NTNU

Norwegian University of
Science and Technology

Model for Prediction of Cement Sheath Failure

Marte Bustgaard
Marie Houge Nesheim

Master of Science in Petroleum Geoscience and Engineering
Submission date: June 2016
Supervisor: Sigbjørn Sangesland, IPT
Co-supervisor: Bjørn A. Brechan, IPT

Norwegian University of Science and Technology
Department of Petroleum Engineering and Applied Geophysics

Summary

In casing design, the casing is required to withstand all loads it is exposed to during the well life. These loads are normally modeled in an industry leading software (ILS), which determines whether the casing can withstand the loads. The well cement is also subjected to the operational loads. However, the cement strength is not included in the ILS. Other complementary softwares are available, but are not always included as standard practice.

In this thesis, a cement sheath mechanical model has been developed in order to investigate the necessity of considering the cement. Safety factors (SF) for the cement resulting from the model, and for the casing resulting from the ILS have been compared. This is done in order to determine if the cement fails before the casing fails in some scenarios. Through this comparison, the necessity of an additional feature in the ILS have been determined.

The model have been developed by the use of axisymmetric thick-walled cylinder theory, considering three cylinders; one for the casing, one for the cement and one for the formation. By considering this theory, the stresses through a cross-section of the cylinders have been calculated, and further, failure criteria have been applied to the stresses. Three failure modes have been considered; debonding of the cement at the casing and formation interfaces, radial cracks and shear failure in the bulk cement. In order to thoroughly investigate how the cement SFs change with variable cement mechanical properties, sensitivity analyses have been performed at various pressure and temperature changes. For one load case, the worst- and the best-case combinations of mechanical properties for each failure mode have been identified, and included in the comparison with the ILS. This has been done to achieve a broad knowledge, and to more effectively conclude whether complementing the ILS is necessary.

The results indicated that debonding was likely at well pressure decreases, while radial cracks mostly occurred at pressure increases. Shear failure occurred at both large pressure increases and pressure decreases. When the worst-case burst and collapse loads, for typical casing and cement properties, were considered, the cement failed in tension before the casing failed. However, the results were less prominent when the worst- and best-case of mechanical properties of the cement and formation were considered. The cement was mostly exposed to lose its integrity through debonding, due to several combinations of mechanical properties resulting in debonding for a worst-case collapse load. It was therefore concluded that it could be beneficial to include an additional feature to the ILS, which analyzes the cement integrity when performing casing design.

Sammendrag

I fôringsrørdesign, må fôringsrørene tåle alle belastningene de er utsatt for gjennom brønnens levetid. Dette blir vanligvis modellert ved hjelp av en industriledende programvare (ILS). Denne vil da kunne avgjøre om fôringsrørene vil tåle lastene de blir utsatt for. Sementen i brønnen blir også utsatt for ulike laster, men den overnevnte programvaren tar ikke hensyn til dette. Det finnes likevel andre programvarer som ivaretar dette, men slike programvarer er normalt ikke en del av standard praksis i brønnkonstruksjon.

I denne masteroppgaven har det blitt utviklet en mekanisk sementmodell. Sikkerhetsfaktorene for sementsvikt som resulterer fra denne, har blitt sammenliknet med sikkerhetsfaktorene for fôringsrørsvikt som resulterer fra ILS. Dette har blitt gjort for å kunne bestemme om det er tilfeller hvor sementen svikter før fôringsrørene svikter. Ved denne sammenligningen har det blitt mulig å bestemme nødvendigheten av å evaluere sementen, og nødvendigheten av å tilføye dette som en tilleggsfunksjon i ILS.

Sementmodellen har blitt laget ved å anta tre sylindre i aksesymmetrisk tykkvegget sylinder teori. De tre sylinderne inkluderer én for fôringsrøret, én for sementen og én for formasjonen. Ved å bruke denne teorien har spenningene gjennom et tverrsnitt av sementen blitt regnet ut, og et bruddkriterium har blitt benyttet for å bestemme når sementen svikter. Sementen kan i hovedsak svikte på tre måter; den kan miste bindingen til fôringsrør- og formasjons grenseflaten, det kan oppstå radielle sprekker og det kan oppstå skjærbrudd i sementmassen. Sensitivitetsanalyser har blitt gjennomført for å undersøke nærmere hvordan sementens sikkerhetsfaktorer varierer med ulike sementegenskaper, trykk og temperaturer. I tillegg har dette blitt brukt til å finne den beste og den verste kombinasjonen av mekaniske egenskaper for hver lastsituasjon. Dette har blitt gjort for å oppnå en bedre sammenlikning med ILS. Dermed har det blitt mulig å konkludere mer presist om det er nødvendig å komplementere ILS, ved å implementere en sementmodell.

Resultatene indikertr at en trykkreduksjon i brønnen førte til at sementen mistet bindingen til både formasjonen og fôringsrøret, og at radielle sprekker oppstod ved trykkøkning i brønnen. Skjærbrudd skjedde ved både høy økning og reduksjon i trykk. Resultatene viste også at en sement med vanlige egenskaper sviktet, i form av radielle sprekker eller avbinding, da typiske fôringsrør ble utsatt for høyt innvendig eller utvendig trykk. Ved endrede sementegenskaper, bla. stivheten til sement, viste det seg at den største risikoen er at bindingen mellom sement og fôringsrøret svikter. Det ble derfor konkludert at det kan være hensiktsmessig å implementere en tilleggsfunksjon i ILS, som analyserer sementens integritet.

Acknowledgements

This master thesis is submitted as the final product of the master's degree programme 'Petroleum Geoscience and Engineering - Drilling Engineering'. The thesis is carried out at the Norwegian University of Science and Technology (NTNU) at the Department of Petroleum Engineering and Applied Geophysics.

The authors would like to thank supervisor Professor Sigbjørn Sangesland (NTNU) for coordinating this project. He has provided great guidance and his calm presence have been highly comforting.

A special appreciation goes to co-supervisor Assistant Professor Bjørn A. Brechan (NTNU) for proposing and supervising this project. His thoroughly and motivating feedback during the work with the thesis, and with the specialization project have been greatly appreciated. The authors are thankful for him imparting his knowledge and providing real life examples. His positive attitude and passion for drilling is transmittable, and will be remembered. The authors will be forever grateful for learning how to use Landmark's WellCat.

The authors would like to express a deep gratitude to Postdoctoral Researcher Jesús De Andrade (NTNU) for his great guidance, grounded presence and all his knowledge about cement sheath modelling. The authors are deeply grateful for his willingness to share his expertise, and believe that without his guidance this thesis would not have been possible.

The authors would also like to thank each other for the good discussions, motivational speeches and excellent cooperation during the development of the cement sheath model, and during the writing process to complete this thesis.

Best regards,

Marte Bustgaard and Marie Houge Nesheim

June 2016

Table of Contents

List of Figures

List of Tables

Abbreviations

BC	Best-Case
CBL	Cement-Bond-Log
DF	Design Factor
ILS	Industry Leading Software
NTNU	Norwegian University of Science and Technology
SBT	Segmented Bond Tool
SCP	Sustained Casing Pressure
SF	Safety Factor
TOC	Top Of Cement
UCS	Unconfined Uniaxial Compressive Strength
UF	Utilization Factor
USIT	Ultrasonic Imagine Tool
VDL	Variable Density Log
WC	Worst-Case

Cem	Cement
Form	Formation

1. Introduction

Motivation

The presence of leak paths through the cement sheath barrier is one of the primary causes of integrity issues in wells today. The interest in improving the cement design in order to avoid such issues is therefore present. The main purpose of the cement is to provide zonal isolation and mechanical support to the casing. When the integrity of the cement is compromised, it might lead to hazardous consequences. Cement bond logs is usually performed to confirm the quality of the cement. However, these logs have been claimed to be inaccurate or difficult to interpret, which can make the logs unreliable when determining the integrity of the cement.

In casing design, the casing is required to withstand all loads it is exposed to during the well life. These loads are normally modeled in an industry leading software (ILS), which determines whether the casing can withstand the loads it is exposed to. The well cement is also subjected to loads. The ILS for casing design takes the cement properties as inputs, but does not incorporate them in terms of stresses in the cement, zonal isolation or mechanical support. It might be a shortcoming for the ILS to not include any calculations on zonal isolation. However, other complementary softwares are available, but are not always included as standard practice.

Goals

The goal has been to develop a model that calculates the stresses in the cement sheath and determines when failures may occur. Additionally, the goal has been to investigate whether including cement sheath failure prediction should be a part of standard practice. If it turns out that the cement fails in cases where the casing is safe, complementing ILS might be necessary.

Approach

In order to investigate whether the cement fails for conditions where the casing is safe, safety factors (SF) have been determined for the different failure modes of the cement. These failure modes include tensile failures, in terms of debonding and radial crack, and shear failure. The SFs for the failure modes have been plotted together with the SFs of the casing, resulting from

the ILS, for the same load case. Production load cases for the 9 5/8-in production casing have been investigated, with a special focus on the worst-case collapse and burst loads.

Sensitivity analyses have been performed for the mechanical properties of the cement and the formation. The analyses have been used to obtain a general conclusion when comparing the SFs from the cement model and the ILS. This is done by varying the cement and formation properties, and determining the worst and the best combination of the mechanical properties in order to avoid failure.

When complementing the ILS, some features can be included in the cement sheath model. These features include the effect of the initial stress condition in the cement, the well geometry and the change in formation pressure. An investigation of how these features affects the SF for the various failure modes have been performed.

2. Theory

2.1 Cement

2.1.1 Casing Cement Purpose

The well cement is placed in the annulus between the casing and the formation exposed to the wellbore. Some part of the cement is often a part of the primary and secondary barrier envelope. Hence, the consequences of a failure in the cement sheath can range from minor, such as sustain casing pressure, to fatal in terms of a blowout.

According to NORSOK (2013 p. 178) the purpose of the cement "is to provide continuous, permanent and impermeable hydraulic seal along hole in the casing annulus or between casing strings, to prevent flow of formation fluids, resist pressures from above or below, and support casing or liner strings structurally". In other words, providing zonal isolation and casing support.

2.1.2 Cement in Terms of Well Integrity

NORSOK (2013 p. 6) defines well integrity to be "application of technical, operational and organizational solutions to reduce risk of uncontrolled release of formation fluids throughout the life cycle of a well". Generally, the hydrocarbons can flow to the environment through four distinct ways: Through the tubing, through the completion annulus, through the cement, and through communication path in the formation.

In a technical perspective, the well needs to be designed with appropriate and sufficient well barrier elements to prevent flow to the surface. The well barrier elements are divided into two categories; primary and secondary barrier elements, where the primary barrier elements are closer to the wellbore fluids. The cement can often be a part of the primary barrier envelope, secondary barrier envelope or both envelopes. Hence, the cement is important to secure the integrity of the well.

2.1.3 Zonal Isolation

The main purpose of the cement is to provide zonal isolation. This involves excluding formation fluids from other zones than the reservoir. In order to achieve zonal isolation, it is necessary to create a hydraulic seal in the annulus, including good bonding and without fluid channels (Nelson and Guillot, 2006).

A consequence of insufficient zonal isolation maintenance is sustained casing pressure (SCP). Normally there are three sources of annuli pressure; intentionally applied pressure used by the operator for a specific purpose, thermally induced pressure from thermal expansion of trapped fluids, and SCP (Petrowiki, 2016). SCP occur when unintended pressure appears from communication between the annulus, and the formation or another annulus, from a defect or failed barrier. In an offshore case, there is a significant difference between a subsea well and a platform well. In a subsea well, the A annulus, which is the annulus outside the tubing, is often the only monitored annulus. Hence, a buildup of pressure in B or C annulus, which are the annuli outside the production- and intermediate casing respectively, could occur without being detected. In severe cases, this could result in a high collapse load for the inner casing and a burst load for the outer casing. For a platform well, the consequences are less severe since it is possible to monitor and bleed down the pressure in the annulus if SCP is detected. However, in severe cases, a remedial cement job might be necessary, or the well might be required to be shut in or abandoned.

It is also worth mentioning that zonal isolation loss can occur from other situations than cement failure. A chemical attack or changes in the downhole temperature and pressure could result in loss of zonal isolation. Additionally, fracturing of the wrong zone could result in loss of zonal isolation (Nelson and Guillot, 2006 p. 269).

2.1.4 Cement Bonding

Together with the cement mechanical properties, the cement bonding is an important quality of the cement to provide zonal isolation. Bonding of cement includes both bonding between the casing and the cement, and the formation and the cement. In order to obtain adequate bond to the casing and the formation, shear bond and hydraulic bond are two criteria that needs to be satisfied at the interfaces. The shear bond mechanically supports the casing, and constitutes the shear bond strength. If the axial forces overcome the shear bond strength, movement of the casing will occur (Nelson and Guillot, 2006 p. 219). The hydraulic bond is related to zonal isolation, because it works by blocking the fluids that are traveling along the casing-cement and the cement-formation interfaces. It is measured by applying pressure at the two interfaces until leakage occur (Nelson and Guillot, 2006 p. 219).

Several variables can affect the quality of the cement bonding; the formation composition, the drilling fluid composition and the cement slurry composition. Furthermore, temperature and pressure conditions can also affect the bonding quality (Nelson and Guillot, 2006).

An acoustic cement bond log is used to qualify the bonding quality. Acoustic logs do not measure the hydraulic seal, but the fraction of the casing covered with cement. This is done by measuring loss of acoustic energy as it propagates through the casing. There are two classes of sonic logging tools; sonic and ultrasonic. For the sonic logs there are two types; cement-bond-log, also called variable density log (CBL/VDL), or segmented bond tool (SBT). For the ultrasonic logging, the ultrasonic imagine tool (USIT) is commonly used (Bybee, 2007).

However, several factors can affect the interpretation and the reliability of the cement bond log. Bybee (2007) mentions that the presence of a microannulus in the cement can lead to misinterpretation of the CBL/VDL, and that some of the logs demand adequate centralization in order to be interpretable. Additionally, fast formation and lightweight cement can negatively affect the interpretation of some logs (Bybee, 2007).

NORSOK (2013) states that in critical cement cases the cement shall be logged. These cases include when the production casing or liner is set into a source of inflow of hydrocarbons, or when the cement is a part of the primary and secondary well barriers. Additionally, the cement is required to be logged if the injection pressure exceeds the formation integrity at the cap rock

2.1.5 Cement Mechanical Properties

Well cement has in general a brittle behavior in tension, and a ductile behavior in compression. Ductile failures (i.e. compressive) in the cement is harder to achieve than brittle failures (i.e. tensile) (Nelson and Guillot, 2006 p .277). Until recently, the unconfined uniaxial compressive strength (UCS) has been the most important mechanical property used when qualifying the cement design. The UCS represents the ability to support the casing and to survive the perforation stresses. However, the ability of the cement to withstand loads and to ensure zonal isolation throughout the lifetime of the well, have had a larger focus. To ensure this ability, mechanical parameters such as the tensile strength, the elasticity and the ductility of the cement have received more attention in later years. Additionally, laboratory experiments have shown that the principal cause of cement sheath damage is due to stresses induced by varying downhole conditions (Nelson and Guillot, 2006 p.269).

Figure 1 shows a typical tensile test curve for porous cement, carried out with a constant confining pressure. In the figure, the axial stresses, which are positive, are compressive. The radial strain curve illustrates the typical brittle tensile behavior of the cement.

Some characteristics are differentiating from a tensile test carried out for a non-porous media. Firstly, the line from 0 to A is not linear. This is due to the collapse of pores when the cement is subjected to the applied stress. However, the curve has a nearly elastic region, where the stress-strain relationship is proportional to the Young's modulus, E. This region is from A to B in the figure. After B, which is the yield point, the plastic behavior of the cement takes place and large deformations occur. Point C is the largest load the cement can take under the given confining pressure. Failure of the cement will occur at this point, and the cement will lose its integrity (Nelson and Guillot, 2006).

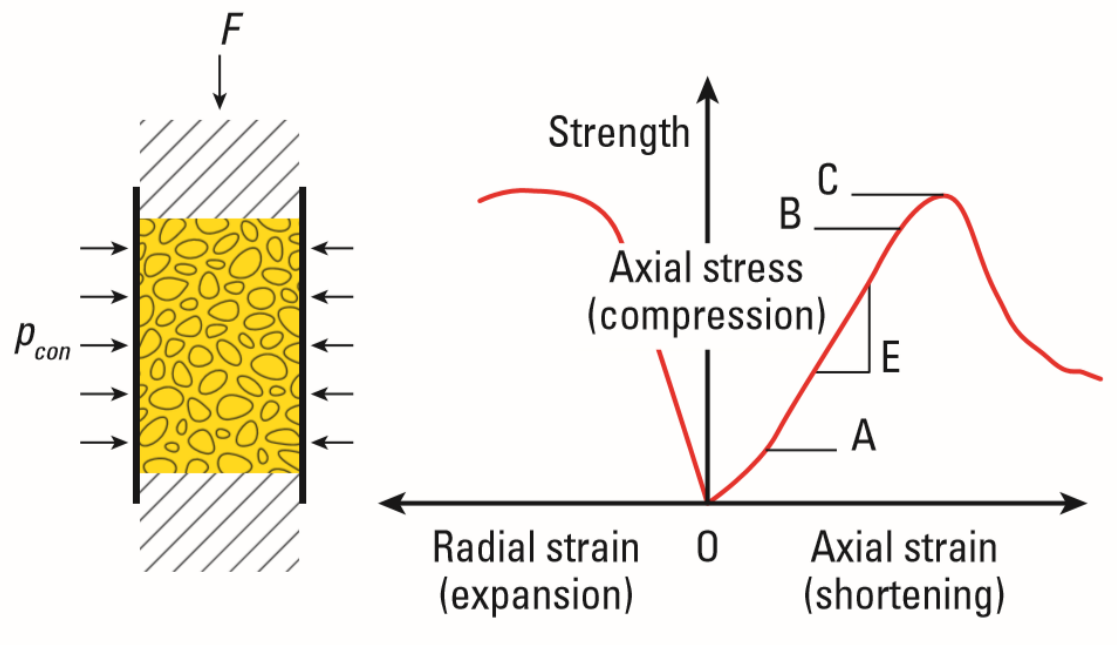

Figure 1: Tensile test curve for cement (Nelson and Guillot, 2006 p. 271)

2.1.6 Typical Cement Properties

As mentioned above, some mechanical properties of the cement are of great importance in order to determine the quality of the design. Among these properties are the cement Young's modulus (E), the Poisson's ratio (ν) and the coefficient of linear thermal expansion (α). Table 1 shows a typical range of these properties for the cement and the formation. The ranges are based on De Andrade (2015 p.41).

Table 1: Typical mechanical property ranges for cement and formation (De Andrade, 2015 p.41).

Mechanical Property	**Range**
Cement Young's modulus	1-20 GPa
Formation Young's modulus	1-70 GPa
Poisson's ratio of cement	0.1-0.3
Poisson's ratio of formation	0.18-0.40
Coefficient of linear expansion of cement	$10*10^{-6}$-$14*10^{-6}$ 1/C
Coefficient of linear expansion of formation	$8*10^{-6}$-$18*10^{-6}$ 1/C

When considering cement strength data, the USC and the uniaxial tensile strength (T_0) are developed with Eq. (2.1) (De Andrade and Sangesland, 2016) and Eq. (2.2) (De Andrade, 2015) respectively.

$$UCS = 0.0354 \cdot Ecem^2 + 3.1509 \cdot Ecem + 4.0642 \tag{2.1}$$

$$T_0 = \frac{UCS}{10} \tag{2.2}$$

Where,

UCS= Uniaxial compressive strength [Pa]

E_{cem}= Young's Modulus of cement [Pa]

T_0= Uniaxial tensile strength [Pa]

Hence, both the UCS and the T_0 are related to the cement Young's modulus.

2.2 Modeling Stresses in the Cement

The state of stress in the cement sheath must be calculated and entered into an expression in order to determine whether the cement sheath will fail or debond in the annulus. The stress state is calculated by assuming a deformation behavior (e.g. elasticity). Convenient boundaries, such as the casing-cement and cement-formation interfaces, should be used. Considering the influence of pore pressure and temperature is necessary in some cases (Nelson and Guillot, 2006 p. 280).

This section will cover the development of stresses in the cement sheath model. The basic mechanical theory is explained in Appendix C.

2.2.1 Stresses in a Cylinder

In a cylinder subjected to temperature, internal and external pressures, three mutually perpendicular principal stresses are set up in the material. These principal stresses are shown in Figure 2, where $\sigma_r, \sigma_t, \sigma_a$ represent the radial, hoop(tangential or circumferential), and axial (longitudinal) stress respectively (Hearn, 1997).

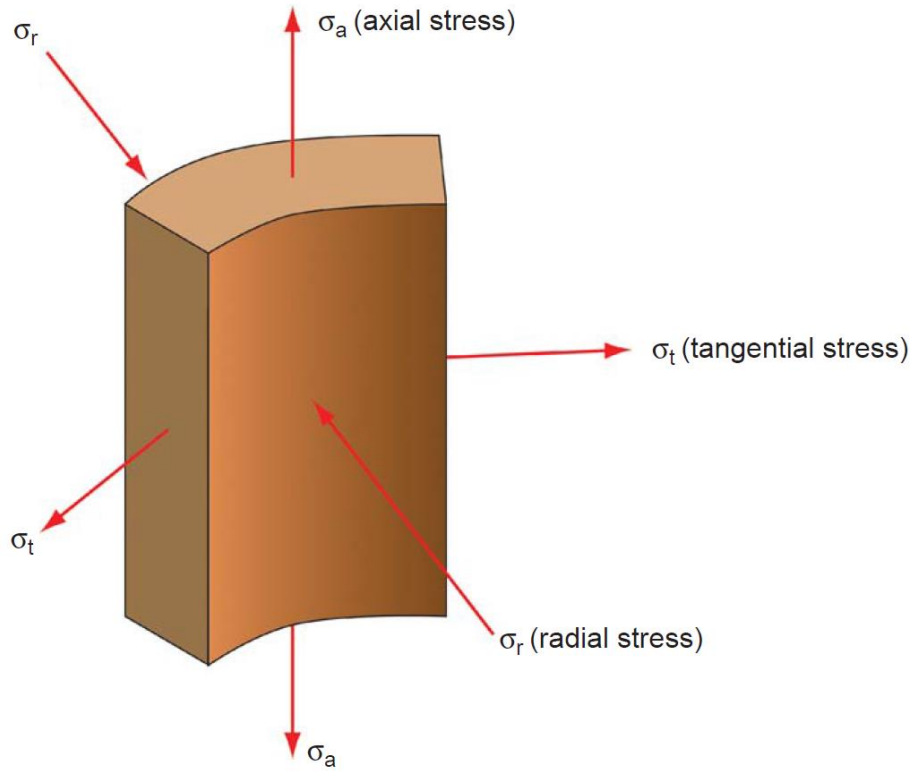

Figure 2: Hoop, axial and radial stress illustrated (Bellarby, 2009 p. 514)

As seen in Figure 2, hoop stresses are the normal stresses that are in the tangential (azimuth) direction, acting around the circumference of the cylinder. Any pressure differential across a cylinder pipe will result in hoop stress. Axial stresses are the stresses along the axis of the cylinder, while radial stresses are acting away from or towards the cylinder axis. According to thick-walled cylinder theory, the internal pressure is the radial stress at the inner wall, while the external pressure is the radial stress at the outer cylinder wall interface. In thin-walled cylinder theory the radial stresses are considered constant through the cylinder wall (Hearn, 1997).

2.2.2 Thin- and Thick-Walled Cylinder Theory

Thin-walled cylinder theory can be used to determine stresses in terms of the hoop, radial and axial directions in a cylinder. However, this theory assumes that the radial and the axial stresses are constant across the wall thickness, and that the magnitudes of the radial stresses set up are small compared to the hoop and axial stresses. Consequently, the radial stresses can be neglected. Furthermore, thin-walled cylinder theory assumes that the ratio of wall thickness to inside diameter of the cylinder is less than 1/20. This is not applicable for the casing, nor for the cement. Hence, stress theory for thick-walled cylinder should be used. Lamé has developed a theory for stresses in thick-walled cylinders, which has been applied in this project. This theory account for a pressure gradient across the cylinder wall and varying hoop stresses across the thickness of the cylinder (Hearn, 1997).

2.2.3 Development of Lamé's Theory

The derivation of Lamé's theory can be shown in Appendix D, while Eq.(2.3) shows the main result. Eq.(2.3) can be used for different radii, to determine the hoop and the radial stresses in a thick-walled cylinder.

$$\sigma_r = A - \frac{B}{r^2}$$
$$\sigma_H = A + \frac{B}{r^2} \tag{2.3}$$

Where,

σ_r = Radial Stress [Pa]
σ_H = Hoop Stress [Pa]
A = Lamé constant A [Pa]
B = Lamé constant B [Pa $\cdot$ m^2]
r = radius [m]

The constants A and B are determined for the relevant boundary conditions (Hearn, 1997).

2.2.4 Defining the Boundary Conditions

In order to develop a model for the stresses in the cement, Lamé's equations have to be used for a cylinder experiencing both internal and external pressure. The boundary conditions where the cylinder experiences both internal and external pressure are shown in Eq. (2.4)

$$\begin{aligned} \sigma_r(r_i) &= -P_i \\ \sigma_r(r_o) &= -P_o \end{aligned} \tag{2.4}$$

Where,

r_i = internal radius of the cylinder [m]
r_o = external radius of the cylinder [m]
P_i = internal pressure [Pa]
P_o = external pressure [Pa]

By inserting the boundary conditions into Lamé's equation, the constants A and B are obtainable as shown in Eq. (2.5):

$$\begin{aligned} -P_i &= A - \frac{B}{r_i^2} \\ -P_o &= A - \frac{B}{r_o^2} \\ A &= \frac{r_i^2 P_i - r_o^2 P_o}{r_o^2 - r_i^2} \\ B &= \frac{(P_i - P_o) r_i^2 \cdot r_o^2}{(r_o^2 - r_i^2)} \end{aligned} \tag{2.5}$$

Then, equations for the hoop and radial stress in a cylinder can be obtained as shown in Eq. (2.6):

$$\sigma_r = \frac{r_i^2 P_i - r_o^2 P_o}{r_o^2 - r_i^2} - \frac{(P_i - P_o) r_i^2 \cdot r_o^2}{(r_o^2 - r_i^2) \cdot r^2}$$
$$\sigma_H = \frac{r_i^2 P_i - r_o^2 P_o}{r_o^2 - r_i^2} + \frac{(P_i - P_o) r_i^2 \cdot r_o^2}{(r_o^2 - r_i^2) \cdot r^2} \quad (2.6)$$

Axial stress is shown in Eq. (2.7).

$$\sigma_z = \upsilon \cdot (\sigma_r + \sigma_H) \quad (2.7)$$

Where,

σ_z = axial stress [Pa]

2.2.5 Implementing the Equations into a Casing-Cement-Formation System

Lamé's equations (Eq.(2.6)) needs to be implemented into a casing-cement-formation system. Figure 3 shows this system with relevant radii. R_a is defined as the inner radius of the casing, r_b is the radius to the outside of the casing. R_c is the radius to the outer border of the cement, and r_d is the radius from the center of the well to the outer border of the formation.

In order to obtain equations applicable for the cement, casing and formation a determination of the contact pressures is also necessary. A contact pressure is the pressure applied between two surfaces in contact with one another. The applicable contact pressures are at the casing-cement interface and at the cement-formation interface (at r_b and r_c). These contact pressures are called P_{c1} and P_{c2}, respectively (De Andrade, 2015). The derivation of the contact pressures are based on the work of De Andrade (2015) and are shown in Appendix E. Nevertheless, it is worth mentioning the main assumptions behind the derivation. The contact pressures are determined by assuming that the radial displacement of the cement and the casing are equal, due to bonded interfaces. Additionally, it is assumed that there is no axial movement.

In order to calculate the contact pressures, it is necessary to calculate the change in temperature in the cement caused by the operational loads. The temperature change at the

cement-formation interface, ΔT_2, is obtained by assuming conduction through the cement and the formation. Eq.(2.8) and Eq.(2.9) represent conduction set up for the cement and the formation, respectively.

$$\Delta T_1 - \Delta T_2 = \frac{\dot{Q}}{2\pi} \cdot \frac{\ln\left(\frac{r_c}{r_b}\right)}{k_{cem}} \tag{2.8}$$

$$\Delta T_2 - \Delta T_{geo} = \frac{\dot{Q}}{2\pi} \cdot \frac{\ln\left(\frac{r_d}{r_c}\right)}{k_{form}} \tag{2.9}$$

Where,

$\Delta T_1 =$ Change in temperature in casing [C°]
$\Delta T_2 =$ Change in temperature in cement [C°]
$\Delta T_{geo} =$ Change in temperature in formation [C°]
$\dot{Q} =$ Heat [W]
$k_{cem} =$ Thermal conductivity of cement $\left[W/m \cdot C°\right]$
$k_{form} =$ Thermal conductivity of formation $\left[W/m \cdot C°\right]$

It is assumed that $\Delta T_{geo} \approx 0$. Since ΔT_{geo} is the change in temperature at r_d, ΔT_2 is dependent on the chosen r_d.

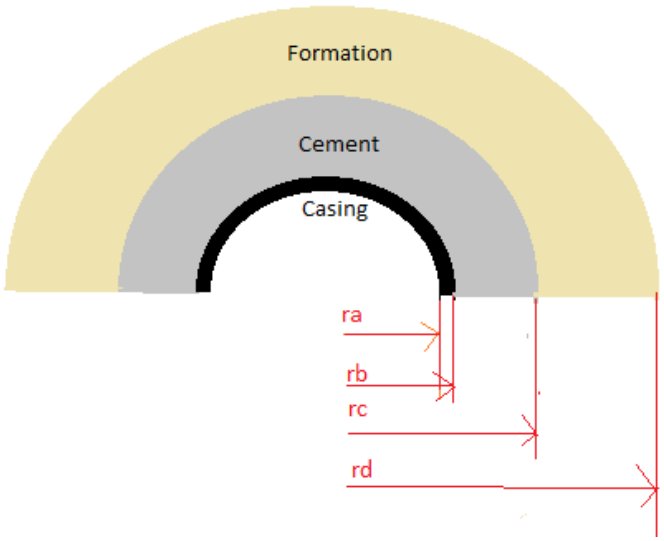

Figure 3: Casing, cement and formation system with defined radii, free from De Andrade (2015)

In order to model the stresses in the cement sheath cross-section, Eq. (2.6) will be used, now by including the radii presented for the casing-cement-formation system, and the contact pressures. Eq. (2.10) to Eq. (2.12) show the results.

In rock mechanics, the sign convention states that compaction is positive and tension is negative. This is because most stresses in rock mechanics are compressive. However, the sign convention in other mechanics might be defined as the opposite, and one must therefore be aware of this when the sign convention is inconsistent (Fjær et al., 2008 p. 1)

In Eq. (2.4)-Eq. (2.7) the input pressure differential values are positive for pressure increases, and negative for pressure decreases. In Eq. (2.8) and Eq. (2.9) the input temperature differential values are positive for heating and negative for cooling. The equations will then give positive values for tensile stresses, and negative values for compressive stresses.

In the cement sheath model, it is desirable that tension is negative and compaction is positive. Hence, a sign conversion is necessary to comply with rock mechanics. This is done by multiplying all the stresses with (-1) as shown in Eq. (2.10)-Eq.(2.12).

For a radius between r_a and r_b, the resulting hoop and radial stresses are given by:

$$\sigma_{r,casing} = (-1)\cdot\frac{r_a^{\,2}P_i - r_b^{\,2}P_{c1}}{r_b^{\,2} - r_a^{\,2}} - \frac{(P_i - P_{c1})\,r_a^{\,2}\cdot r_b^{\,2}}{(r_b^{\,2} - r_a^{\,2})\cdot r^2}$$
$$\sigma_{H,casing} = (-1)\cdot\frac{r_a^{\,2}P_i - r_b^{\,2}P_{c1}}{r_b^{\,2} - r_a^{\,2}} + \frac{(P_i - P_{c1})\,r_a^{\,2}\cdot r_b^{\,2}}{(r_b^{\,2} - r_a^{\,2})\cdot r^2} \quad (2.10)$$

For a radius between r_b and r_c, the resulting hoop and radial stresses are given by:

$$\sigma_{r,cement} = (-1)\cdot\frac{r_b^{\,2}P_{c1} - r_c^{\,2}P_{c2}}{r_c^{\,2} - r_b^{\,2}} - \frac{(P_{c1} - P_{c2})\,r_b^{\,2}\cdot r_c^{\,2}}{(r_c^{\,2} - r_b^{\,2})\cdot r^2}$$
$$\sigma_{H,cement} = (-1)\cdot\frac{r_b^{\,2}P_{c1} - r_c^{\,2}P_{c2}}{r_c^{\,2} - r_b^{\,2}} + \frac{(P_{c1} - P_{c2})\,r_b^{\,2}\cdot r_c^{\,2}}{(r_c^{\,2} - r_b^{\,2})\cdot r^2} \quad (2.11)$$

For a radius between r_c and r_d, the resulting hoop and radial stresses are given by:

$$\sigma_{r\ formation} = (-1)\cdot\frac{r_c^{\,2}P_{c2} - r_d^{\,2}P_f}{r_d^{\,2} - r_c^{\,2}} - \frac{(P_{c2} - P_f)\,r_c^{\,2}\cdot r_d^{\,2}}{(r_d^{\,2} - r_c^{\,2})\cdot r^2}$$
$$\sigma_{H,\,formation} = (-1)\cdot\frac{r_c^{\,2}P_{c2} - r_d^{\,2}P_f}{r_d^{\,2} - r_c^{\,2}} + \frac{(P_{c2} - P_f)\,r_c^{\,2}\cdot r_d^{\,2}}{(r_d^{\,2} - r_c^{\,2})\cdot r^2} \quad (2.12)$$

Where,

$\sigma_{r\ formation}$ = Radial stress in the formation [Pa]
$\sigma_{H,\ formation}$ = Hoop stress in the formation [Pa]
$\sigma_{\mathrm{r,cement}}$ = Radial stress in the cement [Pa]
$\sigma_{H,\mathrm{cement}}$ = Hoop stress in the cement [Pa]
$\sigma_{\mathrm{r,casing}}$ = Radial stress in the casing [Pa]
$\sigma_{\mathrm{H,casing}}$ = Hoop stress in the casing [Pa]
r_a = inner radius of the casing [m]
r_b = outer radius casing/inner radius cement [m]
r_c = outer radius cement/inner radius formation [m]
r_d = outer radius formation [m]
P_i = Change in internal pressure in the casing [Pa]
P_{c1} = Contact pressure at r_b interface [Pa]
P_{c2} = Contact pressure at r_c interface [Pa]
P_f = Change in external (formation) pressure [Pa]

For all radii, the equation for axial stress (Eq.(2.7)) is applicable with the relevant hoop and radial stresses. Appendix A shows how this is modeled in Visual Basic for Applications.

2.2.6 Including Initial Stress Condition

Bosma et al. (1999) mentions the importance of initial stress in the set cement. Figure 4 shows three scenarios for a stable wellbore. Firstly, if there is a net shrinkage of the cement during curing, the initial stresses will be zero. Secondly, if no shrinkage occurs, the initial stress in the cement will be the hydrostatic pressure, which in many cases can be assumed to be the minimum horizontal stress. Furthermore, if an expansion of the cement occurs during curing, the stresses in the cement is the initial hydrostatic pressure plus the expansion restriction in the well.

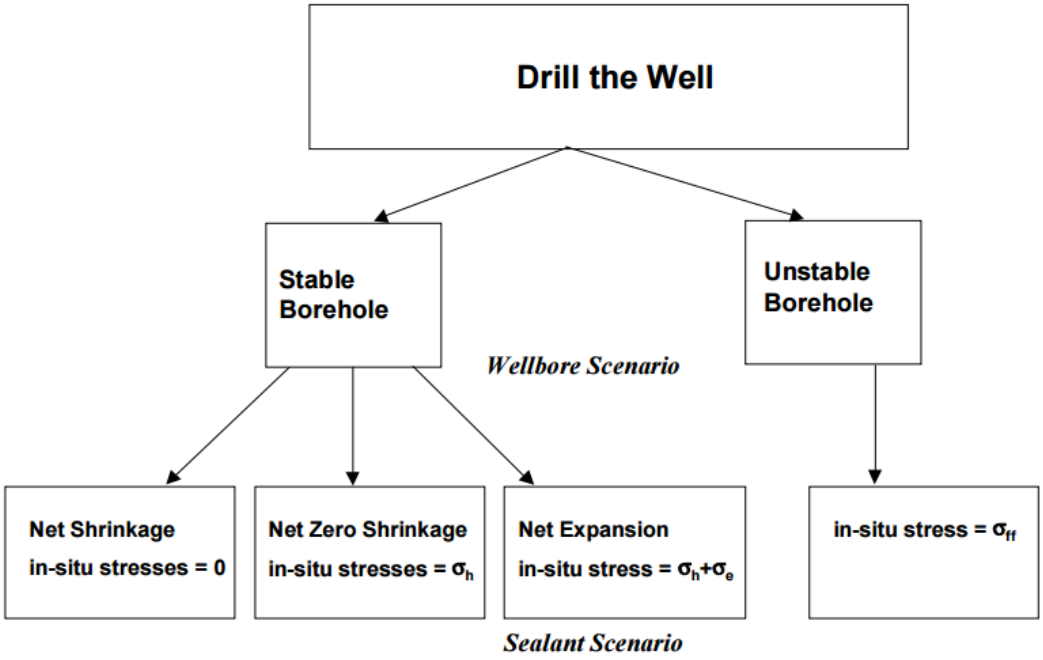

Figure 4: Scenarios for initial stress condition (Bosma et al., 1999 p. 10)

The initial stresses are added to the stress variation that occur from the load case, and then implemented into a failure criterion.

2.3 Failure Criteria

The physical properties of structures or components are usually found by laboratory experiments where the material is only subjected to a simple stress field. This can be done in a simple tensile test, where the material is subjected to stress, and the strains and stresses at fracture can be measured. However, determining the strength of a material subjected to a more complicated stress field, requires calculations that are more complex (Hearn, 1997).

In the past, several failure criteria have been developed in order to determine the conditions where a material is failing. These failure criteria use different inputs, which varies from the case specific principal stresses ($\sigma_1, \sigma_2, \sigma_3$), to other material properties such as Cohesion (c), or friction angle (ϕ).

Nelson and Guillot (2006) describes three failure criteria that can be applicable for cement, these include 'the maximum tensile stress criterion', 'The Tresca criterion' and the 'Mohr-Coulomb criterion'. The first two criteria will be presented in this thesis, while the Tresca criterion can be found in Appendix G. Additionally, the Mogi-Coulomb have received acceptance as an applicable failure criterion for cement. In this thesis, the Maximum tensile stress criterion and the Mogi-Coulomb criterion are used when developing an analytical model to determine the stresses and failure in the cement. In Appendix G a relationship between the Mohr-Coulomb and the Mogi-Coulomb parameters are presented.

2.3.1 The Maximum Tensile Stress Criterion

The maximum tensile stress criterion states that failure occur when the maximum effective principal stress reaches the elastic stress limit in tension (Nelson and Guillot, 2006). However, since tension is defined as negative, tensile failure will occur when the minimum principal stress is less than the negative value of the uniaxial tensile strength:

$$\sigma_3 < -T_0 \tag{2.13}$$

Where,

σ_3 = minimum principal stress [Pa]

2.3.2 The Coulomb Criterion

In 1776, the simplest and most important failure criterion was presented by Coulomb. His theory was that rock failure occurs when the shear stresses (τ) on a specific plane reaches a value that is larger than the rock cohesion (c) together with the friction force that work against motion on the failure plane. According to the criterion, rock failure occurs when (Al-Ajmi, 2006 p. 30):

$$\tau = c + \sigma_n \cdot \tan\phi \tag{2.14}$$

Where,

τ = shear stress [Pa]
c = cohesion of the material [Pa]
σ_n = normal stress acting on the failure plane [Pa]
ϕ = angle of internal friction [radians]

Since failure with this criterion occurs first on a plane in the direction of σ_2, the intermediate stress does not influence the τ or σ_n. This is why the intermediate stress is assumed to not have an effect on the rock strength.

2.3.3 The Mohr Criterion

The Mohr criterion assumes that the normal and shear stresses are related at failure by the following equation (Al-Ajmi, 2006 p. 33):

$$\tau = f(\sigma_n) \tag{2.15}$$

Where,

f = a function obtained experimentally

The curve in the $\tau - \sigma$ space in Figure 5 represents this relation. When the Mohr criterion takes a linear form, it corresponds to the Coulomb criterion of failure. Hence, a linear failure criterion such as Eq.(2.14) is commonly known as the Mohr-Coulomb criterion.

2.3.4 The Mohr-Coulomb Criterion

The Mohr-Coulomb failure criterion is mostly used for highly brittle materials, such as concrete and cement. It is often preferred for materials with a much higher compressive strength compared to the tensile strength. The Mohr-Coulomb failure criterion considers only

the maximum, σ_1, and the minimum, σ_3, principal stresses. It does not consider the intermediate principal stress, σ_2, with regards to the rock strength, which differ from the true triaxial stress state in the rock. In true triaxial tests (i.e polyaxial tests) the stresses can be controlled independently in three dimensions, in contrast to the conventional triaxial test where the stresses are only controlled along two axes (Wawersik et al., 1997). In the Mohr-Coulomb criterion, it is assumed that the intermediate principal stress does not affect the strength of the material.

As seen in Figure 5, the Coulomb failure line is drawn from the tangential point of the Mohr failure envelope and the Mohr circle. Above this line, the rock will experience shear failure.

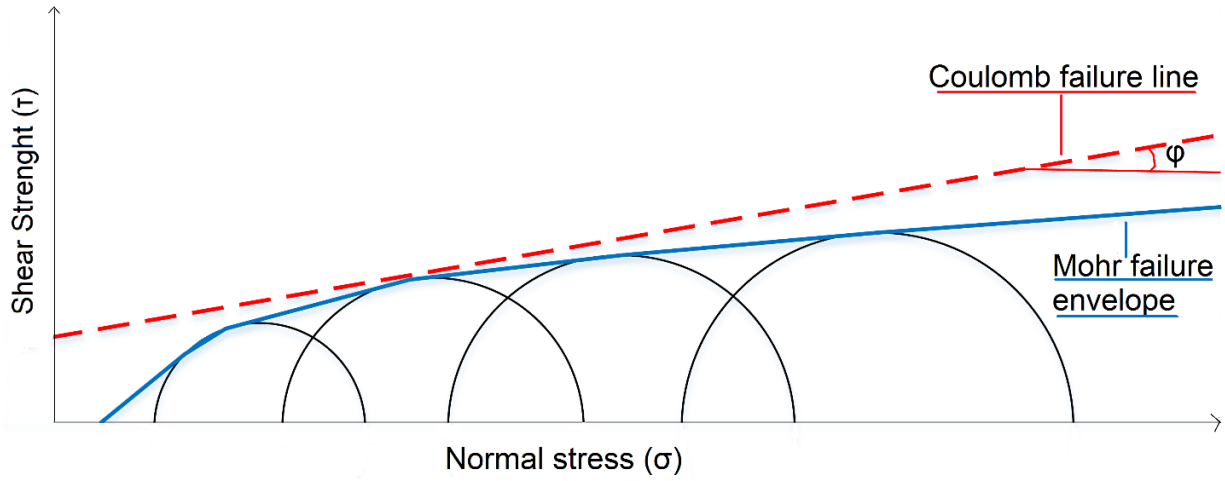

Figure 5: Mohr-Coulomb failure line and combined Mohr circles

2.3.5 The Mogi-Coulomb Criterion

Extensive polyaxial compressive tests in rocks was first performed by Mogi (1971). True triaxial experimental test data have shown that the intermediate stress, σ_2, indeed has a strengthening effect on the rock for several lithology types (Al-Ajmi and Zimmerman, 2005). The Mogi-Coulomb criterion of failure takes the intermediate principal stress into account. When failure occurs, the fracture will propagate along a plane in the direction of the intermediate principal stress. Hence, Mogi concluded that it is the mean normal stress, $\sigma_{m,2}$, that opposes the initiation of fracture. Mogi therefore proposed a new failure criterion, expressed as (Al-Ajmi, 2006):

$$\tau_{oct} = f(\sigma_{m,2}) \tag{2.16}$$

Where,

τ_{oct} = octahedral shear stress [Pa]

$$\tau_{oct} = \frac{1}{3}\sqrt{(\sigma_1 - \sigma_2)^2 + (\sigma_1 - \sigma_3)^2 + (\sigma_2 - \sigma_3)^2}$$

f = monotonically increasing function [-]

$\sigma_{m,2}$ =mean normal stress [Pa]

When the Mogi-Coulomb criterion takes a linear form, the function can be expresses as shown in Eq. (2.17) (Jaeger and Cook, 1979)

$$\tau_{\max} = c \cdot \cos\varphi + \sin\varphi \cdot \sigma_{m,2} \tag{2.17}$$

Where,

$\tau_{\max}$ = the maximum shear stress [Pa]

$$\sigma_{m,2} = \frac{\sigma_1 + \sigma_3}{2}$$
$$c = \frac{UCS(1 - \sin\varphi)}{2 \cdot \cos\varphi}$$

In Figure 6, $\tau_{\max}$ represents the compressive shear failure line. This line is referred to as $\tau_{allowance}$ in Appendix A. If the octahedral shear stresses fall below this line, there will be no shear failure.

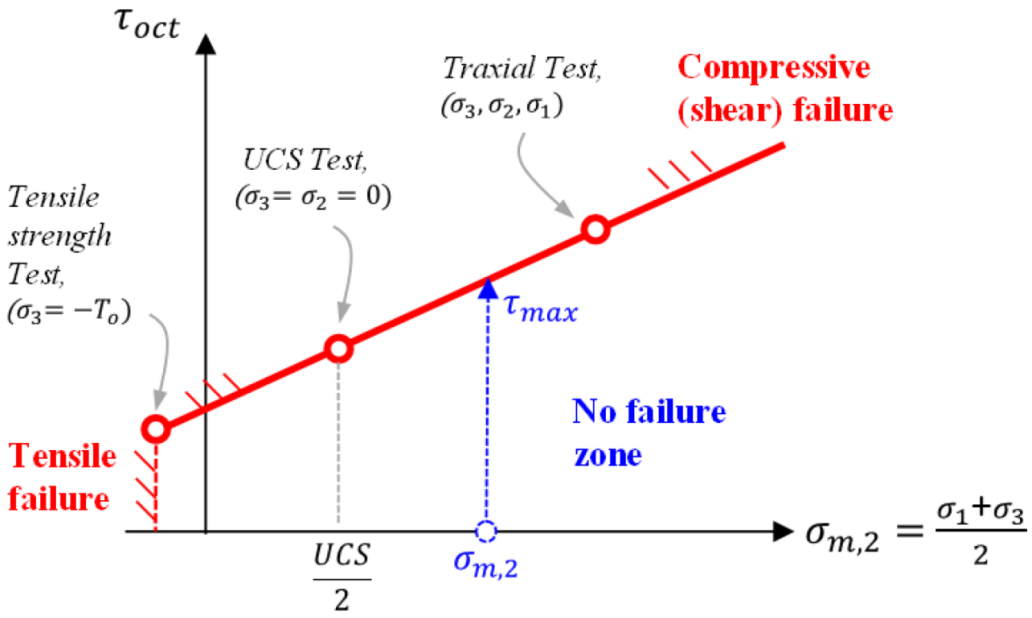

Figure 6: Mogi-Coulomb failure envelope (De Andrade, 2015 p. 36)

2.3.6 Failure Modes

Three modes of failure are applicable for cement, which include debonding, radial cracks and shear failure. These failure modes can result in loss of zonal isolation (De Andrade, 2015). Shear failures are determined with the Mogi-Coulomb criterion, while debonding and radial cracks are determined with the maximum tensile stress criterion. Figure 7 illustrate the various failure modes.

Debonding can occur both at the casing-cement interface and at the cement-formation interface. The bond that is initially set up between casing-cement and cement-formation interface when the cement hardens will fail if the radial stresses reaches a critical value. Debonding might also take place if the shear stresses is significantly large. Debonding can occur if the well experiences a gradual pressure decrease during production, if the casing moves due to subsidence, if temperature and pressure fluctuations occurs or if stimulation operations such as hydraulic fracturing are performed (Nelson and Guillot, 2006 p. 14). If the radial stress at the respective interface exceeds the tensile strength in tension, the following equation describes failure by debonding:

$$\sigma_r < -T_0 \tag{2.18}$$

Radial cracks can occur during the production phase of the well due to thermal or pressure fluctuations. Large variation in temperature or pressure can cause the casing to expand or contract depending on the conditions it is being exposed to. This will give rise to stress

gradients in the wellbore surroundings. If the tensile hoop stress exceeds the tensile strength, voids or cracks in the radial direction will start to form and propagate. When such cracks are present it will compromise the cement integrity (Nelson and Guillot, 2006 p. 14). If several radial cracks are connected, flow paths can be created, which can cause undesirable hydrocarbons to the surface or undesirable uncontrolled pressures (De Andrade, 2015). Cement failure by radial cracks occur when:

$$\sigma_{Hoop} < -T_0 \tag{2.19}$$

Shear failure is the third failure mode which the cement might be subjected to. When the cement experiences shear failure, it typically results in a complete cement sheath failure. The most common cause of shear failure is due to the increased effective stresses around the borehole when the reservoir is being produced. These stresses might rise due to rock subsidence or depletion of the reservoir. Vibrations from downhole pumps or ongoing gas-lift operations may also increase the effective-stresses and result in shear failure (Nelson and Guillot, 2006 p. 14). The Mogi criterion assumes that shear failure takes place when the octahedral shear stress (τ_{oct}) exceeds the allowable shear stress ($\tau_{\max}$) in Eq. (2.20), as shown in the following equation (De Andrade, 2015):

$$\tau_{\max} < \frac{1}{3}\sqrt{(\sigma_1-\sigma_2)^2+(\sigma_1-\sigma_3)^2+(\sigma_2-\sigma_3)^2} \tag{2.20}$$

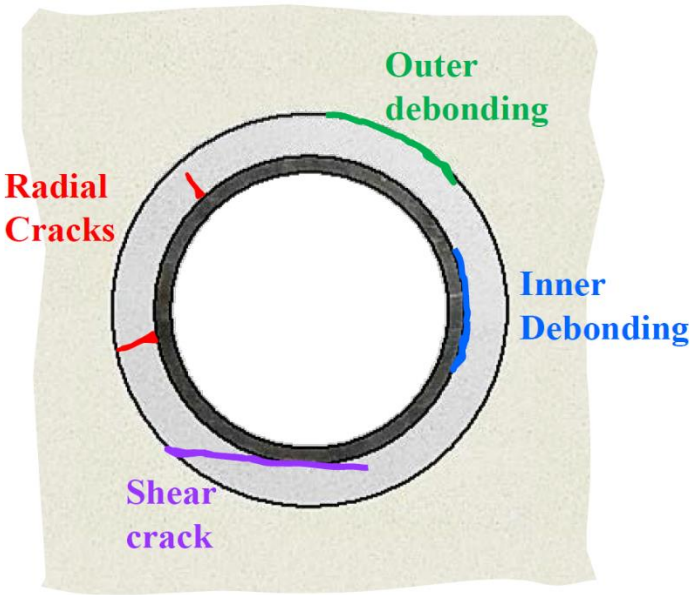

Figure 7: Failure modes in the cement sheath (De Andrade, 2015 p.15)

2.4 The Cement Model

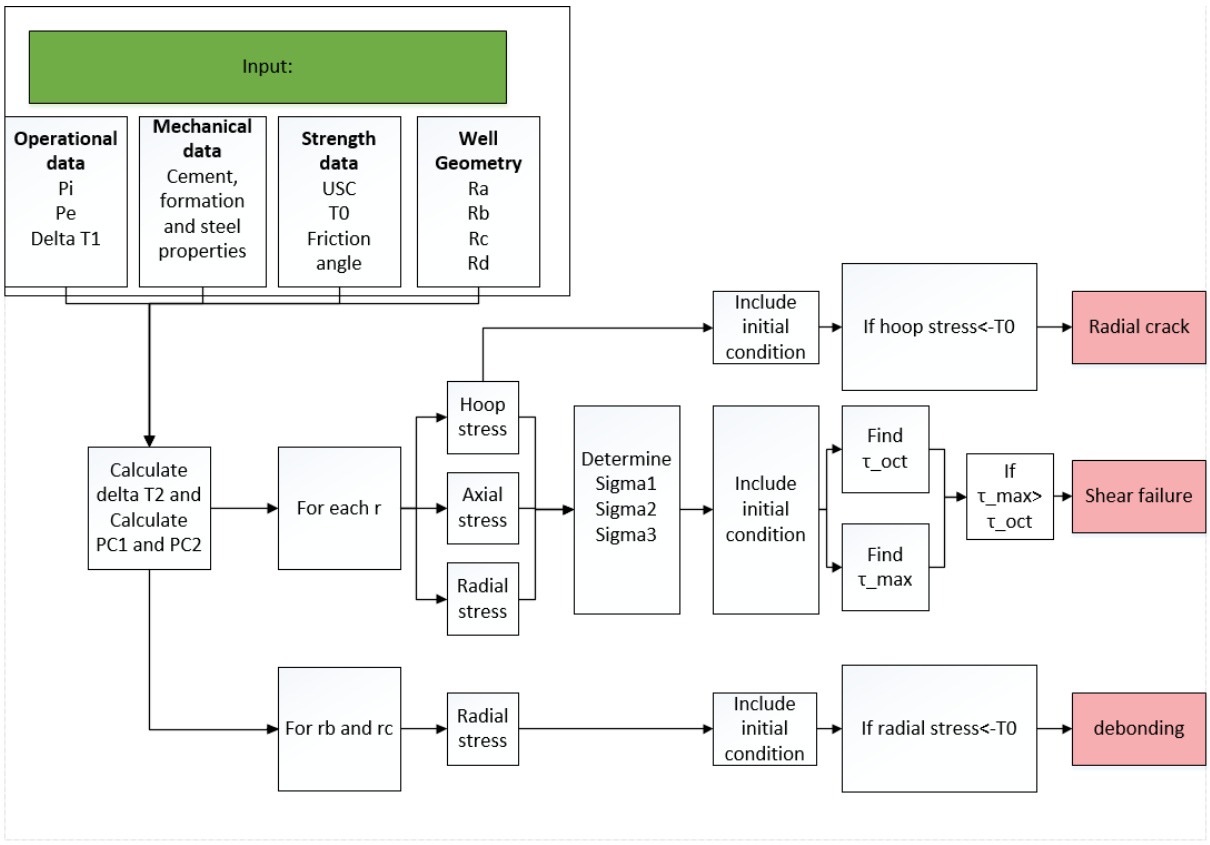

Figure 8: Flowchart of calculations in the cement model

Figure 8 shows a flowchart of how the cement model is working. The main inputs are the operational properties, the mechanical data and the strength data. All operating data are in terms of change from initial condition. Meaning that P_i, is the change in internal pressure from initial condition. P_e is the change in external pressure, which in this model is the formation pressure. ΔT_1 is the change in internal temperature. For the mechanical data; Young's modulus, Poisson's ratio and linear thermal expansion coefficient for formation, steel and cement are entered. The radii are according to Figure 3.

The main output is the type of failure of the cement, in addition to SFs for the failure modes. However, the stresses at different radii are possible to obtain along the cross-section.

The model is used for further analyses, which includes developing SFs for the failure modes in order to see if the cement fails before the casing. Additionally, it is used to complement the ILS when including the cement is necessary, in order to obtain a safe design.

2.5 Load Cases

NORSOK (2013) states that both static and dynamic load cases for well barrier elements shall be defined for each well. What is considered relevant load cases for a well depends on the type of well and what its purpose will be during the entire well life. However, some load case scenarios should always be included for a safe design. NORSOK (2013) also states that design calculations should be performed by competent personnel using software accepted by the industry. In the ILS one can calculate resulting loads from standard or custom scenarios on a preselected grade of casing. When the calculations have been performed, ILS outputs the results as SFs among others. These SFs can be evaluated to see if the design is in good standing, or if it should be altered.

2.5.1 Initial Conditions

The initial condition is defined as the condition the casing is exposed to right after the cement is set and a packer is installed. The initial temperature in the well will be analogues to the geothermal gradient in the formation. Initial internal pressure of the production casing will be due to the fluid column in the annulus. All the load case scenarios calculated for the casing will be analyzed relative to this base case. The initial fluid column is defined as the mud used when running the casing (Bellarby, 2009).

To determine the pressure and temperature changes, the initial pressure and temperature must be subtracted from the final pressure and temperature, resulting from the load cases. This is shown in Eq. (2.21) and (2.22).

$$\Delta P_i = P_{i,\,final} - P_{i,inital} \tag{2.21}$$

$$\Delta T_1 = T_{1,\,final} - T_{1,initial} \tag{2.22}$$

ΔP_i = Change in internal temperature from initial to final condition [Pa]

$P_{i,\,final}$ = Initial pressure, in final condition [Pa]

$P_{i,inital}$ = initial pressure in internal [Pa]

ΔT_i = Change in internal temperature from initial to final condition [°C]

$T_{i,\,final}$ = Initial temperature, in final condition [°C]

$T_{i,inital}$ = initial temperature in internal [°C]

2.5.2 Pressure Test

The casing must always be tested for the highest burst load it might experience during the well life. For the production casing, the worst burst load scenario is often resulting from a tubing leak. In the load case tubing leak, it is assumed that a leak in the tubing occur right below the wellhead. Hence, pressure is applied to the fluid column in A annulus. In order to account for this in the pressure test, the testing pressure is set to the highest burst load pressure, including a kill margin. The kill margin for a 9 5/8-in casing is set to 35 bar (Brechan, 2014). The internal pressure during a pressure test can be calculated by (Economides et al., 1998):

$$P(z) = P_{surface} + \mu_m \cdot z \tag{2.23}$$

Where,

P(z)= pressure at depth z [Pa]

$P_{surface}$=test pressure at surface [Pa]

μ_m= mud weight gradient [Pa/m]

z= depth [m]

This burst load will increase with depth as the test pressure is applied to the fluid column in the A annulus. Since the pressure test is based on the worst case burst load scenario, the pressure test itself will be the highest burst load.

The load case used in ILS have the same fluid in the annulus as the initial condition. Hence, the only variable input is the test pressure, which in turn will determine the internal pressure change from initial to final conditions. This pressure change will be constant with depth, as the fluid gradients are equal. The temperature change during a pressure test will be zero.

2.5.3 Casing Evacuation

Casing evacuation might occur in gas-lift wells when the well loses its injection pressure. As the injection pressure drops to zero, the annulus will be filled with gas down to the deepest gas-lift valve. Full evacuation might also happen if there is a leak in the packer, which can result in a complete loss of the packer fluid. During the casing evacuation, the inside of the production casing is emptied out due to buoyancy forces and the completion fluid is replaced with gas (Bellarby, 2009).

Casing evacuation will cause an increased collapse load due to the lighter fluid in the A annulus, which results in a larger differential pressure across the casing. Hence, the pressure change from initial to final conditions will depend on depth, and be greatest at the bottom of the gas column. The temperature change during casing evacuation will be zero.

2.5.4 Production/Injection

During production and injection operations thermal loads must be considered. Production fluid from the reservoir tend to warm up the surrounding wellbore as it is transported up the well. If the injection fluid is cold, it will cool down the casing. The resulting temperature change during these operations, might have an effect on the strength of both the casing and the cement in the annulus. The internal pressure change from initial to final conditions will not be constant with depth, since it is assumed that the mud column from initial conditions is replaced with completion fluid during production or injection operations.

2.6 Safety Factor, Design factor and Utilization factor

The SF is defined as the component strength divided by the design load. This is shown in Eq. (2.24)

$$SF = \frac{\text{Actual component strength}}{\text{Design load}} \tag{2.24}$$

In a design approach, it is necessary to ensure that the SF is higher than the design factor (DF). DF is a set value, larger than or equal to 1. It is essential in order to determine the maximum allowable load that the well can be exposed to. The set DF can vary from company to company or from well to well.

In a modeling perspective, a utilization factor (UF) can be used. UF has the same objective as the DF, but from the modeling perspective. If Eq.(2.25) is applicable, it is guaranteed that no cement failure will occur. The UF is determined by the modeling uncertainty and is less than 1. A low UF imply large modeling uncertainty (De Andrade, 2015).

$$\frac{load}{capacity} \leq UF \tag{2.25}$$

For the failure modes applicable for the cement the SF are defined as showed in Eq. (2.26)-(2.28)

Shear Failure

$$SF=\frac{\tau_{max}}{\tau_{oct}} \tag{2.26}$$

Debonding

$$SF=\frac{-T_0}{\sigma_r} \tag{2.27}$$

Radial Cracks

$$SF=\frac{-T_0}{\sigma_H} \tag{2.28}$$

Tensile failure can result in negative SFs. It can be shown from Eq. (2.27)-(2.28), that it is due to stresses in compression. A large negative SF is not necessarily worse than a low negative SF. If a low negative SF results from high compressive stresses, it is further from tensile failure than when the stresses are only slightly compressive.

3. Results

This chapter consists of three main parts. First, the resulting stresses from the cement sheath model through the cross-section of the well are presented. Second, the failure modes are presented with the conditions for failure, both in terms of pressure and temperature. Finally, the resulting SFs from the comparison between the cement sheath model and the ILS are shown.

The results are based on the inputs for the cement sheath model listed in Table 2, Table 3 and Table 4. These inputs will from now on be referred to as the base case. All temperatures, pressures and resulting stresses are always in terms of change from initial condition.

It is important to mention that the cement sheath model contains uncertainties, and the results can be altered if the approach is expanded.

Table 2: Standard inputs in the cement sheath model. Well geometry

Well geometry	
R_a	0,1083945 m
R_b	0,1222375 m
R_c	0,155575 m
R_d	10 m

Table 3: Standard inputs in the cement sheath model. Casing, cement and formation properties

Properties	Casing	Cement	Formation
E	2,04E+11 Pa	1,00E+10 Pa	1,50E+10 Pa
ν	0,31	0,26	0,4
α	0,000013 1/°C	0,000016 1/°C	0,00001 1/°C
κ		1 W/m-K	2 W/m-K

Table 4: Standard inputs in the cement sheath model. Initial stress condition in the cement

Initial Condition in the Cement	
Shrinkage	In-situ stress=0

3.1 Resulting Stresses in the Cement

By using the base case inputs in the cement sheath model, the stresses at all radii have been calculated. The resulting stresses are shown in Figure 9 and Figure 10, for a positive and negative pressure change respectively. The cement is located between the black line at the casing-cement interface (r_b) and the gray line at the cement-formation interface (r_c). Positive pressure changes without temperature changes results in high compressive radial stresses, tensile hoop stresses and low tensile axial stresses in the cement. On the other hand, negative pressure changes without temperature changes results in high tensile radial stresses, compressive hoop stresses and low compressive axial stresses in the cement. From Figure 9 and Figure 10 it can be seen that the internal pressure is equal to the radial stress on the inside of the casing, in compliance with thick-walled cylinder theory.

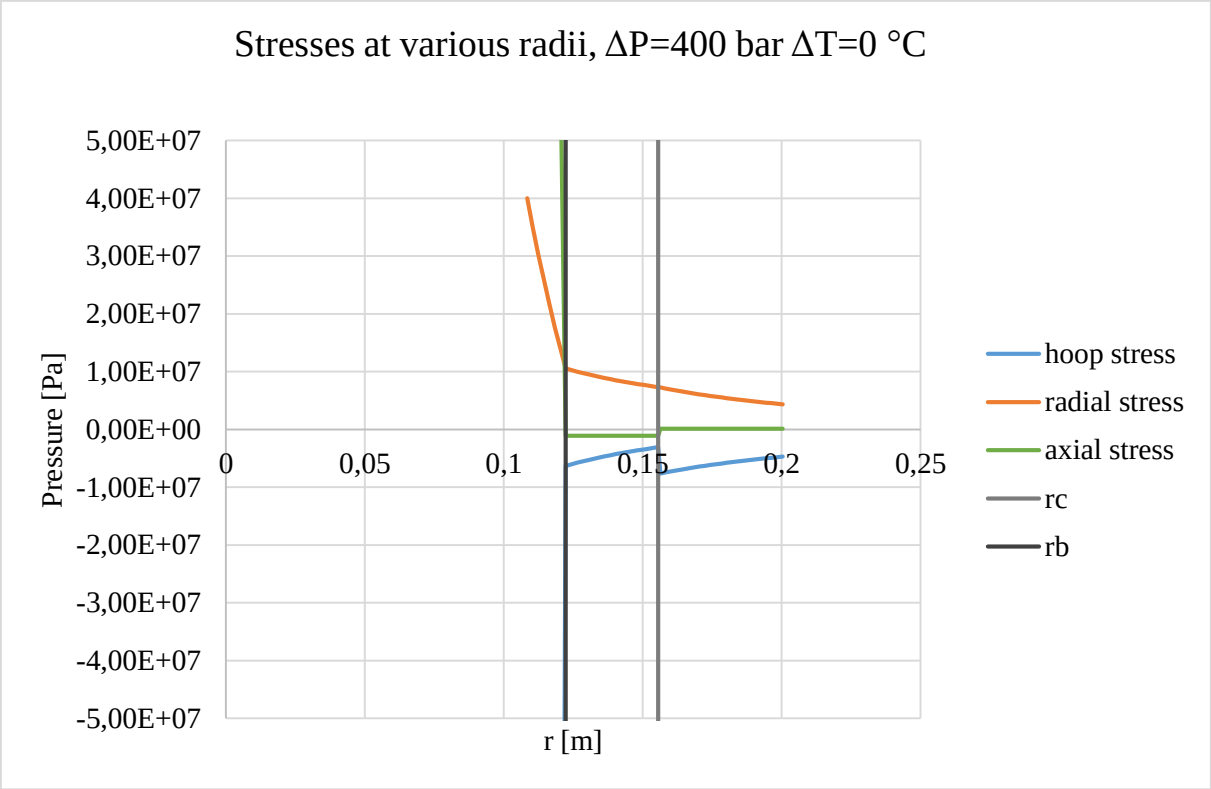

Figure 9: Hoop, radial and axial stress as a function of radius through a cross-section of the well. Positive pressure change of 400 bar, ΔT=0 °C.

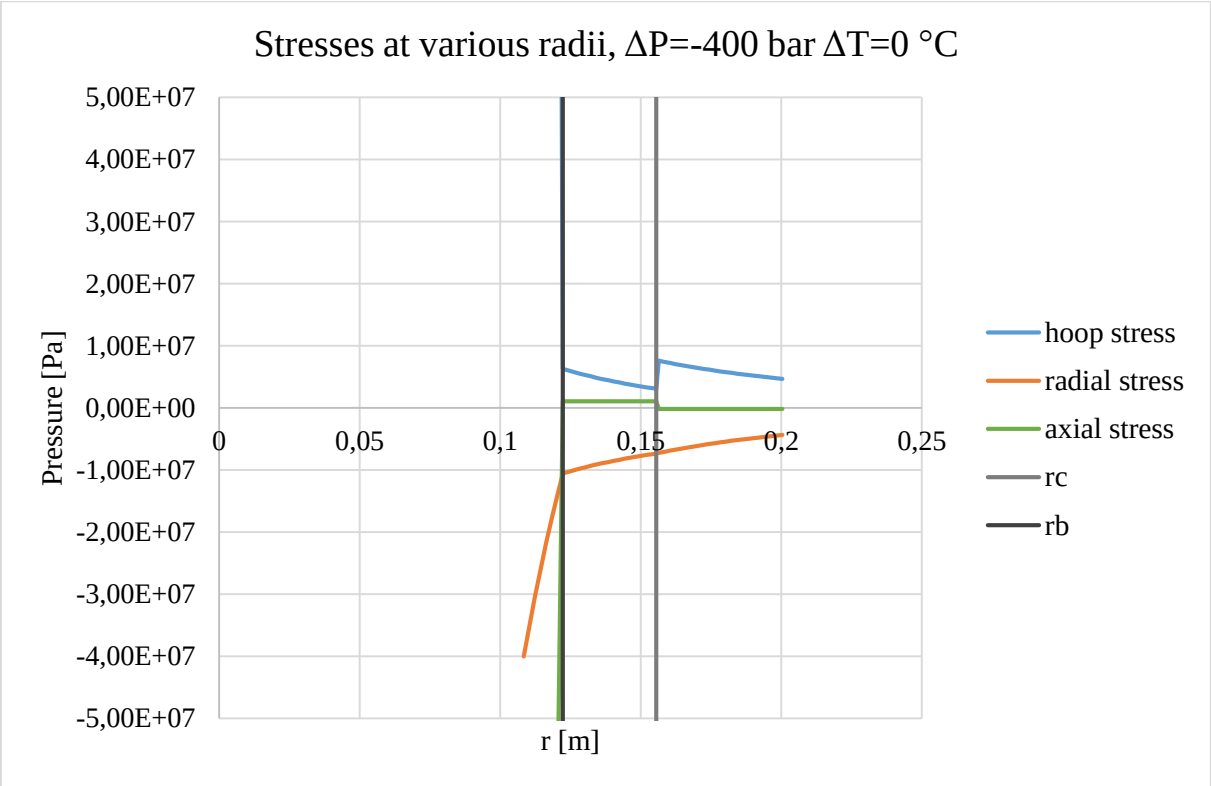

Figure 10: Hoop, radial and axial stresses as a function of radius through a cross-section of the well. Negative pressure change of 400 bar, ΔT=0 °C.

3.2 Typical Failure Conditions, Regarding Pressure and Temperature Variations

The failure conditions for the three failure modes: debonding, radial crack and shear failure, will be presented in this section. The results are carried out in terms of SFs, where the SFs are plotted as a function of pressure, with three graphs representing different temperature changes (in °C).

3.2.1 Debonding

In this model, debonding will mainly occur at negative pressure changes. Therefore, the results from debonding will not be presented for positive pressure changes. It is worth mentioning that debonding only can occur at the casing-cement interface (r_b) and the cement-formation interface (r_c). It is therefore important to analyze the stresses at these locations. Figure 11 and Figure 12 show the SFs for debonding at r_b and r_c, respectively.

As seen in Figure 11 and Figure 12, the general tendency of debonding is that a large pressure drop will cause failure. A pressure drop accompanied by a temperature drop will increase the risk of debonding. This is true at both the casing-cement interface and the cement-formation interface.

However, debonding is more likely to occur at r_b than at r_c, due to the lower SFs at this point. This is because r_b is located closer to the well, where the cement may be more affected by the pressure change in the well.

The effect of temperature is larger at r_c than at r_b. This can be seen in Figure 12 as a wider spread between the graphs for different temperature changes. This may be due to the reduced influence of pressure at this point.

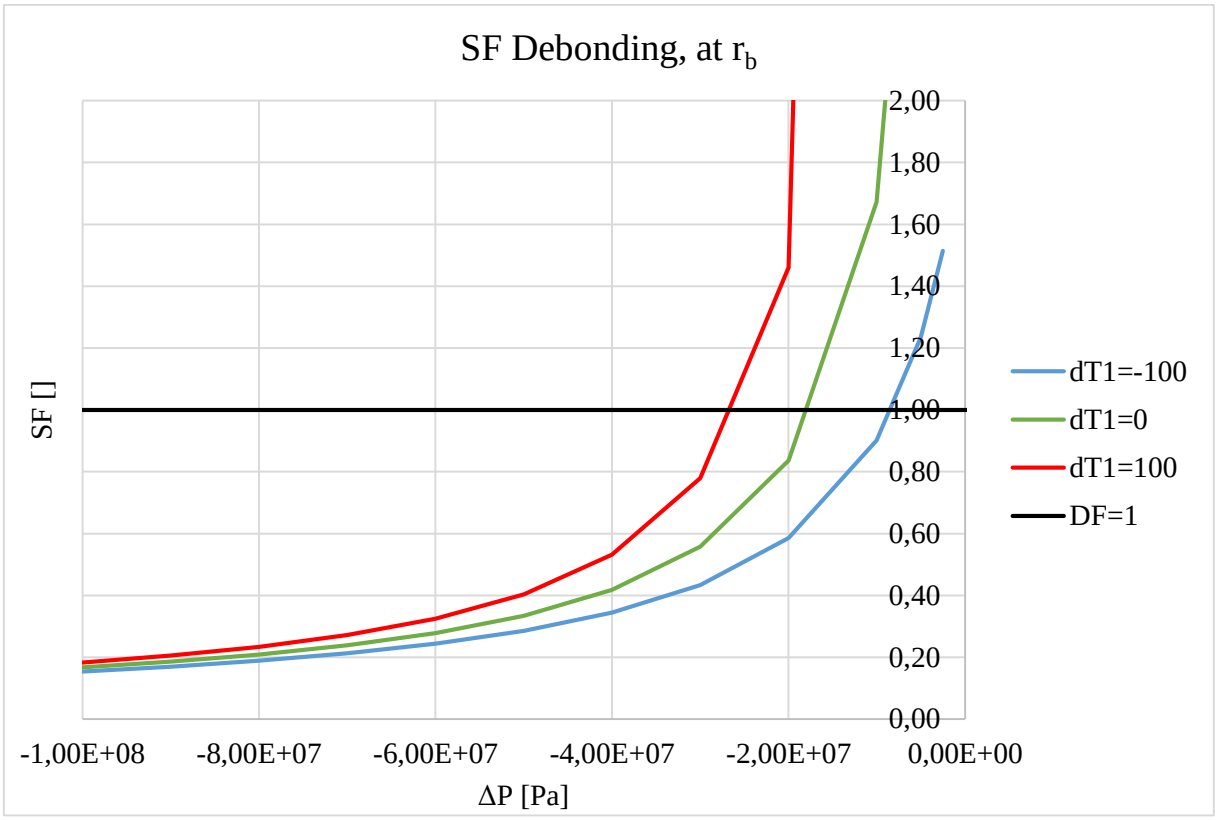

Figure 11: SF debonding as a function of pressure changes for various temperature changes, at r_b.

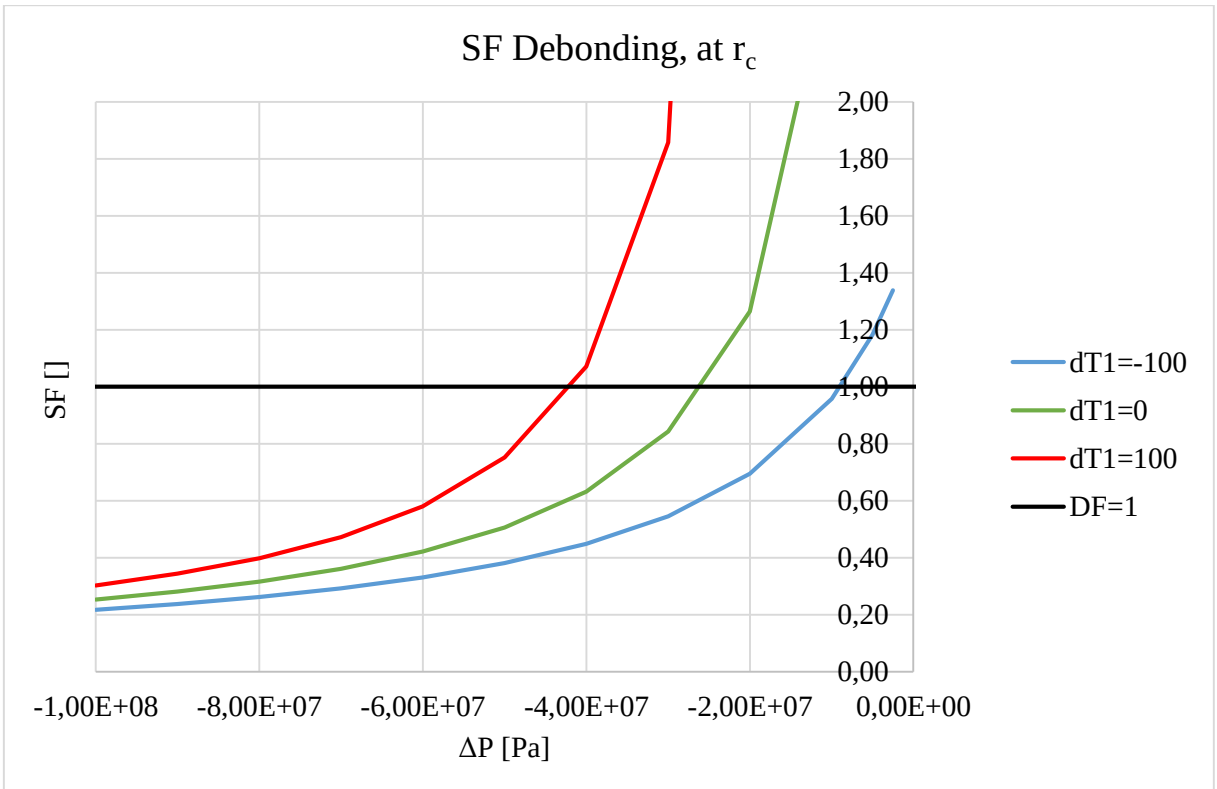

Figure 12: SF debonding as a function of pressure changes for various temperature changes, at r_c.

3.2.2 Radial Crack

Radial cracks will mostly occur at positive pressure changes. Therefore, the general results from radial cracks will not be presented for negative pressure changes. Figure 13 and Figure 14 show the SFs for radial cracks at the casing-cement interface (r_b) and the cement-formation interface (r_c), respectively.

Radial cracks tend to form when the wellbore experiences a large pressure increase. Figure 13 and Figure 14 show that if the temperature drops, radial cracks can form at r_b and r_c at lower pressure increases.

When a positive internal pressure change occur, the results indicate that radial cracks will first begin to form at the casing-cement interface. Hence, the effect of positive internal pressure changes has the largest consequences for radial cracks when the investigated radius is close to the wellbore. Once a radial crack initiates, the crack will propagate radially outwards until the entire cement sheath fails in radial cracks. One can therefore assume, that when a radial crack initiates at r_b, radial cracks will be present in the entire cement sheet.

A large pressure increase results in the lowest SFs for radial cracks. However, these SFs are higher than the SFs for debonding at equivalent negative pressure. Hence, the initiation of debonding is easier than the initiation of radial cracks. However, this is dependent on the load case the well is exposed to.

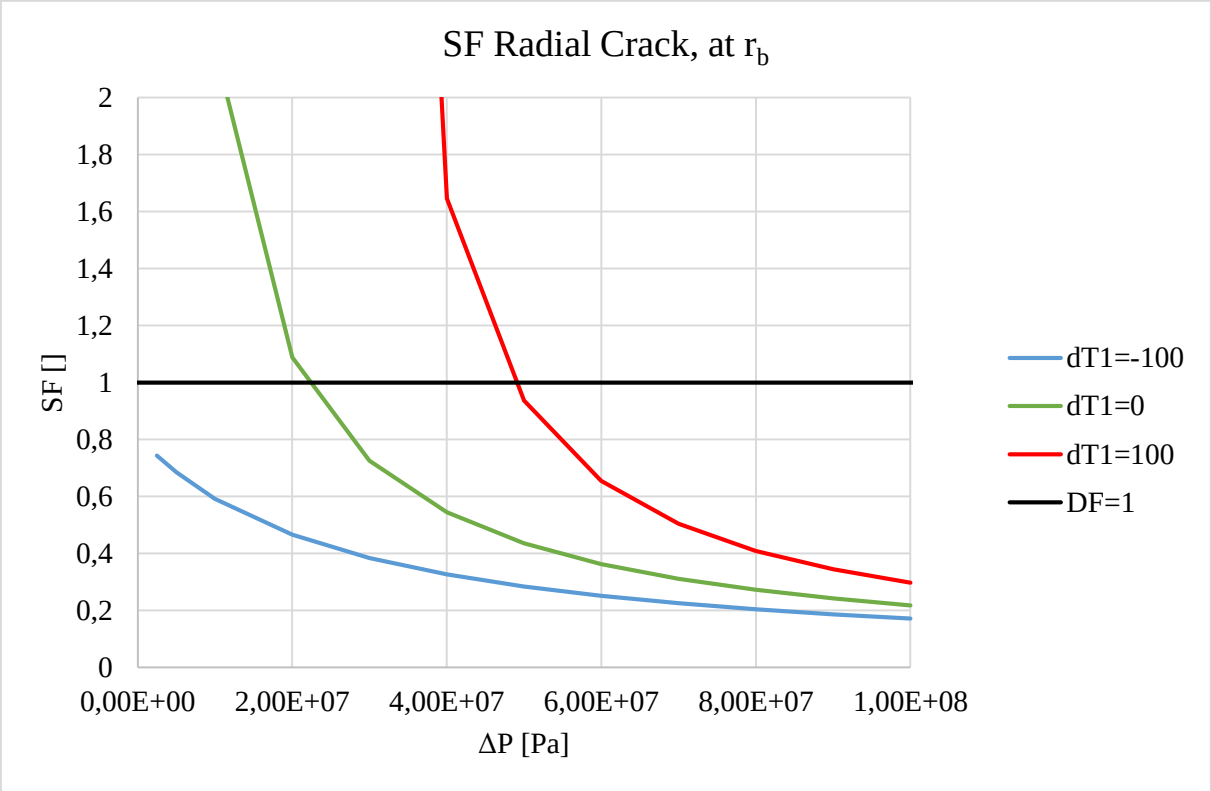

Figure 13: SF radial crack as a function of pressure changes for various temperature changes, at r_b.

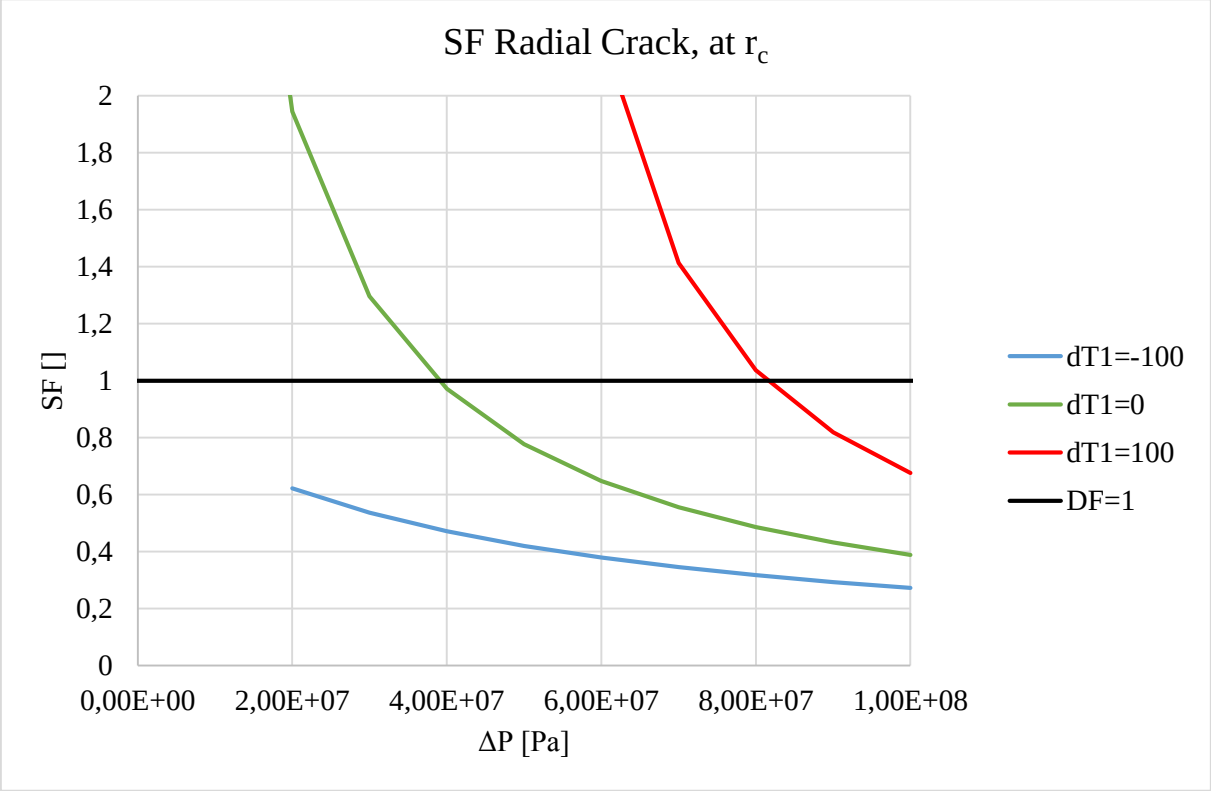

Figure 14: SF radial crack as a function of pressure changes for various temperature changes, at r_c.

When the well experiences a large negative temperature change, radial cracks can also be initiated at low negative pressure changes, as shown for r_b in Figure 15. Two graphs with large temperature drops are plotted for small pressure changes. There is a portion of the blue graph (i.e. dT1=-100) that falls below the black line (DF) on the left side of the y-axis. At these conditions, the casing cement is at risk of radial crack.

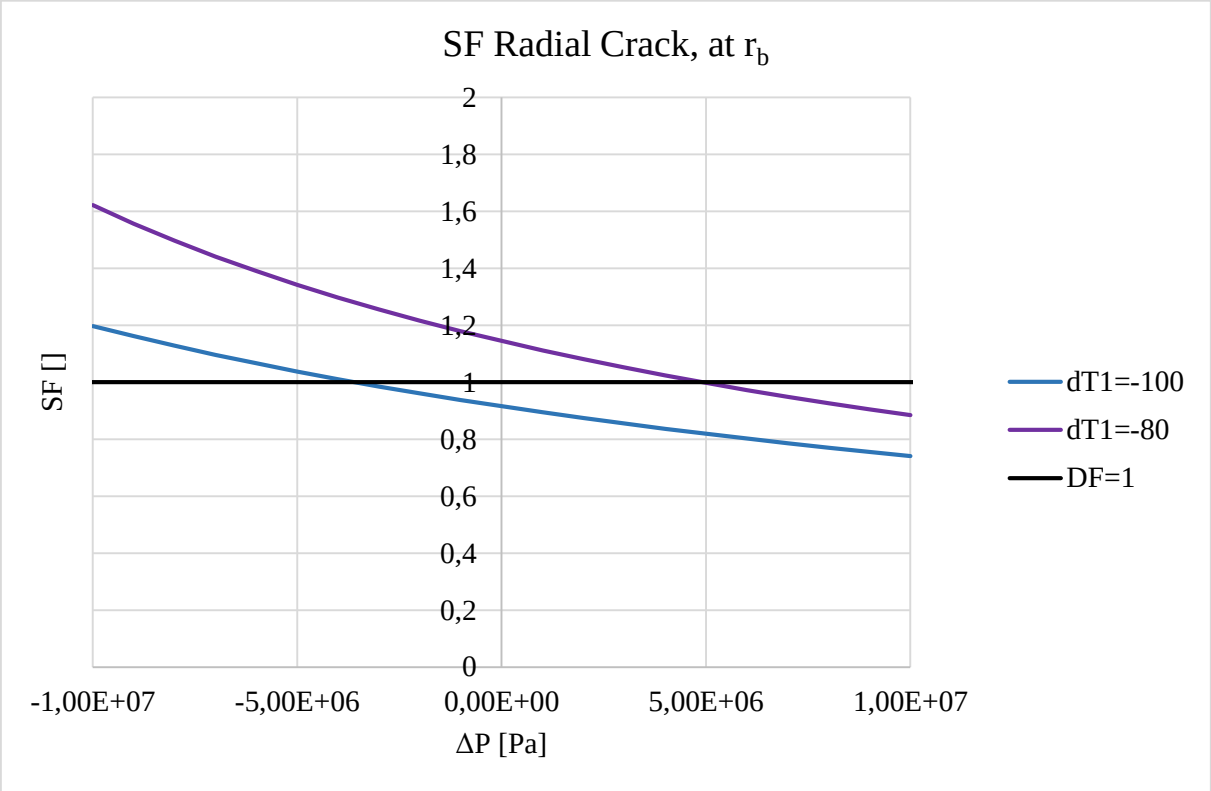

Figure 15: SF radial crack as a function of low pressure changes, various temperature change, at r_b

3.2.3 Shear Failure

Shear failures can occur at both pressure increases and decreases. Therefore, the results from shear failure will be presented for both positive and negative pressure changes. Figure 16 and Figure 17 show the SFs for shear failure plotted at r_b and r_c, respectively.

Table 5 shows the required Δp to cause shear failure at r_b and r_c. These pressure changes are only valid for the given temperature changes and the base case inputs. For the temperatures given in Table 5, it can be seen that a pressure increase is less critical to initiate failure than a pressure decrease. Additionally, failure will initiate easier if a temperature drop occurs. This is illustrated in Figure 16 and Figure 17.

It is also interesting to point out that when the well experiences a pressure drop, the required pressure change to initiate failure through the whole cross-section, is not much higher than the required pressure to initiate failure only at the casing-cement interface. For positive pressures, this difference is higher.

Table 5: Required pressure change for shear failure for specific temperature changes, at r_b and r_c

Required pressure change for shear failure for specific temperature changes, at r_b and r_c		
Temperature change	r_b	r_c
100 °C	-640 bar	-1040 bar
	843 bar	1349 bar
0°C	-623 bar	-962 bar
	713 bar	1194 bar
-100°C	-571 bar	-829 bar
	548 bar	985 bar

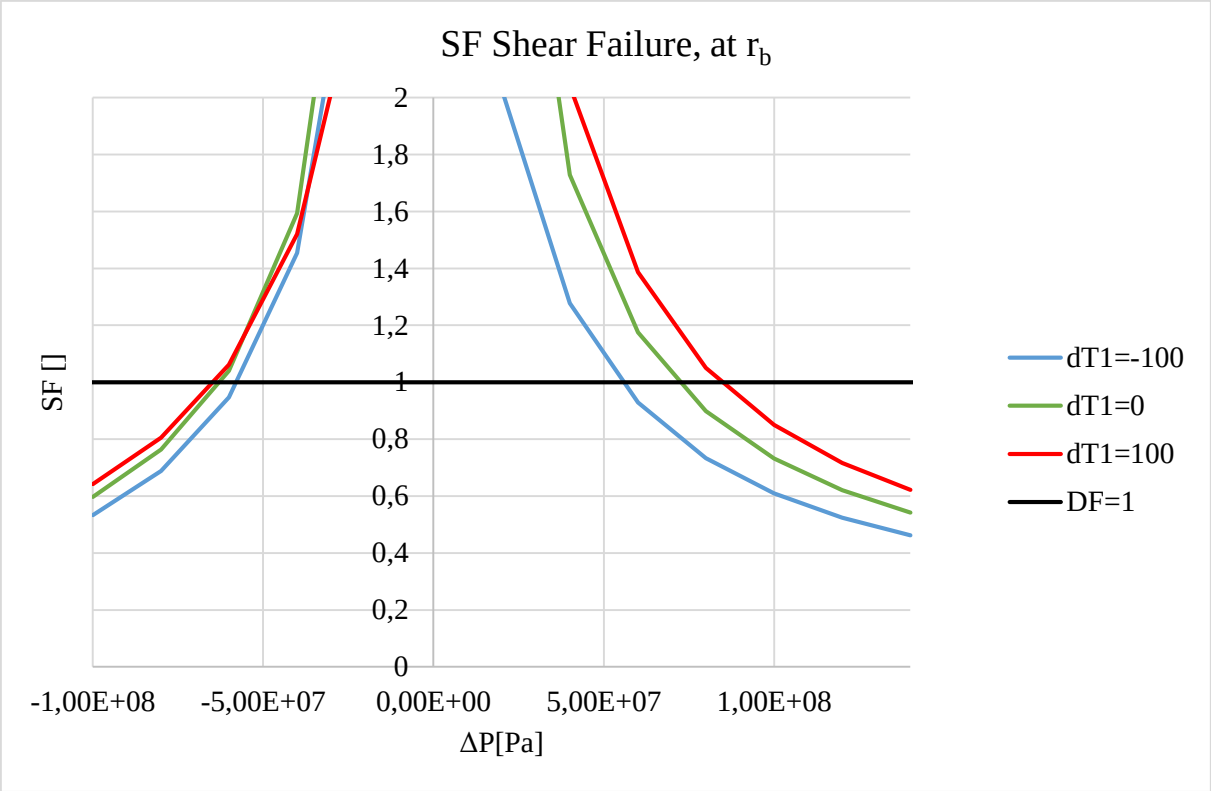

Figure 16: SF shear failure as a function of pressure changes for various temperature changes, at r_b

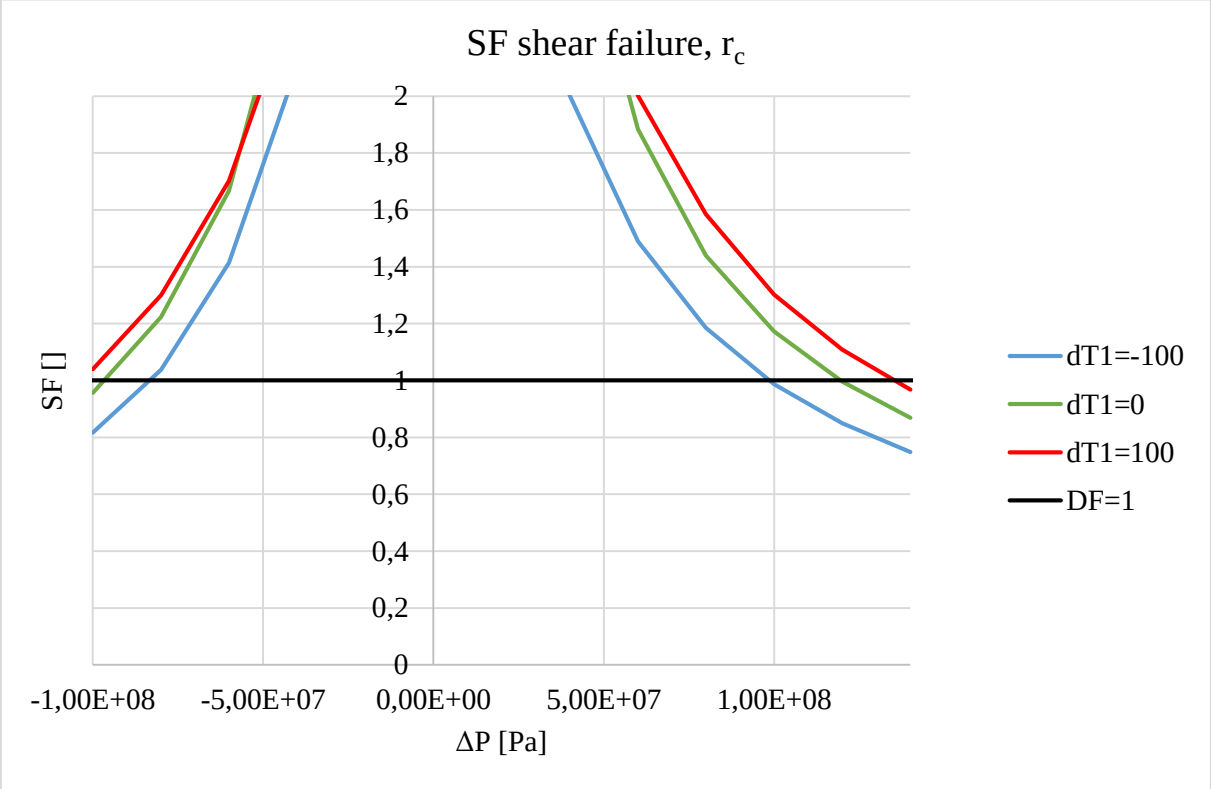

Figure 17: SF shear failure as a function of pressure changes for various temperature changes, at r_c

3.3 Determining when the Cement Fails before the Casing Fails for Various Production Load Cases and if Complementing ILS is Necessary

The motivation have been is to see if the ILS considers failure of the cement, to investigate the necessity of including a cement model in standard practice and to complement the ILS if required. In order to investigate the necessity of including a cement sheath model, the casing SFs from ILS will therefore be plotted together with the cement SFs. This is done for various production load cases. By determining whether it is the casing or the cement that fail first, the necessity can be obtained. This is from now on referred to as a comparison.

All casing SFs are based on a vertical well, with a 9 5/8-in production casing shoe at 3000 m, which is cemented from 2500-3000m. The Casing DF for burst in ILS is set equal to 1.1. The cement properties correspond to the base case values found in Table 2, Table 3 and Table 4. The casing types are mostly selected arbitrary for illustration purposes. However, one of the most commonly used casing grades on the Norwegian continental shelf, #53.5 P-110, is always included.

Normally, UF should be used to ensure that the well has a safe design and that the cement will not be exposed to failure, even if the cement model have some uncertainties. If UF is set to 0.8, uncertainties are accounted for in order to make sure that there is no failure when the model reports no failure. 1/UF=1.25 is the equivalent in order to compare with SF to know when the design is safe. When comparing with ILS the DF for cement is set equal to 1. This is done to make sure that when the SFs for cement fall below this value, failure in the cement will be guaranteed. If there is failure in the cement, and ILS provides no failure in the casing, this might be a weakness in the program and complementing is necessary.

The black and dashed vertical line and the black vertical line in the figures represents the DF for cement and casing, respectively. When the SFs for shear failure, debonding or radial crack is less than the DF for cement, the cement will experience failure. When the SF for casing falls below the burst or collapse design factor, the casing will experience failure.

The production load cases investigated in this section are pressure test, casing evacuation, steady stage production, steady stage injection and tubing leak. The internal pressure gradient for the initial condition and the pressure test load will be the mud gradient, while the other load cases will have an internal gradient from the completion fluid.

The results from the cement sheath model is calculated with no external pressure change. The external pressure profiles from ILS is therefore set equal to the initial condition. The external profile, for all load cases, will therefore consists of the mud gradient the production casing is run in, and the cement-mix-water gradient in the cemented zone. This is done for simplicity and to better match the conditions in the cement sheath model. The external pressure profile options available in ILS is described in Appendix F.

It is important to mention that all the load cases can differentiate from well to well. For example, a pressure test could be necessary to perform at a high pressure to account for a tubing leak occurring right below the wellhead if the main bore fluid is light and the reservoir pressure is high. However, if the reservoir pressure is low and the wellbore fluid is heavy, a tubing leak will be less hazardous to the production casing, and the pressure test can be performed at a lower pressure.

Later in this thesis, a sensitivity analysis regarding the load cases from this section will be performed for various cement properties.

3.3.1 Load Cases

Each load case will be presented in a separate plot. The SFs from the casing design is plotted together with the DF for burst or collapse, for the entire depth. The SFs and DF for cement is only plotted in the cemented section. Firstly, observations of the SF with the related DF for cement for all load cases are presented. Secondly, observations concerning the casing SFs are presented. Lastly, the results are compared and discussed.

When performing a pressure test, the ΔP inside the casing will depend on the applied pressure at surface. Since the fluid column in annulus is the same as the one initial, ΔP will be constant with depth. The resulting SFs in the cement from this load will therefore also be constant with depth, as seen in Figure 18 for the SF line for shear failure (green) and the SF line for radial crack (purple). This is not the case with the other load scenarios: casing evacuation, production, injection and tubing leak. For these loads, Figure 18-Figure 22 show that the SFs for cement failure are depth dependent. This is due to Δp changing with depth, as the internal fluid column differentiates from the one initial. In Figure 18, which illustrates the pressure test load, the SF line for shear failure (dashed green) is high, and safe from failure. The SF line for radial cracks (dashed purple) is however lower than the DF for the cement, which indicates that the cement will fail in radial cracks when exposed to the pressure test load. For

the casing evacuation load case in Figure 19, debonding in the cement will occur. For the production load in Figure 20, there is no failure in the cement, and the radial stresses is compressive. The SF line for debonding (pink) are close to failure when considering injection in Figure 21, though it will be on the safe side of the cement DF. No radial crack or shear failure will occur with the tubing leak load in Figure 22.

In Figure 18, the #43.5 N-80 casing (blue) will burst when exposed to the pressure test load. The #53.5 P-110 (yellow) will not experience burst. Figure 19 shows that the lower grade casing will fail in collapse in the casing evacuation load. In the rest of the load cases, the casing types investigated will withstand the applied load. The SFs for the tubing leak load with a wellhead pressure of 365 bar in Figure 22 is low, but for the selected casing grades, the casing design is safe.

One interesting thing to point out is that the cement will fail in radial cracks in Figure 18, even if the #53.5 P-110 casing holds. Figure 19 shows that the cement will have debonding failure regardless of if the casing holds. These scenarios may prove that the ILS have a shortcoming regarding the cement and safe zonal isolation.

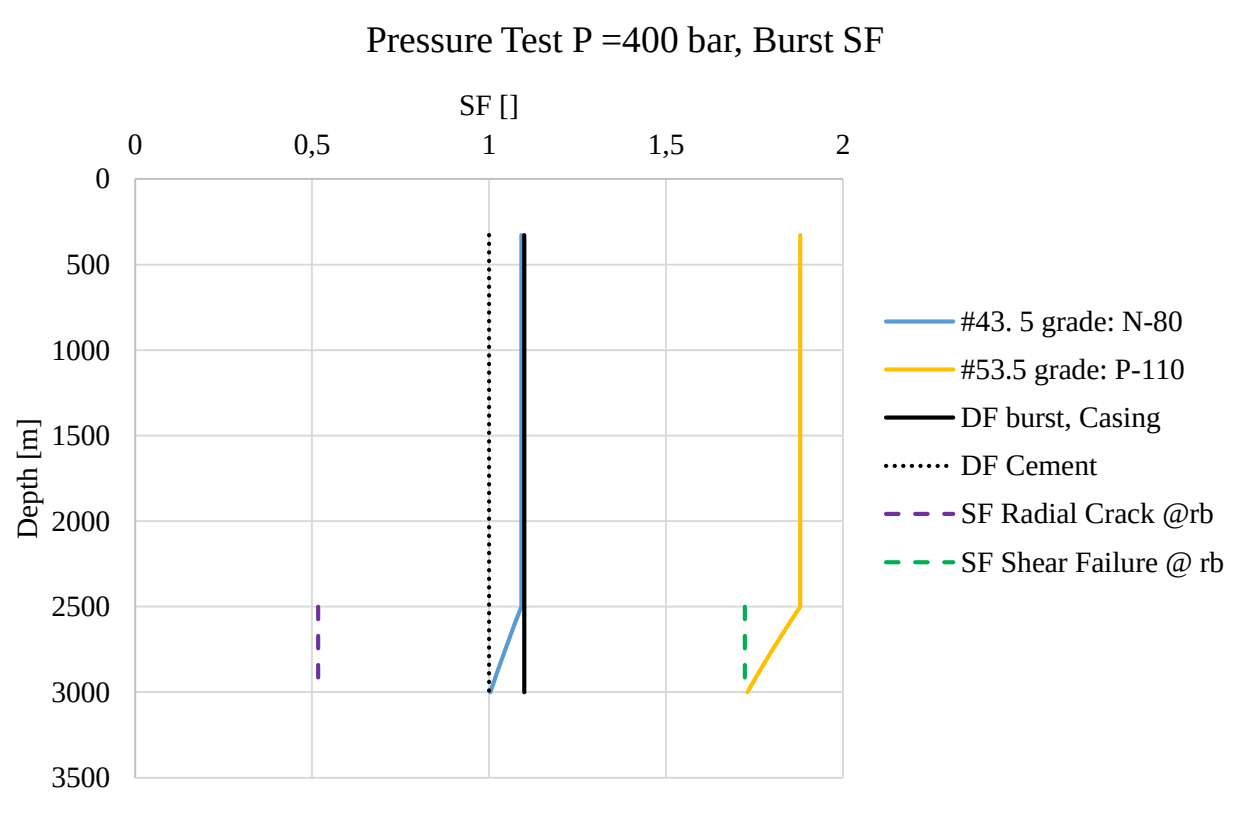

Figure 18: SF and DF for both cement (at r_b) and casing exposed to a pressure test with ΔP=400 bar from initial condition.

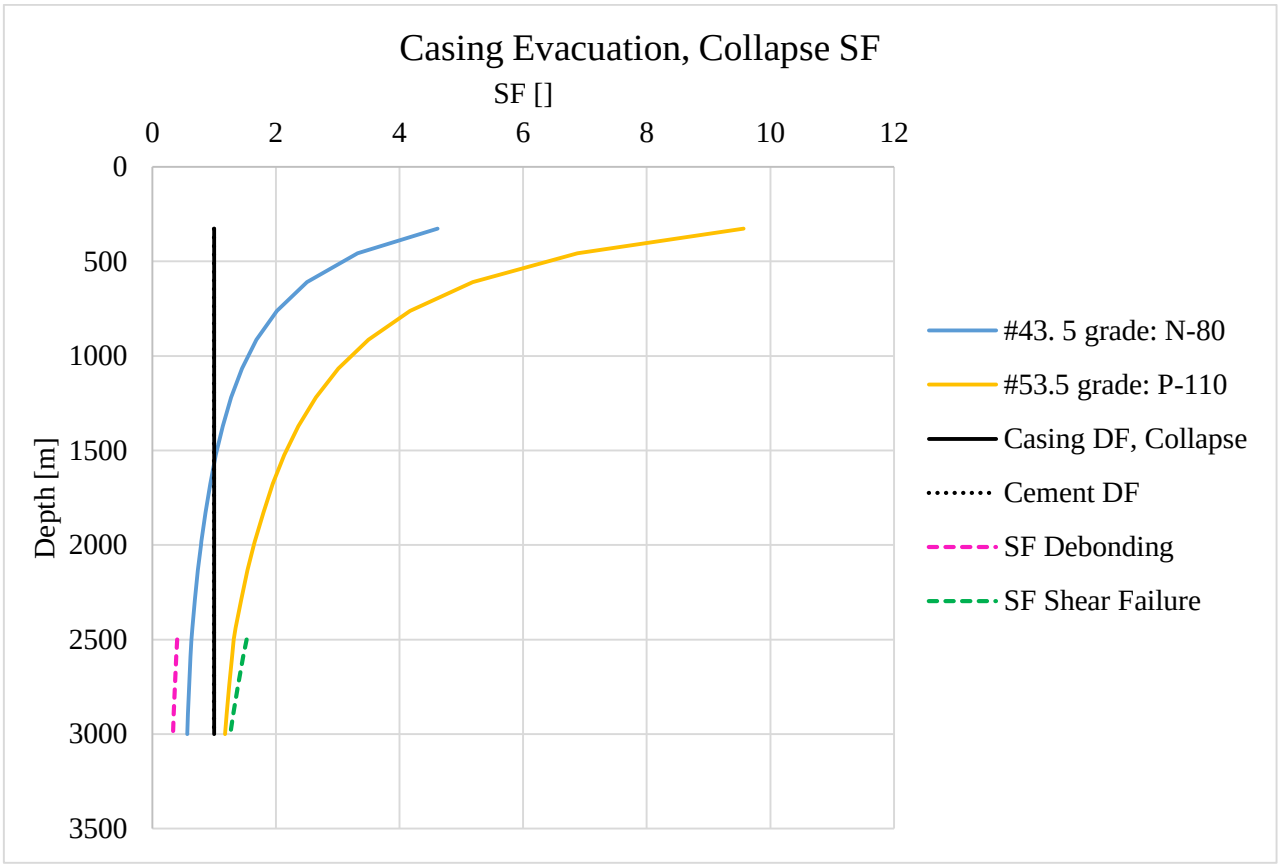

Figure 19: SF and DF for both cement (at r_b) and casing exposed to a casing evacuation

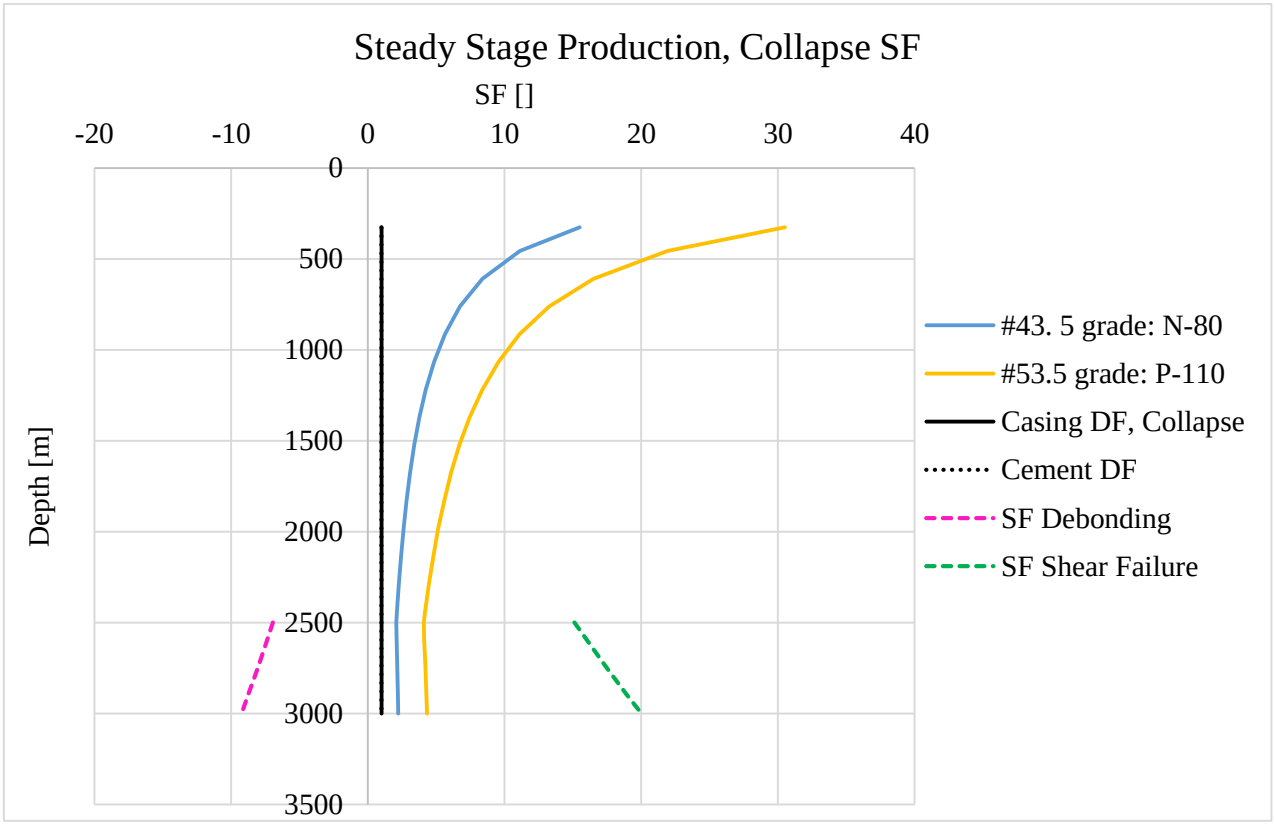

Figure 20: SF and DF for both cement (at r_b) and casing exposed to steady stage production.

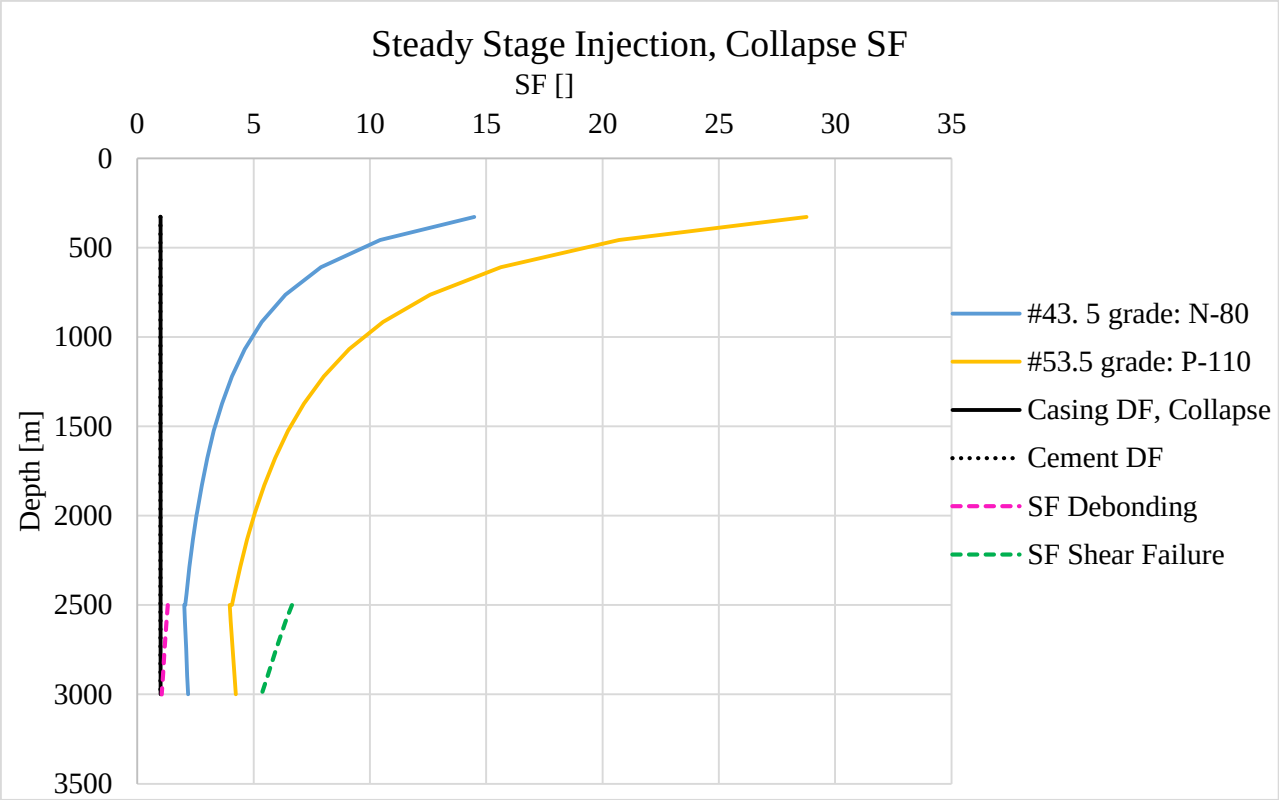

Figure 21: SF and DF for both cement (at r_b) and casing exposed to steady stage injection.

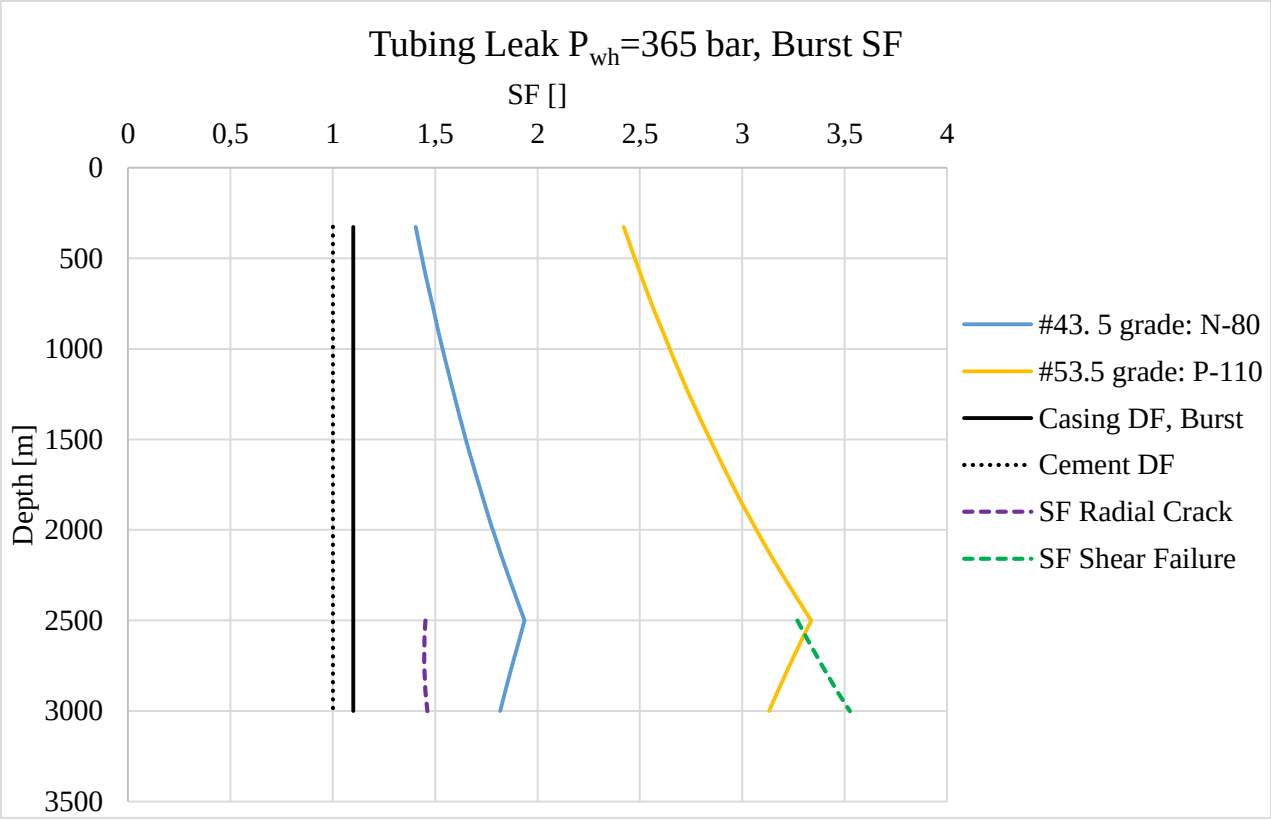

Figure 22: SF and DF for both cement (at r_b) and casing exposed to a tubing leak, with a wellhead pressure of 365 bar.

4. Discussion

This part will cover the sensitivity analyses performed on the mechanical properties of the cement and the formation. The results from the sensitivity analyses are later included in the comparison with the ILS, and used to determine whether an additional feature should be implemented in the ILS. Additionally, the discussion will cover some features in the cement sheath model, and the uncertainties resulting from not including these features in the comparison.

4.1 Sensitivity Analyses on Mechanical Properties

Sensitivity analyses are performed on several parameters in order to see how these parameters will affect the safety factors for the different failure modes. Only mechanical properties of the cement and the formation are investigated. The variables analyzed are the Young's modulus, the Poisson's ratio and the coefficient of linear thermal expansion. For all sensitivity analyses, the variables not investigated are according to base case.

All plots in this section will show the SF lines resulting from the various mechanical properties, with varying pressure at constant temperature. Appendix H will show the plots not included in this section, which contain the effect of changing the temperature, among other.

It is observed for all sensitivity analyses that if one parameter is investigated at a condition resulting in a very low SF, the effect of changing this parameter is reduced. For instance, if radial crack is investigated at very large pressures increases, a change in a mechanical parameter will not alter the safety factor for radial crack to a great extent. In contrast, if the pressure and temperature condition are favorable to avoid failure, the parameter investigated will affect the SFs for the relevant failure mode to a greater extent. This is seen in the plots when the lines have a large spread between them.

4.1.1 Young's Modulus

An investigation, of how sensitive the SFs for the different failure modes are to change in the Young's modulus of the cement and the formation, is performed. Eight cases with different combinations of Young's moduli have been investigated. The Young's moduli ranges are shown in Table 1. A discussion about the most favorable and unfavorable combination to prevent failure, and the general trend observed for the failure mode are presented. A discussion about the differences between considering the casing-cement interface (r_b) and the cement-formation interface (r_c) is also included.

It is important to mention that in order to obtain more accurate results, and hence achieve a more general conclusion; a more extensive analysis should be performed.

4.1.1.1 Debonding

Figure 23 shows the SFs for various combinations of cement and formation stiffness, E_{cem} and E_{form} respectively. From the values evaluated, the probability of debonding at the casing-cement and the cement-formation interfaces are highest when the Young's modulus of cement is low, and the Young's modulus of the formation is high ($E_{form} > E_{cem}$). This means that when the cement is placed next to a stiff formation, it is more prone to debonding. The combination that will result in the largest SFs is the largest cement Young's modulus, and the lowest formation Young's modulus ($E_{cem} > E_{form}$). The best-case combination when considering the ranges in Table 1 is then; E_{cem} = 20 GPa and E_{form} = 1 GPa. It has been found that as long as the cement Young's modulus is larger than the formation Young's modulus, the highest value of cement Young's modulus is the most desirable. In contrast, the lowest SFs would be expected with E_{cem} = 1 GPa and E_{form} = 70 GPa. However, this has been found not to be the worst-case. The lowest SF, obtained by only considering round numbers Young's moduli (in GPa), occurs when E_{cem}= 2 GPa and E_{form} = 70 GPa. There could be different reasons for this observation, however one reason could be that if the cement Young's modulus is 1 GPa, the cement is very elastic, and is not as exposed to failure.

As shown in the results, the likelihood of debonding increases at negative temperature changes, and this is true for all combinations of E_{cem} and E_{form} investigated. There are no major differences between the casing-cement interface and the cement-formation interface.

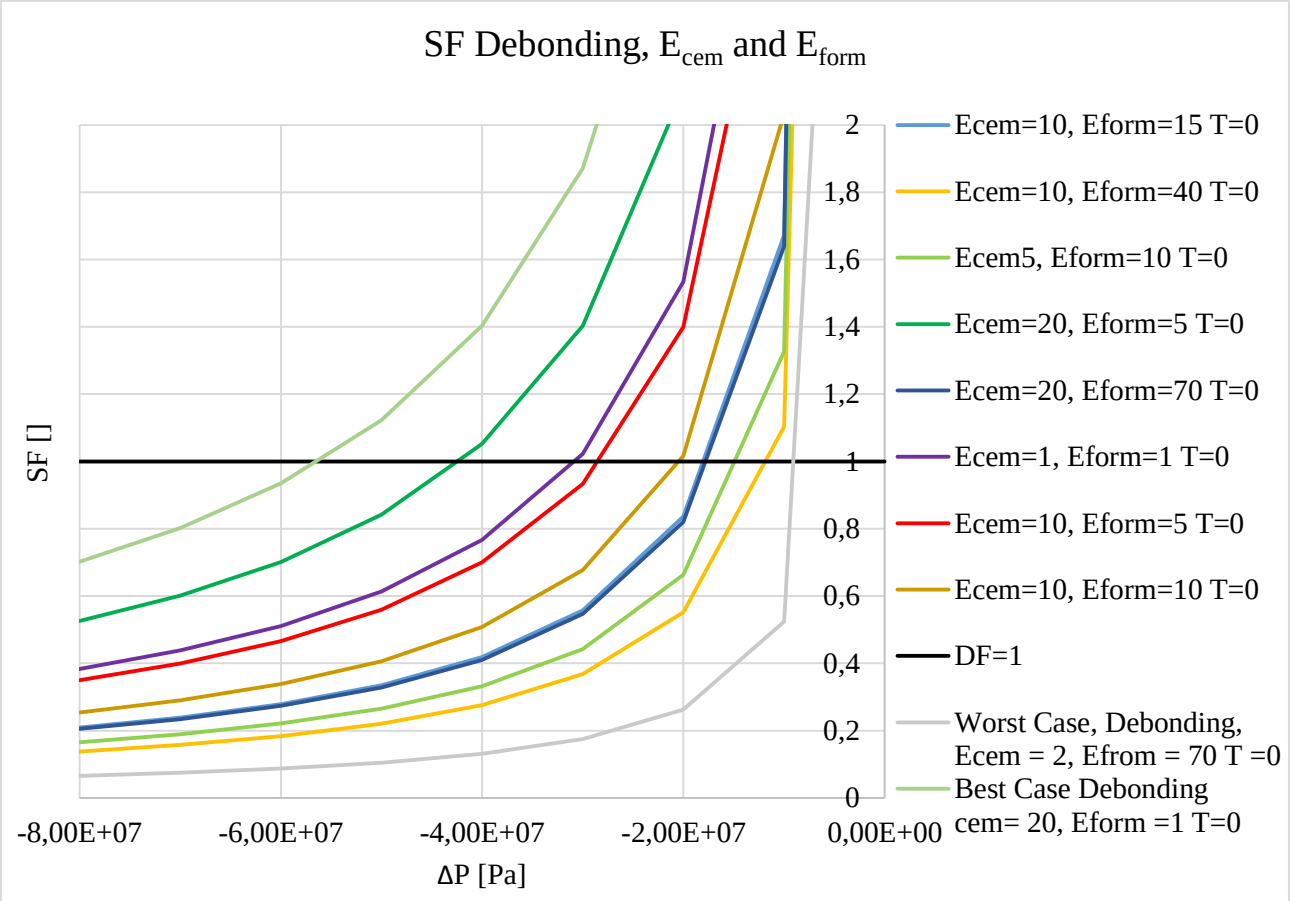

Figure 23: Effect of Young's modulus for the cement and formation in GPa, on SF for debonding, ΔT = 0, at r_b

4.1.1.2 Radial Crack

Figure 24 shows the SFs for various combinations of cement and formation stiffnesses, E_{cem} and E_{form}. The SFs are plotted at no temperature variation, and as a function of positive pressure changes, which is where radial crack is most likely to occur. Some trends are observed when considering positive pressures:

First, a large formation Young's modulus tends to result in large SFs. Additionally, in combination with a low cement Young's modulus, the largest SFs can be obtained. This results in the best-case scenario with values at the edges of the ranges shown in Table 1, that is E_{cem} = 1 GPa and E_{form} = 70 GPa. However, it seems like the formation Young's modulus is more dominating on the resulting radial crack SF, than the Young's modulus of cement.

From Figure 24 it can be seen, for zero temperature change at r_b, that the best-case described above result in the highest SFs for all pressures. This is also applicable for positive and negative temperature changes, and at both the casing-cement interface and the cement-

formation interface. However, a second observation is that the worst-case scenario is present if the formation Young's modulus is very small. According to the range presented in the theory, this means E_{form}= 1 GPa. Considering round numbers of Young's moduli, the worst-case scenario is present when the cement Young's modulus is 9 GPa. The reason for this may be that the tensile strength in the cement sheath model is only dependent on the cement Young's modulus. Hence, a very large cement Young's modulus will result in a large tensile strength. On the other side, a low cement Young's modulus can be favorable in order to avoid failure, because creating failures in a very elastic cement can be difficult.

Thirdly, when considering the difference on the two interfaces it can be observed that the order in which the failure occur, when considering the eight cases, is slightly different. However, the best- and worst-case combinations are the same at both interfaces.

A final observation when considering positive pressure changes is that for the most favorable combination of Young's moduli, the hoop stresses can be compressive, as illustrated by the green line in Figure 24. This occur when the formation Young's modulus is very large compared to the Young's modulus of the cement. In these conditions, a radial crack can occur at negative pressures.

For negative pressure changes, it has been observed for the base case, that a radial crack can only occur if a negative temperature change occurs at the same time. Additionally, this radial crack will only occur at small negative pressure changes. However, when the combinations of the Young's moduli are changed, this result also changes. It has been observed that with a large Young's modulus for the formation, radial crack can occur for a larger range of negative pressures. This range is also larger at r_c than r_b.

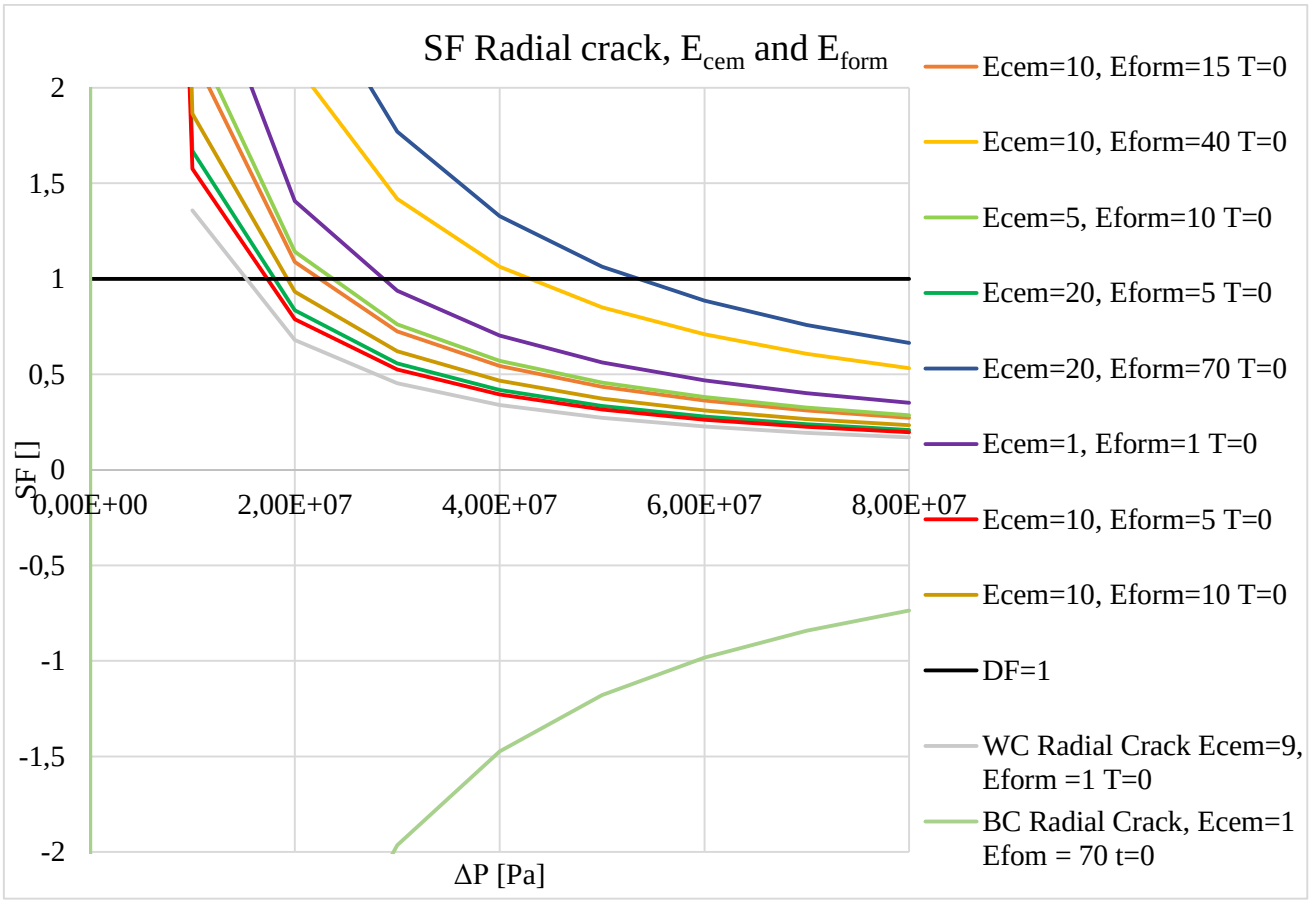

Figure 24: Effect of Young's modulus, for the cement and formation in GPa, on SF for radial crack, ΔT = 0, at r_b

4.1.1.3 Shear Failure

Figure 25 shows the SFs for various combinations of cement and formation stiffness, E_{cem} and E_{form} respectively. Since shear failure can occur for both pressure drops and increases, the SFs are plotted as a function of both positive and negative pressure changes. This is done for no temperature variation.

The best case for all temperatures and pressures is observed when the Young's moduli of the cement and the formation are 1 GPa. The worst-case for negative temperature changes and pressures increases at r_b, is when E_{cem} = 10 GPa and E_{form} = 5 GPa. All the other scenarios have E_{cem} =2 GPa and E_{form} =70 GPa as a worst-case. The general trend is that for negative pressure changes, a high formation Young's modulus will increase the probability of shear failure. Positive pressures do not have an as easily identifiable trend.

For a range of pressures where the lines are spread in Figure 25, the resulting SFs will be significantly influenced by the Young's moduli. However, where the lines are concurrent, the significance of the Young's moduli are less. There is a clear difference at r_b and r_c at zero temperature change regarding this, where r_c is more affected by the Young's moduli.

Temperature will have an effect on the order of failure at both r_b and r_c. The plots show similar trends, but the degree of concurrent lines varies. At r_b, the Young's moduli will be significant for the resulting SFs for negative pressures. At r_c, the Young's moduli will mainly be significant for the resulting SFs for negative pressures, except for positive temperatures where there is no clear trend.

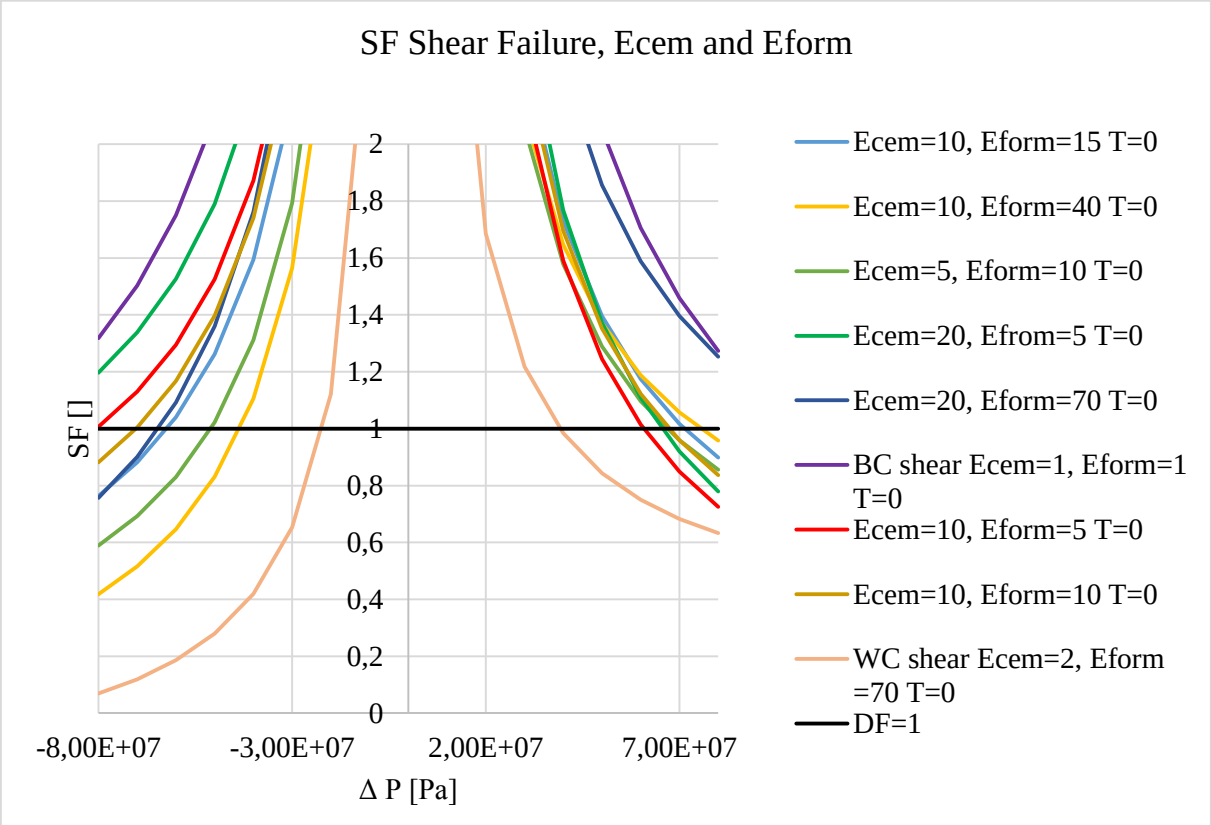

Figure 25: Effect of Young's modulus, for the cement and formation in GPa, on SF for shear failure, ΔT = 0, at r_b

4.1.2 Poisson's Ratio

Generally, the effect of changing the Poisson's ratio is less significant than changing the Young's modulus. However, some trends are observed:

First, when considering no temperature change, different Poisson's ratios will not have a large impact on the SFs for any of the failure modes. Secondly, what combinations of Poisson's ratio for the cement and the formation that is most desirable to obtain large safety factors, are opposite from positive to negative temperatures. This is valid for both radial crack and debonding. For example, in Figure 26 it is observed for debonding that the most favorable condition to prevent failure for positive temperature changes is a large Poisson's ratio for the cement, and a low for the formation. For negative temperature changes, the most favorable Poisson's ratios are a low value for the cement, and a high value for the formation. These observed trends are applicable at both r_b and r_c, for both radial crack and debonding. A third observation is that the combination of Poisson's ratio for cement and formation that is most desirable to prevent shear failure, is not consistent for negative and positive pressure changes, nor for positive and negative temperature changes.

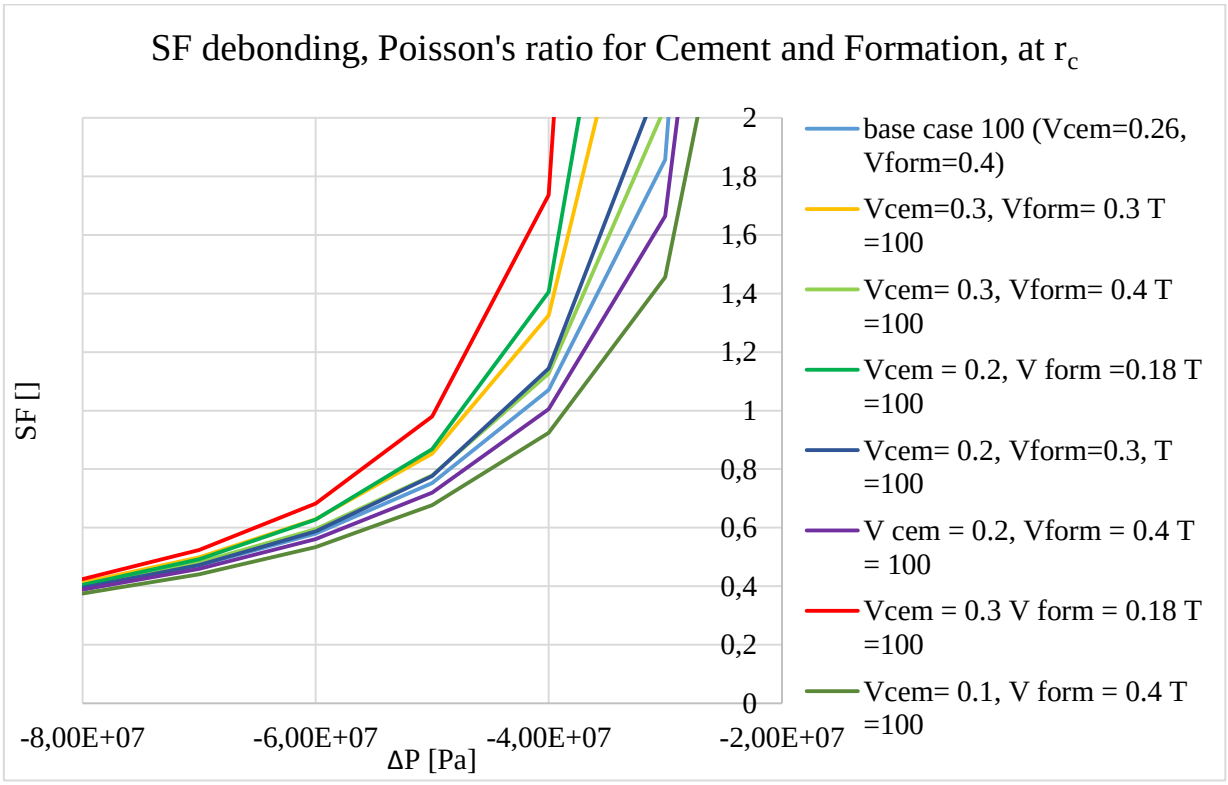

Figure 26: SF Debonding, varying Poisson's ratio for cement and formation. Positive temperature change of 100 °C, at r_c.

4.1.3 Coefficient of Linear Thermal Expansion

The effect of changing the coefficient of linear thermal expansion on resulting SFs for each failure mode has been investigated. By changing the coefficients for both the cement and the formation, and by plotting the SFs for various pressure and temperature changes, some distinct trends are observed. Firstly, when there is no temperature change in the well, the coefficient will as expected not have any impact on the resulting SFs. Hence, for the pressure test and evacuation load cases, all values of the coefficient (α) will give the same results. Secondly, debonding and radial crack seem to have the same trend when considering which combinations of the coefficient that result in the most favorable condition. For positive temperature changes, it is most desirable to have a large coefficient for the cement, and a low coefficient for the formation. Figure 27 illustrates this statement. It can be seen from the figure that the line, which has the highest SFs for all pressures, is the combination with the highest value for the cement and the lowest value for the formation. However, the opposite combination is favorable for negative temperature changes. Thirdly, an interesting trend is observed when considering the difference between r_b and r_c. The same combinations are desirable for each failure modes at both r_b and r_c, though the trends are more distinct when considering r_c. For example, it can be seen at r_c that a large thermal expansion coefficient for the cement together with a small coefficient for the formation is the most desirable. However, at r_b, only low values for the formation are seen as the best alternative, and with no distinct trend in the cement's value. This may be because when failure occurs at an interface, it is more sensitive to the properties at this interface. However, this does not explain why the coefficient of linear expansion for the formation is more dominant at r_b.

When discussing how shear failure is dependent on the coefficient of liner thermal expansion the trends are not as clear as for debonding and radial crack. However, it seems like opposite trends tend to appear when considering r_b and r_c. At r_b, a high value for the formation is undesirable, while at r_c a low value for the formation is undesirable. Generally, the most favorable combination is not consistent neither for negative or positive pressure changes, nor for positive or negative temperature changes.

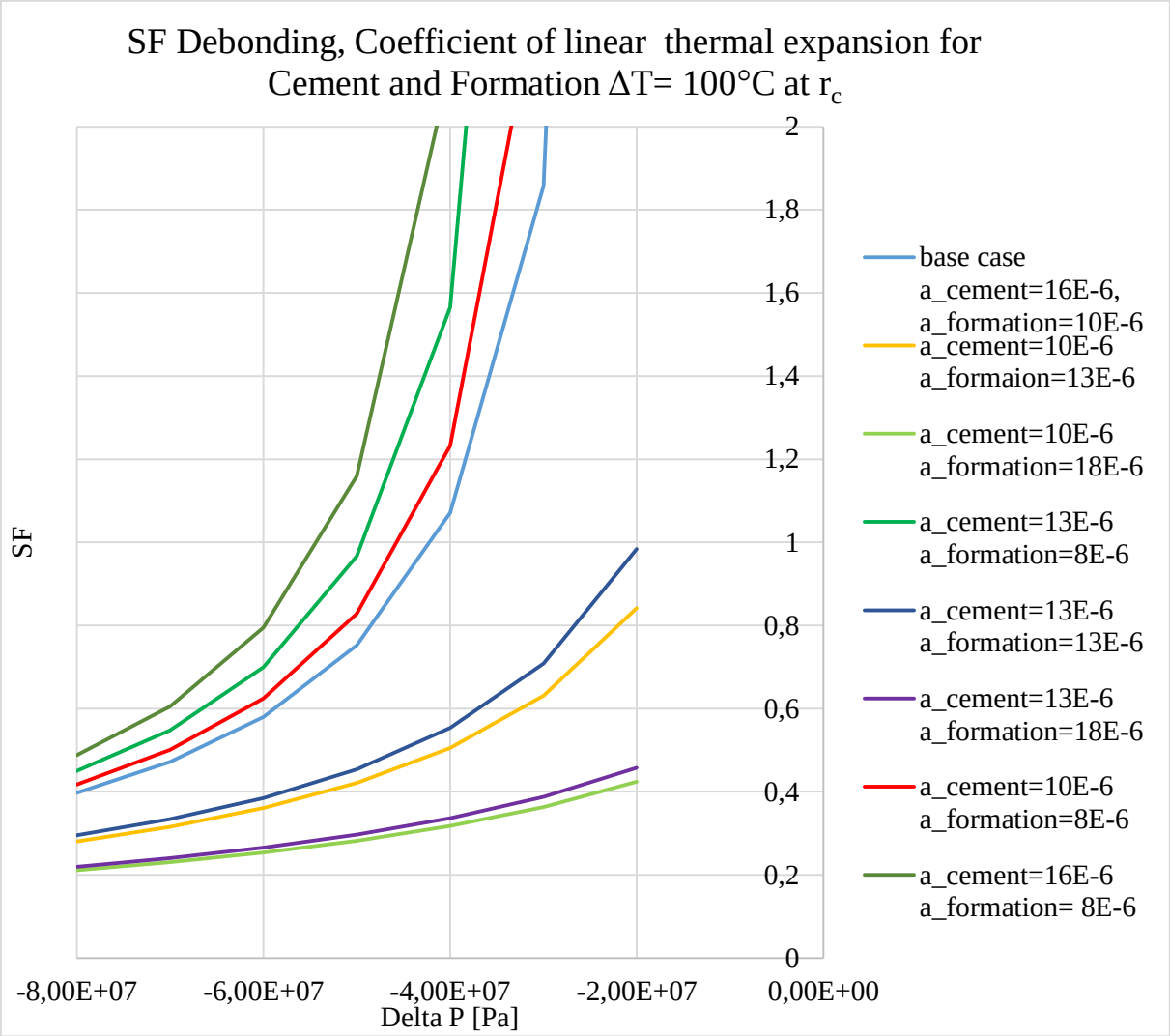

Figure 27 SF Debonding with varying coefficient of liner thermal expansion of cement and formation. Positive temperature change of 100 °C, at r_c

4.2 Complementing the ILS

4.2.1 Approach

In order to investigate the necessity of complementing the ILS, it is necessary to see if the cement fails in cases where the casing does not. In these cases, it would be desirable that the ILS could provide information to the user that the cement could be at risk of losing its integrity. In chapter 3.3 it has been shown that for the base case, radial cracks or debonding can occur, even if the casing is safe for the same load case. It is in these cases an improved user function could be added to the ILS. In order to expand these analyses, to be more general, various cement and formation properties have been added to the analyses. However, only the worst-case collapse and burst load cases, which are casing evacuation and pressure test, respectively, are discussed further. It is important to mention that these load cases vary for the different conditions the well are subjected to. However, it has been decided to expand the analyses from Chapter 3.3, by only changing the cement and formation properties, while the load cases remains the same. This is done by including the results from the sensitivity analyses, in terms of a worst- and a best-case scenario for each failure mode. By determining the combinations of Young's moduli and Poisson's ratios, for both the cement and the formation, that result in the most favorable and unfavorable conditions, the best- and the worst-case can be developed. The reason for not including the coefficient of linear thermal expansion is because the SFs does not vary when there is no temperature change. This is the case for pressure test and casing evacuation. Since r_b is more exposed to failure in the various load cases, it has been decided to only consider this interface.

When determining the combinations of Young's moduli for the cement and the formation that result in the largest and lowest SFs for each failure mode, the results from Chapter 4.1 are used. In this case, the theoretical values of Young's moduli are used; hence, worst- and best-case scenarios tend to appear from the outer edges of the ranges. Meaning that the combinations not always are realistic, but they are necessary in order to quality check the results from the base case. It is important to mention that in order to develop the selected combinations of Young's moduli for each case, only round values in GPa are considered.

Since the Young's moduli affect the resulting safety factors to a greater extent than the Poisson's ratios, the Young's moduli are determined fist. The trends observed in the sensitivity analysis for the Poisson's ratios, are not consistent when the Young's moduli are changed. That is why the combinations of Poisson's ratios that result in the worst- and the

best-case scenarios, are not the same as shown earlier. This is evident in the worst-case mechanical properties of radial crack. Here, the Poisson's ratios do not influence the results to any extent, and that is why the base case values are chosen.

4.2.2 Pressure Test

The cement and formation properties for best- and worst-case of the pressure test load are shown in Table 6. These properties are determined by investigating one failure mode at the time, for a pressure test performed at 400 bar.

Table 6: Best- and worst-case combinations for mechanical properties, pressure test

Failure mode	**Radial Crack**	**Shear Failure**
Best-Case	E_{cem} = 1 GPa E_{form} = 70 GPa V_{cem}= 0.3 V_{form}= 0.18	E_{cem} = 1 GPa E_{form} = 1 GPa V_{cem}= 0.3 V_{form}= 0.4
Worst-Case	E_{cem} = 9 GPa E_{form} = 1 GPa V_{cem}= independent (base case) V_{form}= independent (base case)	E_{cem} = 2 GPa E_{form} = 70 GPa V_{cem}= 0.3 V_{form}= 0.18

Figure 28 shows a SF plot for both casing and cement for a pressure test performed at 400 bar. In this plot the SF graph for the commonly used 9 5/8-in casing, #53.5 P-110, is shown together with the base-, best- and worst-case of the two applicable failure modes for a pressure test; radial crack and shear failure. From this figure, the following are observed.

First, when considering shear failure it was determined from the base case that a shear failure of the cement was not likely to happen during a pressure test. However, it can be seen from the figure that with the least desirable conditions, a shear failure can occur. This can be seen by the worst-case scenario SF line being located to the left of the cement DF line. However, this occurs at very unfortunate conditions, and may not be worth considering, due to unrealistic mechanical properties, and a small possibility for failure. It can be seen from the range in the figure, which is between the worst- and the best-case scenarios, that a larger

portion of the range is located to the right of the DF line, meaning that the design is safe for most of the cases.

Secondly, when considering radial crack it is not that easy to see the range. This is because for some combinations of the mechanical properties, the hoop stresses will be in compression resulting in negative SFs. This is a safe state when considering radial cracks. However, it can be seen that the distance from the worst-case SF line to the DF line is larger compared to the SF line for shear failure. This means that more combinations of Young's moduli will lead to radial crack than to shear failure.

It can therefore be concluded that for a pressure test, radial crack is the failure mode that is most important to consider. Radial cracks propagate radially from its initiation point, and can result in a loss of zonal isolation. Multiple radial cracks can result in a connected channel, which equalizes the pressure above and below the cement, and undesirable communication occur. The consequences of a zonal isolation loss are, as mentioned in the theory, in terms of both economics and safety.

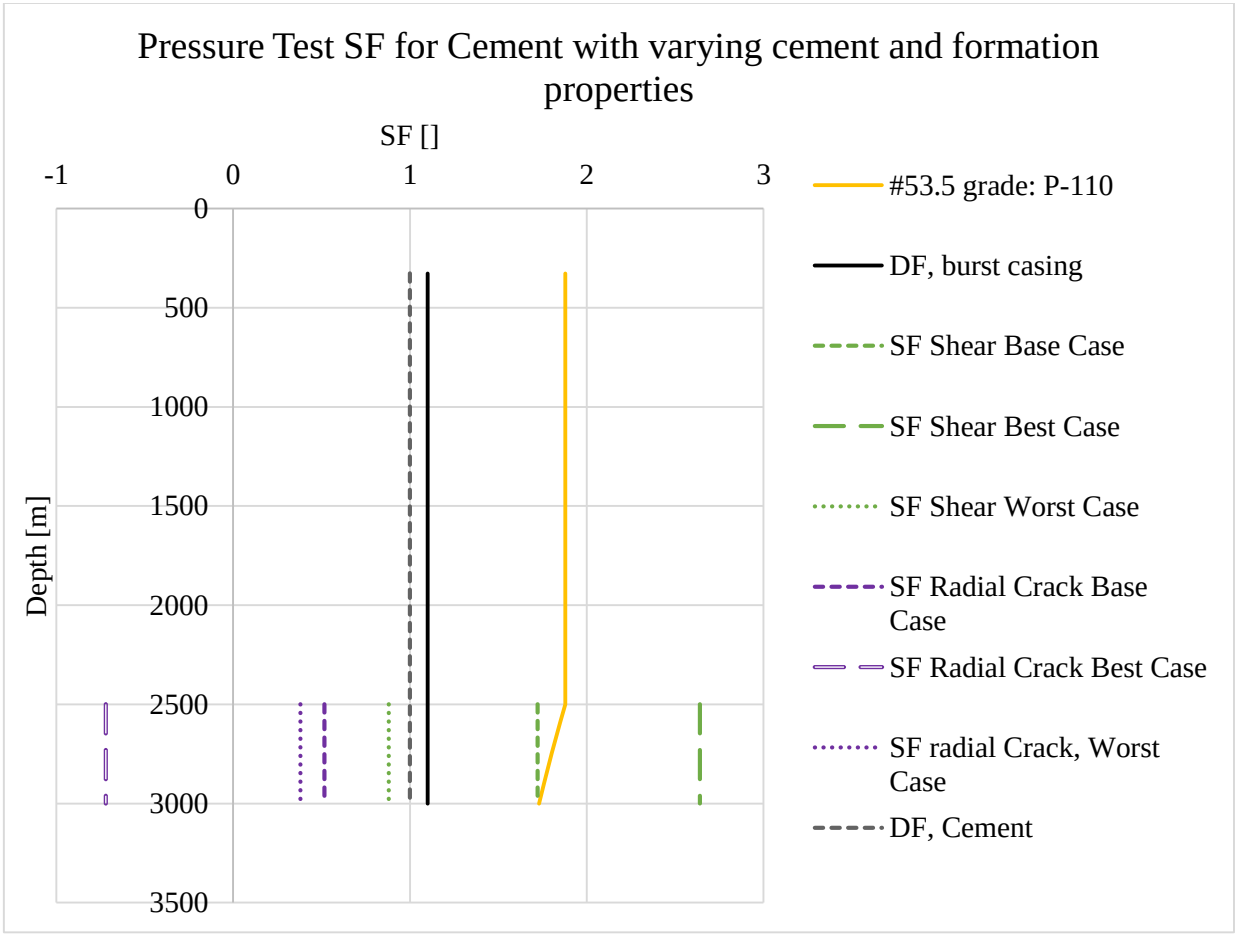

Figure 28: Pressure test SF for casing and cement with varying properties

4.2.3 Casing Evacuation

When considering the worst-case collapse load, casing evacuation, .

Table 7 shows the combinations of Young's moduli and Poisson's ratios of the cement and the formation, which results in the worst- and the best-case scenarios.

Even though the evacuation results in different negative pressure changes along the well depth, the worst- and best-case mechanical property combinations are the same.

Table 7: Best- and worst-case combinations for mechanical properties, casing evacuation

Casing Evacuation		
Failure mode	**Debonding**	**Shear Failure**
Best-Case	E_{cem} = 20 GPa E_{form} = 1 GPa V_{cem} = 0.1 V_{form} = 0.4	E_{cem} = 1 GPa E_{form} = 1 GPa V_{cem} = 0.3 V_{form} = 0.4
Worst-Case	E_{cem} = 2 GPa E_{form} = 70 GPa V_{cem} = 0.3 V_{form} = 0.18	E_{cem} = 2 GPa E_{form} = 70 GPa V_{cem} = 0.3 V_{form} = 0.18

Figure 29 shows the SF lines for a #53.5 P-110 casing and the cement failure modes, with their worst- and best-case scenarios.

First, when considering shear failure, the range where shear failure can occur, extend across the DF line. This means that various combinations of mechanical properties can result in both a safe and an unsafe design. Additionally, the SFs for the worst-case are lower than when comparing to the worst-case of pressure test. It is therefore more important to consider shear failure, when a negative pressure change occur.

Secondly, debonding is also more critical than what radial crack was in the pressure test. This can be seen when the best-case scenario is within the safe zone by a small margin. This

means, that for most of the cases, if an evacuation occurs, the cement will be in risk of debond from the casing. However, with favorable combinations of mechanical properties, the design can be safe.

If debonding occurs, and the cement is not bonded to the casing or the formation, a microannulus or a cavity at these interfaces are created. As for radial crack, this means that in order to develop communication through the cement, a continuous pathway is necessary. Normally this is not the case, however according to the governing documentation for the various companies; a certain length of good bonded cement is required. This is normally confirmed by a cement bond log, which has been claimed to be inadequate in certain situations. Hence, a thoroughly model, to accurately determine situations where debonding occur in order to avoid these situations, could be of great need in the industry.

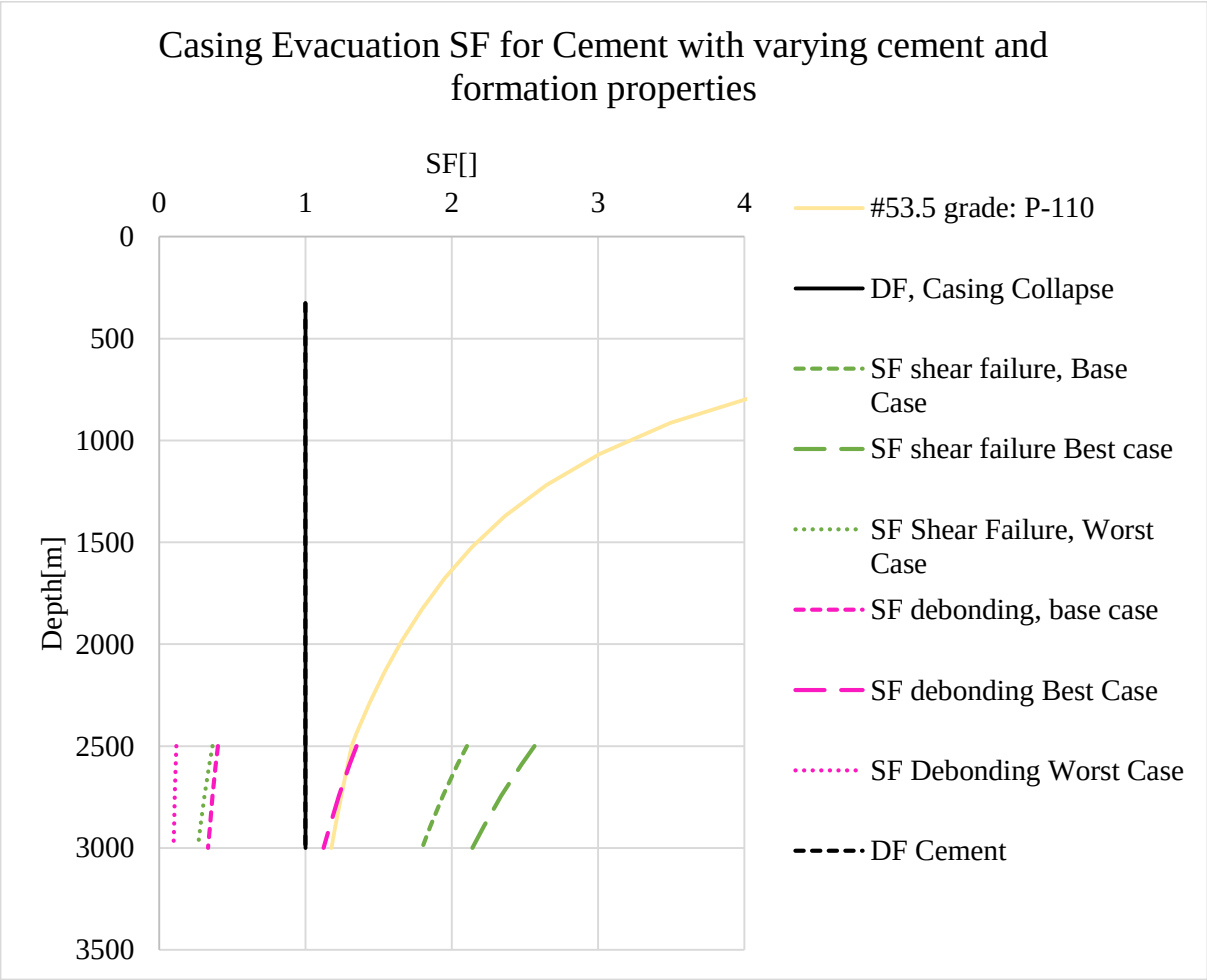

Figure 29: Casing evacuation SF for casing and cement with varying properties

4.2.4 Shortcoming with the Approach

Generally, it is important to mention that it could be an unrealistic approach to only consider one failure mode at the time. Meaning that if more failure modes are considered at the same time, the difference between the worst- and the best-case scenarios, are less, implying a narrower range. It could be called a conservative approach from the analysis perspective, since the range obtained is larger than what it would be if multiple failure modes were included. This is because the worst- and the best-case scenarios differentiate with the various failure modes. Additionally, it is conservative to only account for one load at the time when the well is exposed to both collapse and burst loads. A narrower range, between the best- and the worst-case would be developed if multiple loads where considered together. Then a more precise and realistic conclusion could be drawn.

4.3 Model Features and Uncertainties

In order to complement the ILS, some features, and how they affect the previous results will be discussed. These features include the effect of initial condition, the effect of change in formation pressure, the effect of changing the cement thickness and the effect of varying the outer boundary of the cement model. For all analyses of the features, the base case properties shown in Table 2, Table 3 and Table 4 are used as the main inputs. The most important plots are shown in the relevant section, while the remaining plots are shown in Appendix I.

4.3.1 Effect of Initial Condition

One feature of the model is to include the initial stress condition in the cement. Until now, shrinkage of the cement has been considered, meaning that the initial stress is zero. Zero net shrinkage, which means that hydrostatic stress is the initial stress in the cement, is another approach that can be used. The assumption behind the hydrostatic pressure can vary, but one approach is to set the minimum horizontal stress as the hydrostatic stress. Then the minimum horizontal stress is added to all the stresses before it is set into the failure criterion. Appendix B shows the pore pressure plot, where the used values of minimum horizontal stress can be found. In this case, the initial condition is analyzed at 2500 m, which is the top of cement (TOC). It is important to mention that if zero net shrinkage is included when considering the entire depth of the cement section, the load cases will have a larger depth dependency due to the minimum horizontal stress varying with depth.

In this chapter, a comparison between the two approaches is performed, finally leading to a discussion about the uncertainty resulting from the assumed initial condition. The effect of the initial condition has been investigated for the three failure modes. The results are plotted in terms of SF, with different pressure and temperature.

Figure 30, Figure 31 and Figure 32 show the effect of initial stress in the cement for radial crack, debonding and shear failure respectively. This is illustrated by plotting the SF for the failure mode as a function of radius through the cement. The figures show the results for constant temperature, but with varying pressures, which will be the case during a pressure test or an evacuation of the casing.

As seen in both Figure 30 and Figure 31 when considering zero net shrinkage, the SFs will be negative for all pressures. A negative SF means that the cement stress is in compression, and

neither radial crack nor debonding occurs. The pressure effect is canceled out by the effect of initial stress when no shrinkage occurs. When shrinkage occurs, the effect of pressure is larger than for zero net shrinkage. When considering constant pressure with varying temperatures, the result will be the same. For zero net shrinkage the temperature effect is also canceled out.

As seen from the figures, the effect of initial condition on radial crack and debonding differentiate from shear failure. Shear failure can occur with large pressure changes, even if initial stresses are present. However, initial stresses reduce the risk of shear failure. Figure 32 shows the effect of initial condition on shear failure SF with varying pressures. The plot consists of graphs for -300 bar, 300 bar, -600 bar and 600 bar for both shrinkage and zero net shrinkage. Zero net shrinkage results in the highest safety factors, and none less than one. Hence, if hydrostatic stress is the initial condition, no shear failure will occur, even if the well is subjected to a 600 bar pressure decrease. However, if the cement shrunk during setting, a 600 bar pressure decrease would result in SFs less than one, and hence a shear failure would be likely. It can also be seen from Figure 32 that the effect of the initial condition is larger when the pressure is low. This is evident from the distance between the lines; for 300 bar, the distance between shrinkage and no shrinkage is larger than for 600 bar.

These results prove that the choice of initial condition is important when analyzing and determining what happens with the cement when it is subjected to loads. Hence, the initial condition represents a major uncertainty, especially when tensile failures are considered.

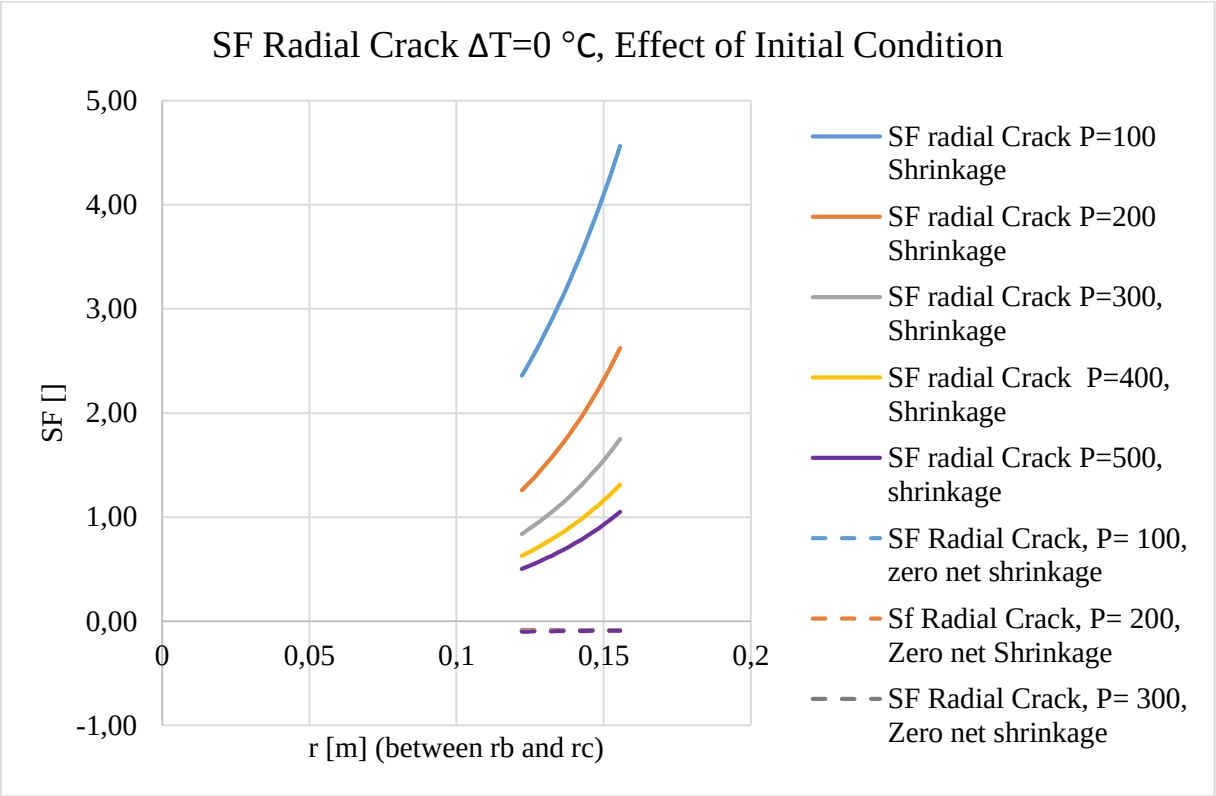

Figure 30: Effect of initial stress on radial crack SF, for different pressure changes in bar

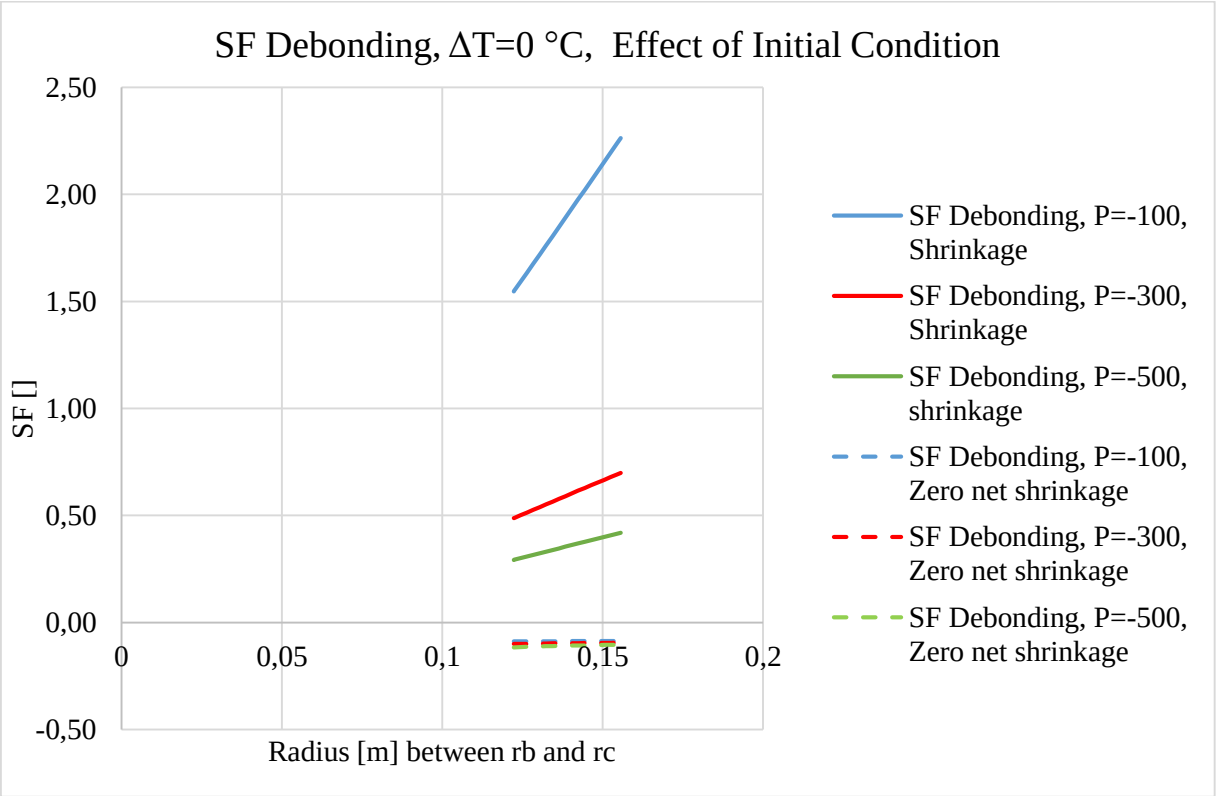

Figure 31: Effect of initial stress on debonding SF, for different pressure changes in bar

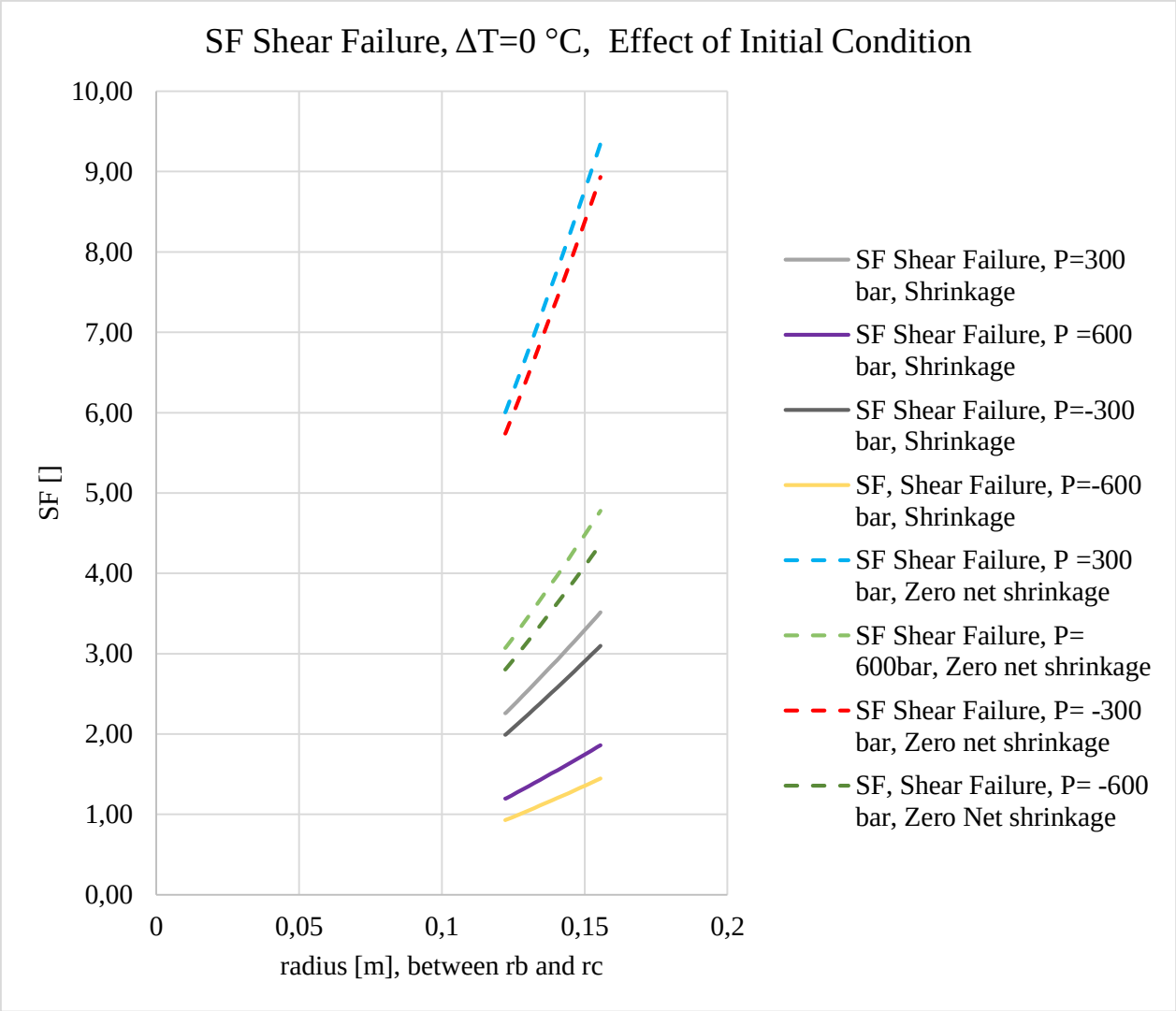

Figure 32: Effect of initial stress on shear failure SF, for different pressure changes in bar

4.3.1 Change in External Pressure

Several applications of the model are available, for example considering change in external pressures. The external pressure change is the change in the formation pressure. For all the examples already presented, this has been set to zero. This represents an uncertainty in the analyses, because a change in the external pressure can alter the SFs for all failure modes.

Mainly two occasions could cause external pressure change, namely subsidence, where the sea bottom sinks, or depletion. Depletion means that the pore pressure is reduced, while subsidence can occur if depletion occurs. In this thesis, the production casing is the casing that has been investigated. The production casing shoe is normally set above the reservoir, and hence it is not directly affected by the depletion of the reservoir. However, subsidence induced pressure alternation is applicable for the production casing.

In order to investigate the effect of changing the external pressure, the SFs for debonding, radial crack and shear failure have been calculated. This is done by varying the external pressure change for several fixed internal pressure and temperature changes. The results for debonding, radial crack and shear failure are plotted at r_b.

4.3.1.1 Debonding

Generally, an external pressure increase is favorable to avoid debonding at both the casing-cement and the cement-formation interfaces. A pressure reduction both internally and externally will increase the probability of debonding. As seen in Figure 33, P_i = -500 bar and T = -50 °C will never be higher than the DF-line when the radial stresses are in tension. Additionally, and the stresses will go straight into compression when the external pressure increase exceeds 100 bar. The pressure effects will attenuate the temperature effects when varying the external pressure. However, this trend is more visible at r_b than at r_c.

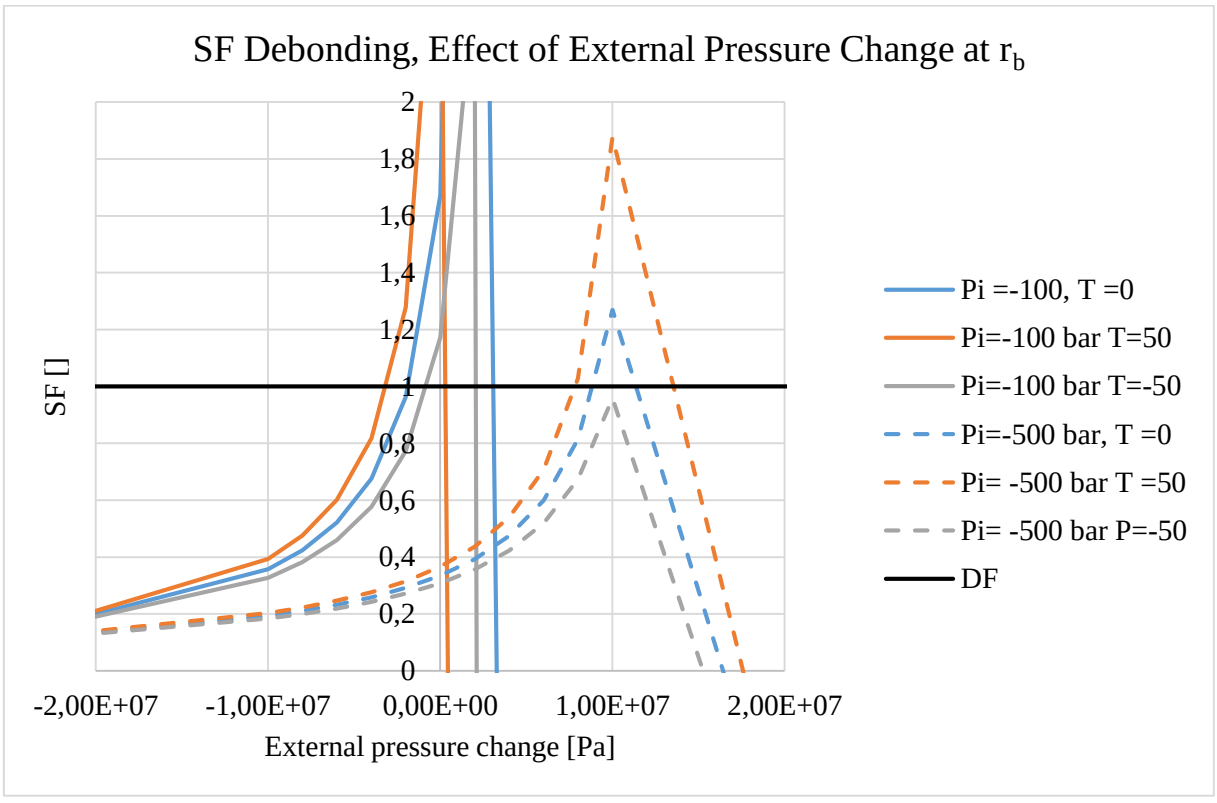

Figure 33: SF Debonding, change of external pressure, at r_b. Temperature change in °C.

4.3.1.2 Radial Crack

In Figure 34, the SFs for radial cracks at r_b show the same trend as the debonding SFs. Generally, an external pressure increase is favorable to avoid radial crack at both the casing-cement and the cement-formation interfaces. However, there are larger differences between the required external pressure change in order to avoid failure for the diverse temperatures, compared to debonding. In contrast to debonding, will a pressure reduction externally combined with a pressure increase internally, increase the probability of radial crack.

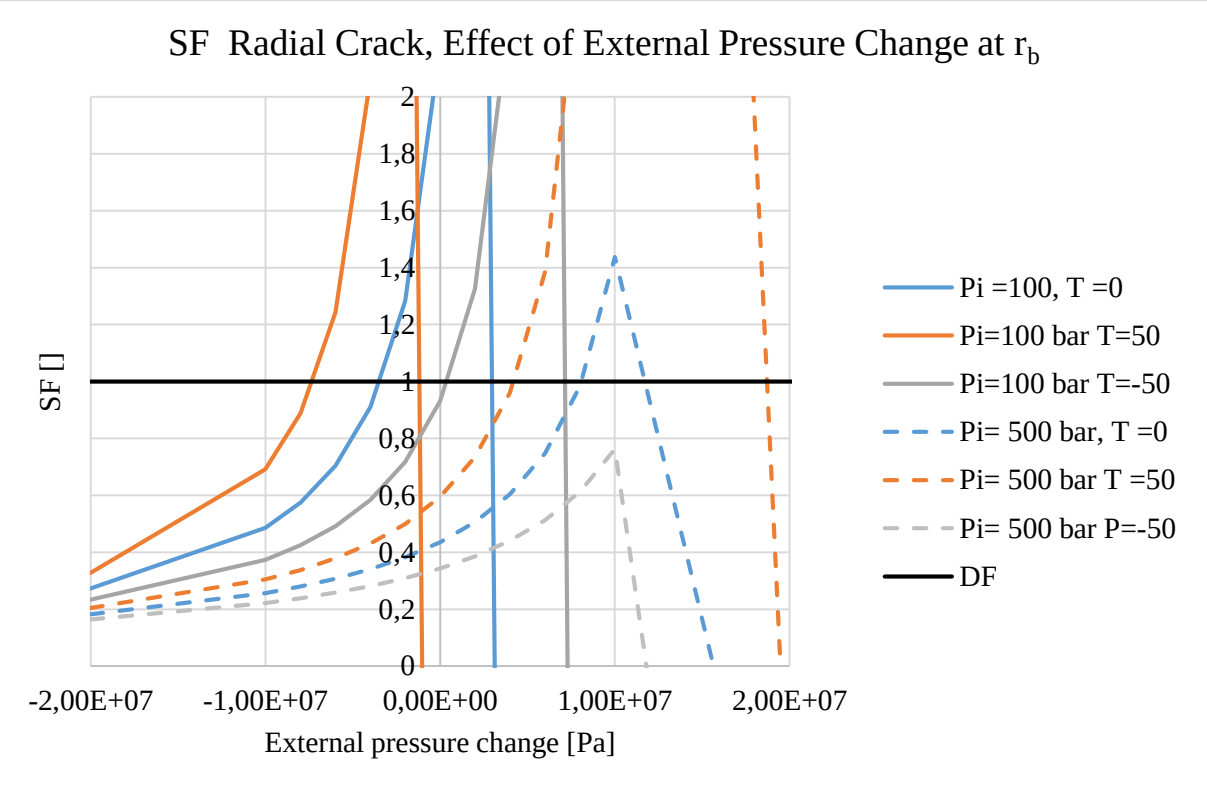

Figure 34: SF Radial crack, change of external pressure, at r_b. Temperature change in °C

4.3.1.3 Shear Failure

It can be seen from Figure 35 at r_b, that a low external pressure increase is favorable to avoid shear failure, especially when there is a high internal pressure drop in the well. When there is an internal pressure increase together with an external pressure decrease, and vice versa, the effect of the pressure cancels out, and the cement is less exposed to shear failure. At r_c, the SFs are more dependent on the external pressure change, than the internal pressure change.

A temperature decrease together with an external pressure drop is unfavorable for shear failure, while the opposite is true for external pressure increases. This may represent a large uncertainty in the previous work, as it differs from the base case results for shear failure.

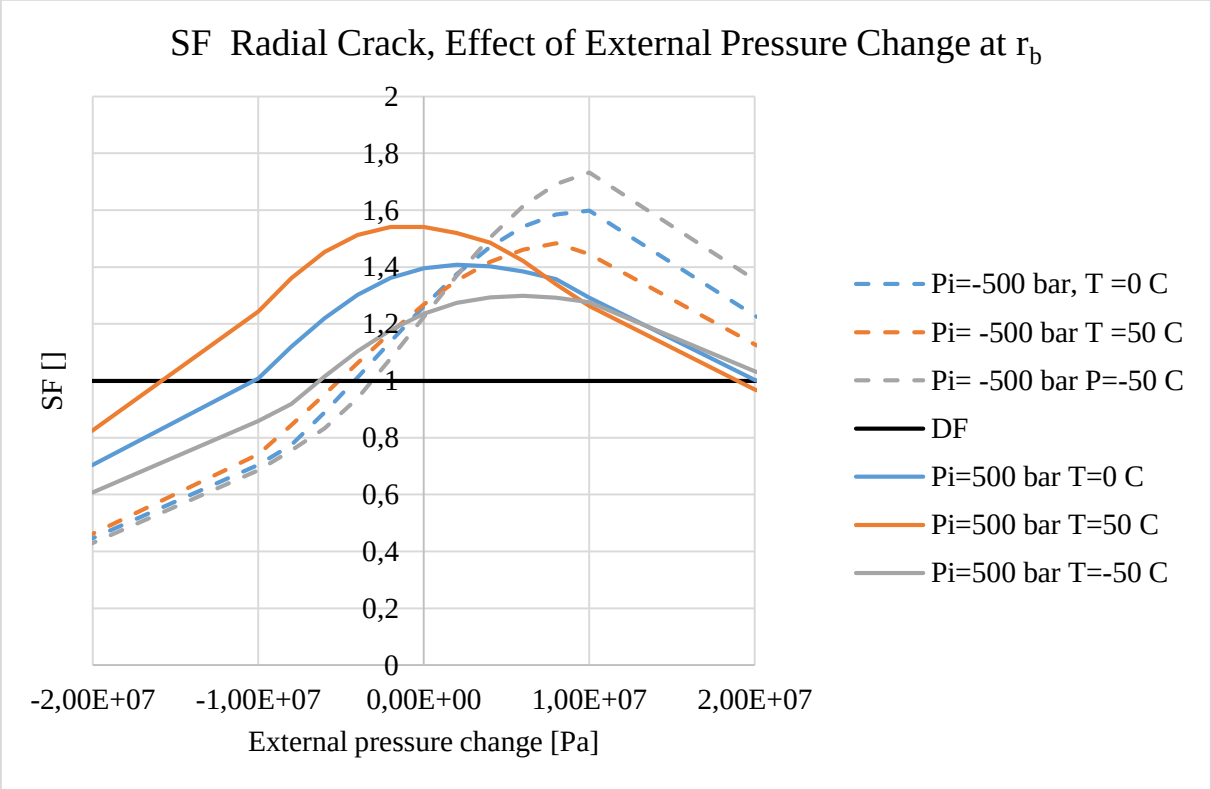

Figure 35: SF Shear failure change of external pressure, at r_b. Temperature change in °C

4.3.1 Thickness of the Cement

One feature of the model is to investigate the effect of a thin and a thick cement. The way this is done is by changing r_c, the cement-formation interface. It is important to mention that the model assumes that there is contact between the casing, cement and formation. This means that a large r_c could represent a washout, and not necessarily a thick cement. The same is applicable for a small r_c, which could represent an under gauged hole, and not necessarily a thin cement. This will increase the uncertainties of the investigation presented in this section. The effect of another medium between the cement and casing or formation (e.g. microannuli, voids etc) will therefore not be considered.

In order to determine how the cement thickness influences the safety factors for the different failure modes, an analysis with varying r_c has been performed. Values between 0.13 m to 0.2 m have been chosen for r_c.

Some trends are detected when investigating how a change in the cement thickness affects the SFs for the various failure modes.

It has been observed for debonding and radial crack that there is a difference when considering r_b or r_c. As seen from Figure 36, at r_b the cement thickness does not influence the SFs of radial crack to a large extent. However, Figure 37 shows that a thin cement will fail for a larger range of pressures than a thick cement at r_c. The main reason for this difference is that when the thickness is changed, the location where the stresses are considered is also changed when considering r_c. This is not the case when considering r_b, and hence the effect of the cement thickness is less. This is also due to the lower SFs at rb, since this interface is closer to the pressure and temperature source.

For shear failure, the spread between the SF-lines is small for r_b, but large for r_c. Hence, the cement thickness has a greater influence at the cement-formation interface. A special case is at rb, with a temperature drop: the negative pressure side will have a larger spread between the graphs than the positive pressure side. The opposite is observed with temperature increases.

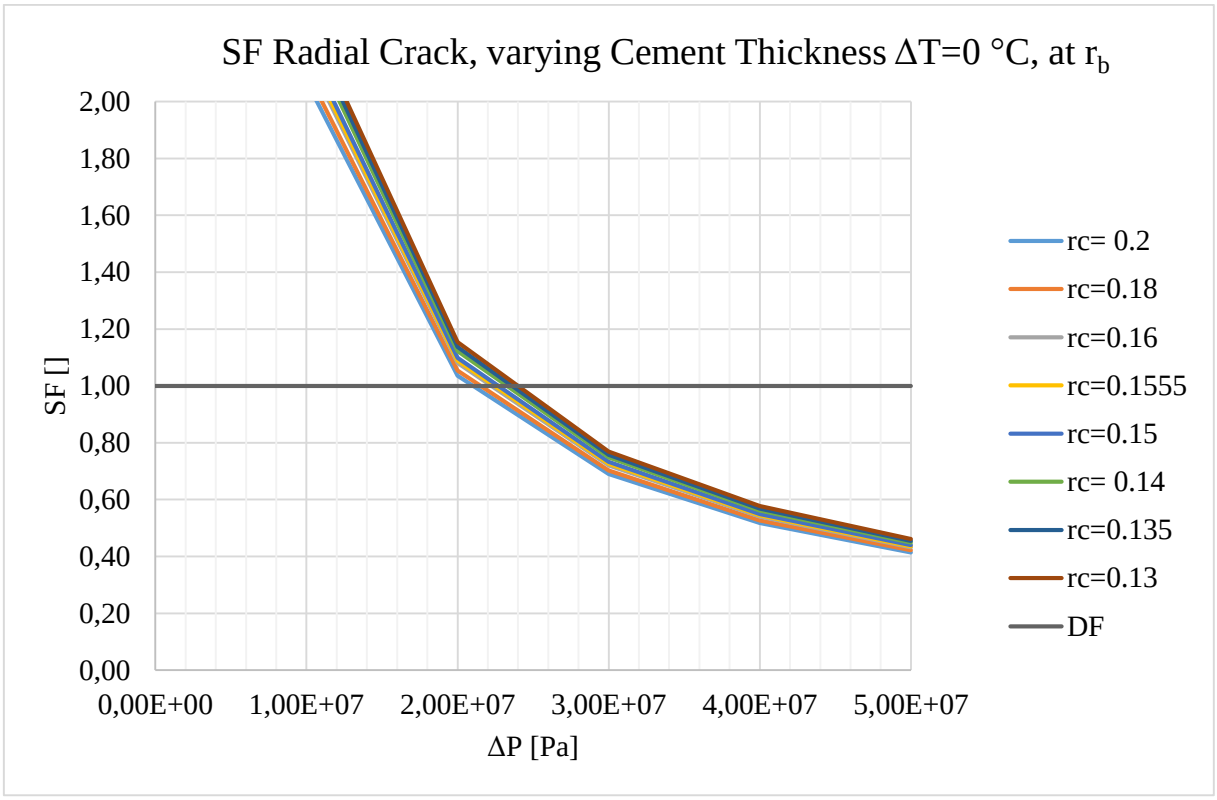

Figure 36: SF Radial Crack, for varying thicknesses, ΔT=0°C, at r_b, r_c in meter

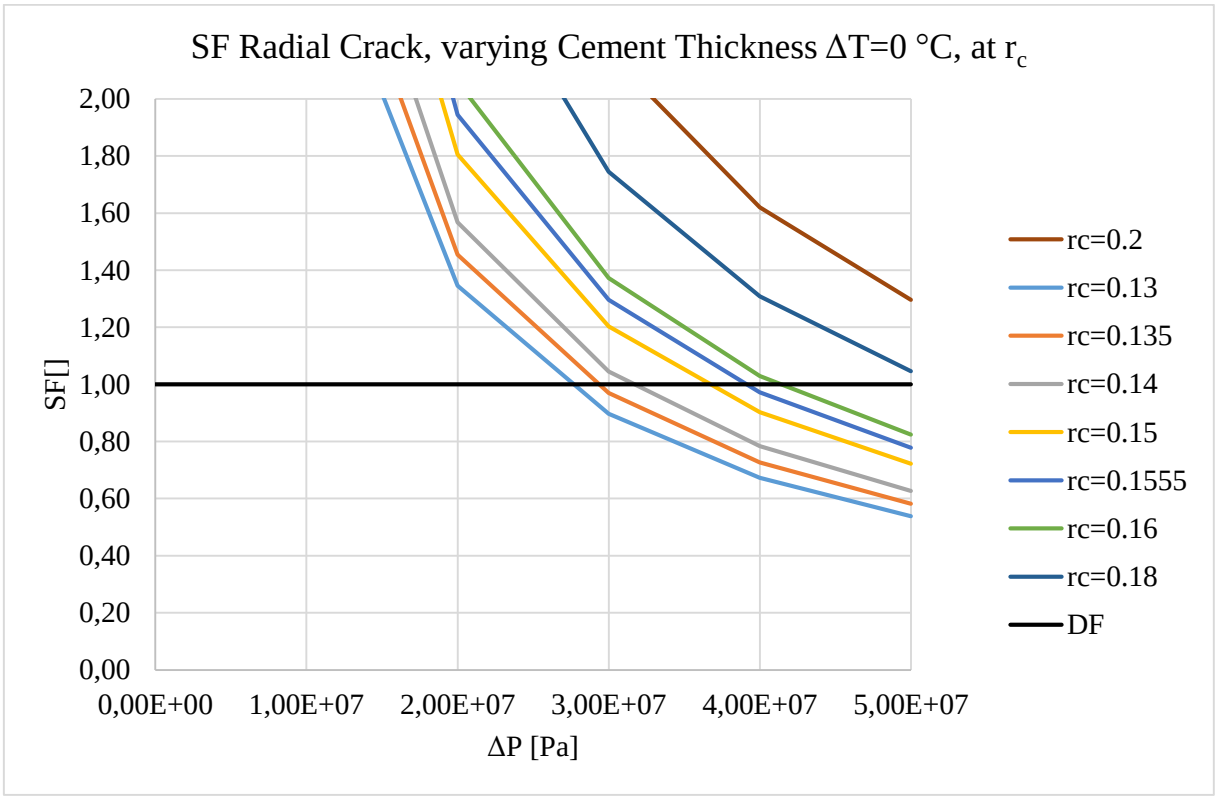

Figure 37: SF Radial Crack, for varying thicknesses, ΔT=0°C, at r_c, r_c in meter.

4.3.2 Choice of R_d

In order to tune in the model to be as correct as possible, it is necessary to decide the outer boundary of the model, r_d. R_d is mostly important for the temperature calculations, but it affects other parts through the resulting temperatures. This section will cover the effect of changing the r_d, and a discussion about the most suitable r_d.

4.3.2.1 General Effect of R_d on $\Delta T2$

R_d affects the temperature calculations, because it is an important part in the calculations of ΔT_2, which is the temperature change at the outer cement interface during the load case. In the calculations of ΔT_2, it is assumed that the temperature change at r_d is zero. Hence, a small r_d will reduce the accuracy of the result. It is important that r_d is chosen to be large enough so that this assumption is applicable.

In Figure 38, ΔT_2 is plotted against r_c for each r_d, for ΔT_1 = -100°C. The temperature change is less than 100°C for all cases in the cement, but for large r_d it is closer to 100°C than for the small r_ds. This is because, if r_d is chosen to be small compared to the well radius, the temperature change in the cement is more affected by the temperature change in the formation (which is zero) than the temperature change in the well. This is why the largest r_c (0.2 m) results in the smallest temperature change in the cement, even if the internal temperature change is large (-100°C).

It is possible to see a convergence towards one common temperature for the large r_ds. It is therefore applicable to assume that these radii are the most accurate, and therefore adequate for the rest of the investigation.

Figure 38 is sufficient to decide on an applicable r_d. However, the next session will show a short overview of how changing the r_d affect the SFs for the different failure modes, at r_b and r_c.

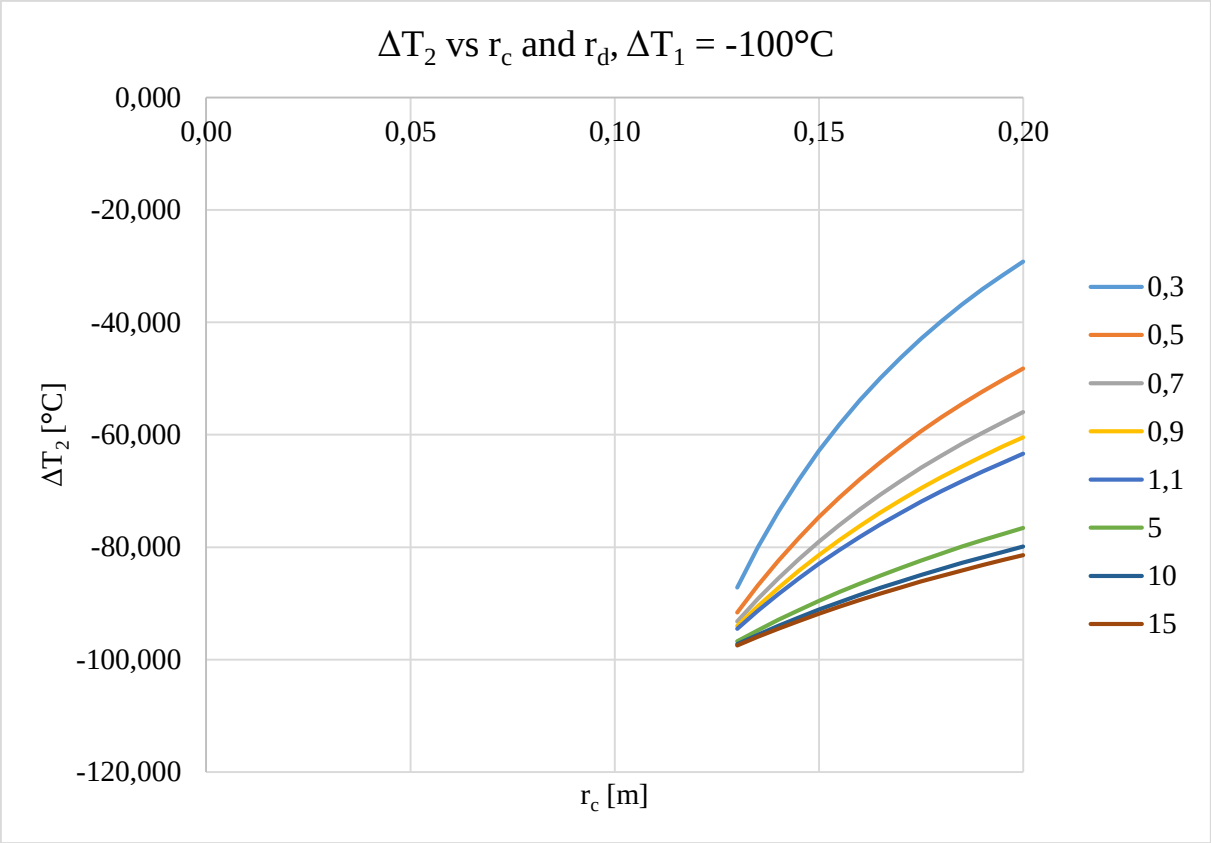

Figure 38: Effect of r_d on ΔT_2, ΔT_1=-100°C, r_d in meters.

4.3.2.2 R_d Effect on the SF for the Different Failure Modes

Through an investigation, where the SFs have been plotted for different r_ds and temperatures, some trends have been observed. Figure 39 shows radial crack as an example of how the investigation is performed. The figure illustrates the affected SFs, when r_d is changing for radial crack at r_b. The plot shows the SFs as a function of temperature, at a given pressure, for different r_d

Firstly, it is observed for all failure modes, when choosing an outer radius larger than 5 meter, the SFs converge towards the same values for all pressure and temperature conditions. This is the reason for choosing 10 m in the base case.

Secondly, when comparing how the SFs change at r_b and r_c, some similar trends can be seen for all the failure modes. At r_b, the pressure and temperature source is closer, because it is closer to the well where the changes occur. It can therefore be observed that the effect of changing the r_d does not overcome the effect of pressure and temperature at r_b compared to r_c. This effect is mostly applicable when the pressure and temperature conditions are undesirable, and a failure occur, or is close to occur. This is seen by the less separated lines at r_b compared

to at r_c. Additionally, one more trend is observed when comparing the difference in SFs at r_b and r_c for the failure modes. It can be seen that the SFs at r_c have little dependency on temperature change in the well for small r_ds. This is because the temperature change at r_d (which is zero) is much closer, and therefore affect the temperature change at r_c in a greater extent. This results in small changes in temperature at r_c, which will result in small changes in the SFs for different temperatures.

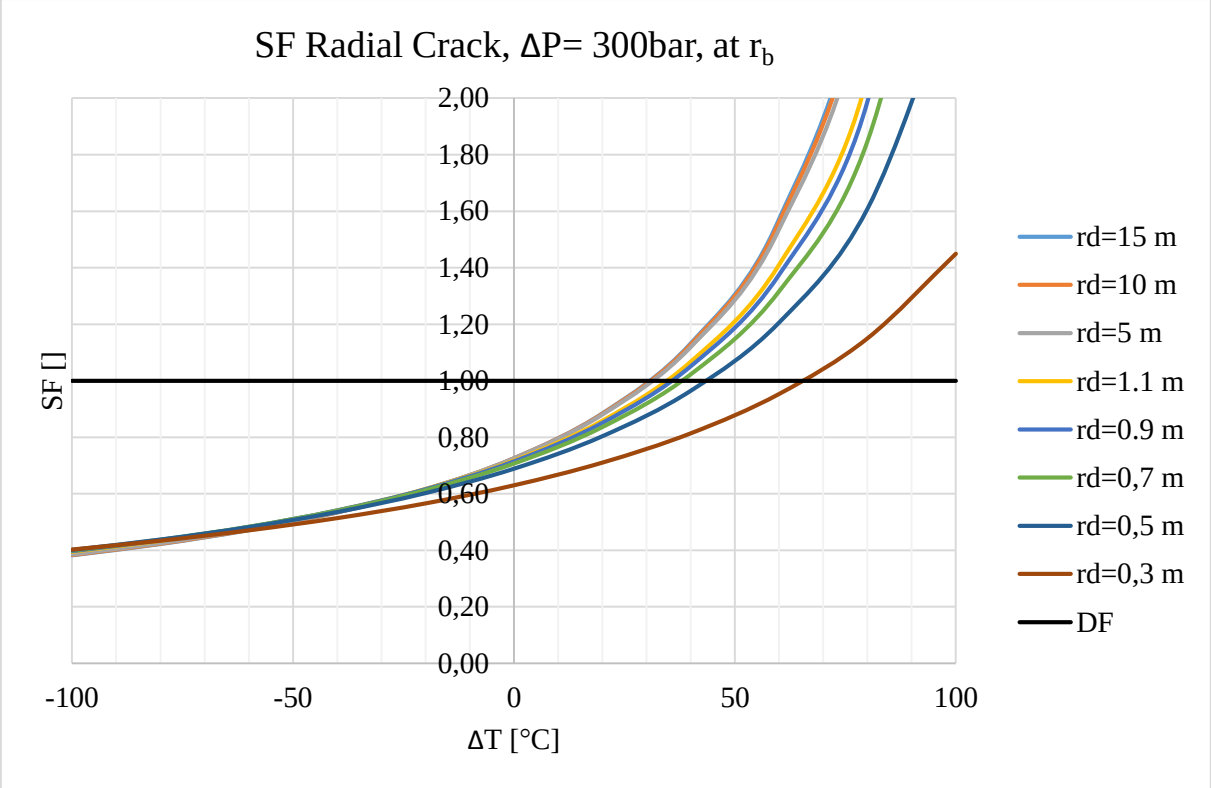

Figure 39: SF Radial Crack, with varying r_d at r_b

4.3.3 Uncertainties

The model and the analyses contain some uncertainties that are not as susceptible to modifications as the parameters shown in the previous chapters. Additionally, some shortcomings are present in the model, which are related to the assumptions behind the model. These uncertainties and shortcomings are in terms of external pressure profile when comparing the cement model and ILS, in addition to the fact that the model disregards pore pressure and successive loads.

In the comparison with ILS, the external pressure profiles differentiate in the model and in the ILS. The cement model does not account for any annulus pressure, which is sufficient since this pressure does not affect the resulting SF for the cement. However, the casing SF is largely dependent on the annulus pressure. Hence, a comparison of the two SFs are not directly applicable. This is why the cement model is mainly useful to complement the ILS. However, if considering normal annulus pressures, the comparison may be applicable.

Another uncertainly, which reduces the credibility to the results, is that the pore pressure in the cement is not included. By not including the pore pressure, the effect of considering a porous media is not included. The pore pressure will change the results because it is included by altering the stresses to effective stresses. However, pore pressures vary from field to field, and could therefore not be used in a general solution. In addition, the change in pore pressure is difficult to determine, especially if the initial stress condition in the cement affects it.

Successive loads can alter when the initiation of failure occurs. For example, it is possible that debonding can occur after a large pressure increase resulting in a plastically deformed cement. If it then experiences a reduced positive pressure load, debonding can occur. However, this is not accounted for in this project.

5. Conclusion

In the work performed with the casing-cement-formation mechanical model together with the ILS, the following conclusions are made:

- Debonding may take place at the casing-cement or the cement- formation interface. The cement is more exposed to debonding at negative internal pressure changes, and negative temperature changes. When the cement Young's modulus is large, and the formation Young's modulus is small, the probability of debonding decreases in the cases investigated.
- In the cases investigated, radial cracks will first initiate at the casing-cement interface. The cement is more exposed to radial cracks when the well experiences a pressure increase. A temperature drop will lower the required pressure change to initiate radial cracks at r_b and r_c. A high formation Young's modulus is favorable in order to avoid radial crack, while a low Young's modulus of the formation is unfavorable. It seems like the formation Young's modulus is more dominating on the resulting radial crack SF than the Young's modulus of cement.
- Shear failure may occur at both pressure increases and decreases. However, it is more likely when the well experiences a pressure decrease. Shear failure generally demands a large pressure change in order to occur. However, the mechanical properties of the cement can alter this result. Negative temperature changes lower the required pressure changes to initiate failure, as long as there is no external pressure change.
- Neither the Poisson's ratio nor the coefficient of linear thermal expansion will significantly affect the SFs of the failure modes.
- Some failure modes will occur in the cement sheath before the casing fails, for the burst and collapse load investigated. This is mostly applicable for the stronger casing grades, which includes the widely used 9 5/8-in casing; #53.5 P-110.
    - Shear failure is not likely to occur for the burst load nor for the collapse load considered. However, collapse loads are more critical. Nevertheless, with the most undesirable combinations of the mechanical properties, meaning mainly large values of the formation Young's modulus, it can occur.
    - It can be concluded that for a pressure test, radial crack is the failure mode that is most important to consider. Radial cracks can occur when the casing experiences a pressure test load, while the casing remains safe. However, this case is highly dependent on the mechanical properties of the cement. Therefore

is it difficult to conclude whether ILS needs to be complemented, when considering radial crack. With the most desirable properties of the cement and the formation, the SFs are negative, meaning that no radial crack can occur.

  - Debonding is the most important failure mode to consider during a casing evacuation. For most combinations of the mechanical properties, the cement will fail, when the casing does not fail. However, a few combinations of the mechanical properties will result in a safe cement design. If the company considers debonding as a critical failure, complementing ILS would be desirable. NORSOK (2013) states that some cases requires logging of the cement, and in these cases, a complementary program is recommended to be included in the standard practice. It can therefore be concluded that debonding is the failure that is the most important to evaluate if an additional cement feature should be included in the ILS. The ILS should at least provide a warning when the well is not safe in terms of zonal isolation, even if the casing design is safe.

- Model features, that can increase the uncertainty of the obtained results, include:
  - If no shrinkage of the cement is included, then no tensile failure will occur for the base case investigated.
  - By including external pressure profile, it is possible to implement the effect of depletion or subsidence of the formation. Generally, a drop in external pressure will increase the probability of failure for the cases investigated. External pressure will change the favorable temperature condition for shear failure, which represent a large uncertainty in the analyses.
  - By including a thin cement sheath, the SFs for all failure modes will be reduced. This effect is more significant when considering the cement-formation interface. However, this analysis does not incorporate the presence of fluid channels or microannuli.
  - By changing the boundary of the model in terms of the outer radius, the SFs for all failure modes are altered. The chosen radius has a large impact on the temperature calculations. An r_d of 10 m seems like an appropriate outer boundary in order to obtain an accurate prediction of the temperature variations.

6. Further Work

In order to expand the thesis to conclude more thoroughly on cement sheath failure estimates, several measures could be taken. These measures include improvements of the model and improvements of the analyses already performed. Additionally, suggested investigations, using the features of the model, are presented.

- Some model improvements may be:
    - Include assumption of porous cement, by including pore pressure in terms of effective stress for various initial stress conditions.
    - Investigate the stresses in the cement, when failure has occurred.
    - Incorporate transient load cases, i.e. effect of successive load cases, for investigation of thermal or pressure cycling.
    - Include the possibility to retrieve the degree of debonding, radial crack and shear failure in the cement sheet.
- Some improvements to the analyses could be performed:
    - Include more cases in the sensitivity, or make a program that runs several cases for all the variable mechanical properties for the different pressures and temperatures.
    - Include sensitivity of altered cement strength data to investigate the effect on SFs. Additionally, this could be included into the already existing sensitivity analyses on mechanical properties.
    - Find, if possible, a combination of Young's modulus and Poisson's ratio that will be the best case for both burst and collapse loads for all failure modes.
    - An improvement in the analysis considering the cement thickness could be performed. In order to improve this part, a cylinder of fluid, representing the space between the cement and the formation should be included. This could be done by including one more cylinder with Lamé's theory, and then obtaining a third contact pressure and a new interface radius.
    - Expand the analyses to include more than one casing, in order to see if the results are applicable for other casing sizes.
    - Determine applicable pressure changes that result from depletion and subsidence.

- Some further investigations, using the features of the model, could be performed:
    - Compare the stresses in the casing provided by the model, with the stresses provided by the ILS. From the ILS by using the resulting SF on the load, from the model by considering radii between r_a and r_b. Then the mechanical support from the cement may be determined.
    - The model can be verified by comparing with a load history of real well. By exposing the model to the same loads as the well, and by comparing the debonding results from the model with the associated CBL, a verification can be obtained.

7. Nomenclature

Roman letters

A = Areal [m^2]

A =intersection of the line on the τ axis

A = Lamé constant A

B = inclination of the line

B = Lamé constant B

c = cohesion of the material [Pa]

d = original diameter [m]

E = Young's Modulus [Pa]

$E_{formation}$ = Young's Modulus formation [Pa]

E_{cement} = Young's Modulus cement [Pa]

E_{steel} = Young's Modulus steel [Pa]

F = Force [N]

f = a function obtained experimentally [-]

f = monotonically increasing function [-]

k_{cem} = Thermal conductivity of cement $\left[W/m \cdot C^{\circ} \right]$

k_{form} = Thermal conductivity of formation $\left[W/m \cdot C^{\circ} \right]$

L = Original Length [m]

P_{c1} = Contact pressure at r_b interface [Pa]

P_{c2} = Contact pressure at r_c interface [Pa]

P_i = internal pressure [Pa]

P_i = Change in internal pressure in casing [Pa]

$P_{i,final}$ = Initial pressure, in final condition [Pa]

$P_{i,inital}$ = Initial pressure in internal [Pa]

P_f = Change in external (formation) pressure [Pa]

P_o = external pressure [Pa]

$P_{surface}$=test pressure at surface [Pa]

P(z)= pressure at depth z [Pa]

r = radius [m]

r_a = inner radius of casing [m]

r_b = outer radius casing/inner radius cement [m]

r_c =outer radius of the cement/inner radius of the formation [m]

r_d = outer radius formation [m]

r_i = internal radius of the cylinder [m]

r_o = external radius of the cylinder [m]

$T_{i,final}$ = Internal temperature, in final condition [°C]

$T_{i,inital}$ = Internal temperature in initial condition [°C]

T_0 = Tensile Strength [Pa]

$\dot{Q}$ = Heat [W]

z= depth [m]

Y_{co} = Cohesion [Pa]

Greek letters

α = coefficient of linear thermal expansion [1/C]

$\alpha_{formation}$ = coefficient of linear expansion for formation [1/C]

α_{cement} = coefficient of linear expansion for cement [1/C]

α_{steel} = coefficient of linear expansion for steel [1/C]

δd = change in diameter [m]

δL = Length Change [m]

$\delta r_{formation}$ = radial displacement of formation [m]

δr_{cement} = radial displacement of cement [m]

δr_{steel} = radial displacement of steel [m]

ΔP_i = Change in internal pressure from initial to final condition [Pa]

ΔT = Change in temperature [°C]

ΔT_{geo} = Change in temperature in formation [C°]

ΔT_i = Change in internal temperature from initial to final condition [°C]

ΔT_1 = Change in temperature in casing [C°]

ΔT_2 = Change in temperature in cement [C°]

ΔT_1 = Change in temperature at ra [°C]

ΔT_2 = Change in temperature at rb [°C]

ΔT_3 = Change in temperature at rc [°C]

ΔT_4 = Change in temperature at rd [°C]

ε = Strain []

ϕ = angle of internal friction [radians]

μ_m = mud weight gradient [Pa/m]

σ = stress [Pa]

σ_c = Compressive strength [Pa]

σ_H = Hoop Stress [Pa]

$\sigma_{H,casing}$ = Hoop stress in casing [Pa]

$\sigma_{H,cement}$ = Hoop stress in cement [Pa]

$\sigma_{H,formation}$ = Hoop stress in formation [Pa]

σ_r = Radial Stress [Pa]

$\sigma_{r,casing}$ = Radial stress in casing [Pa]

$\sigma_{r,cement}$ = Radial stress in cement [Pa]

$\sigma_{r\ formation}$ = Radial stress in formation [Pa]

$\sigma_{m,2}$ = mean normal stress [Pa]

σ_n = normal stress acting on the failure plane [Pa]

σ_n'=effective normal stress acting on the failure plane [Pa]

σ_z = axial stress [Pa]

σ_1 = maximum principal stress [Pa]

σ_2 = intermediate principal stress [Pa]

σ_3 = minimum principal stress [Pa]

σ_1' = effective maximum principal stress $(\text{confining stress})$[Pa]

σ_2' = effective intermediate principal stress [Pa]

σ_3' = effective minimum principal stress [Pa]

τ = shear stress [Pa]

τ_{max} = maximum allowable shear stress [Pa]

τ_{oct} = octahedral shear stress [Pa]

ν = Poisson's ratio []

$\upsilon_{formation}$ = Possions ratio of the formation []

υ_{cement} = Possions ratio of the cement []

υ_{steel} = Possions ratio of the steel []

8. References

AL-AJMI, A. 2006. *Wellbore stability analysis based on a new true-triaxial failure criterion.* PhD thesis, KTH, Stockholm.

AL-AJMI, A. M. & ZIMMERMAN, R. W. 2005. 'Relation between the Mogi and the Coulomb failure criteria'. *International Journal of Rock Mechanics and Mining Sciences,* vol.42, no.3**,** pp. 431-439.

BELLARBY, J. 2009. *Well Completion Design,* Amsterdam, Amsterdam : Elsevier Science.

BOSMA, M., RAVI, K., VAN DRIEL, W. & SCHREPPERS, G. J. 1999. 'Design Approach to Sealant Selection for the Life of the Well' SPE-56536-MS. *SPE Annual Technical Conference and Exhibition.* Houston, Texas: Society of Petroleum Engineers.

BRECHAN, B. 2014. NTNU Governing Documentation Casing Design. Trondheim: NTNU.

BYBEE, K. 2007. 'Cement-Bond-Log Interpretation Reliability', SPE-0207-0064-JPT. *Journal of Petroleum Technology,* vol. 59, no. 2**,** pp. 64-66.

DE ANDRADE, J. 2015. *Cement Sheat Integrity During Thermal Cycling.* PhD Thesis, Norwegian University of Science and Technology, Trondheim.

DE ANDRADE, J. & SANGESLAND, S. 2016. Cement Sheath Failure Mechanisms: Numerical Estimates to Design for Long-Term Well Integrity.

ECONOMIDES, M. J., DUNN-NORMAN, S. & WATTERS, L. T. 1998. *Petroleum well construction,* Chichester, Wiley.

FJÆR, E., HOLT, R. M., HORSRUD, P., RAAEN, A. M. & RISNES, R. 2008. *Petroleum Related Rock Mechanics,* Amsterdam, Elsevier Science.

HEARN, E. J. 1997. *Mechanics of Materials : An Introduction to the Mechanics of Elastic and Plastic Deformation of Solids and Structural Materials,* Burlington, Elsevier Science.

JAEGER, J. C. & COOK, N. G. W. 1979. *Fundamentals of rock mechanics,* 3rd edn, London, Chapman and Hall.

JAEGER, J. C., COOK, N. G. W. & ZIMMERMAN, R. W. 2007. *Fundamentals of rock mechanics,* Malden, Mass, Blackwell.

LANDMARK 2001. WellCat. Houston: Landmark Graphics Corporation.

MOGI, K. 1971. 'Fracture and flow of rocks under high triaxial compression'. *Journal of Geophysical Research,* vol. 76 (5)**,** pp. 1255-1269.

NELSON, E. B. & GUILLOT, D. (eds.) 2006. *Well cementing,* 2nd edn, Amsterdam: Schlumberger.

NORSOK 2013. Well Integrity in drilling and well operations. *NORSOK-D010.* rev 4, Standards Norway.

PETROWIKI. 2016. *Well Integrity* [Online]. Available: http://petrowiki.org/Well_integrity [Accessed 02.06.16.

RAHIMI, R. 2014. *The effect of using different rock failure criteria in wollbore stability analysis.* Master of Science, Missouri University of Science and Technology.

WAWERSIK, W. R., CARLSON, L. W., HOLCOMB, D. J. & WILLIAMS, R. J. 1997. 'New method for true-triaxial rock testing'. *International Journal of Rock Mechanics and Mining Sciences,* vol. 34(3-4)**,** pp. 330.e1-330.e14.

Appendix A
Visual Basic for Applications code

Stresses

```
Function hoop_stress(r, ra, rb, rc, rd, Pi, Pc1, Pc2, Pf)

If ra <= r And r < rb Then

    hoop_stress = (-1) * (((ra ^ 2 * Pi - rb ^ 2 * Pc1) / (rb ^ 2 - ra ^ 2)) + (((Pi - Pc1) * ra ^ 2 * rb ^ 2) / ((rb ^ 2 - ra ^ 2) * r ^ 2)))

ElseIf rb <= r And r <= rc Then

    hoop_stress = (-1) * (((rb ^ 2 * Pc1 - rc ^ 2 * Pc2) / (rc ^ 2 - rb ^ 2)) + (((Pc1 - Pc2) * rb ^ 2 * rc ^ 2) / ((rc ^ 2 - rb ^ 2) * r ^ 2)))

ElseIf rc < r And r < rd Then

    hoop_stress = (-1) * (((rc ^ 2 * Pc2 - rd ^ 2 * Pf) / (rd ^ 2 - rc ^ 2)) + (((Pc2 - Pf) * rc ^ 2 * rd ^ 2) / ((rd ^ 2 - rc ^ 2) * r ^ 2)))

End If

End Function
```

```
Function radial_stress(r, ra, rb, rc, rd, Pi, Pc1, Pc2, Pf)

If ra <= r And r < rb Then

    radial_stress = (-1) * (((ra ^ 2 * Pi - rb ^ 2 * Pc1) / (rb ^ 2 - ra ^ 2)) - (((Pi - Pc1) * ra ^ 2 * rb ^ 2) / ((rb ^ 2 - ra ^ 2) * r ^ 2)))

ElseIf rb <= r And r <= rc Then

    radial_stress = (-1) * (((rb ^ 2 * Pc1 - rc ^ 2 * Pc2) / (rc ^ 2 - rb ^ 2)) - (((Pc1 - Pc2) * rb ^ 2 * rc ^ 2) / ((rc ^ 2 - rb ^ 2) * r ^ 2)))

ElseIf rc < r And r < rd Then

    radial_stress = (-1) * (((rc ^ 2 * Pc2 - rd ^ 2 * Pf) / (rd ^ 2 - rc ^ 2)) - (((Pc2 - Pf) * rc ^ 2 * rd ^ 2) / ((rd ^ 2 - rc ^ 2) * r ^ 2)))

End If
```

```
End Function
```

```
Function axial_stress(vform, vcem, vsteel, sigmar, sigmah, r, ra, rb, rc, rd)
If ra <= r And r < rb Then
    axial_stress = (-1) * (vsteel * (sigmar + sigmah))
    ElseIf rb <= r And r <= rc Then
    axial_stress = (-1) * (vcem * (sigmar + sigmah))
ElseIf rc < r And r < rd Then
    axial_stress = (-1) * (vform * (sigmar + sigmah))
End If
End Function
```

Contact Pressures

```
Function T1_steel(alpha_steel, deltaT1, v_steel)
T1_steel = alpha_steel * deltaT1 * (v_steel + 1)
End Function
```

```
Function T2_steel(alpha_steel, deltaT2, v_steel)
T2_steel = alpha_steel * deltaT2 * (v_steel + 1)
End Function
```

```
Function T1_form(alpha_form, deltaT1, v_form)
T1_form = alpha_form * deltaT1 * (v_form + 1)
End Function
```

```
Function T2_form(alpha_form, deltaT2, v_form)
T2_form = alpha_form * deltaT2 * (v_form + 1)
```

End Function

Function T1_cem(alpha_cem, deltaT1, v_cem)

T1_cem = alpha_cem * deltaT1 * (v_cem + 1)

End Function

Function T2_cem(alpha_cem, deltaT2, v_cem)

T2_cem = alpha_cem * deltaT2 * (v_cem + 1)

End Function

Function A_cem(v_cem, rb, rc)

A_cem = (v_cem ^ 2 - 1) * (((rb ^ 2) / (rb ^ 2 - rc ^ 2)) + ((rc ^ 2) / (rb ^ 2 - rc ^ 2)))

End Function

Function A_steel(v_steel, ra, rb)

A_steel = (v_steel ^ 2 - 1) * (((ra ^ 2) / (ra ^ 2 - rb ^ 2)) + ((rb ^ 2) / (ra ^ 2 - rb ^ 2)))

End Function

Function A_form(v_form, rc, rd)

A_form = (v_form ^ 2 - 1) * (((rc ^ 2) / (rc ^ 2 - rd ^ 2)) + ((rd ^ 2) / (rc ^ 2 - rd ^ 2)))

End Function

Function B_1(Pi, ra, rb, v_steel, E_steel)

B_1 = ((2 * Pi * ra ^ 2 * rb * (v_steel ^ 2 - 1)) / (E_steel * (ra ^ 2 - rb ^ 2)))

End Function

Function B_2(Pf, rc, rd, v_form, E_form)

B_2 = (2 * Pf * rc * rd ^ 2 * (v_form ^ 2 - 1)) / (E_form * (rc ^ 2 - rd ^ 2))

End Function

Function PC_1(rb, rc, T1_steel, T1_cem, T2_cem, T2_steel, T2_form, v_steel, v_cem, v_form, B_1, B_2, A_steel, A_cem, A_form, E_steel, E_cem, E_form)

PC_1 = (rb * T1_steel - rb * T1_cem + B_1 - ((2 * rb * rc ^ 2 * (v_cem ^ 2 - 1) * (rc * T2_cem - rc * T2_form + B_2)) / (E_cem * (rb ^ 2 - rc ^ 2) * (((rc * (v_cem + v_cem ^ 2 - A_cem)) / (E_cem)) - ((rc * (v_form + v_form ^ 2 + A_form)) / (E_form)))))) / ((((rb * (v_steel + v_steel ^ 2 - A_steel)) / (E_steel)) - ((rb * (v_cem + v_cem ^ 2 + A_cem)) / (E_cem))) * (((4 * rb ^ 3 * rc ^ 3 * (v_cem ^ 2 - 1) ^ 2) / (E_cem ^ 2 * (rb ^ 2 - rc ^ 2) ^ 2 * (((rb * (v_steel + v_steel ^ 2 - A_steel)) / (E_steel)) - ((rb * (v_cem + v_cem ^ 2 + A_cem)) / (E_cem))) * (((rc * (v_cem + v_cem ^ 2 - A_cem)) / (E_cem)) - ((rc * (v_form + v_form ^ 2 + A_form)) / (E_form)))) - 1)))

End Function

Function PC_2(rb, rc, v_steel, v_cem, v_form, A_steel, A_cem, A_form, E_steel, E_cem, E_form, T1_steel, T1_cem, T2_cem, T2_form, B_1, B_2)

PC_2 = (rc * T2_cem - rc * T2_form + B_2 - ((2 * rb ^ 2 * rc * (v_cem ^ 2 - 1) * (rb * T1_steel - rb * T1_cem + B_1)) / (E_cem * (rb ^ 2 - rc ^ 2) * (((rb * (v_steel + v_steel ^ 2 - A_steel)) / (E_steel)) - ((rb * (v_cem + v_cem ^ 2 + A_cem)) / (E_cem)))))) / ((((rc * (v_cem + v_cem ^ 2 - A_cem)) / (E_cem)) - ((rc * (v_form + v_form ^ 2 + A_form)) / (E_form))) * (((4 * rb ^ 3 * rc ^ 3 * (v_cem ^ 2 - 1) ^ 2) / (E_cem ^ 2 * (rb ^ 2 - rc ^ 2) ^ 2 * (((rb * (v_steel + v_steel ^ 2 - A_steel)) / (E_steel)) - ((rb * (v_cem + v_cem ^ 2 + A_cem)) / (E_cem))) * (((rc * (v_cem + v_cem ^ 2 - A_cem)) / (E_cem)) - ((rc * (v_form + v_form ^ 2 + A_form)) / (E_form)))) - 1)))

End Function

Failure

Function UCS(Ecem)

UCS = 0.0354 * (Ecem * 10 ^ (-9)) ^ 2 + 3.1509 * (Ecem * 10 ^ (-9)) + 4.0642

End Function

Function T0(UCS)

T0 = UCS * 10 ^ 6 / 10

End Function

Function c(UCS, angle)

```
c = (UCS * (1 - Sin(angle))) / (2 * Cos(angle))

End Function
```

```
Function t_allowance(c, angle, sigmam)

t_allowance = c * Cos(angle) + Sin(angle) * sigmam

End Function
```

```
Function sigmam(sigma1, sigma3)

sigmam = (sigma1 + sigma3) / (2)

End Function
```

```
Function t_max(sigma1, sigma2, sigma3)

t_max = (1 / 3) * ((sigma1 - sigma3) ^ 2 + (sigma2 - sigma3) ^ 2 + (sigma1 - sigma2) ^ 2) ^ (0.5)

End Function
```

Appendix B

Pore Pressure Plot

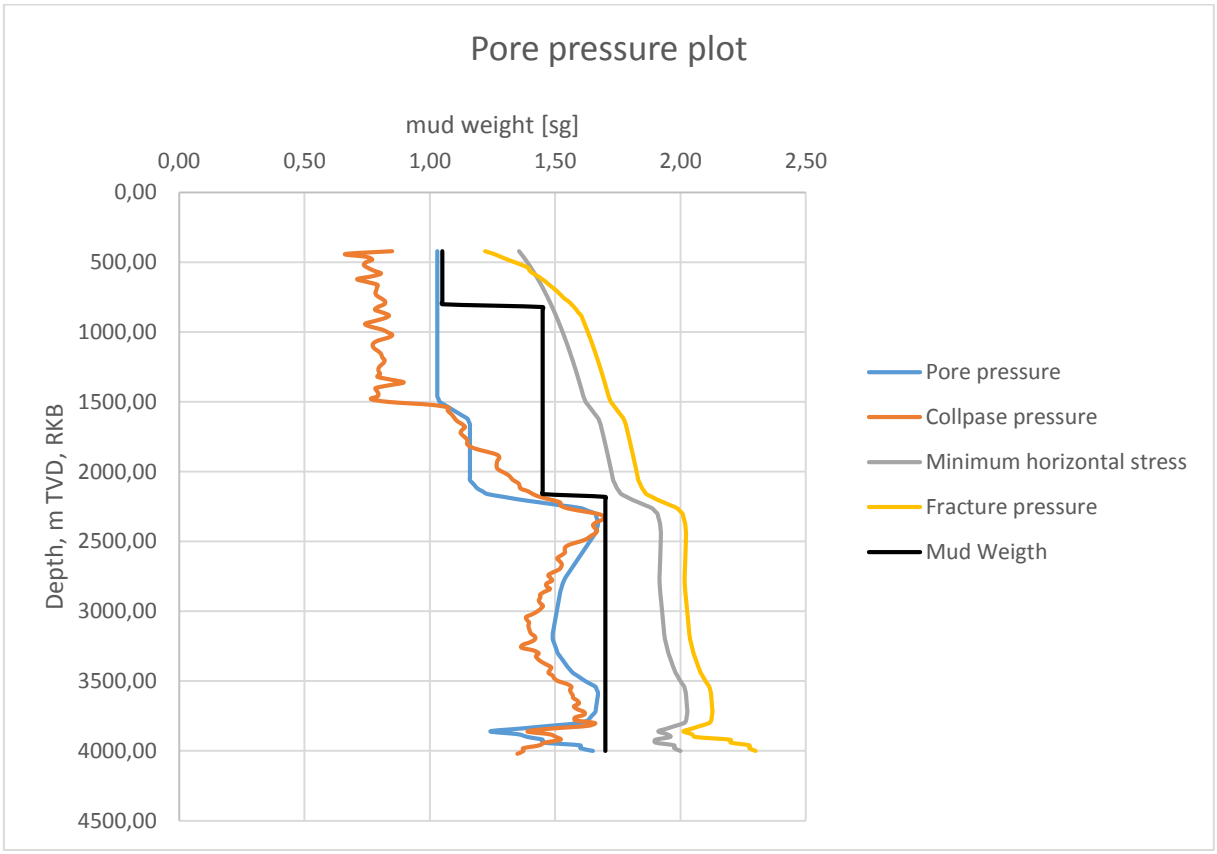

Appendix Figure 1: Pore pressure plot used in model and ILS

Appendix C

Definition of Basic Mechanics

If a bar is subjected to a direct force that causes a uniform tension or compression of the bar over the cross sectional area, the bar is subjected to a uniform direct or normal stress. Eq. (C.1) shows how stress is defined (Hearn, 1997).

$$stress(\sigma) = \frac{Force}{Area} = \frac{F}{A} \tag{C.1}$$

Where,

F = Force [N]
A= Area [m^2]

When the bar is subjected to stress, a length change will occur. The length change δl , divided by the original length L, gives the strain as defined in Eq. (C.2).

$$Strain(\varepsilon) = \frac{\delta L}{L} \tag{C.2}$$

Where,

δL = Length Change [m]
L= Original Length [m]

The relationship between the stress and the strain can be shown in a tensile test curve. A tensile test is carried out to compare the strength of different materials. A typical tensile test curve is shown in Appendix Figure 2. The curve consists of mainly two parts; an elastic part and a plastic region. In the elastic region, the deformation of the bar is reversible, meaning that it returns to its original shape when the pressure is released. In this region the stress is proportional to the strain with E, Young's modulus, as the proportional constant. In this region Hook's law apply (Hearn, 1997). This is shown in Eq. (C.3)

$$\sigma = E\varepsilon \tag{C.3}$$

Where,

σ = stress [Pa]
E = Young's modulus [Pa]
ε = Strain []

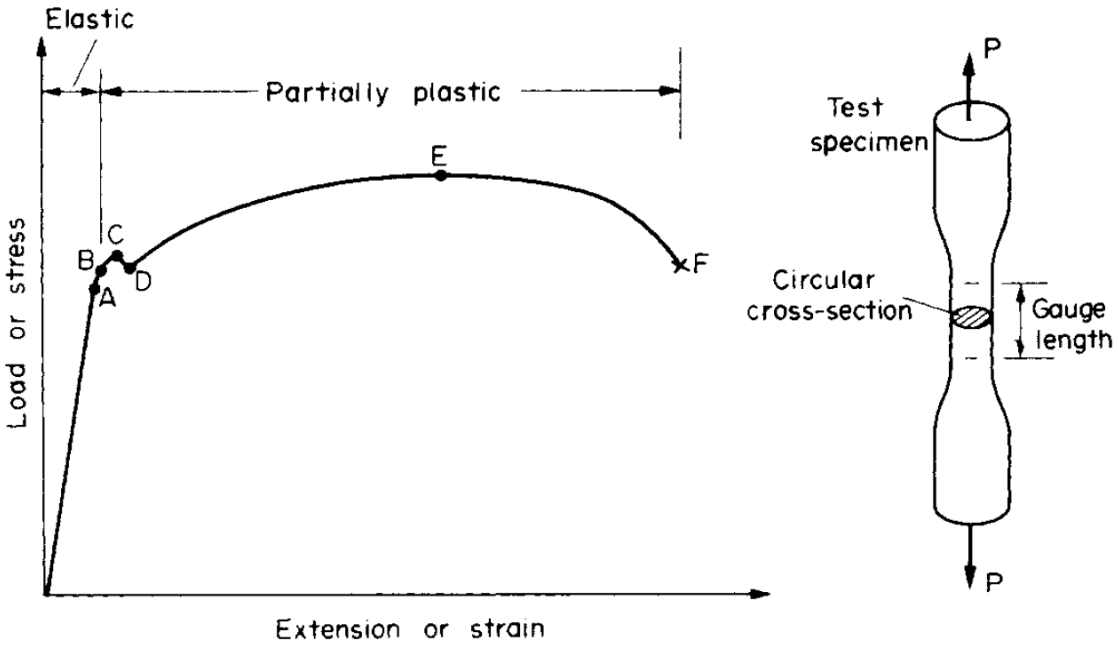

Appendix Figure 2: Tensile test curve (Hearn, 1997)

In the plastic region the strain occurring from the exerted stress is not recoverable and the bar experiences a permanent deformation. The capacity of a material to allow for the plastic deformation is the measure of the materials ductility (Hearn, 1997).

When applying the defined terms in two-dimensions, Hook's law is useful for modeling the stresses and strains in a bar. However, it is useful to introduce the term, Poisson's ration. Poisson's ratio is defined in Eq. (C.4)

$$\text{Poissons ratio } (\nu) = \frac{\text{Latitudal strain}}{\text{Longitudial strain}} = \frac{-\delta d / d}{\delta L / L} \tag{C.4}$$

ν=poissons ratio []
δd = change in diameter [m]
d = original diameter [m]

By using Hook's law the strains in the different directions can be expressed as shown in Appendix Table 1.

Appendix Table 1: Strain in different directions by use of Hook's law

Strain in x direction resulting from:	$\frac{\sigma_x}{E}$
Strain in y direction resulting from	$\frac{\sigma_y}{E}$
Strain in x direction resulting from	$-\upsilon\frac{\sigma_y}{E}$
Strain in y direction resulting from	$-\upsilon\frac{\sigma_x}{E}$

Using the strains from Appendix Table 1, two-directional strain can be obtained

$$\varepsilon_x = \frac{\sigma_x}{E} - \upsilon\frac{\sigma_y}{E} = \frac{1}{E}(\sigma_x - \upsilon\cdot\sigma_y) \tag{C.5}$$

$$\varepsilon_y = \frac{\sigma_y}{E} - \upsilon\frac{\sigma_x}{E} = \frac{1}{E}(\sigma_y - \sigma_x\cdot\upsilon) \tag{C.6}$$

By including three dimensions and strain due to temperature change Eq. (C.5) and (C.6) becomes Eq. (C.7)-Eq.(C.9).

$$\varepsilon_x = \frac{\sigma_x}{E} - \upsilon\frac{\sigma_y}{E} - \upsilon\frac{\sigma_z}{E} + \alpha\Delta T = \frac{1}{E}\left[\sigma_x - \upsilon(\sigma_y + \sigma_z)\right] + \alpha\Delta T \tag{C.7}$$

$$\varepsilon_y = \frac{\sigma_y}{E} - \upsilon\frac{\sigma_x}{E} - \upsilon\frac{\sigma_z}{E} + \alpha\Delta T = \frac{1}{E}\left[\sigma_y - \upsilon(\sigma_x + \sigma_z)\right] + \alpha\Delta T \tag{C.8}$$

$$\varepsilon_z = \frac{\sigma_z}{E} - \upsilon\frac{\sigma_y}{E} - \upsilon\frac{\sigma_x}{E} + \alpha\Delta T = \frac{1}{E}\left[\sigma_z - \upsilon(\sigma_x + \sigma_y)\right] + \alpha\Delta T \tag{C.9}$$

Where,

α = coefficient of linear thermal expansion

ΔT =change in temperature

Appendix D

Development of Lamé's Theory

This sections purpose is to describe the development of Lamé's equation for thick-walled cylinders. This information is mainly collected from Hearn (1997), due to the good description of the theory.

Considering a cylinder with stresses acting on an element with length L and radius r, as shown in Appendix Figure 3 and Appendix Figure 4. The radial equilibrium of the element can be expressed as Eq. (D.1)

$$(\sigma_r + d\sigma_r)(r+dr)d\theta \cdot 1 - \sigma_r \cdot r d\theta \cdot 1 = 2\sigma_H \cdot dr \cdot 1 \cdot \sin\left(\frac{d\theta}{2}\right) \tag{D.1}$$

For small angles Eq.(D.2) is applicable

$$\sin\frac{\theta}{2} \approx \frac{\theta}{2} radians \tag{D.2}$$

By neglecting second-order small quantities, a simplification of Eq. (D.1) can be developed by using the assumption as shown in Eq. (D.2). This is shown in Eq.(D.3)

$$(\sigma_r \cdot r + d\sigma_r \cdot r + \sigma_r \cdot dr + d\sigma_r \cdot \mathrm{d}\theta) \cdot d\theta - \sigma_r r d\theta = 2\sigma_H \cdot dr \cdot \frac{d\theta}{2}$$

Simplifying, by neglecting second order small quanitity

$$\sigma_r \cdot r + d\sigma_r \cdot r + \sigma_r \cdot dr + d\sigma_r \cdot \mathrm{d}\theta - \sigma_r r = \sigma_H \cdot dr$$

$$d\sigma_r \cdot r + \sigma_r \cdot dr = \sigma_H \cdot dr$$

Reconstructing

$$\sigma_H - \sigma_r = r\frac{d\sigma_r}{dr} \tag{D.3}$$

Assuming constant axial strain ε_L and axial stress σ_L at points remote from the ends

$$\varepsilon_L = \frac{1}{E} \cdot \left[\sigma_L - \upsilon(\sigma_r + \sigma_H)\right] = \text{constant} \tag{D.4}$$

$$\sigma_r + \sigma_H = \text{constant} = 2\text{A(say)} \tag{D.5}$$

Substituting in Eq.(D.5) for σ_H in Eq.(D.3), Eq. (D.6) can be developed

$$2A - \sigma_r - \sigma_r = r\frac{d\sigma_r}{dr} \tag{D.6}$$

Multiplying through by r, and rearranging

$$2\sigma_r r + r^2\frac{d\sigma_r}{dr} - 2Ar = 0$$

$$\frac{d}{dr}(\sigma_r r^2 - Ar^2) = 0$$

Therefore, integrating

$$\sigma_r r^2 - Ar^2 = \text{constant} = \text{-B(say)} \tag{D.7}$$

From Eq.(D.7) and (D.6) Eq. (D.8) can be developed

$$\sigma_r = A - \frac{B}{r^2}$$

$$\sigma_H = A + \frac{B}{r^2} \tag{D.8}$$

Where,

σ_r = Radial Stress [Pa]
σ_H = Hoop Stress [Pa]
A = Lamé constan A
B = Lamé constan B
r = radius [m]

Eq. (D.8) can be used for different r, to determine hoop and radial stresses in a thick-walled cylinder. The constants A and B are determined for different boundary conditions. This Equation is referred to as Eq. (2.3) in the theory.

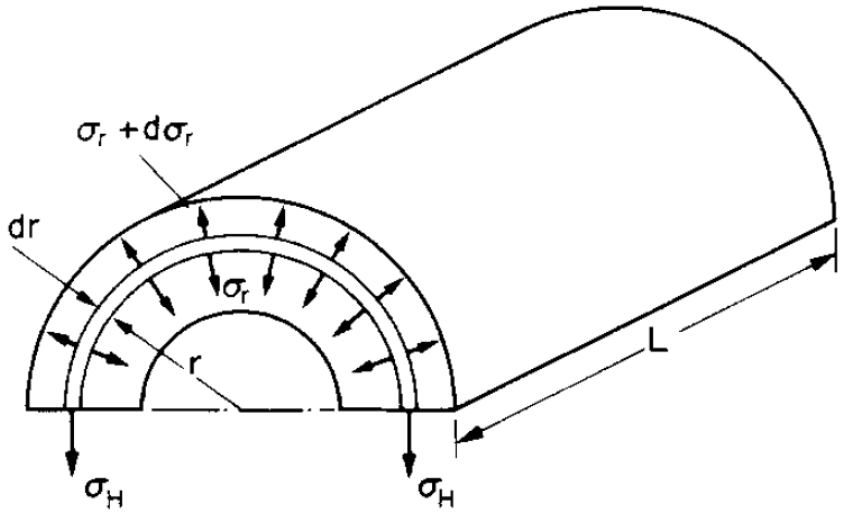

Appendix Figure 3: Stresses acting on a cylinder (Hearn, 1997)

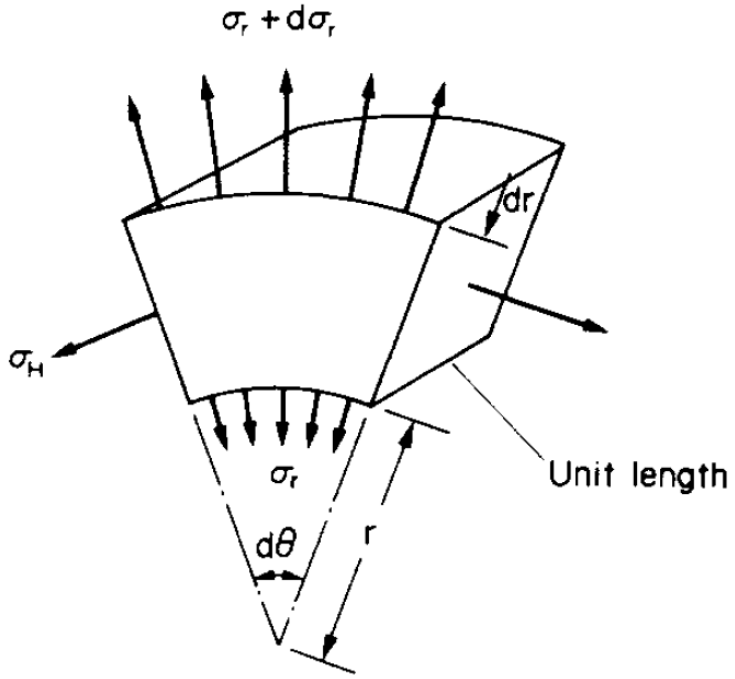

Appendix Figure 4: Stresses acting on an element of the cylinder wall (Hearn, 1997)

Appendix E

Derivation of Contact Pressures

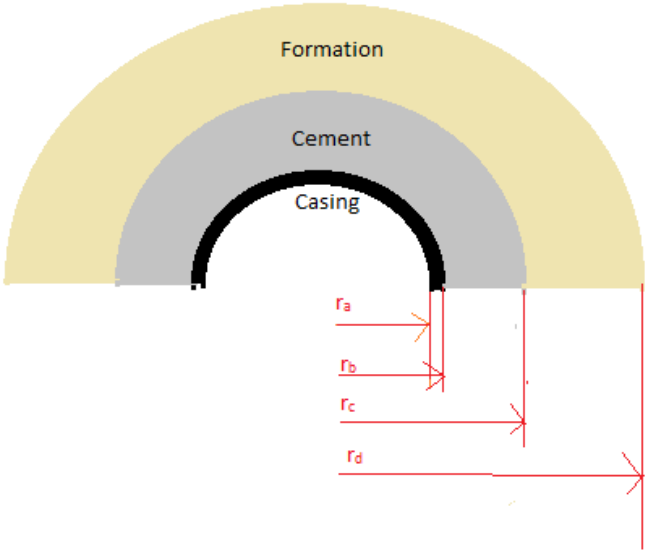

Appendix Figure 5: Casing-cement-formation system with respective radii, free from De Andrade (2015)

This derivation is developed through conversation with Jesus De Andrade.

In order derive the contact pressures, Lamé's equation has to be used. This is done by assuming that the radial displacement is equal for the cement (δcem) and the casing (δcasing) and that there is no axial movement. This is shown through Appendix Figure 6 and (E.1)

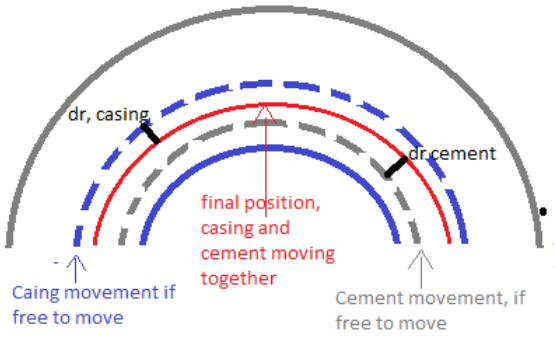

Appendix Figure 6: Thermal expansion of a compound cylinder with the final position of the casing-cement interface, free from De Andrade (2015)

$$\delta r_{cement} - \delta r_{casing} = 0 \tag{E.1}$$

To be able to derive the contact pressure from Eq. (E.1) it is necessary to develop an expression for the strain in the cement, casing and formation and implement it into the casing, formation and cement system.

Developing an expression for the strain in the cement, casing and formation

First, writing Hook's law for axial and hoop strain

$$\varepsilon_H = \frac{1}{E}\left[\sigma_H - \upsilon\left(\sigma_L - \sigma_r\right)\right] + \alpha\Delta T \tag{E.2}$$

$$\varepsilon_L = \frac{1}{E}\left[\sigma_L - \upsilon\left(\sigma_H - \sigma_r\right)\right] + \alpha\Delta T \tag{E.3}$$

With the assumption that strain in axial direction is negligible.

$$\varepsilon_L = 0 \tag{E.4}$$

From Eq.(E.4), Eq.(E.5) can be developed assuming Hook's law

$$\sigma_L = \upsilon\left[\sigma_r + \sigma_H\right] - \alpha E\Delta T \tag{E.5}$$

Substituting Eq.(E.5) in Eq.(E.2)

$$\varepsilon_H = \frac{1}{E}\left[\sigma_H \cdot (1-\upsilon^2) - (\upsilon+\upsilon^2)\cdot\sigma_r + (1+\upsilon)\cdot\alpha E\Delta T\right] \tag{E.6}$$

Finding contact pressures

Following, a derivation of the contact pressures is shown. These are used in Eq. (2.10)-Eq.(2.12).

Expressing Eq. (E.6) in terms of strain in casing and in cement as shown in Eq.(E.7) and Eq.(E.8) respectively

$$\varepsilon_{casing} = \frac{1}{E_{steel}}\left[\sigma_H \cdot (1-\upsilon_{steel}{}^2) - (\upsilon_{steel} + \upsilon_{steel}{}^2)\cdot\sigma_r + (1+\upsilon_{steel})\cdot\alpha_{steel}E_{teel}\Delta T\right] \quad \text{(E.7)}$$

$$\varepsilon_{cement} = \frac{1}{E_{cement}}\left[\sigma_H \cdot (1-\upsilon_{cement}{}^2) - (\upsilon_{cement} + \upsilon_{cement}{}^2)\cdot\sigma_r + (1+\upsilon_{cement})\cdot\alpha_{cement}E_{cement}\Delta T\right] \quad \text{(E.8)}$$

Expressing Eq.(E.6) in terms if radial dispalcement δr

$$\delta r = \frac{r}{E}\left[\sigma_H \cdot (1-\upsilon^2) - (\upsilon + \upsilon^2)\cdot\sigma_r + (1+\upsilon)\cdot\alpha E\Delta T\right] \quad \text{(E.9)}$$

And in terms of casing (Eq.(E.10)), cement(in contact with casing) (Eq.(E.11)), cement (in contact with formation) (Eq. (E.12)) and formation Eq. ((E.13)) using the terms presented in Appendix Figure 5

$$\delta r_{casing} = \frac{r_b}{E_{steel}}\left\{\sigma_{H,casing}\cdot(1-\upsilon_{steel}{}^2) - (\upsilon_{steel} + \upsilon_{steel}{}^2)\cdot\sigma_{r,casing}\right\} + \left[(1+\upsilon_{steel})\,\mathrm{r_b}\,\alpha_{steel}\Delta T_1\right] \quad \text{(E.10)}$$

$$\delta r_{cement} = \frac{r_b}{E_{cement}}\left\{\sigma_{H,cement}\cdot(1-\upsilon_{cement}{}^2) - (\upsilon_{cement} + \upsilon_{cement}{}^2)\cdot\sigma_{r,cement}\right\} + \left[(1+\upsilon_{cement})\,\mathrm{r_b}\,\alpha_{cement}\Delta T_2\right] \quad \text{(E.11)}$$

$$\delta r_{cement} = \frac{r_c}{E_{cement}}\left\{\sigma_{H,cement}\cdot(1-\upsilon_{cement}{}^2) - (\upsilon_{cement} + \upsilon_{cement}{}^2)\cdot\sigma_{r,cement}\right\} + \left[(1+\upsilon_{cement})\,\mathrm{r_c}\,\alpha_{cement}\Delta T_3\right] \quad \text{(E.12)}$$

$$\delta r_{formation} = \frac{r_c}{E_{formation}}\left\{\sigma_{H,\,formation}\cdot(1-\upsilon_{formation}{}^2) - (\upsilon_{formation} + \upsilon_{formation}{}^2)\cdot\sigma_{r,\,formation}\right\} + \left[(1+\upsilon_{formation})\,\mathrm{r_b}\,\alpha_{formation}\Delta T_4\right]$$

(E.13)

Where,

$\delta r_{formation}$ = radial displacement of formation [m]
δr_{cement} = radial displacement of cement [m]
δr_{steel} = radial displacement of steel [m]
$E_{formation}$ = Young's Modulus formation [Pa]
E_{cement} = Young's Modulus cement [Pa]
E_{steel} = Young's Modulus steel [Pa]
$\sigma_{H,\,formation}$ = Hoop stress in the formation [Pa]
$\sigma_{H,cement}$ = Hoop stress in the cement [Pa]
$\sigma_{H,\text{steel}}$ = Hoop stress in the steel [Pa]
$\sigma_{\text{r},\,formation}$ = Radial stress in the formation [Pa]
$\sigma_{\text{r},cement}$ = Radial stress in the cement [Pa]
$\sigma_{\text{r,steel}}$ = Radial stress in the steel [Pa]
$\upsilon_{formation}$ = Possions ratio of the formation []
υ_{cement} = Possions ratio of the cement []
υ_{steel} = Possions ratio of the steel []
$\alpha_{formation}$ = coefficient of linear expansion for formation
α_{cement} = coefficient of linear expansion for cement
α_{steel} = coefficient of linear expansion for steel

ΔT_1 = Change in temperature in at ra [C°]
ΔT_2 = Change in temperature in at rb [C°]
ΔT_3 = Change in temperature in at rc [C°]
ΔT_4 = Change in temperature in at rd [C°]

By assuming that the radial displacement of the casing (Eq.(E.10)) is equal to the radial cement (Eq. (E.11)). And by inserting Eq. (2.6) in (terms of radius mentioned in Appendix Figure 5) for the hoop and radial stresses, one can be able to obtain the contact pressures which are used to obtain the radial and hoop stresses for all r through the casing, cement and formation.

First considering the casing and the cement (P_{c1})

Eq. (2.6) will then be converted to:

$$\sigma_{r,casing} = \frac{r_a^{\,2}P_i - r_b^{\,2}P_{c1}}{r_b^{\,2} - r_a^{\,2}} - \frac{\left(P_i - P_{c1}\right)r_a^{\,2}\cdot r_b^{\,2}}{\left(r_b^{\,2} - r_a^{\,2}\right)\cdot r_b^{\,2}}$$
$$\sigma_{H,casing} = \frac{r_a^{\,2}P_i - r_b^{\,2}P_{c1}}{r_b^{\,2} - r_a^{\,2}} + \frac{\left(P_i - P_{c1}\right)r_a^{\,2}\cdot r_b^{\,2}}{\left(r_b^{\,2} - r_a^{\,2}\right)\cdot r_b^{\,2}} \qquad \text{(E.14)}$$

Here, the radial and hoop stresses in the casing is expressed with regards to ra, rb, Pi and Pc1 (contact pressure). These equations represent the radial and hoop stresses at the contact between the casing and cement.

Second, considering the cement and the formation (P_{c2})

Eq. (2.6): will them be converted to

$$\sigma_{r,cement} = \frac{r_b^{\,2}P_{c1} - r_c^{\,2}P_{c2}}{r_c^{\,2} - r_b^{\,2}} - \frac{\left(P_{c1} - P_{c2}\right)r_b^{\,2}\cdot r_c^{\,2}}{\left(r_c^{\,2} - r_b^{\,2}\right)\cdot r_c^{\,2}}$$
$$\sigma_{H,cement} = \frac{r_b^{\,2}P_{c1} - r_c^{\,2}P_{c2}}{r_c^{\,2} - r_b^{\,2}} + \frac{\left(P_{c1} - P_{c2}\right)r_b^{\,2}\cdot r_c^{\,2}}{\left(r_c^{\,2} - r_b^{\,2}\right)\cdot r_c^{\,2}} \qquad \text{(E.15)}$$

Now, inserting Eq. (E.14) into (E.10)

$$\delta r_{casing} = \frac{r_b}{E_{steel}}\left\{\begin{array}{l}\left[\dfrac{r_a^{\,2}P_i - r_b^{\,2}P_{c1}}{r_b^{\,2} - r_a^{\,2}} + \dfrac{\left(P_i - P_{c1}\right)r_a^{\,2}\cdot r_b^{\,2}}{\left(r_b^{\,2} - r_a^{\,2}\right)\cdot r_b^{\,2}}\right]\cdot\left(1-\upsilon_{steel}^{\,2}\right) \\ -\left(\upsilon_{steel} + \upsilon_{steel}^{\,2}\right)\cdot\left[\dfrac{r_a^{\,2}P_i - r_b^{\,2}P_{c1}}{r_b^{\,2} - r_a^{\,2}} - \dfrac{\left(P_i - P_{c1}\right)r_a^{\,2}\cdot r_b^{\,2}}{\left(r_b^{\,2} - r_a^{\,2}\right)\cdot r_b^{\,2}}\right]\end{array}\right\} + \left[\left(1+\upsilon_{steel}\right)\mathrm{r_b}\,\alpha_{steel}\Delta T_1\right] \qquad \text{(E.16)}$$

and Eq.(E.15) into(E.11)

$$\delta r_{cement} = \frac{r_b}{E_{cement}} \left\{ \begin{array}{l} \left[\frac{r_b^{\,2} P_{c1} - r_c^{\,2} P_{c2}}{r_c^{\,2} - r_b^{\,2}} + \frac{\left(P_{c1} - P_{c2}\right) r_b^{\,2} \cdot r_c^{\,2}}{\left(r_c^{\,2} - r_b^{\,2}\right) \cdot r_c^{\,2}} \right] \cdot (1 - \upsilon_{cement}^{\,2}) \\ -(\upsilon_{cement} + \upsilon_{cement}^{\,2}) \cdot \left[\frac{r_b^{\,2} P_{c1} - r_c^{\,2} P_{c2}}{r_c^{\,2} - r_b^{\,2}} - \frac{\left(P_{c1} - P_{c2}\right) r_b^{\,2} \cdot r_c^{\,2}}{\left(r_c^{\,2} - r_b^{\,2}\right) \cdot r_c^{\,2}} \right] \end{array} \right\} + \left[(1 + \upsilon_{cement}) \, \mathrm{r_b} \, \alpha_{cement} \Delta T_2 \right]$$

(E.17)

Assuming that the radial expansion of the cement is equal the radial compaction of the casing,

$$\delta r_{cement} = \delta r_{casing} \tag{E.18}$$

Eq. (E.16)and Eq. (E.17) can be used to obtain Pc1.

However, Pc2 is also necessary to obtain.

Third, considering the cement and rock interface (contact pressure 2)

By using the radial and hoop stresses in the cement from Eq. (E.15) and the radial expansion of the cement connected to the formation (Eq. (E.12)), an equation for the radial expansion of the cement (in contact with the formation) can be obtained.

$$\delta r_{cement} = \frac{r_c}{E_{cement}} \left\{ \begin{array}{l} \left[\frac{r_b^{\,2} P_{c1} - r_c^{\,2} P_{c2}}{r_c^{\,2} - r_b^{\,2}} + \frac{\left(P_{c1} - P_{c2}\right) r_b^{\,2} \cdot r_c^{\,2}}{\left(r_c^{\,2} - r_b^{\,2}\right) \cdot r_c^{\,2}} \right] \cdot (1 - \upsilon_{cement}^{\,2}) \\ -(\upsilon_{cement} + \upsilon_{cement}^{\,2}) \cdot \left[\frac{r_b^{\,2} P_{c1} - r_c^{\,2} P_{c2}}{r_c^{\,2} - r_b^{\,2}} - \frac{\left(P_{c1} - P_{c2}\right) r_b^{\,2} \cdot r_c^{\,2}}{\left(r_c^{\,2} - r_b^{\,2}\right) \cdot r_c^{\,2}} \right] \end{array} \right\} + \left[(1 + \upsilon_{cement}) \, \mathrm{r_c} \, \alpha_{cement} \Delta T_3 \right]$$

(E.19)

Fourth, considering the rock interface (Pf)

Eq. (2.6) will them be converted to

$$\sigma_{r\ formation} = \frac{r_c^{\,2} P_{c2} - r_d^{\,2} P_f}{r_d^{\,2} - r_c^{\,2}} - \frac{\left(P_{c2} - P_f\right) r_c^{\,2} \cdot r_d^{\,2}}{\left(r_d^{\,2} - r_c^{\,2}\right) \cdot r_d^{\,2}}$$
$$\sigma_{H,\,formation} = \frac{r_c^{\,2} P_{c2} - r_d^{\,2} P_f}{r_d^{\,2} - r_c^{\,2}} + \frac{\left(P_{c2} - P_f\right) r_c^{\,2} \cdot r_d^{\,2}}{\left(r_d^{\,2} - r_c^{\,2}\right) \cdot r_d^{\,2}} \qquad \text{(E.20)}$$

Where Pf is formation pressure.

Inserting (E.20) into Eq.(E.13)

$$\delta r_{formation} = \frac{r_c}{E_{formation}} \left\{ \begin{array}{l} \left[\dfrac{r_c^{\,2} P_{c2} - r_d^{\,2} P_f}{r_d^{\,2} - r_c^{\,2}} + \dfrac{\left(P_{c2} - P_f\right) r_c^{\,2} \cdot r_d^{\,2}}{\left(r_d^{\,2} - r_c^{\,2}\right) \cdot r_d^{\,2}} \right] \cdot (1 - \upsilon_{formation}^{\,2}) - \\ (\upsilon_{formation} + \upsilon_{formation}^{\,2}) \cdot \left[\dfrac{r_c^{\,2} P_{c2} - r_d^{\,2} P_f}{r_d^{\,2} - r_c^{\,2}} - \dfrac{\left(P_{c2} - P_f\right) r_c^{\,2} \cdot r_d^{\,2}}{\left(r_d^{\,2} - r_c^{\,2}\right) \cdot r_d^{\,2}} \right] \end{array} \right\} + \left[(1 + \upsilon_{formation})\, \mathrm{r_b}\, \alpha_{formation} \Delta T_4 \right]$$

(E.21)

Assuming that the radial displacement of respectively the cement and the formation is equal

$$\delta r_{cement} = \delta r_{formation} \qquad \text{(E.22)}$$

Eq. (E.19)an Eq. (E.21)can be used to obtain Pc2.

Two equations ((E.22) and (E.18)) containing two unknowns (Pc1 and Pc2) are possible to solve. Appendix A shows the symbolic equation, and the calculation method.

Where,

$\sigma_{r\ formation}$ = Radial stress in formation [Pa]

$\sigma_{H,\ formation}$ = Hoop stress in formation [Pa]

$\sigma_{\mathrm{r,cement}}$ = Radial stress in cement [Pa]

$\sigma_{H,\mathrm{cement}}$ = Hoop stress in cement [Pa]

$\sigma_{\mathrm{r,casing}}$ = Radial stress in casing [Pa]

$\sigma_{\mathrm{H,casing}}$ = Hoop stress in casing [Pa]

r_a = inner radius of casing [m]

r_b = outer radius casing/inner radius cement [m]

r_c = outer radius formation [m]

r_d = outer radius formation [m]

P_i = Change in internal pressure in casing [Pa]

P_{c1} = Contact pressure at r_b interface [Pa]

P_{c2} = Contact pressure at r_c interface [Pa]

P_f = Change in external (formation) pressure [Pa]

Appendix F

Industry Leading Software (ILS) Cement Considerations

The ILS software considered in this thesis is only considering the cement in terms of external pressure profiles. For production loads, several external pressure profiles can be selected, and several options are available for each profile. The different external pressure profiles are 'Fluid gradient (w/pore pressure)', 'Mud and Cement mix-water', 'Minimum formation pore pressure', 'Permeable zones', 'Mud and cement slurry', 'Pore pressure with seawater gradient' and 'Minimum formation pore pressure with backup option'. Appendix Table 2 shows the different external profiles and the different options available. The external pressure profile 'Permeable zones' enable choosing "Poor cement" as an option. The ILS assumes that no zonal isolation has been achieved for any permeable zones if "poor cement" is enabled. Pressure communication occurs anywhere along the casing string cement column. Cement mix-water density is used above and below the permeable zones allowing for linear pressure profile from the permeable zone (Landmark, 2001).

The different options for each external profile are shown in Appendix Table 2.

Appendix Table 2: External pressure profile options in ILS

EXTERNAL PRESSURE PROFILES	OPTIONS AVAILABLE FOR THE PRESSURE PROFILE
FLUID GRADIENT (W/PORE PRESSURE)	- Mud weight above TOC - Fluid gradient below TOC - WH pressure *Pore pressure in open hole *Deteriorated mud
MUD AND CEMENT MIX-WATER	- Wellhead pressure *Deteriorated mud
MINIMUM FORMATION PORE PRESSURE	*Allow mud drop *Deteriorated mud - Wellhead pressure
PERMEABLE ZONES	***Poor cement** *Deteriorated mud - Wellhead pressure
MUD AND CEMENT SLURRY	No options
PORE PRESSURE WITH SEAWATER GRADIENT	- Sea water gradient
MINIMUM FORMATION PORE PRESSURE WITH BACKUP OPTION	- Cement backup in cased hole - Cement back up in open hole

*= enable or not enable

- =choose value or other options

Appendix G
Failure Criteria

Tresca Criterion (maximum shear stress)

The Tresca failure criterion is the simplest shear failure criterion based on Mohr's circle of stress. It is assumed that failure will occur when a critical value, the cohesion, is surpassed by the maximum shear failure inside any plane of the rock. Hence, the Tresca criterion is also referred to as the maximum shear stress theory (Hearn, 1997). By taking sign and the possibility that one of the stresses may be zero, the maximum shear stress can be found through the following equation:

$$\tau_{\max} = \frac{\sigma_1 - \sigma_3}{2} = c \tag{G.1}$$

Where,

$\frac{c_o}{2} = c$ (cohesion) $[Pa]$

$c_o =$ Uniaxial compressive strength [Pa]

The Tresca failure envelope takes the form of a regular hexagon in the three dimensional principal stress space. When the internal angle of friction is zero, the Tresca failure criterion is considered a special case of the Mohr-Coulomb criterion (Rahimi, 2014 p. 7). Hence, the Tresca criterion can be expressed as:

$$\sigma_1 = C_o + \sigma_3 \cdot q \tag{G.2}$$

When $\varphi = 0$,

$q = \frac{(1+\sin\varphi)}{(1-\sin\varphi)} = 1$

and

$Co = \sigma_1 - \sigma_3$

The Tresca criterion is mostly applicable for very ductile materials, and not so much for brittle materials. The Von Mises criterion is often preferred over the Tresca criterion. Hence, the Tresca criterion is mostly used as a historical reference.

Mohr-Coulomb Criterion

In the Mohr-Coulomb criterion the materials cohesion and a factor corresponding to the coefficient of friction multiplied with the effective normal stress to the failure plane, are working against the shear stress for compressive failure (Nelson and Guillot, 2006p. 277). According to this criterion, rock failure will occur when:

$$|\tau| = Y_{co} - \tan\phi \cdot \sigma_n' \tag{G.3}$$

Where,

Y_{co} = Cohesion [Pa]

σ_n'=effective normal stress acting on the failure plane [Pa]

ϕ = angle of internal friction [radians]

The shear stress, τ, is written in terms of an absolute value, because the sign of τ only affects the sliding direction. In terms of principal effective stresses, the Mohr-Coulomb failure criterion is expressed by (Nelson and Guillot, 2006 p. 277):

$$\sigma_3' = -\sigma_c + \tan^2\left(\frac{\pi}{4} + \frac{\phi}{2}\right) \cdot (\sigma_1') \tag{G.4}$$

Where,

σ_3' = effective minimum principal stress [Pa]
σ_c = compression strength [Pa]
σ_1' = effective maximum principal stress $(\text{confining stress})[Pa]$

From Eq.(G.4) it can be seen that the compressive strength of the material will increase linearly with increasing confining pressure.

In terms of maximum, σ_1, and minimum, σ_3, principal stresses, the Mohr-Coulomb criterion can be expressed as (Rahimi, 2014 p.5):

$$\sigma_1 = C_0 + \sigma_3 \cdot q \tag{G.5}$$

Where,

$$C_0 = 2c \cdot \frac{\cos\phi}{1-\sin\phi}$$

C_0 = uniaxial compressive strength (UCS) (related to c and ϕ) [Pa]

$$q = \frac{1+\sin\phi}{1-\sin\phi}$$

q=flow factor (function of ϕ)[-]

Mogi-Coulomb Criterion

The Mogi-Coulomb criterion is not described with one specific function, but is assumed to be obtained experimentally (Al-Ajmi, 2006). Al-Ajmi and Zimmerman (2005) presents a linear relationship between the octahedral shear stress (τ_{oct}) and the mean stress ($\sigma_{m,2}$) through the following equations:

$$\tau_{oct} = A + B \cdot \sigma_{m,2} \tag{G.6}$$

Where,

A =intersection of the line on the τ_{oct} axis

B = inclination of the line

This relationship corresponds well to the polyaxial test data. The parameters A and B of the Mogi-Coulomb failure criterion are based on parameters from the Mohr-Coulomb criterion. The relationship between the Mohr-Coulomb parameters, C_0 and q, and the Mogi-Coulomb parameters, A and B, is seen in the equations below:

$$A = \frac{2\sqrt{2}}{3} \cdot \frac{C_0}{(q+1)} \tag{G.7}$$

$$B = \frac{2\sqrt{2}}{3} \cdot \frac{(q-1)}{(q+1)} \tag{G.8}$$

The linear Mogi-Coulomb criterion and the Mohr-Coulomb criterion of failure in the conventional triaxial state of stress are equal. Hence, the Mogi-Coulomb criterion can be

perceived as an extension of the Mohr-Coulomb criterion in the true triaxial space (Rahimi, 2014 p. 7).

Appendix H

Plots for the Sensitivity analyses

For all plots where the legends are not described extensively: the first number represents the value for the cement, the second number is the value for the formation, while the last number is the temperature change.

H.1 Young's Modulus

H.1.1 Debonding

At rb

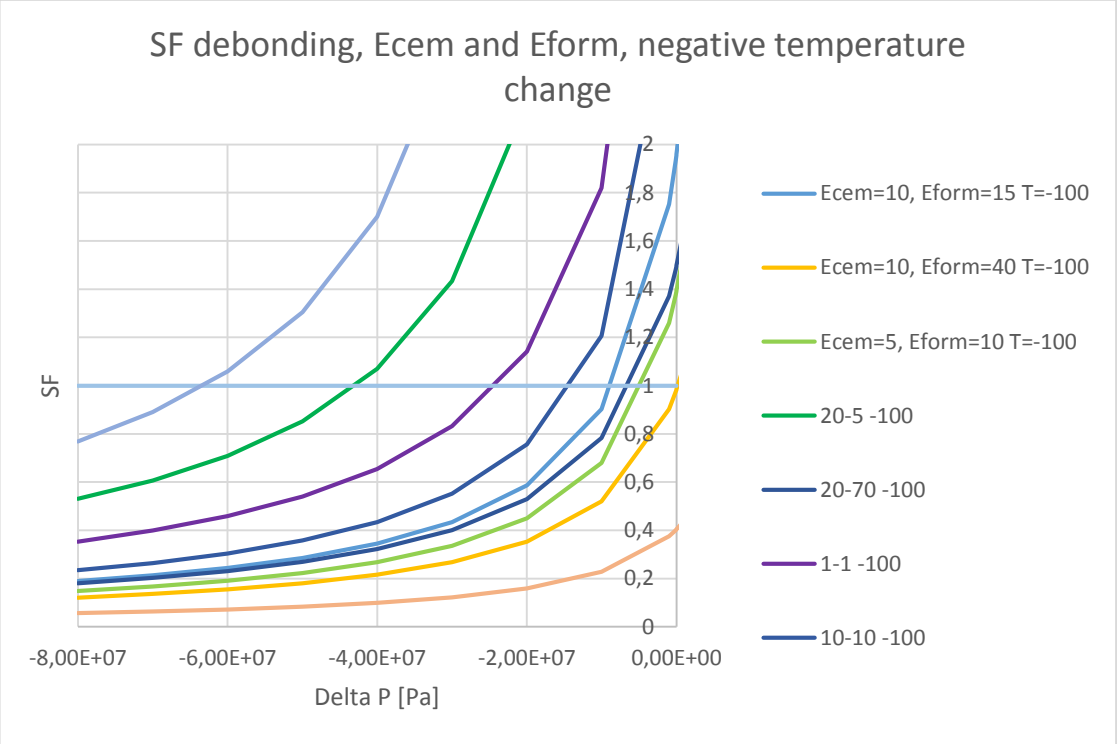

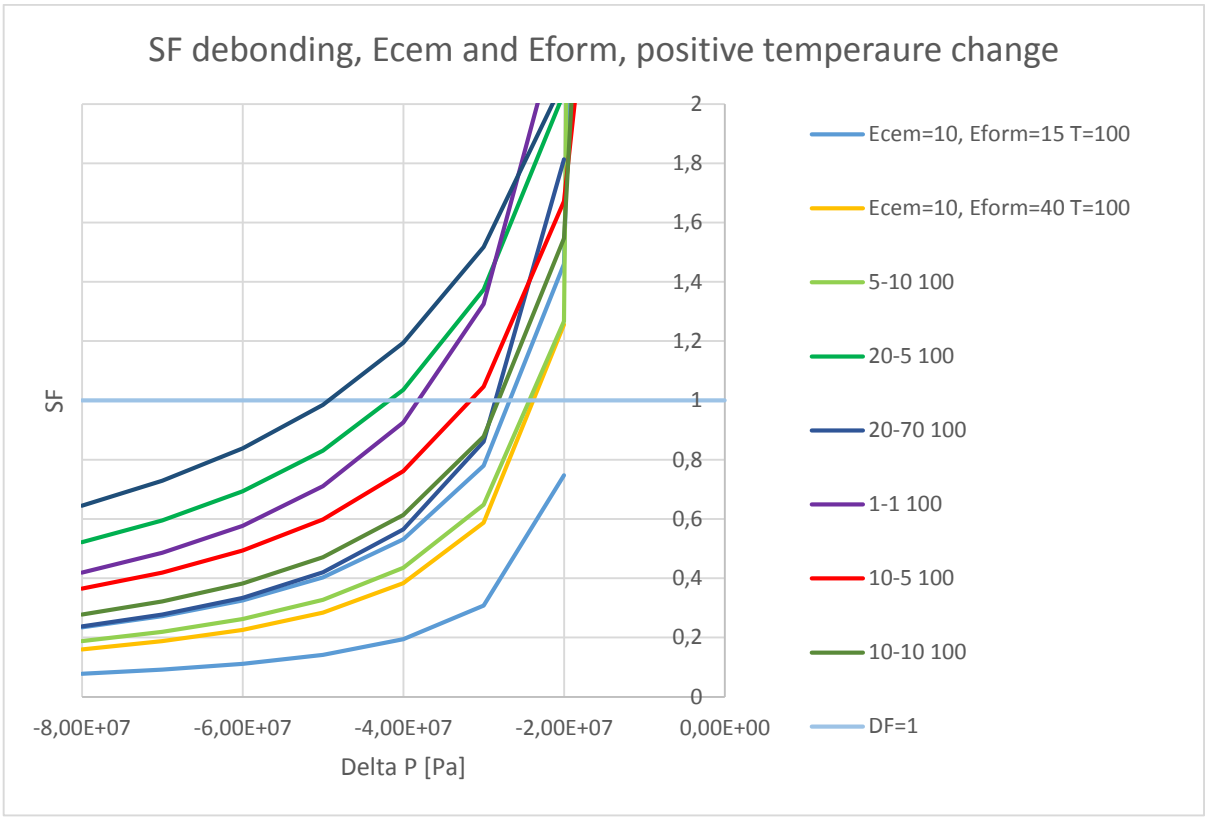
SF debonding, Ecem and Eform, positive temperaure change
SF
2
1,8
1,6
1,4
1,2
1
0,8
0,6
0,4
0,2
0
-8,00E+07
-6,00E+07
-4,00E+07
-2,00E+07
0,00E+00
Delta P [Pa]
Ecem=10, Eform=15 T=100
Ecem=10, Eform=40 T=100
5-10 100
20-5 100
20-70 100
1-1 100
10-5 100
10-10 100
DF=1

At r_c

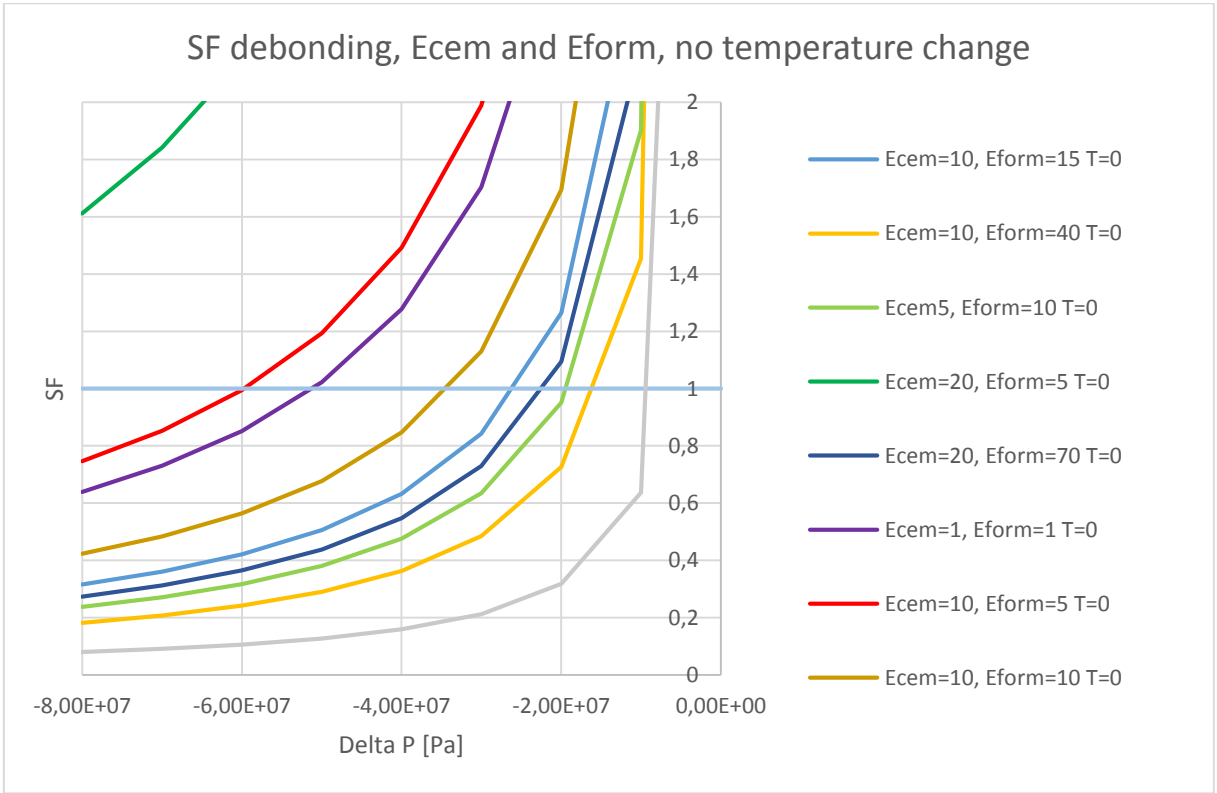
SF debonding, Ecem and Eform, no temperature change
SF
2
1,8
1,6
1,4
1,2
1
0,8
0,6
0,4
0,2
0
-8,00E+07
-6,00E+07
-4,00E+07
-2,00E+07
0,00E+00
Delta P [Pa]
Ecem=10, Eform=15 T=0
Ecem=10, Eform=40 T=0
Ecem5, Eform=10 T=0
Ecem=20, Eform=5 T=0
Ecem=20, Eform=70 T=0
Ecem=1, Eform=1 T=0
Ecem=10, Eform=5 T=0
Ecem=10, Eform=10 T=0

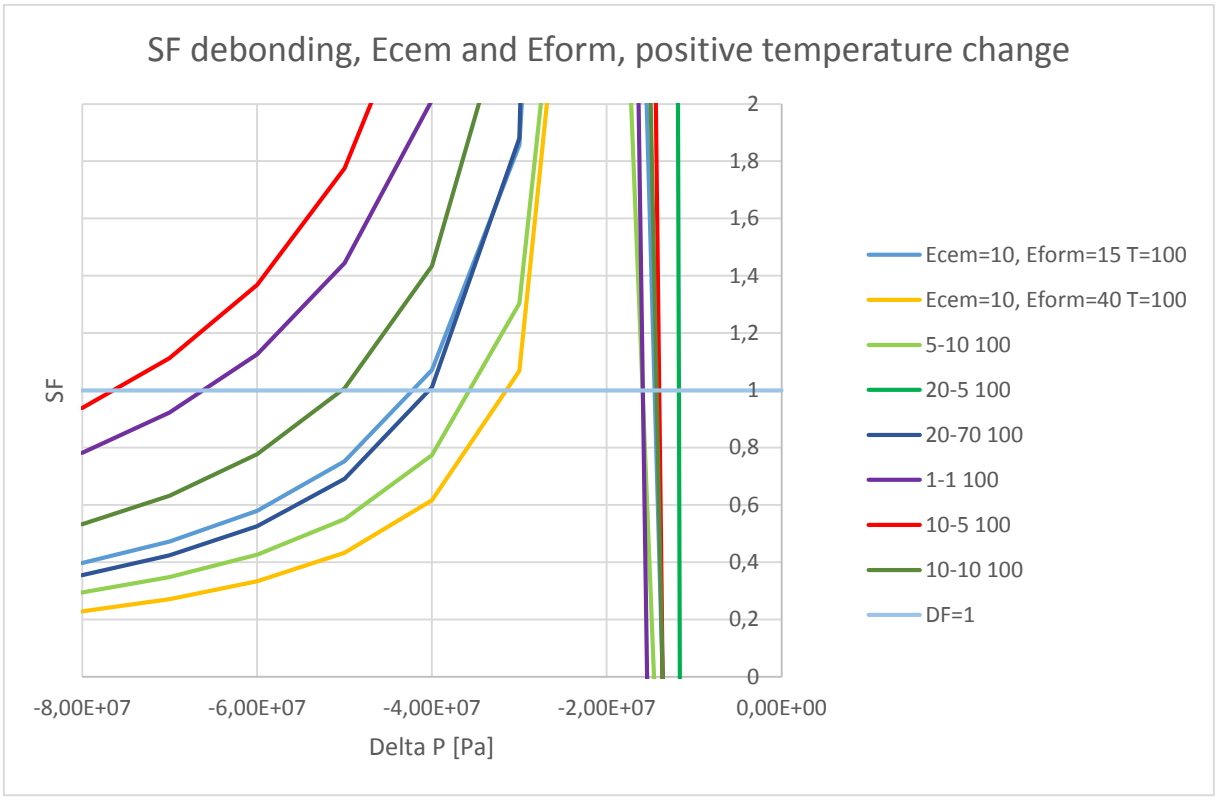
SF debonding, Ecem and Eform, positive temperature change
SF
2
1,8
1,6
1,4
1,2
1
0,8
0,6
0,4
0,2
0
-8,00E+07
-6,00E+07
-4,00E+07
-2,00E+07
0,00E+00
Delta P [Pa]
Ecem=10, Eform=15 T=100
Ecem=10, Eform=40 T=100
5-10 100
20-5 100
20-70 100
1-1 100
10-5 100
10-10 100
DF=1

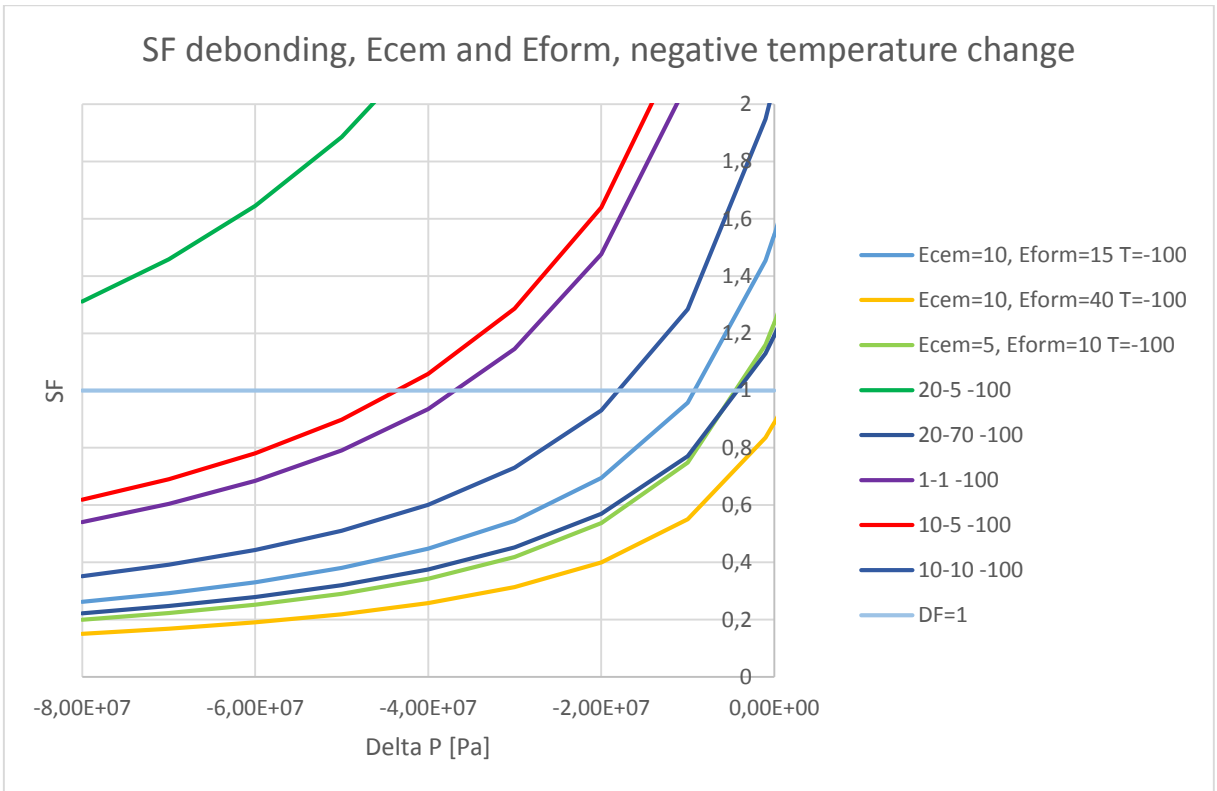
SF debonding, Ecem and Eform, negative temperature change
SF
2
1,8
1,6
1,4
1,2
1
0,8
0,6
0,4
0,2
0
-8,00E+07
-6,00E+07
-4,00E+07
-2,00E+07
0,00E+00
Delta P [Pa]
Ecem=10, Eform=15 T=-100
Ecem=10, Eform=40 T=-100
Ecem=5, Eform=10 T=-100
20-5 -100
20-70 -100
1-1 -100
10-5 -100
10-10 -100
DF=1

H.1.2 Radial Crack

At rb

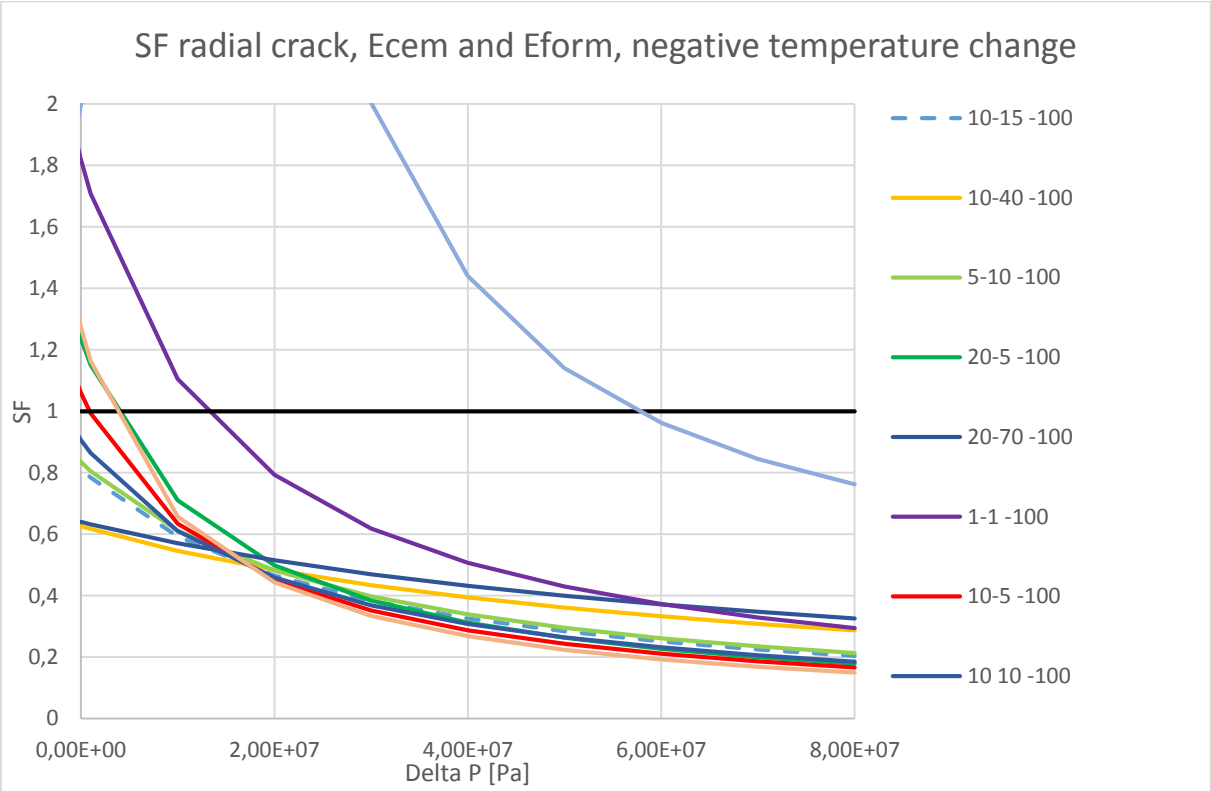

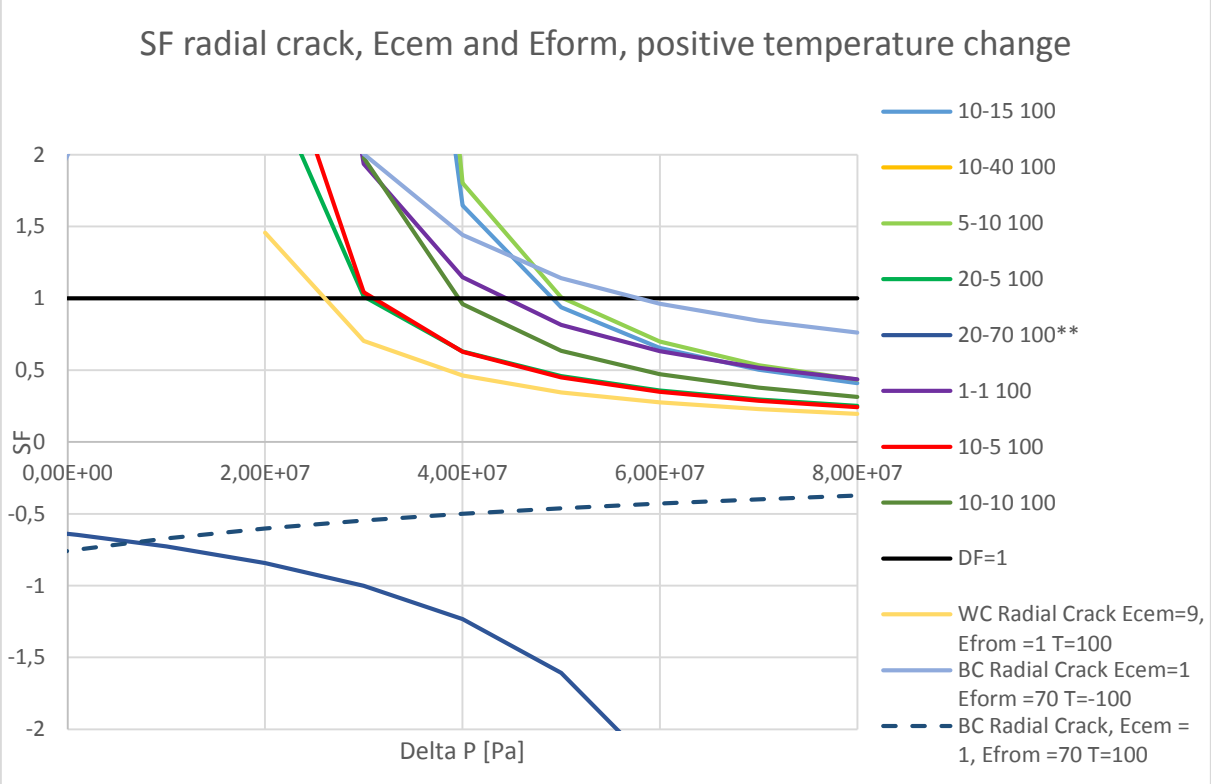

At r_c

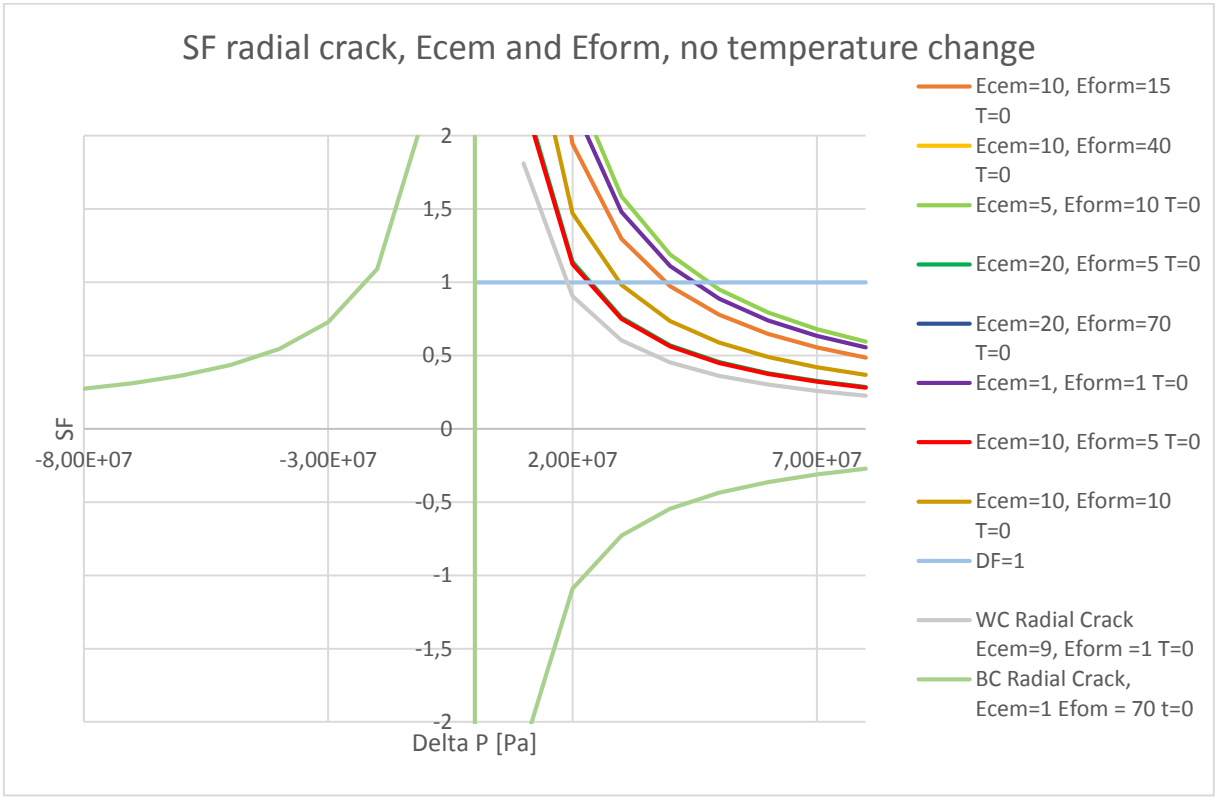
SF radial crack, Ecem and Eform, no temperature change
SF
Delta P [Pa]
-8,00E+07
-3,00E+07
2,00E+07
7,00E+07
2
1,5
1
0,5
0
-0,5
-1
-1,5
-2
Ecem=10, Eform=15 T=0
Ecem=10, Eform=40 T=0
Ecem=5, Eform=10 T=0
Ecem=20, Eform=5 T=0
Ecem=20, Eform=70 T=0
Ecem=1, Eform=1 T=0
Ecem=10, Eform=5 T=0
Ecem=10, Eform=10 T=0
DF=1
WC Radial Crack Ecem=9, Eform =1 T=0
BC Radial Crack, Ecem=1 Efom = 70 t=0

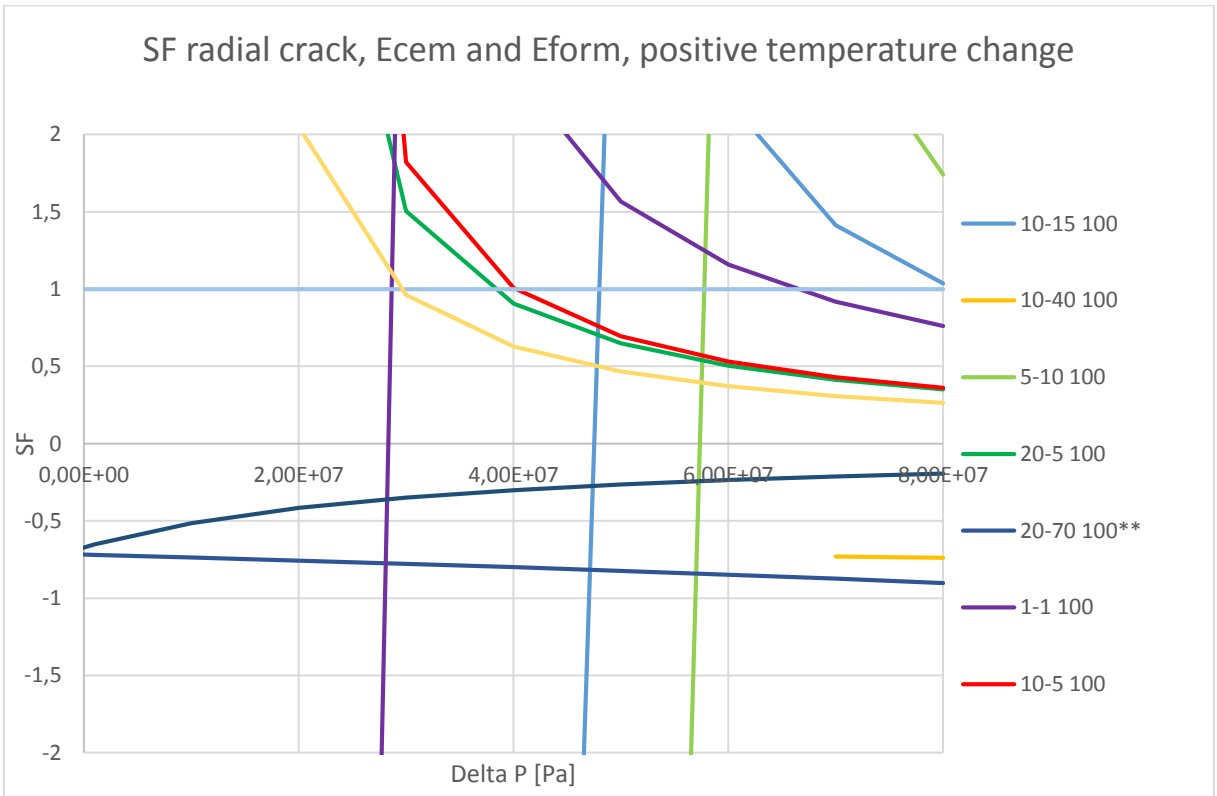
SF radial crack, Ecem and Eform, positive temperature change
SF
Delta P [Pa]
0,00E+00
2,00E+07
4,00E+07
6,00E+07
8,00E+07
2
1,5
1
0,5
0
-0,5
-1
-1,5
-2
10-15 100
10-40 100
5-10 100
20-5 100
20-70 100**
1-1 100
10-5 100

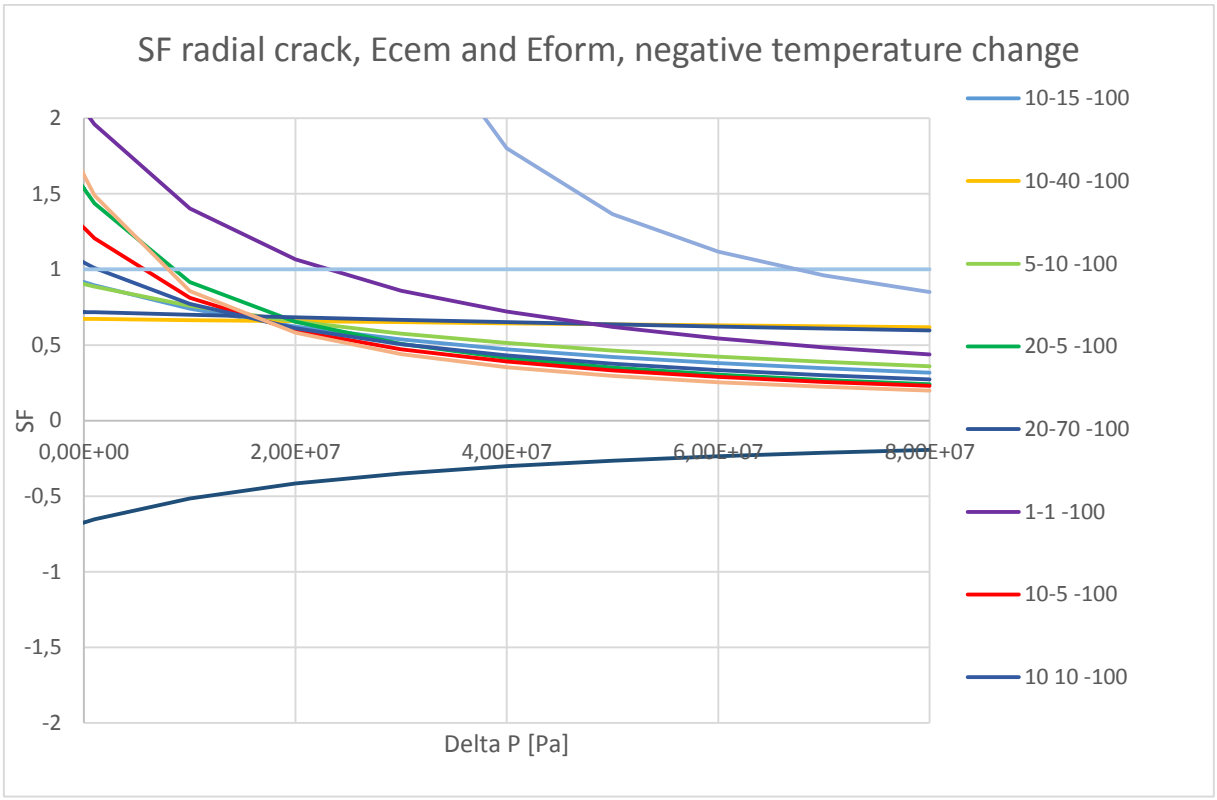

H.1.3 Shear Failure

At rb

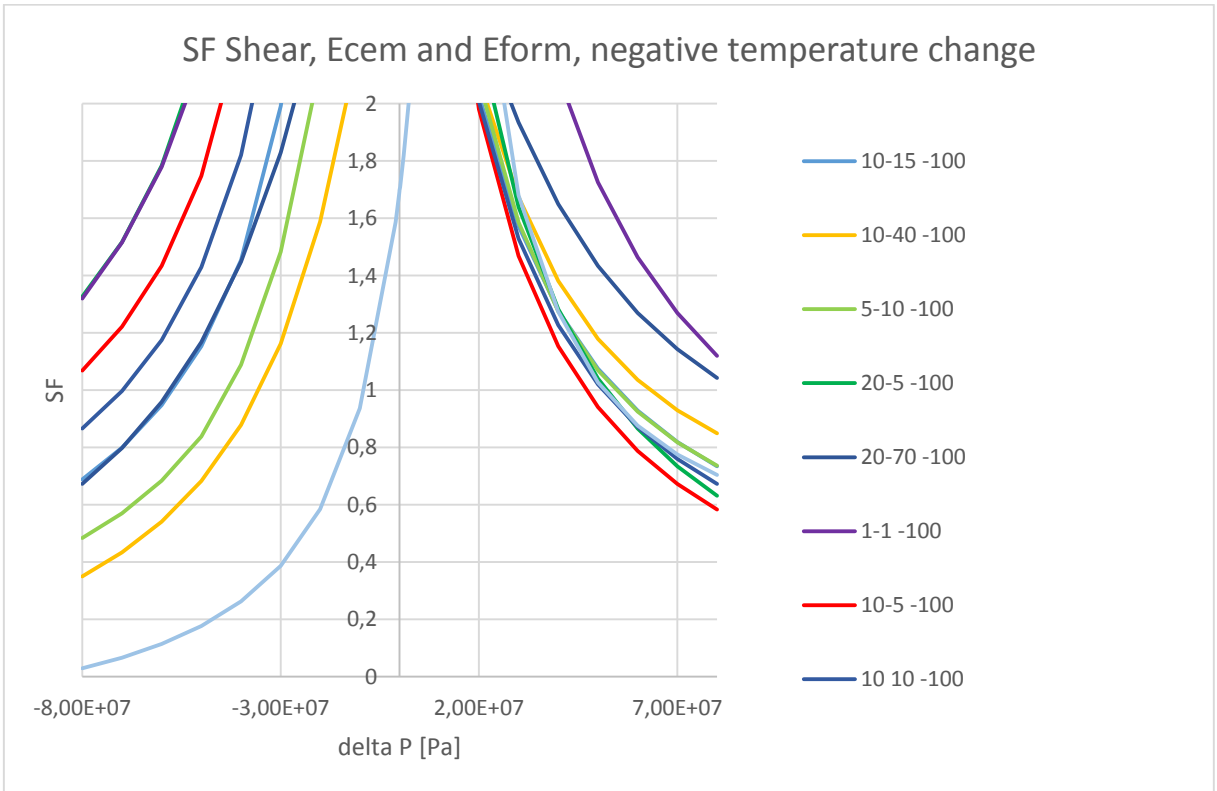

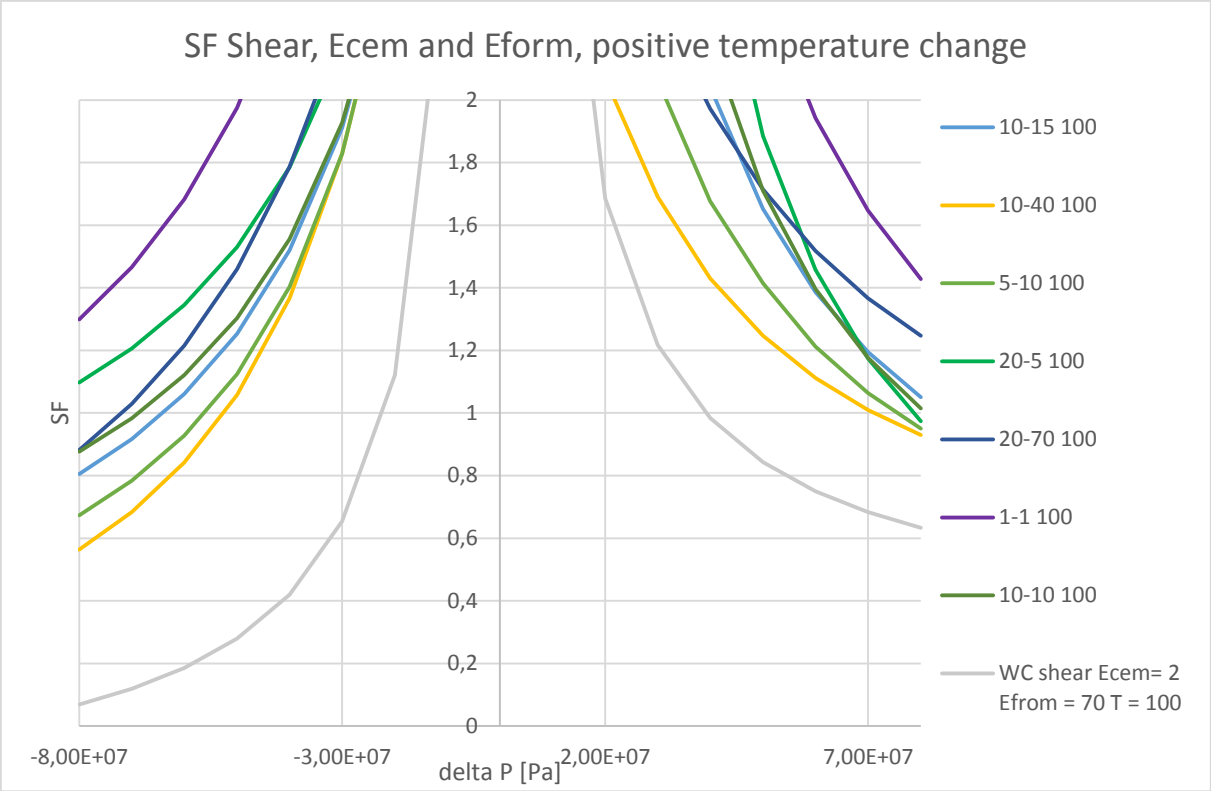
SF Shear, Ecem and Eform, positive temperature change
SF
2
1,8
1,6
1,4
1,2
1
0,8
0,6
0,4
0,2
0
-8,00E+07
-3,00E+07
2,00E+07
7,00E+07
delta P [Pa]
10-15 100
10-40 100
5-10 100
20-5 100
20-70 100
1-1 100
10-10 100
WC shear Ecem= 2
Efrom = 70 T = 100

At r_c

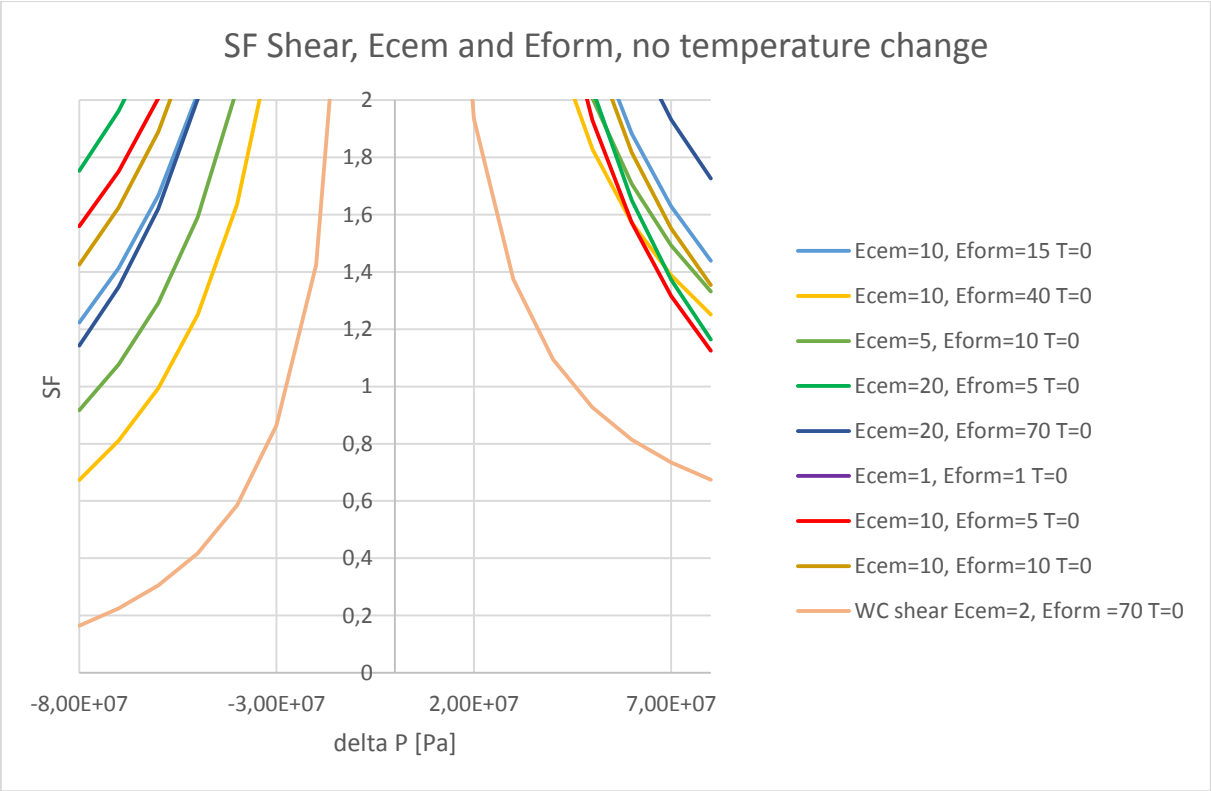
SF Shear, Ecem and Eform, no temperature change
SF
2
1,8
1,6
1,4
1,2
1
0,8
0,6
0,4
0,2
0
-8,00E+07
-3,00E+07
2,00E+07
7,00E+07
delta P [Pa]
Ecem=10, Eform=15 T=0
Ecem=10, Eform=40 T=0
Ecem=5, Eform=10 T=0
Ecem=20, Efrom=5 T=0
Ecem=20, Eform=70 T=0
Ecem=1, Eform=1 T=0
Ecem=10, Eform=5 T=0
Ecem=10, Eform=10 T=0
WC shear Ecem=2, Eform =70 T=0

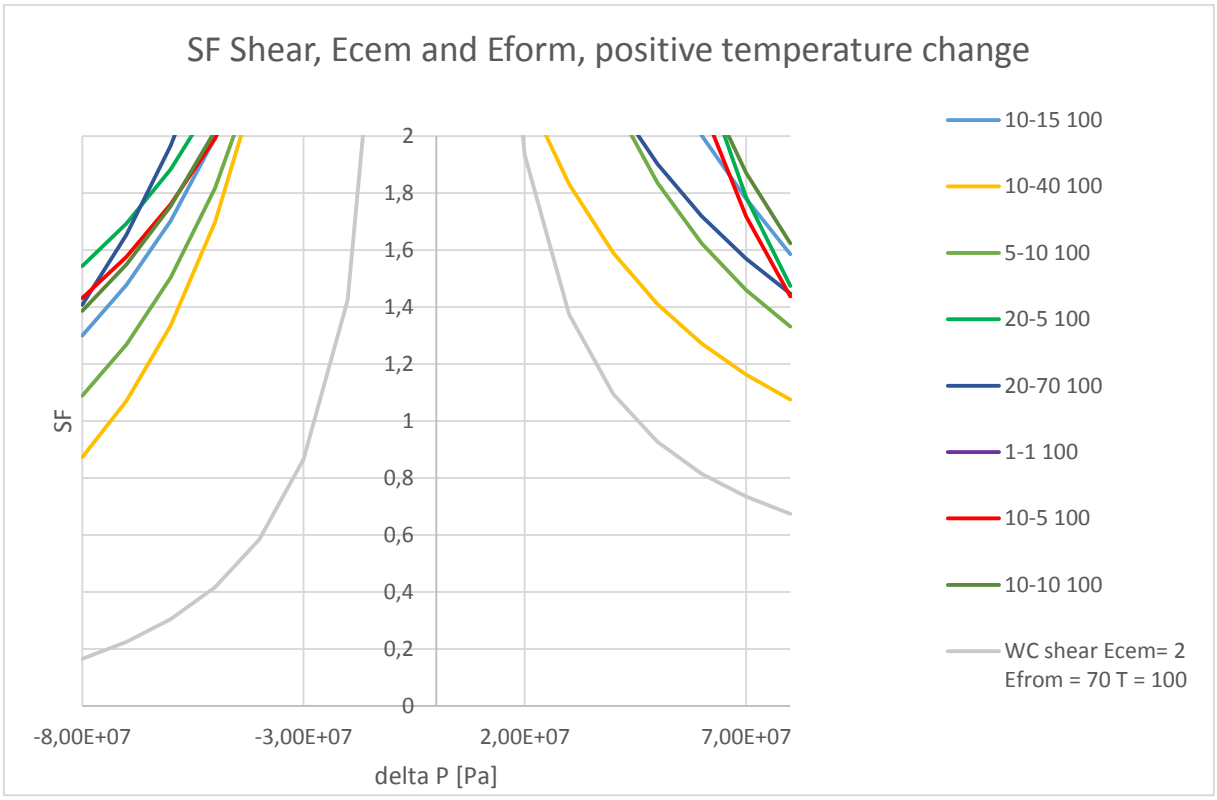
SF Shear, Ecem and Eform, positive temperature change
SF
2
1,8
1,6
1,4
1,2
1
0,8
0,6
0,4
0,2
0
-8,00E+07
-3,00E+07
2,00E+07
7,00E+07
delta P [Pa]
10-15 100
10-40 100
5-10 100
20-5 100
20-70 100
1-1 100
10-5 100
10-10 100
WC shear Ecem= 2
Efrom = 70 T = 100

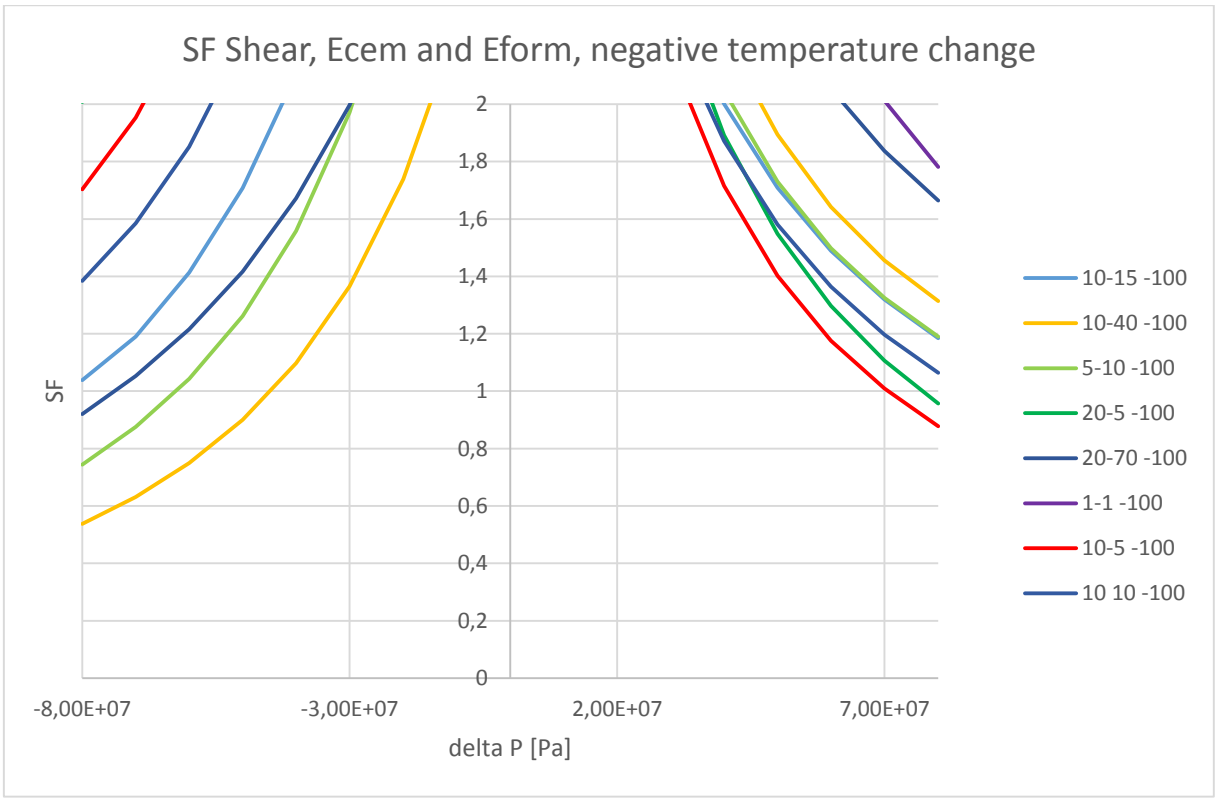
SF Shear, Ecem and Eform, negative temperature change
SF
2
1,8
1,6
1,4
1,2
1
0,8
0,6
0,4
0,2
0
-8,00E+07
-3,00E+07
2,00E+07
7,00E+07
delta P [Pa]
10-15 -100
10-40 -100
5-10 -100
20-5 -100
20-70 -100
1-1 -100
10-5 -100
10 10 -100

H.2 Poisson's Ratio

H.2.1 Debonding

At rb

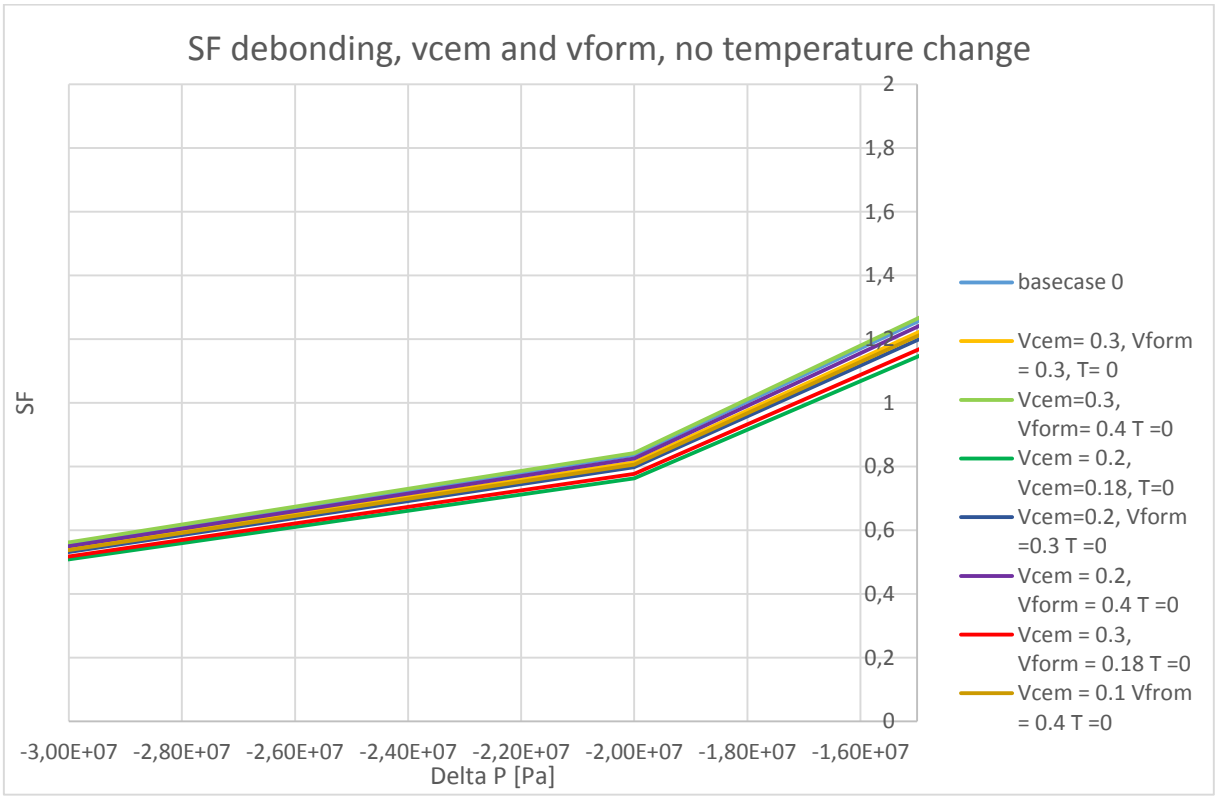

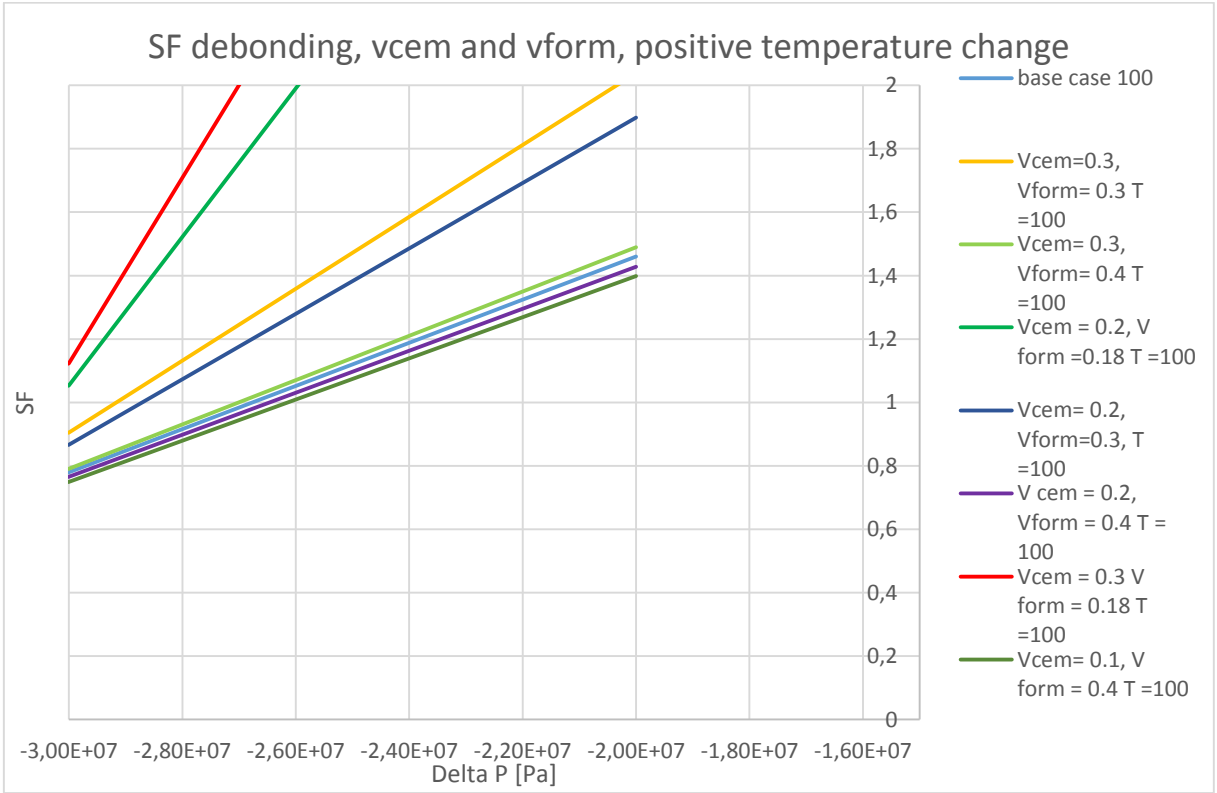

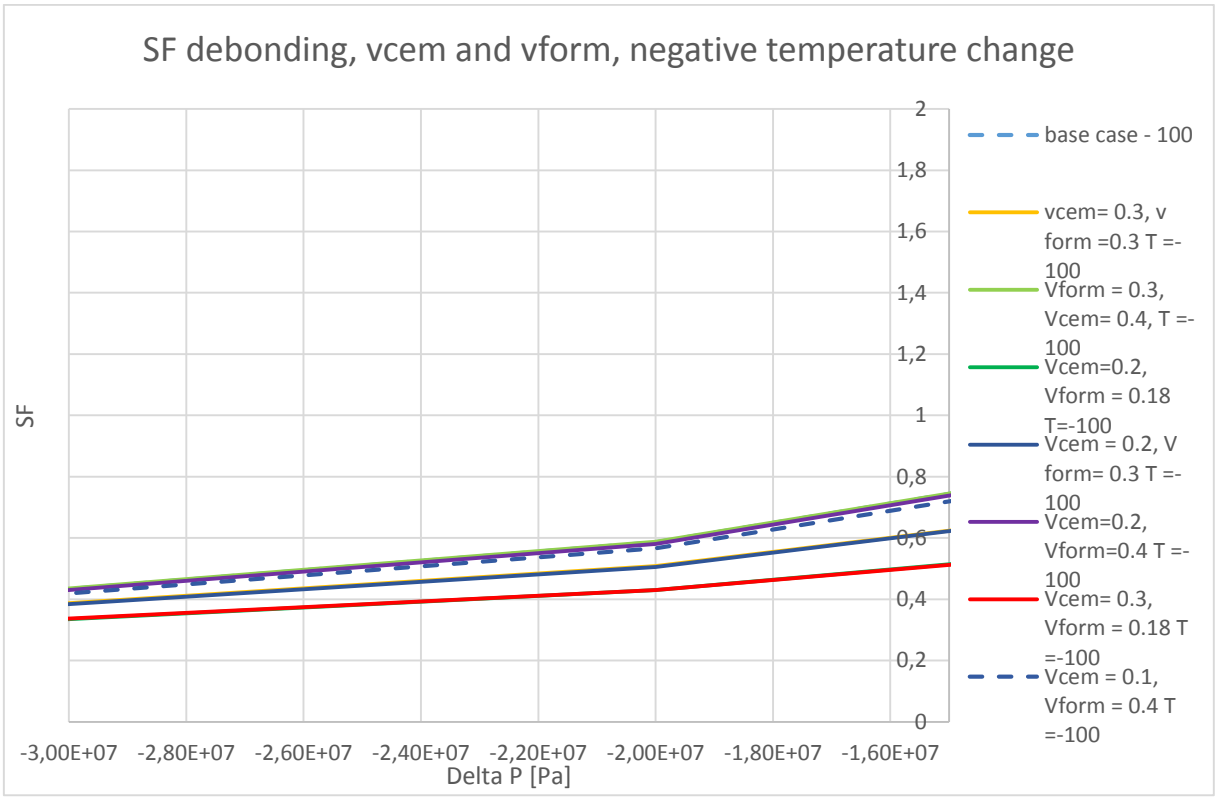
SF debonding, vcem and vform, negative temperature change
SF
Delta P [Pa]
-3,00E+07
-2,80E+07
-2,60E+07
-2,40E+07
-2,20E+07
-2,00E+07
-1,80E+07
-1,60E+07
0
0,2
0,4
0,6
0,8
1
1,2
1,4
1,6
1,8
2
base case - 100
vcem= 0.3, v form =0.3 T =-100
Vform = 0.3, Vcem= 0.4, T =-100
Vcem=0.2, Vform = 0.18 T=-100
Vcem = 0.2, V form= 0.3 T =-100
Vcem=0.2, Vform=0.4 T =-100
Vcem= 0.3, Vform = 0.18 T =-100
Vcem = 0.1, Vform = 0.4 T =-100

At r_c

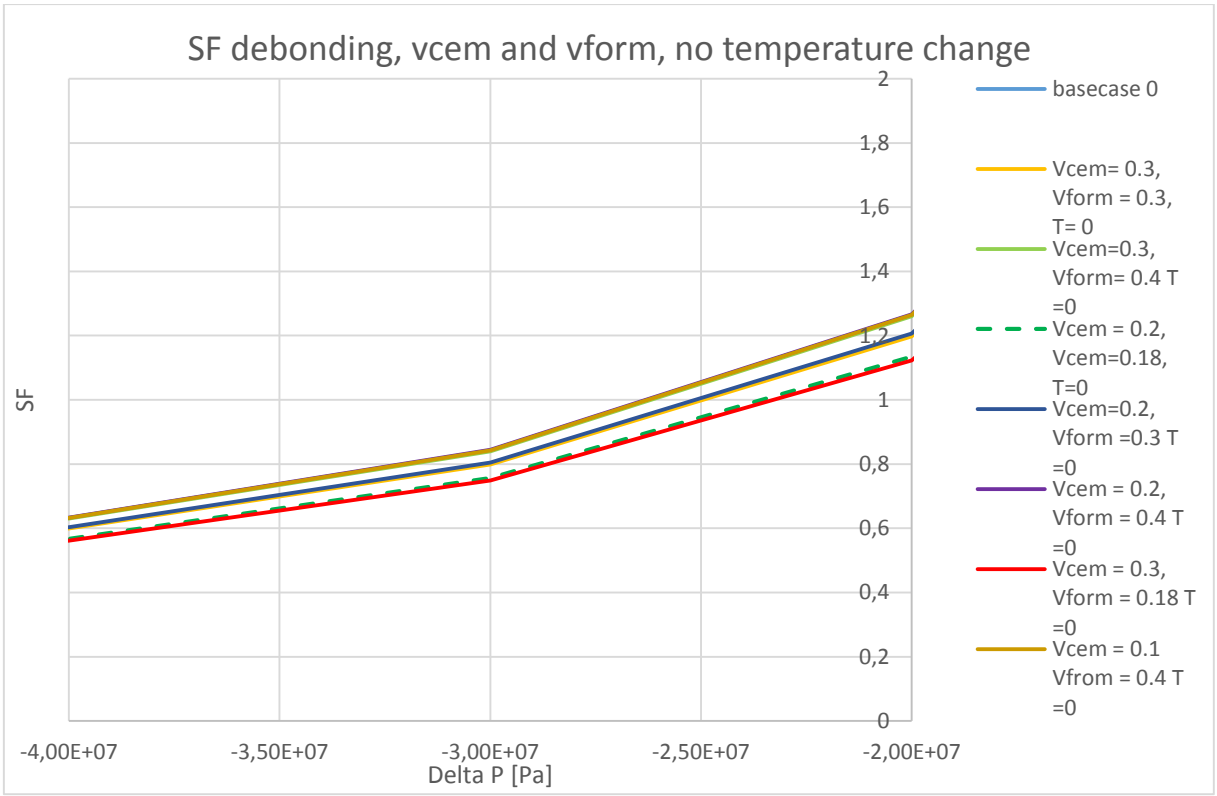
SF debonding, vcem and vform, no temperature change
SF
Delta P [Pa]
-4,00E+07
-3,50E+07
-3,00E+07
-2,50E+07
-2,00E+07
0
0,2
0,4
0,6
0,8
1
1,2
1,4
1,6
1,8
2
basecase 0
Vcem= 0.3, Vform = 0.3, T= 0
Vcem=0.3, Vform= 0.4 T =0
Vcem = 0.2, Vcem=0.18, T=0
Vcem=0.2, Vform =0.3 T =0
Vcem = 0.2, Vform = 0.4 T =0
Vcem = 0.3, Vform = 0.18 T =0
Vcem = 0.1 Vfrom = 0.4 T =0

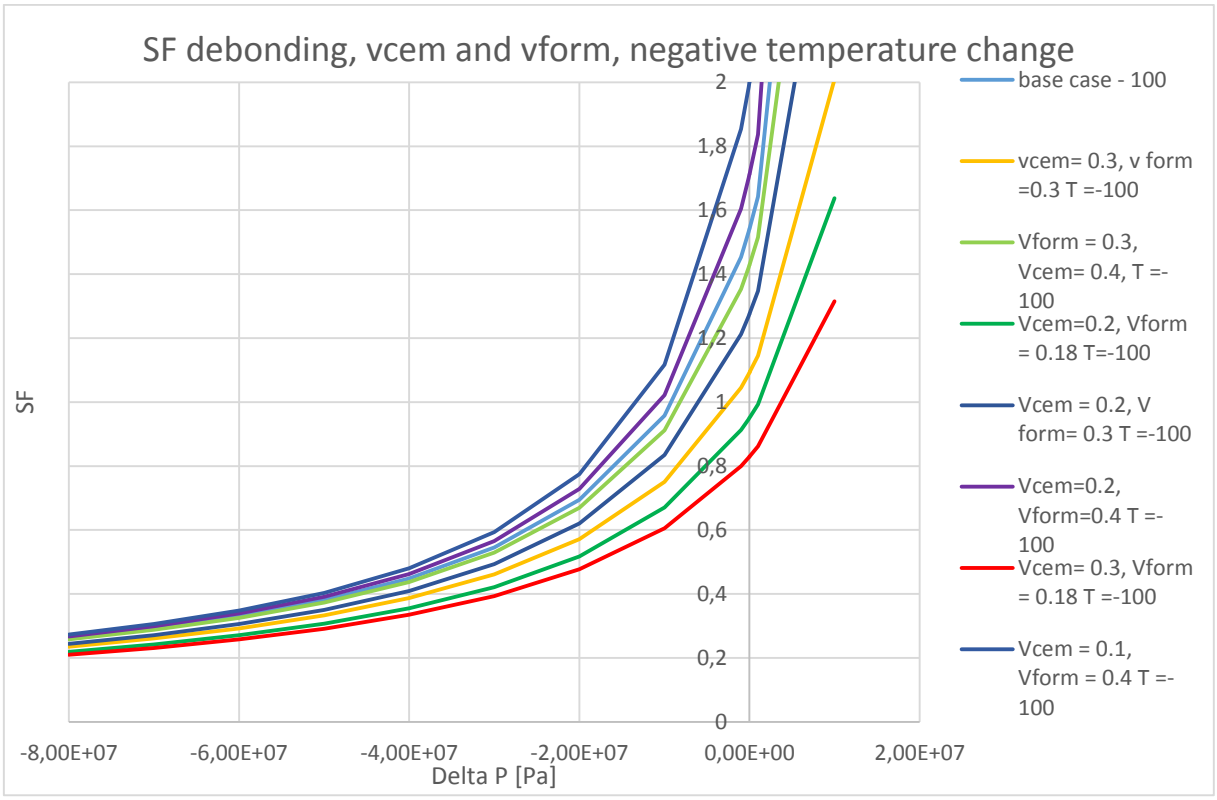

H.2.2 Radial Crack

At rb

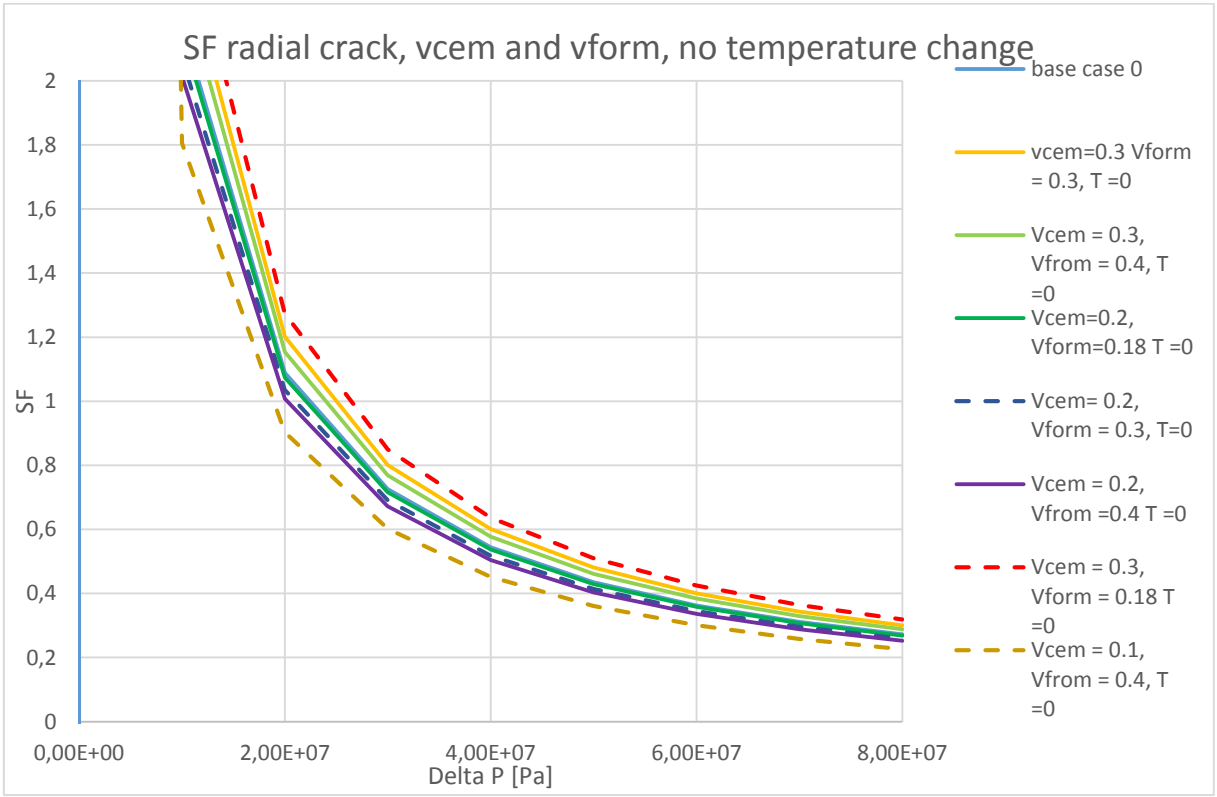

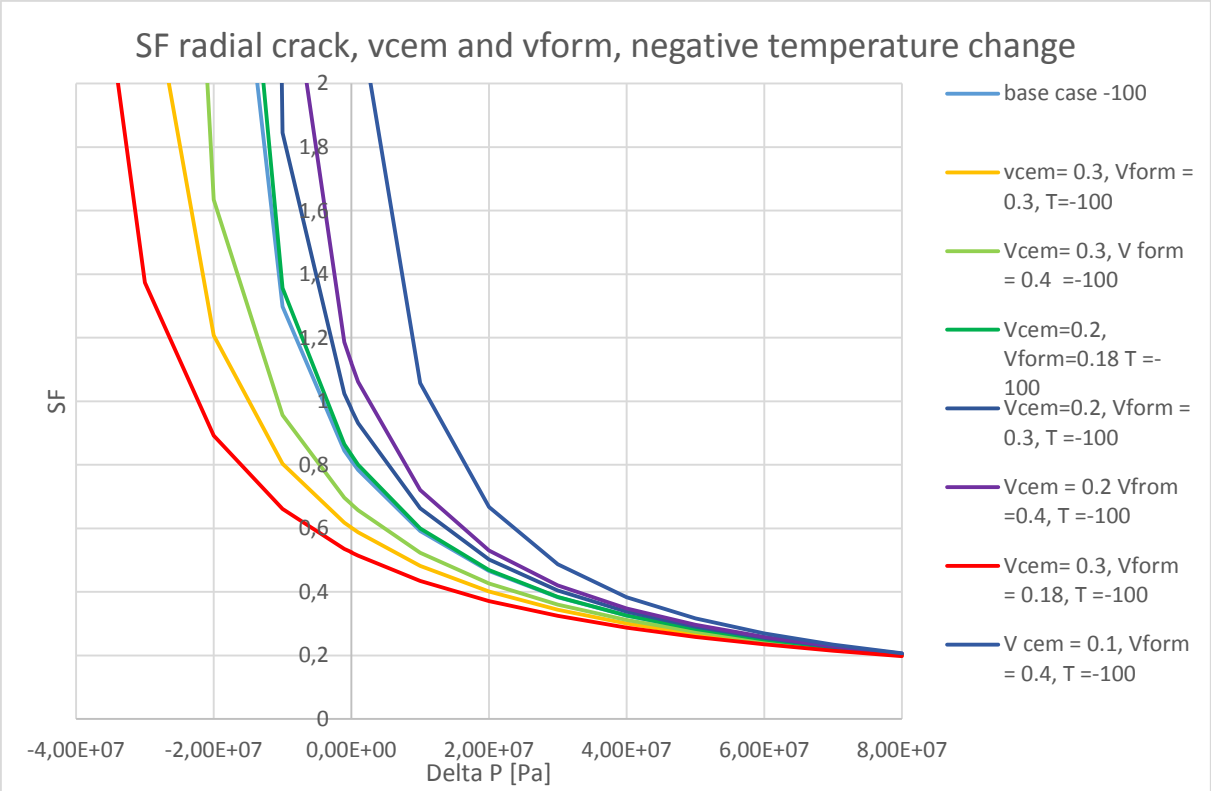
SF radial crack, vcem and vform, negative temperature change
SF
Delta P [Pa]
-4,00E+07
-2,00E+07
0,00E+00
2,00E+07
4,00E+07
6,00E+07
8,00E+07
0
0,2
0,4
0,6
0,8
1
1,2
1,4
1,6
1,8
2
base case -100
vcem= 0.3, Vform = 0.3, T=-100
Vcem= 0.3, V form = 0.4 =-100
Vcem=0.2, Vform=0.18 T =-100
Vcem=0.2, Vform = 0.3, T =-100
Vcem = 0.2 Vfrom =0.4, T =-100
Vcem= 0.3, Vform = 0.18, T =-100
V cem = 0.1, Vform = 0.4, T =-100

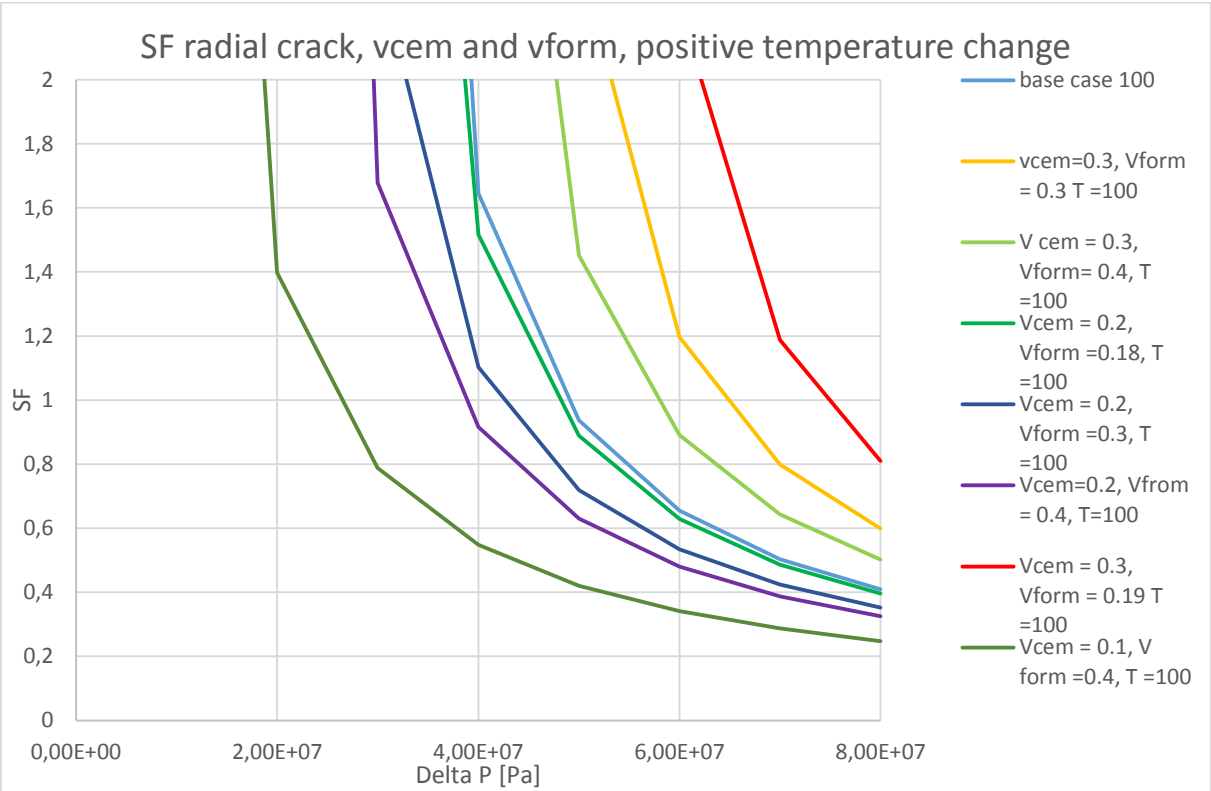
SF radial crack, vcem and vform, positive temperature change
SF
Delta P [Pa]
0,00E+00
2,00E+07
4,00E+07
6,00E+07
8,00E+07
0
0,2
0,4
0,6
0,8
1
1,2
1,4
1,6
1,8
2
base case 100
vcem=0.3, Vform = 0.3 T =100
V cem = 0.3, Vform= 0.4, T =100
Vcem = 0.2, Vform =0.18, T =100
Vcem = 0.2, Vform =0.3, T =100
Vcem=0.2, Vfrom = 0.4, T=100
Vcem = 0.3, Vform = 0.19 T =100
Vcem = 0.1, V form =0.4, T =100

At r_c

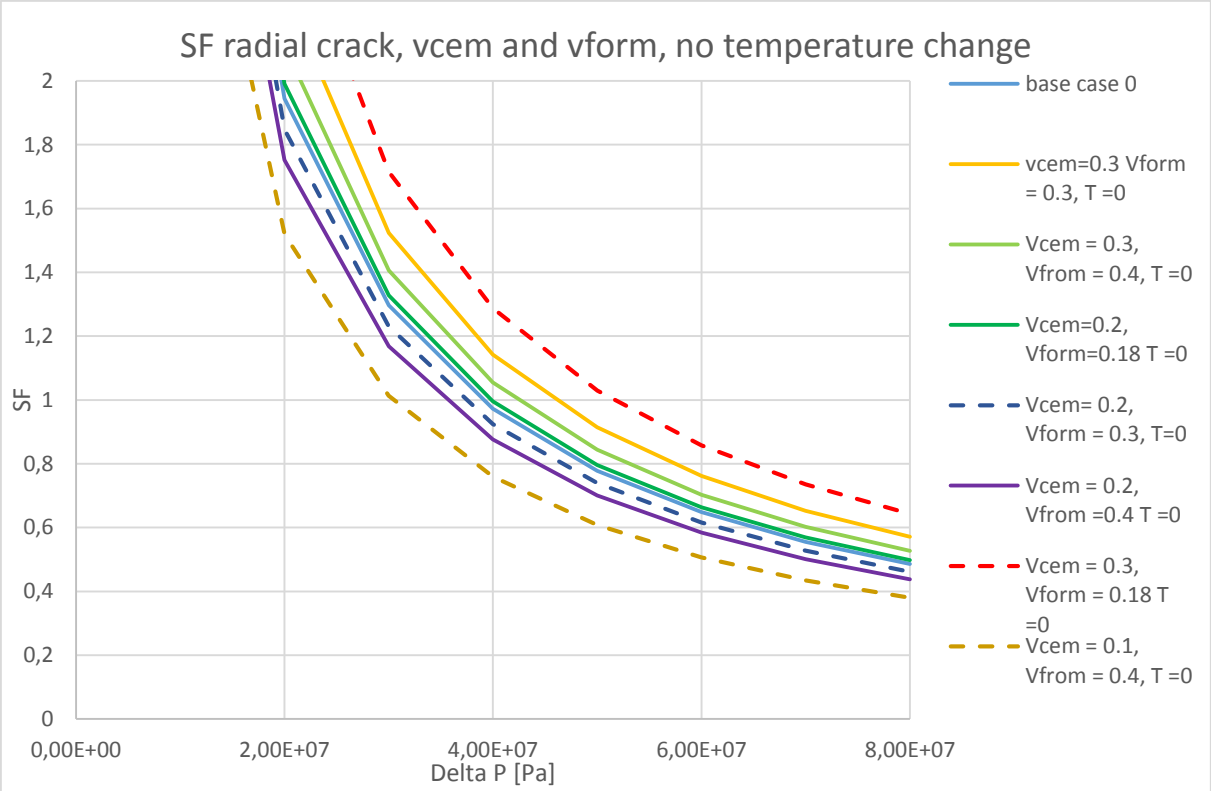
SF radial crack, vcem and vform, no temperature change
SF
Delta P [Pa]
0
0,2
0,4
0,6
0,8
1
1,2
1,4
1,6
1,8
2
0,00E+00
2,00E+07
4,00E+07
6,00E+07
8,00E+07
base case 0
vcem=0.3 Vform = 0.3, T =0
Vcem = 0.3, Vfrom = 0.4, T =0
Vcem=0.2, Vform=0.18 T =0
Vcem= 0.2, Vform = 0.3, T=0
Vcem = 0.2, Vfrom =0.4 T =0
Vcem = 0.3, Vform = 0.18 T =0
Vcem = 0.1, Vfrom = 0.4, T =0

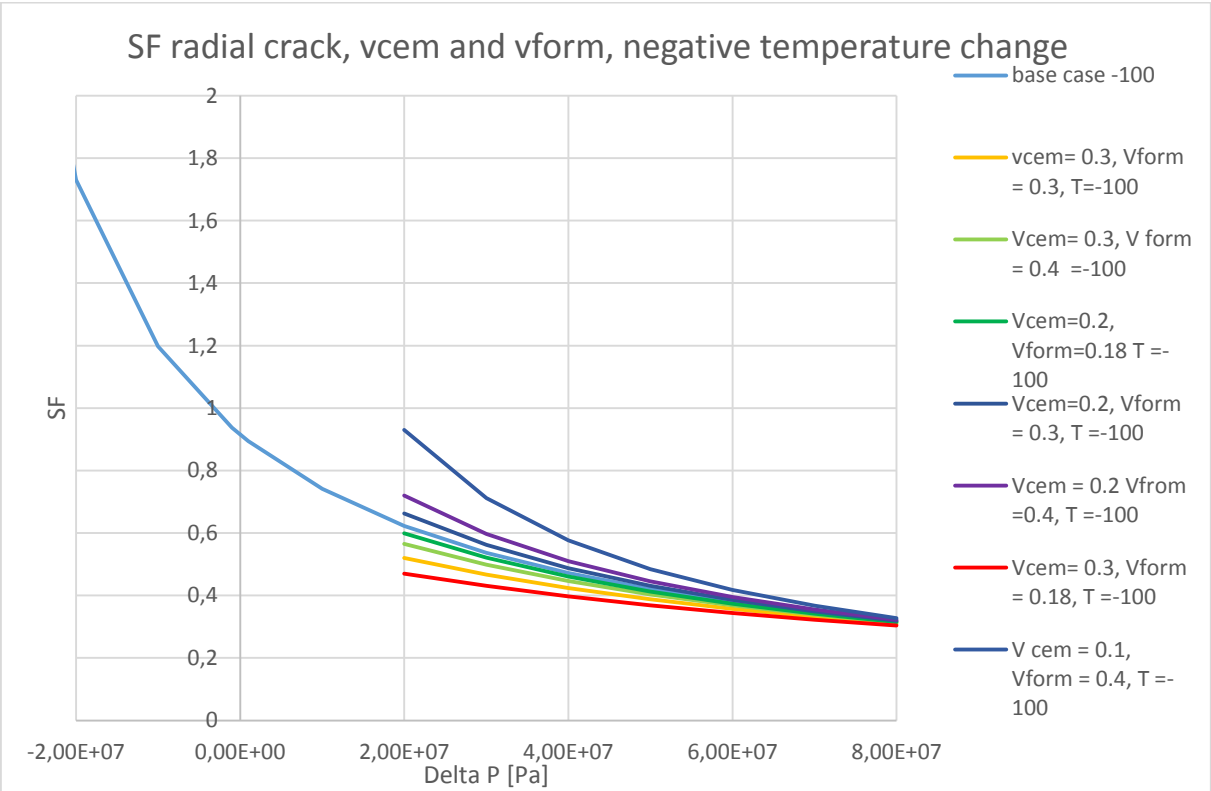
SF radial crack, vcem and vform, negative temperature change
SF
Delta P [Pa]
0
0,2
0,4
0,6
0,8
1
1,2
1,4
1,6
1,8
2
-2,00E+07
0,00E+00
2,00E+07
4,00E+07
6,00E+07
8,00E+07
base case -100
vcem= 0.3, Vform = 0.3, T=-100
Vcem= 0.3, V form = 0.4 =-100
Vcem=0.2, Vform=0.18 T =-100
Vcem=0.2, Vform = 0.3, T =-100
Vcem = 0.2 Vfrom =0.4, T =-100
Vcem= 0.3, Vform = 0.18, T =-100
V cem = 0.1, Vform = 0.4, T =-100

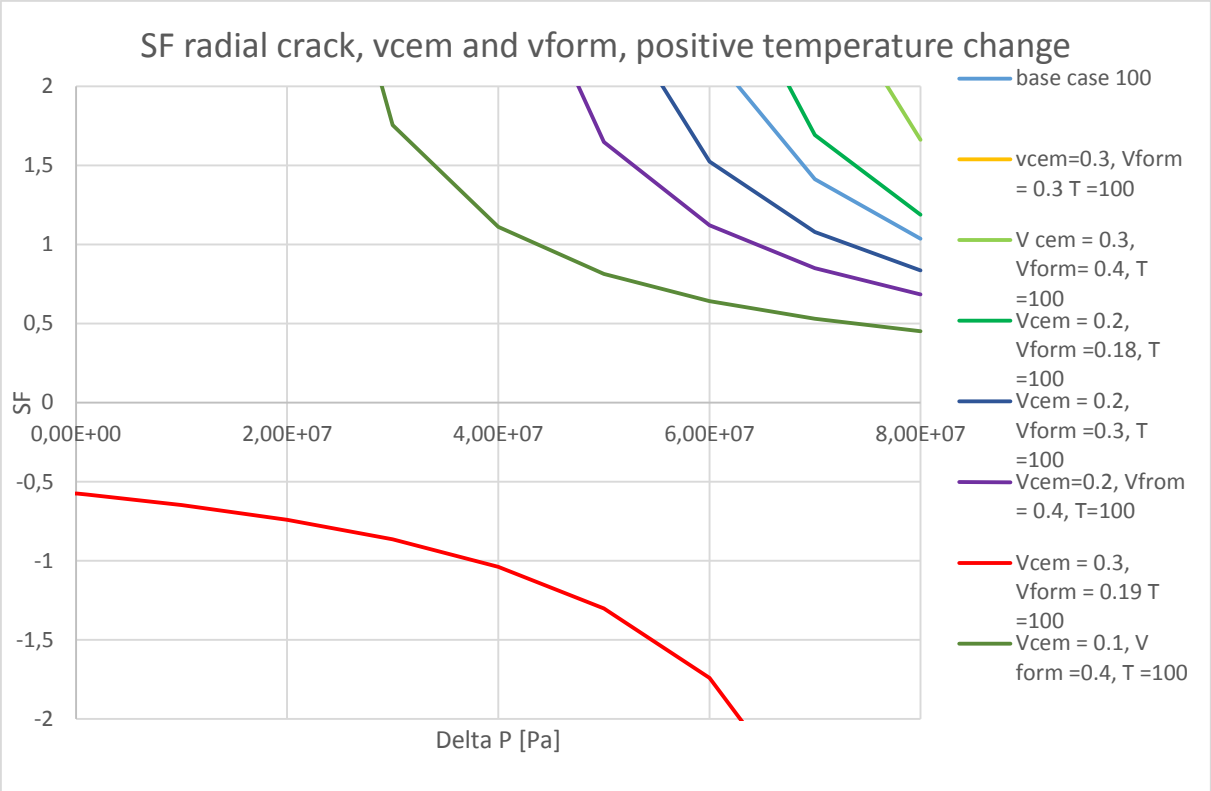

H.2.3 Shear Failure

At rb

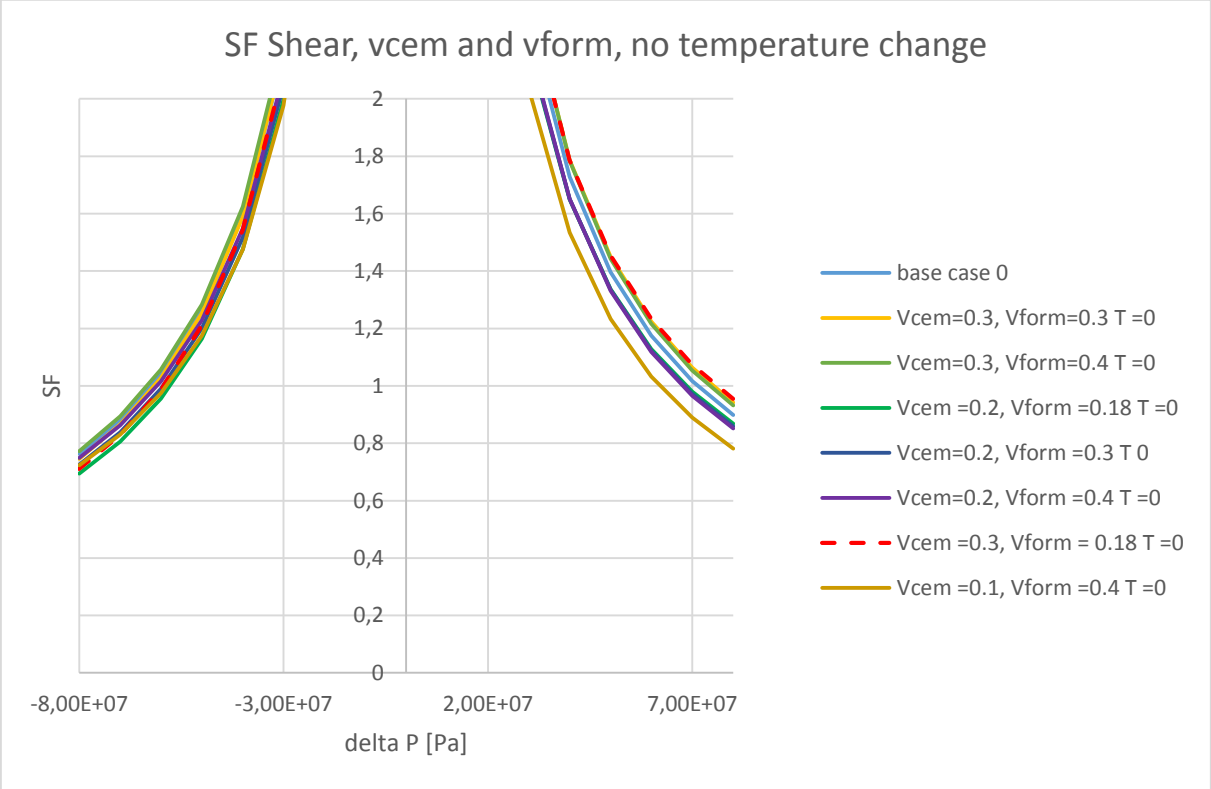

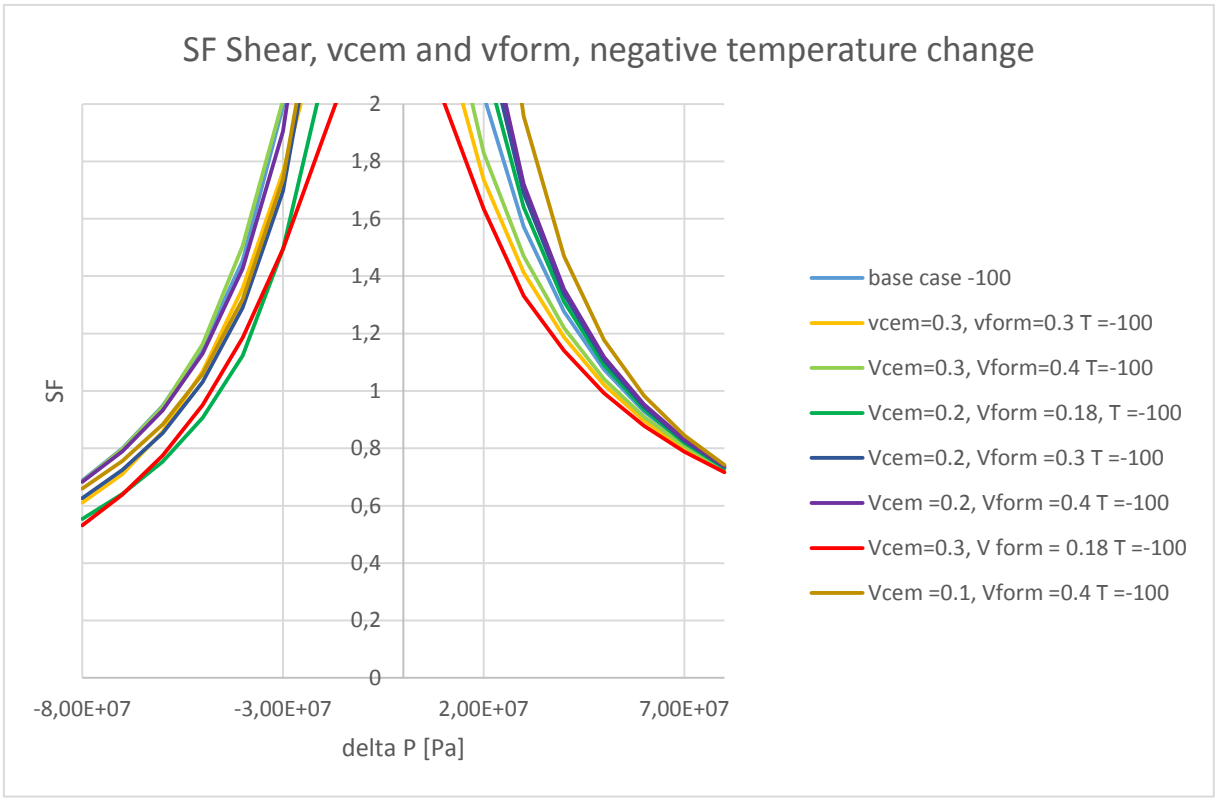
SF Shear, vcem and vform, negative temperature change
SF
2
1,8
1,6
1,4
1,2
1
0,8
0,6
0,4
0,2
0
-8,00E+07
-3,00E+07
2,00E+07
7,00E+07
delta P [Pa]
base case -100
vcem=0.3, vform=0.3 T =-100
Vcem=0.3, Vform=0.4 T=-100
Vcem=0.2, Vform =0.18, T =-100
Vcem=0.2, Vform =0.3 T =-100
Vcem =0.2, Vform =0.4 T =-100
Vcem=0.3, V form = 0.18 T =-100
Vcem =0.1, Vform =0.4 T =-100

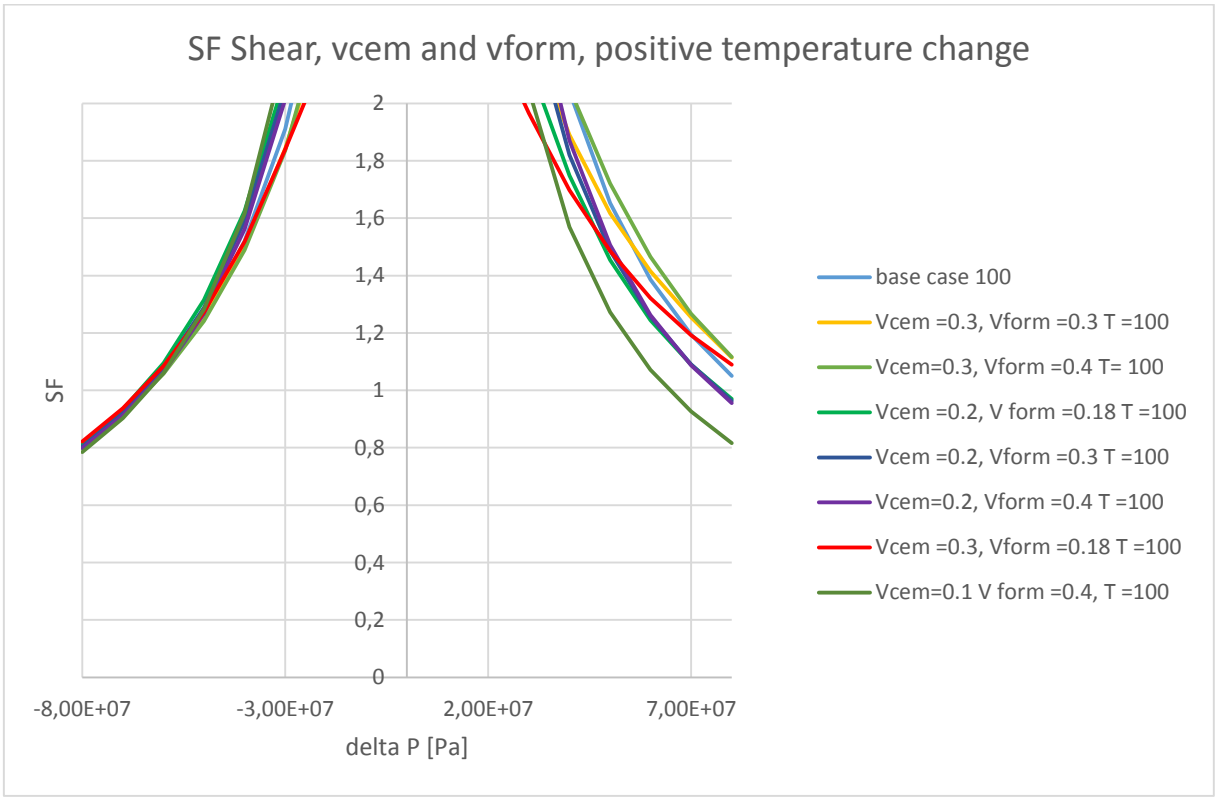
SF Shear, vcem and vform, positive temperature change
SF
2
1,8
1,6
1,4
1,2
1
0,8
0,6
0,4
0,2
0
-8,00E+07
-3,00E+07
2,00E+07
7,00E+07
delta P [Pa]
base case 100
Vcem =0.3, Vform =0.3 T =100
Vcem=0.3, Vform =0.4 T= 100
Vcem =0.2, V form =0.18 T =100
Vcem =0.2, Vform =0.3 T =100
Vcem=0.2, Vform =0.4 T =100
Vcem =0.3, Vform =0.18 T =100
Vcem=0.1 V form =0.4, T =100

At r_c

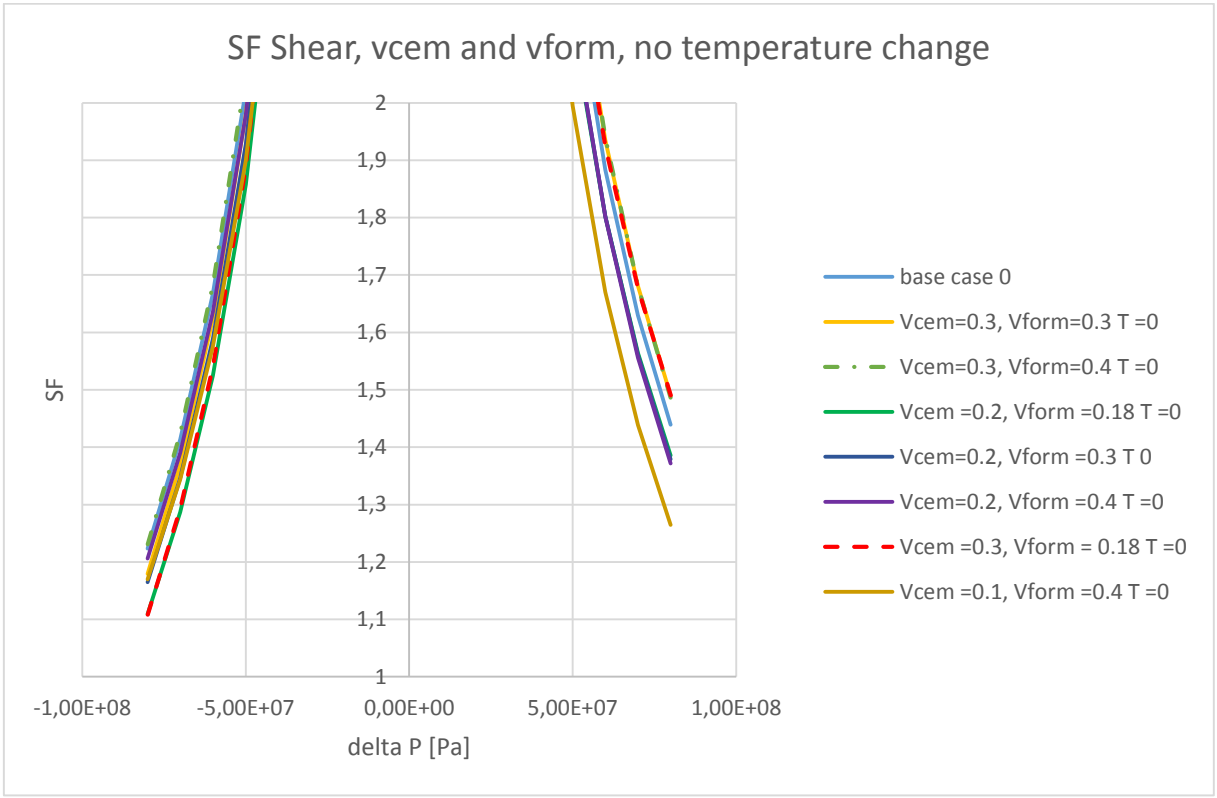
SF Shear, vcem and vform, no temperature change
SF
2
1,9
1,8
1,7
1,6
1,5
1,4
1,3
1,2
1,1
1
-1,00E+08
-5,00E+07
0,00E+00
5,00E+07
1,00E+08
delta P [Pa]
base case 0
Vcem=0.3, Vform=0.3 T =0
Vcem=0.3, Vform=0.4 T =0
Vcem =0.2, Vform =0.18 T =0
Vcem=0.2, Vform =0.3 T 0
Vcem=0.2, Vform =0.4 T =0
Vcem =0.3, Vform = 0.18 T =0
Vcem =0.1, Vform =0.4 T =0

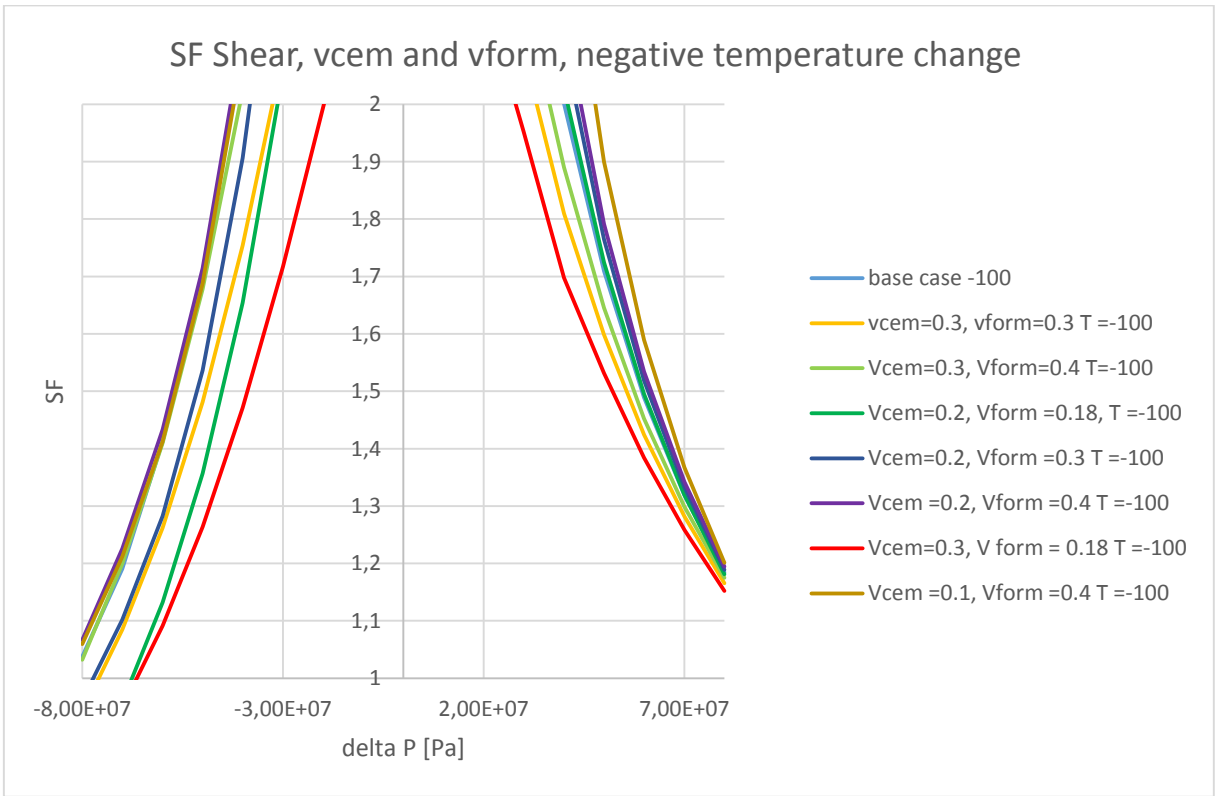
SF Shear, vcem and vform, negative temperature change
SF
2
1,9
1,8
1,7
1,6
1,5
1,4
1,3
1,2
1,1
1
-8,00E+07
-3,00E+07
2,00E+07
7,00E+07
delta P [Pa]
base case -100
vcem=0.3, vform=0.3 T =-100
Vcem=0.3, Vform=0.4 T=-100
Vcem=0.2, Vform =0.18, T =-100
Vcem=0.2, Vform =0.3 T =-100
Vcem =0.2, Vform =0.4 T =-100
Vcem=0.3, V form = 0.18 T =-100
Vcem =0.1, Vform =0.4 T =-100

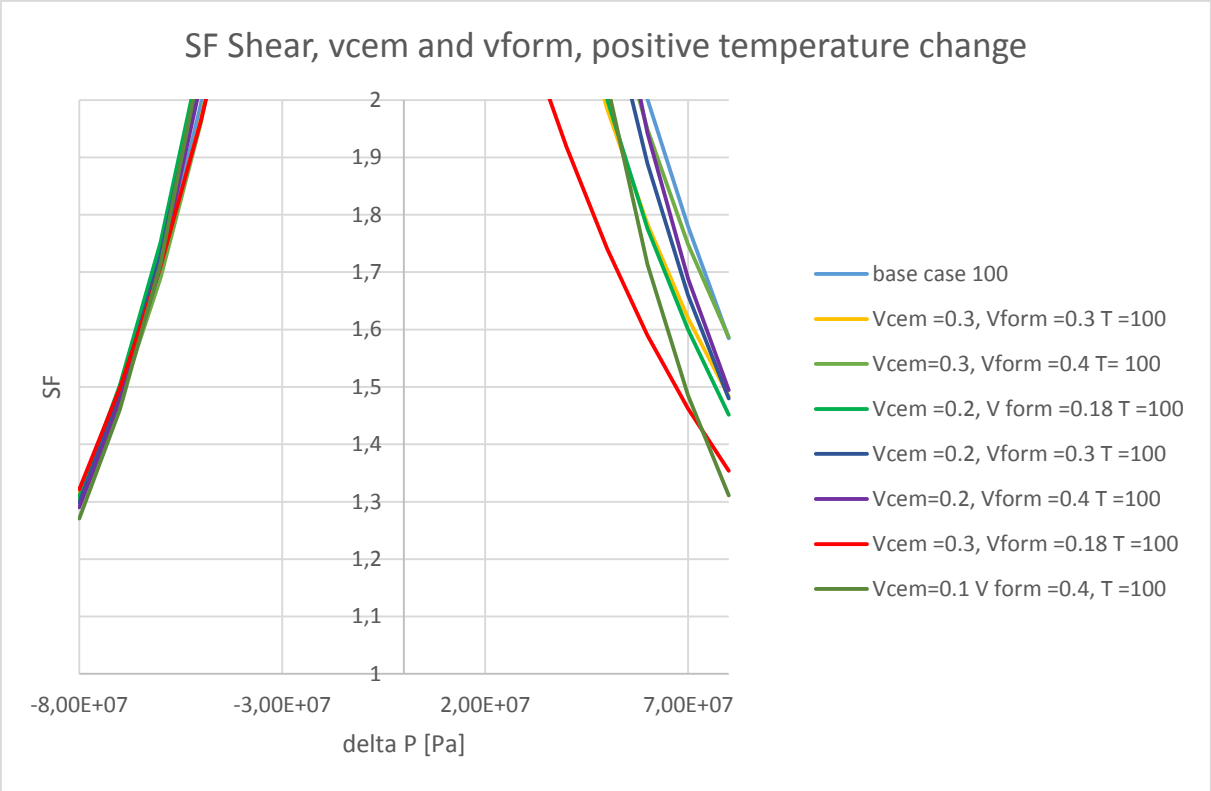

H.3 Coefficient of Linear Thermal Expansion

H.3.1 Debonding

At rb

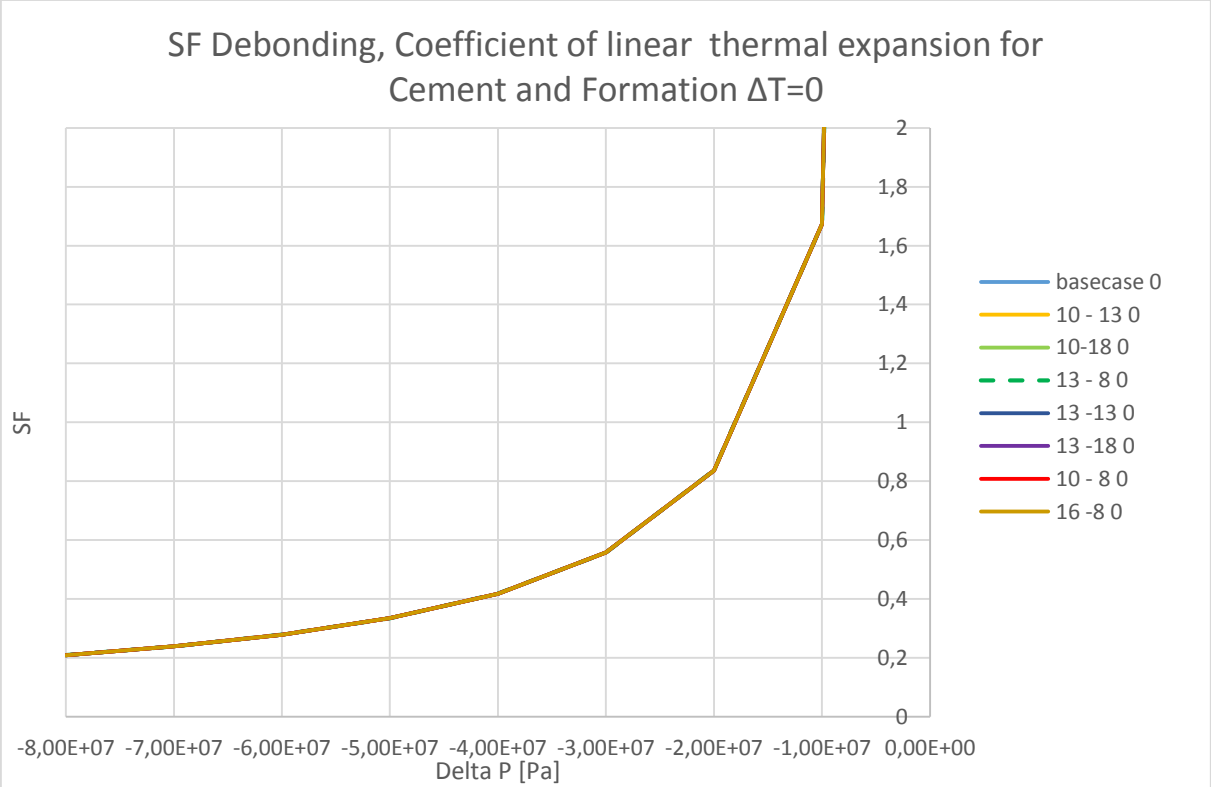

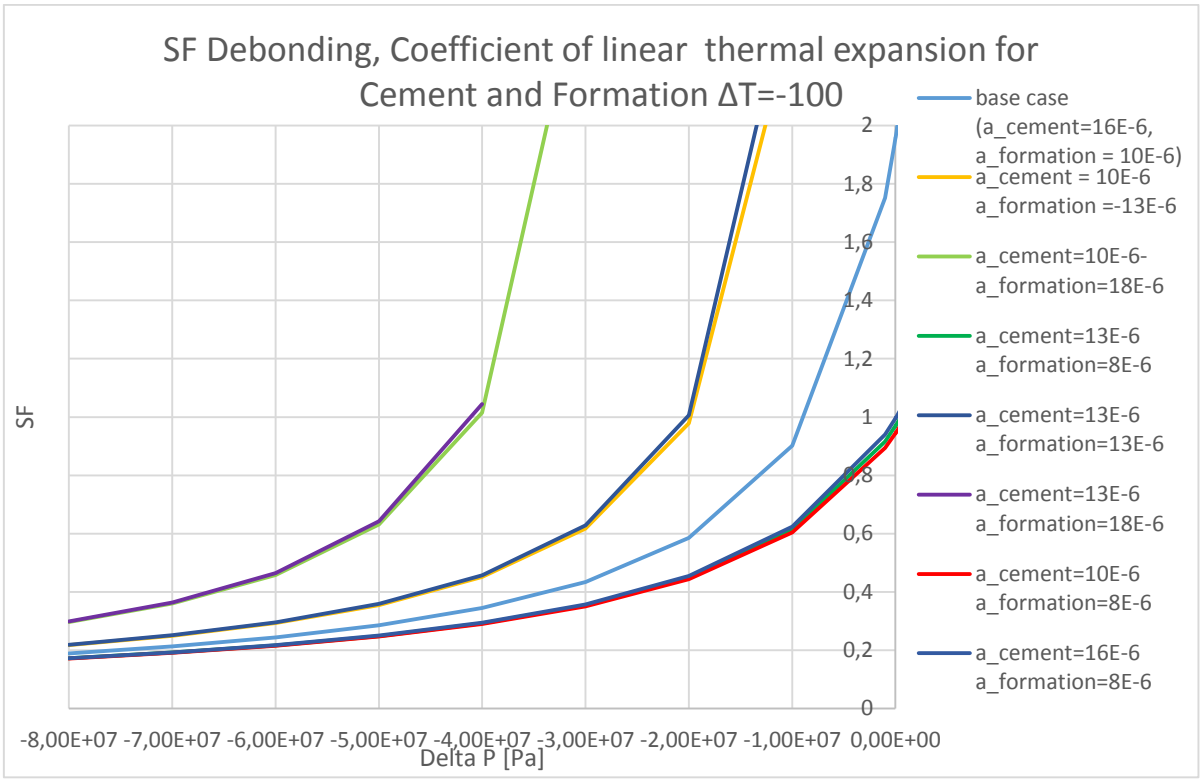
SF Debonding, Coefficient of linear thermal expansion for Cement and Formation ΔT=-100
SF
2
1,8
1,6
1,4
1,2
1
0,8
0,6
0,4
0,2
0
-8,00E+07 -7,00E+07 -6,00E+07 -5,00E+07 -4,00E+07 -3,00E+07 -2,00E+07 -1,00E+07 0,00E+00
Delta P [Pa]
base case (a_cement=16E-6, a_formation = 10E-6)
a_cement = 10E-6 a_formation =-13E-6
a_cement=10E-6- a_formation=18E-6
a_cement=13E-6 a_formation=8E-6
a_cement=13E-6 a_formation=13E-6
a_cement=13E-6 a_formation=18E-6
a_cement=10E-6 a_formation=8E-6
a_cement=16E-6 a_formation=8E-6

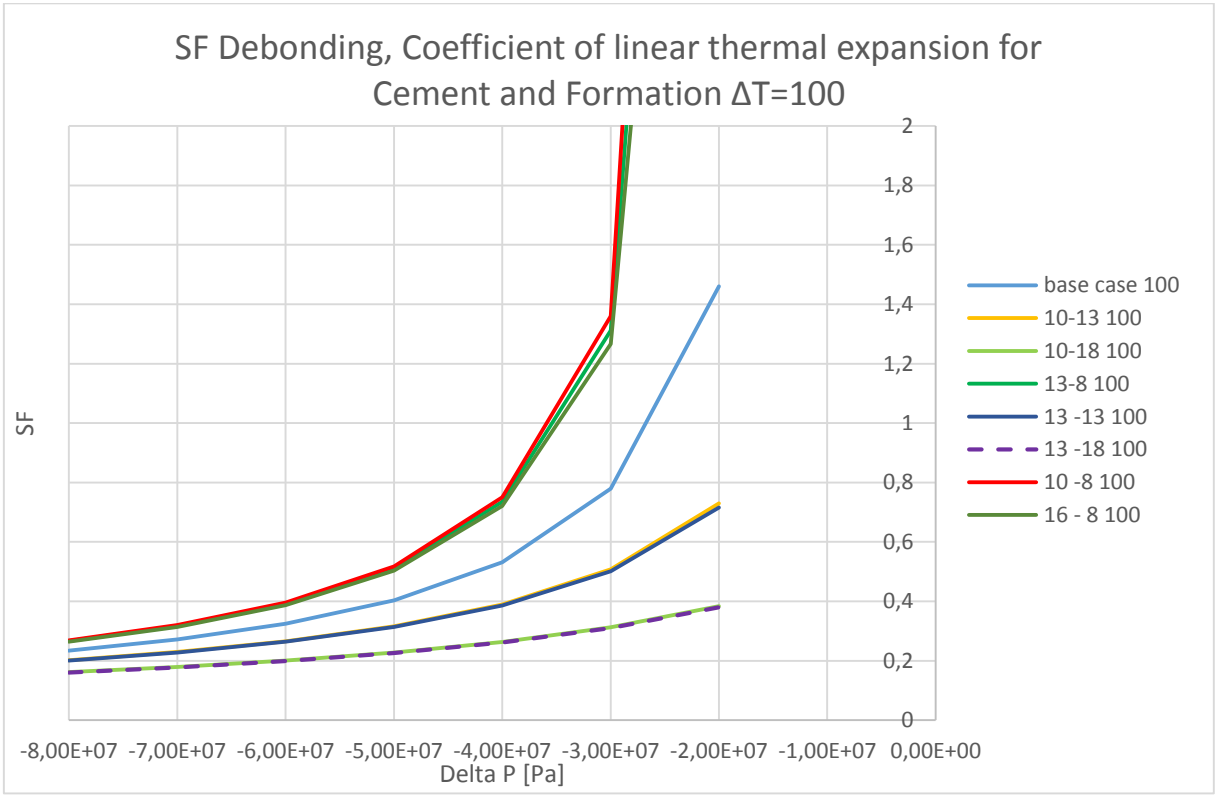
SF Debonding, Coefficient of linear thermal expansion for Cement and Formation ΔT=100
SF
2
1,8
1,6
1,4
1,2
1
0,8
0,6
0,4
0,2
0
-8,00E+07 -7,00E+07 -6,00E+07 -5,00E+07 -4,00E+07 -3,00E+07 -2,00E+07 -1,00E+07 0,00E+00
Delta P [Pa]
base case 100
10-13 100
10-18 100
13-8 100
13 -13 100
13 -18 100
10 -8 100
16 - 8 100

At r_c

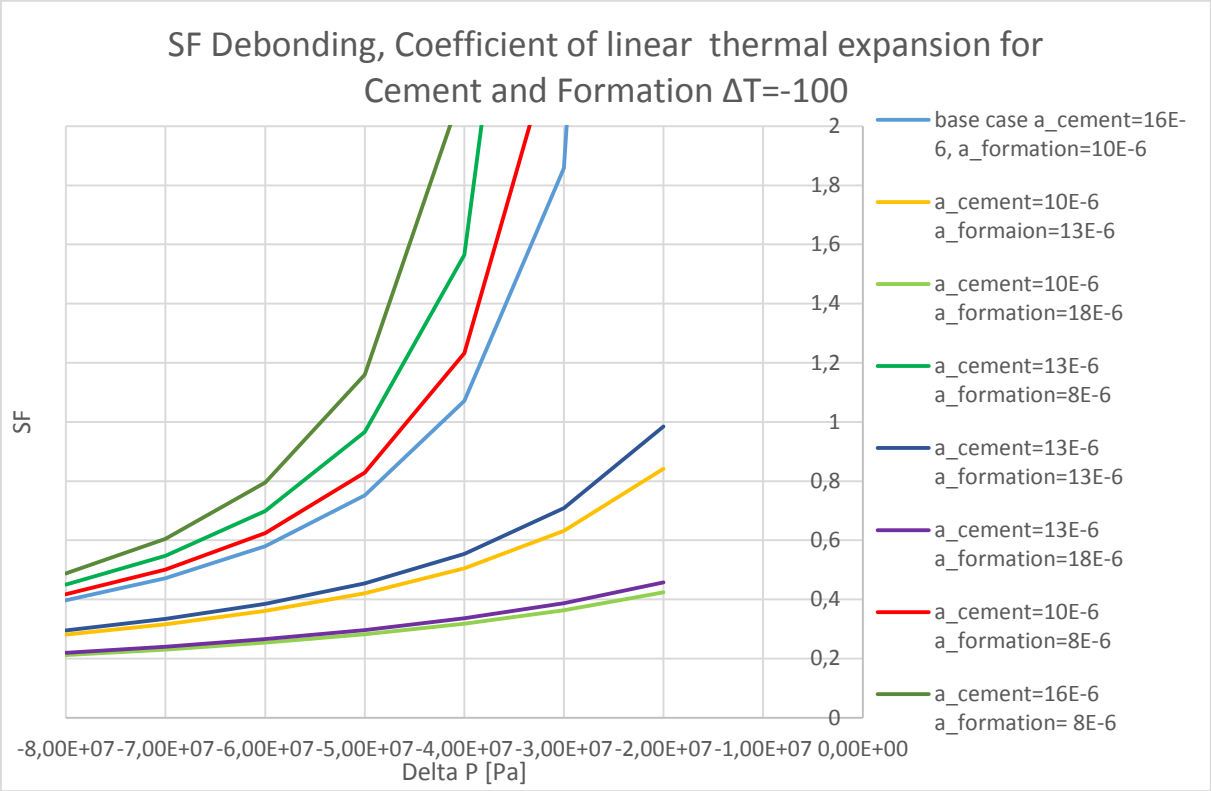
SF Debonding, Coefficient of linear thermal expansion for Cement and Formation ΔT=-100
SF
2
1,8
1,6
1,4
1,2
1
0,8
0,6
0,4
0,2
0
-8,00E+07 -7,00E+07 -6,00E+07 -5,00E+07 -4,00E+07 -3,00E+07 -2,00E+07 -1,00E+07 0,00E+00
Delta P [Pa]
base case a_cement=16E-6, a_formation=10E-6
a_cement=10E-6 a_formaion=13E-6
a_cement=10E-6 a_formation=18E-6
a_cement=13E-6 a_formation=8E-6
a_cement=13E-6 a_formation=13E-6
a_cement=13E-6 a_formation=18E-6
a_cement=10E-6 a_formation=8E-6
a_cement=16E-6 a_formation= 8E-6

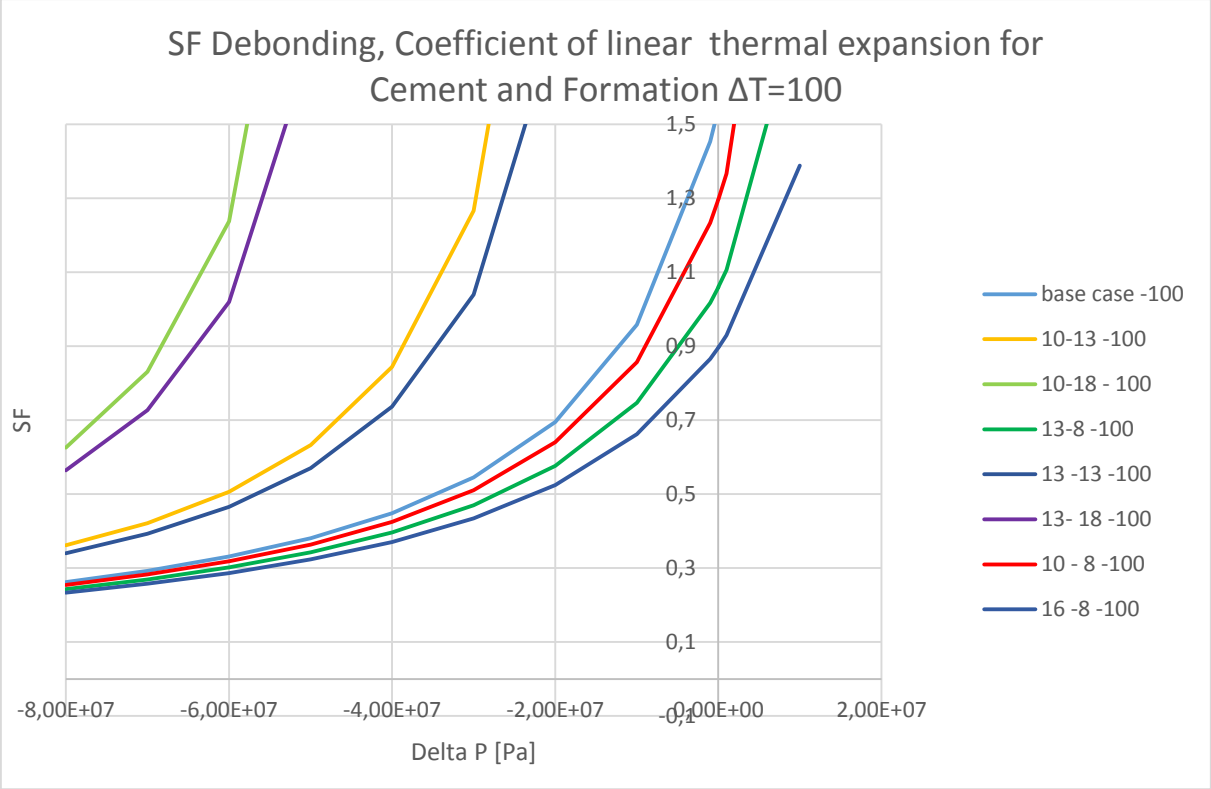
SF Debonding, Coefficient of linear thermal expansion for Cement and Formation ΔT=100
SF
1,5
1,3
1,1
0,9
0,7
0,5
0,3
0,1
-0,1
-8,00E+07
-6,00E+07
-4,00E+07
-2,00E+07
0,00E+00
2,00E+07
Delta P [Pa]
base case -100
10-13 -100
10-18 - 100
13-8 -100
13 -13 -100
13- 18 -100
10 - 8 -100
16 -8 -100

H.3.2 Radial Crack

At rb

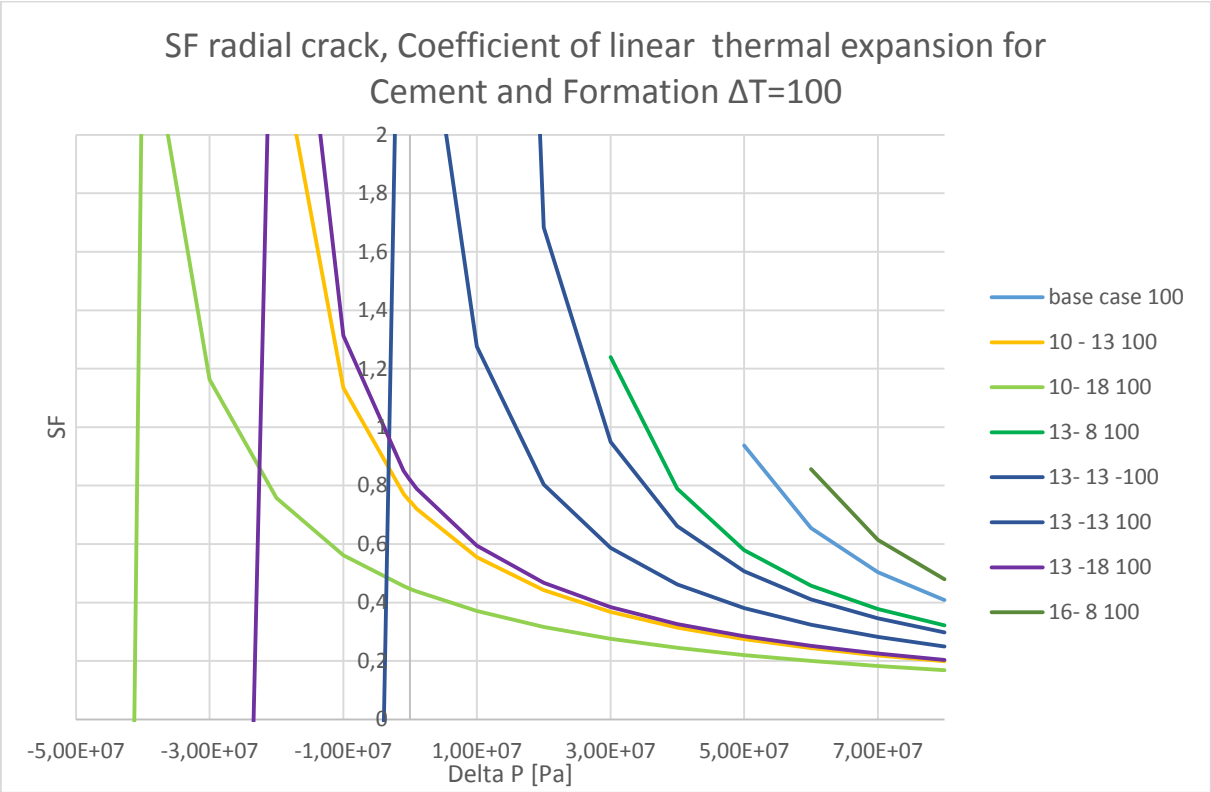

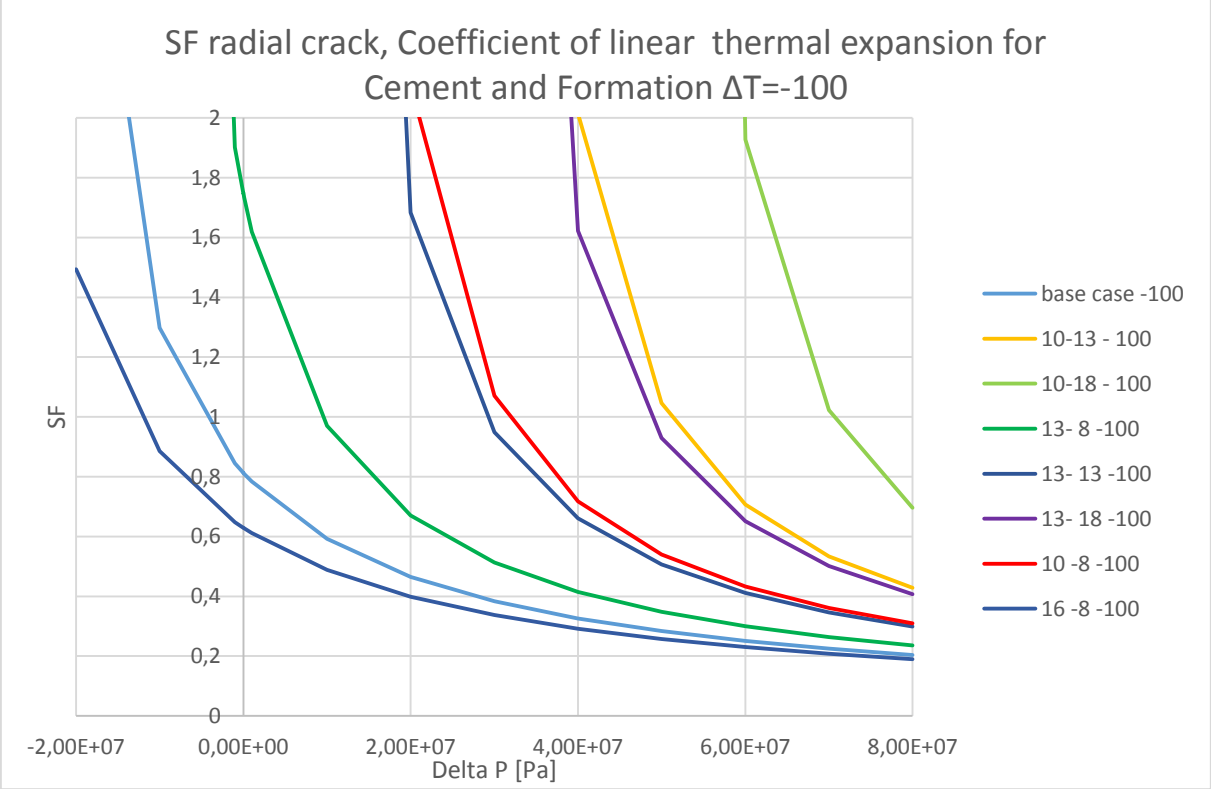

At r_c

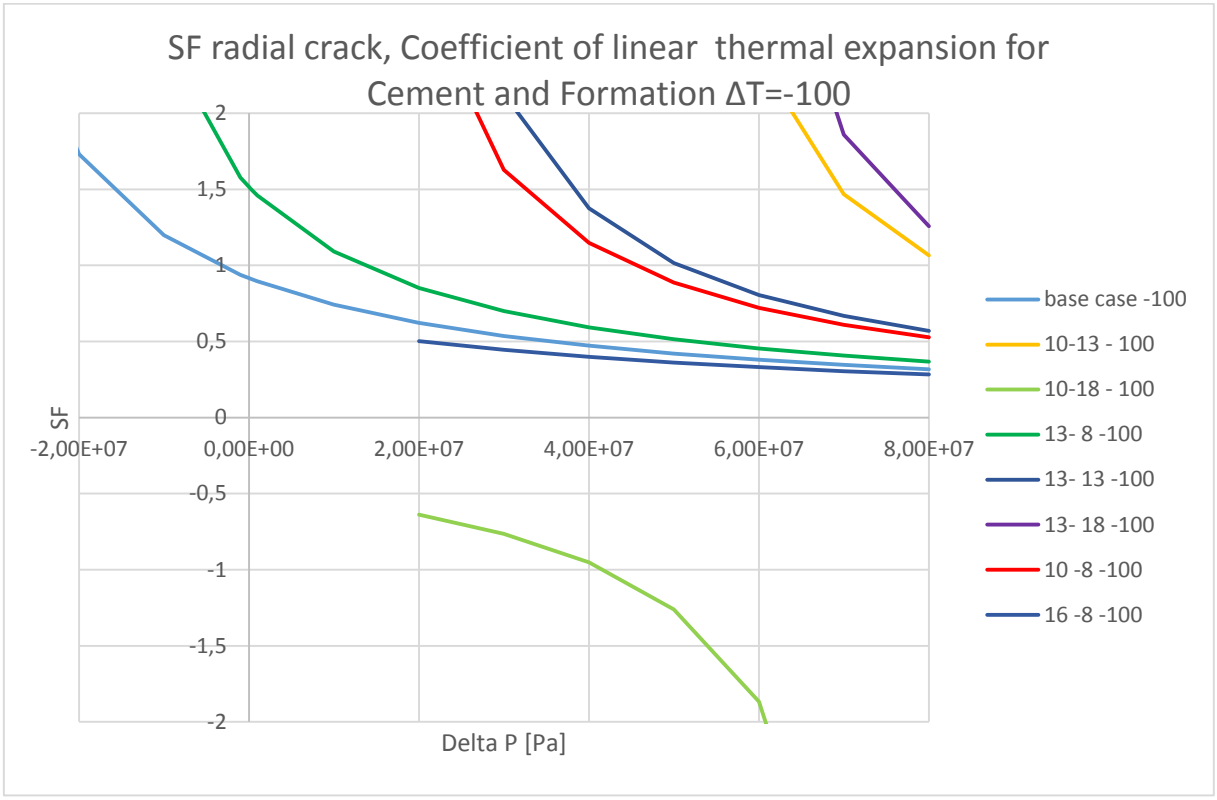
SF radial crack, Coefficient of linear thermal expansion for Cement and Formation ΔT=-100
SF
Delta P [Pa]
2
1,5
1
0,5
0
-0,5
-1
-1,5
-2
-2,00E+07
0,00E+00
2,00E+07
4,00E+07
6,00E+07
8,00E+07
base case -100
10-13 - 100
10-18 - 100
13- 8 -100
13- 13 -100
13- 18 -100
10 -8 -100
16 -8 -100

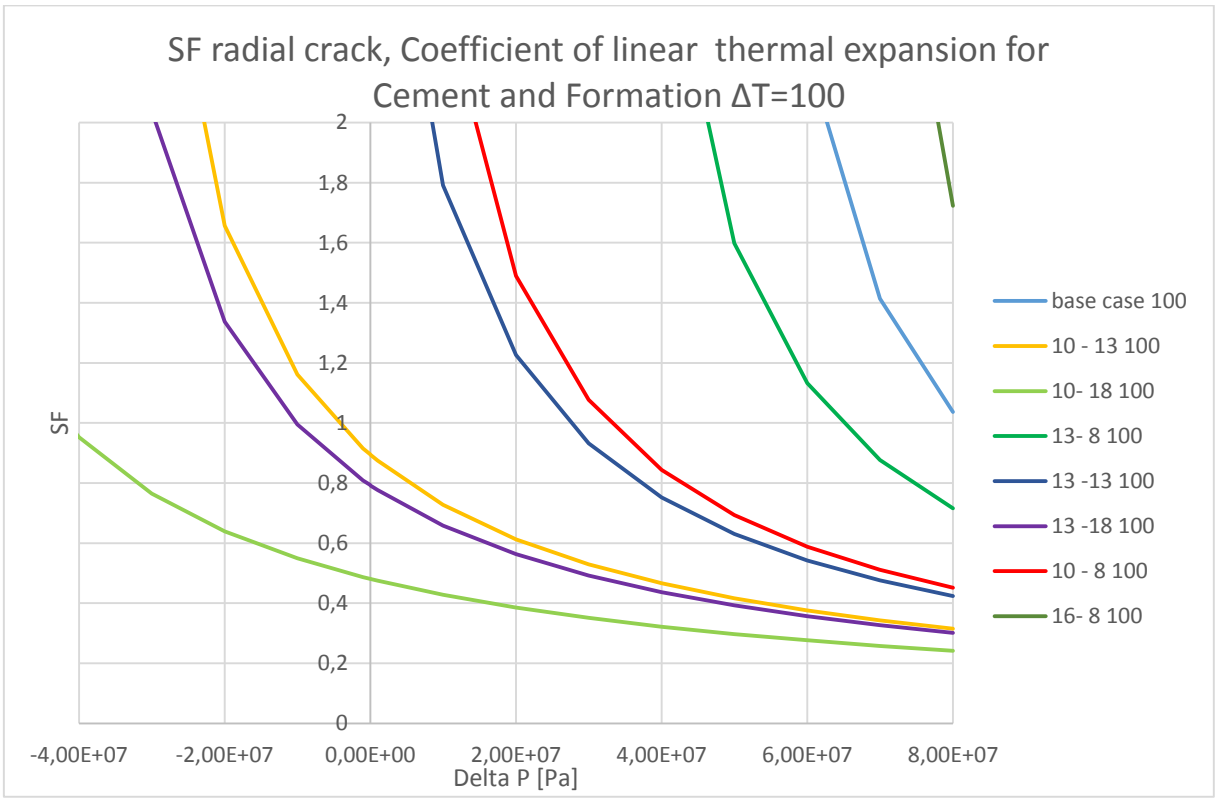
SF radial crack, Coefficient of linear thermal expansion for Cement and Formation ΔT=100
SF
Delta P [Pa]
2
1,8
1,6
1,4
1,2
1
0,8
0,6
0,4
0,2
0
-4,00E+07
-2,00E+07
0,00E+00
2,00E+07
4,00E+07
6,00E+07
8,00E+07
base case 100
10 - 13 100
10- 18 100
13- 8 100
13 -13 100
13 -18 100
10 - 8 100
16- 8 100

H.3.3 Shear Failure

At rb

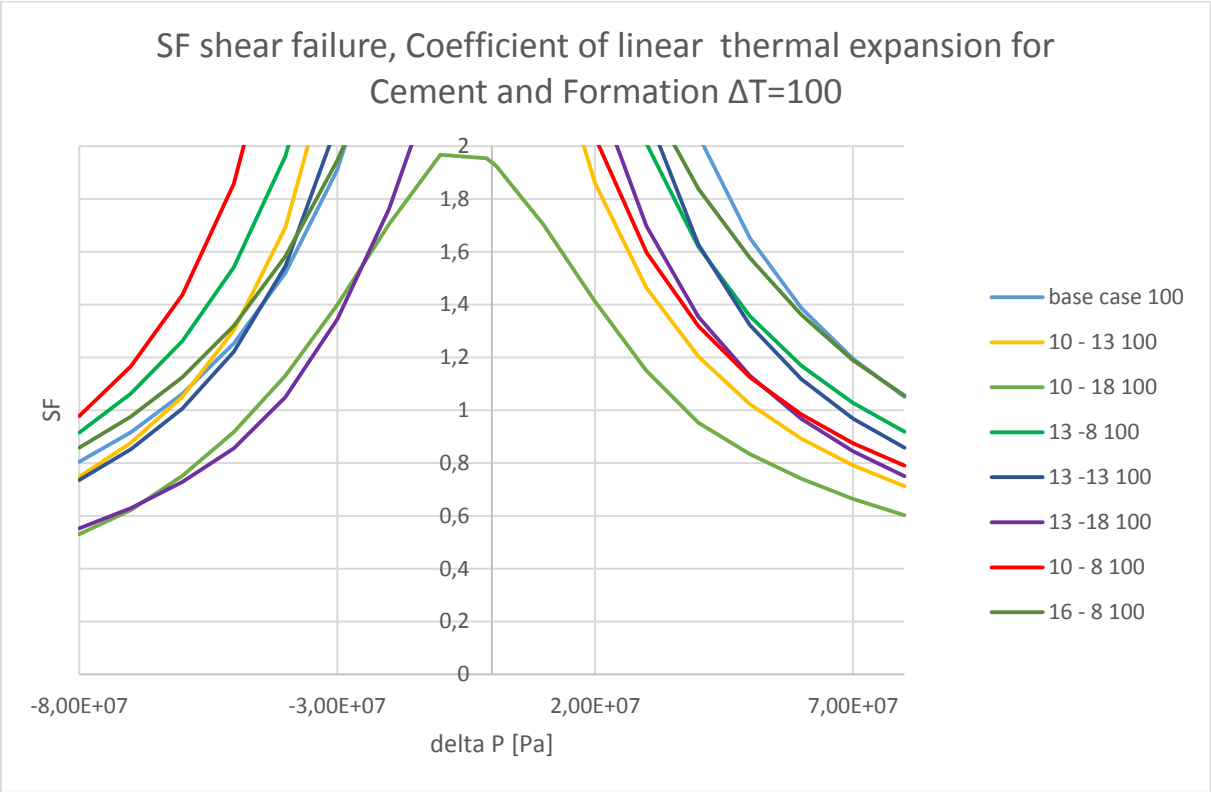

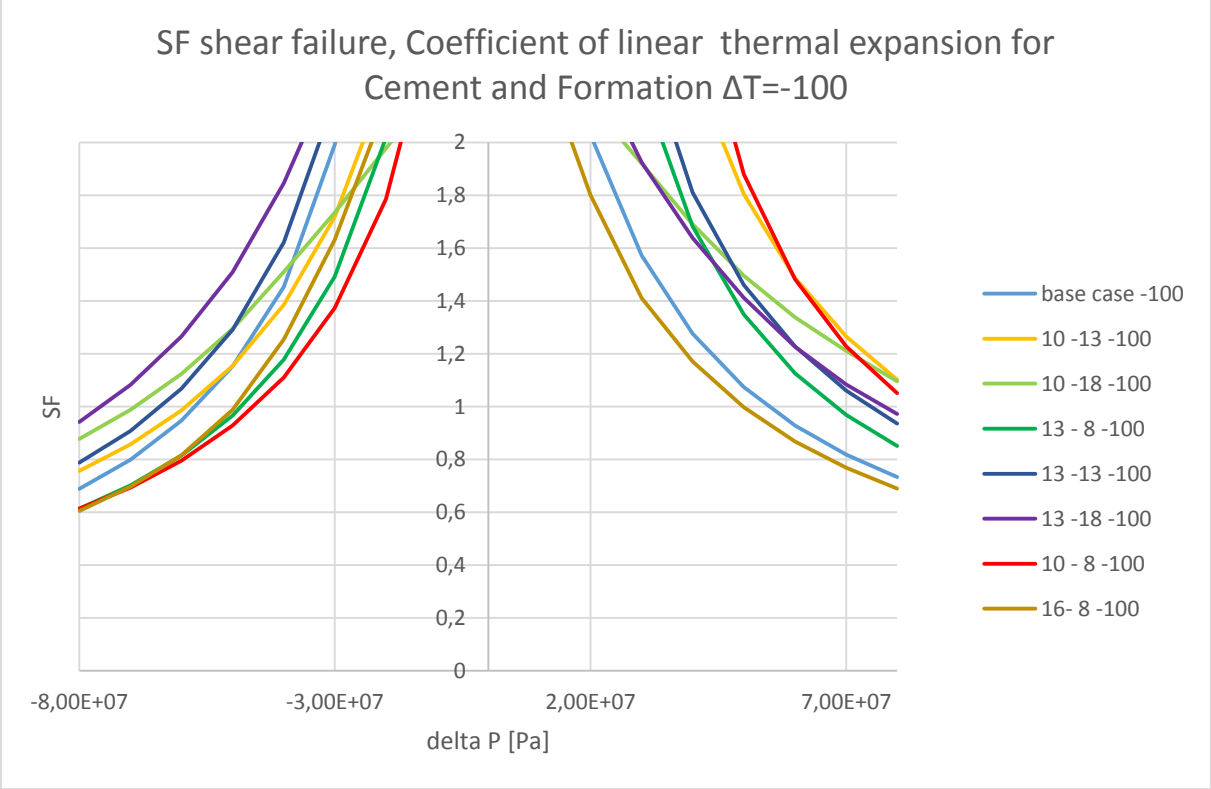

At r_c

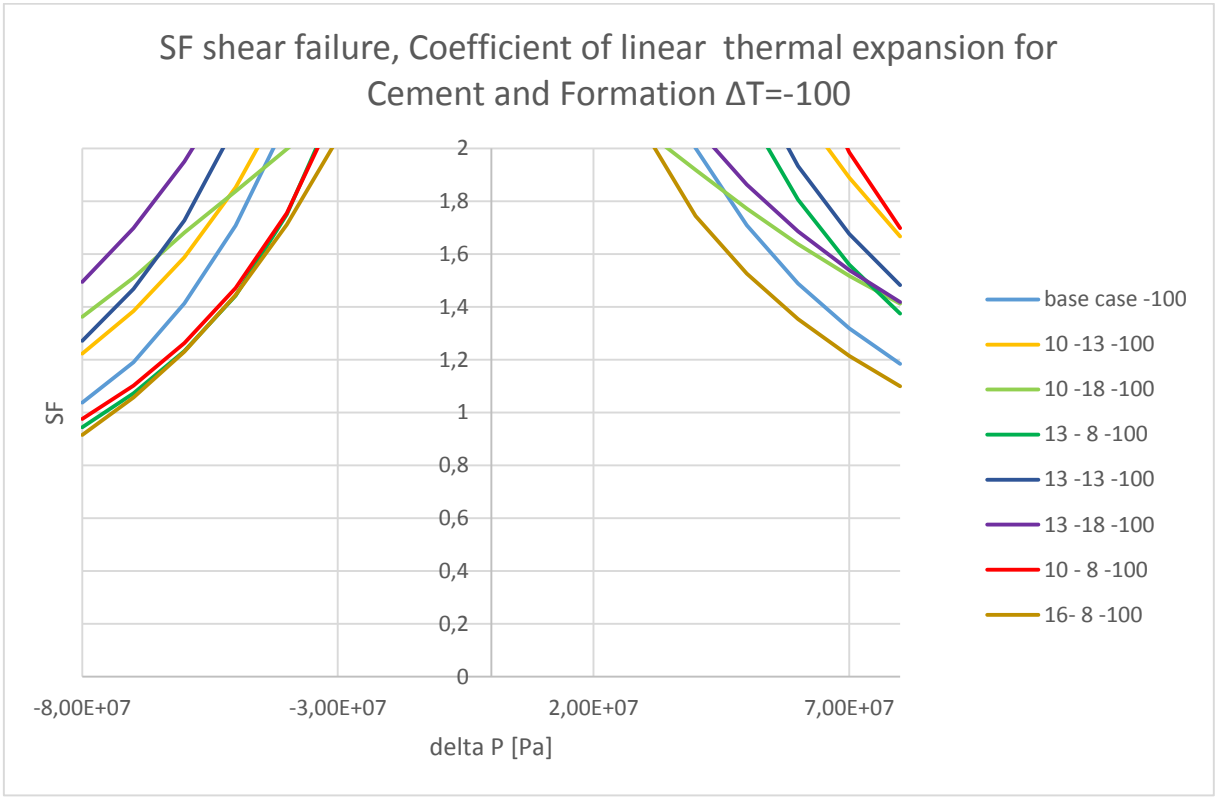
SF shear failure, Coefficient of linear thermal expansion for Cement and Formation ΔT=-100
SF
2
1,8
1,6
1,4
1,2
1
0,8
0,6
0,4
0,2
0
-8,00E+07
-3,00E+07
2,00E+07
7,00E+07
delta P [Pa]
base case -100
10 -13 -100
10 -18 -100
13 - 8 -100
13 -13 -100
13 -18 -100
10 - 8 -100
16- 8 -100

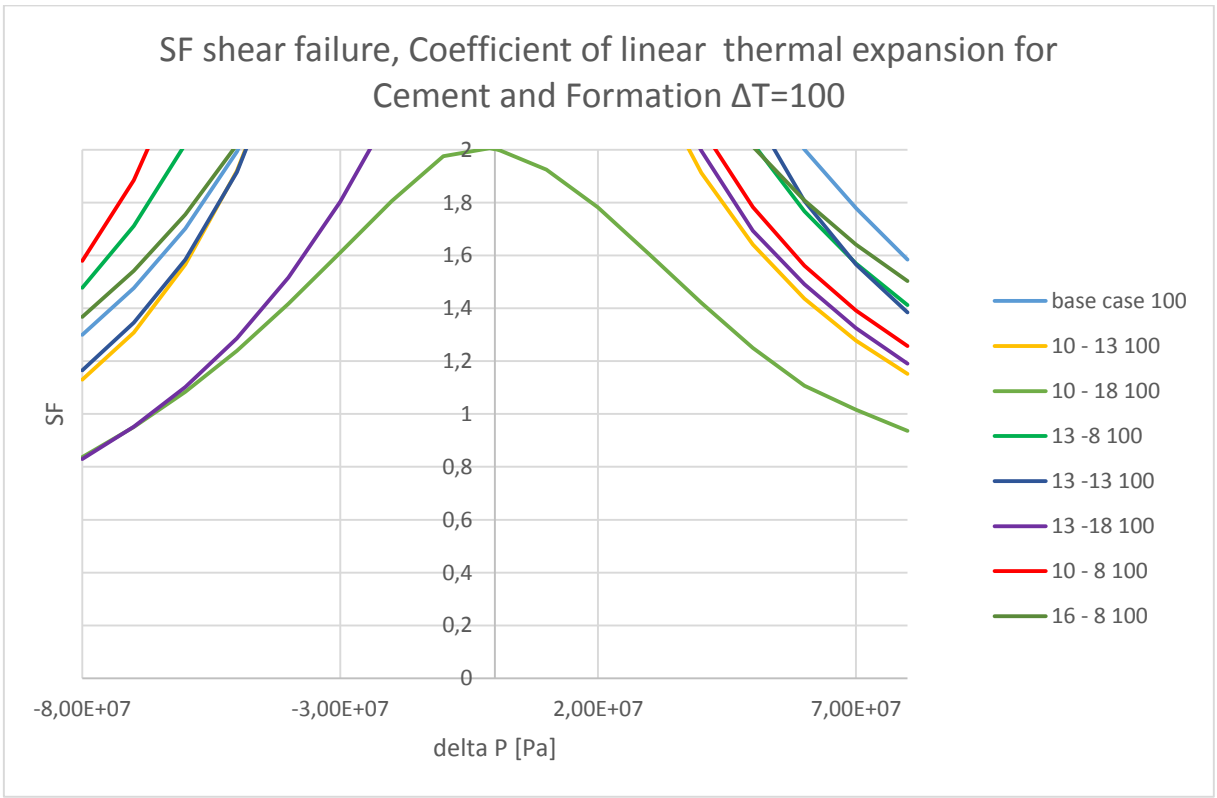
SF shear failure, Coefficient of linear thermal expansion for Cement and Formation ΔT=100
SF
2
1,8
1,6
1,4
1,2
1
0,8
0,6
0,4
0,2
0
-8,00E+07
-3,00E+07
2,00E+07
7,00E+07
delta P [Pa]
base case 100
10 - 13 100
10 - 18 100
13 -8 100
13 -13 100
13 -18 100
10 - 8 100
16 - 8 100

Appendix I

Model Features and Uncertainties

I.1 Initial Condition, remaining plots

Hoop stresses in compression when including initial condition

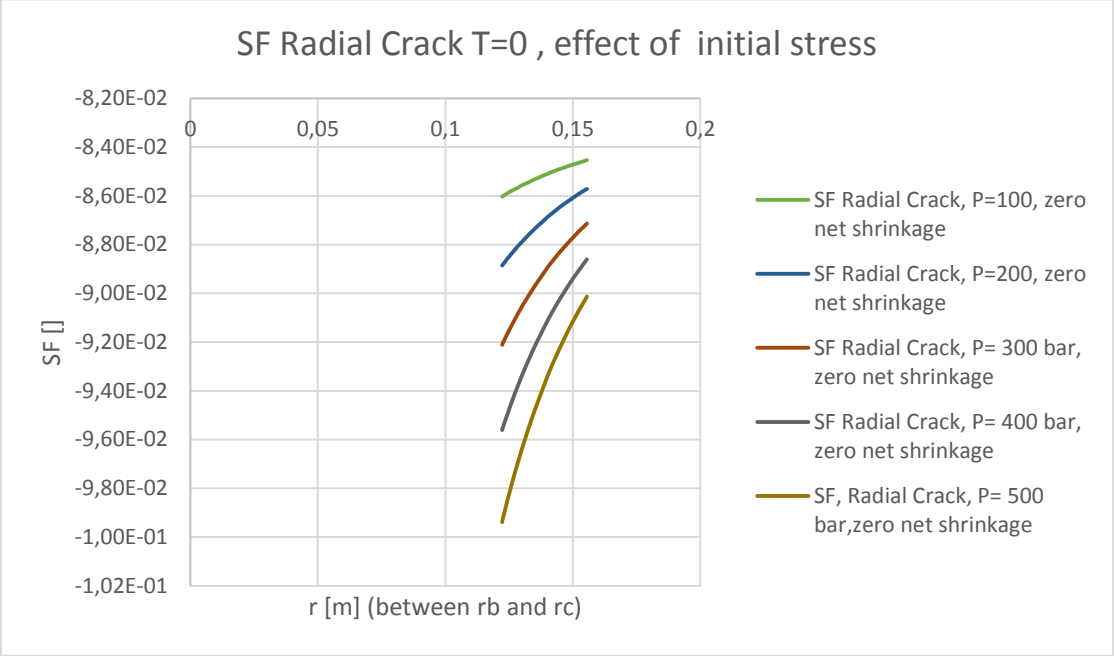

SF for radial crack, considering different temperatures, with constant pressure

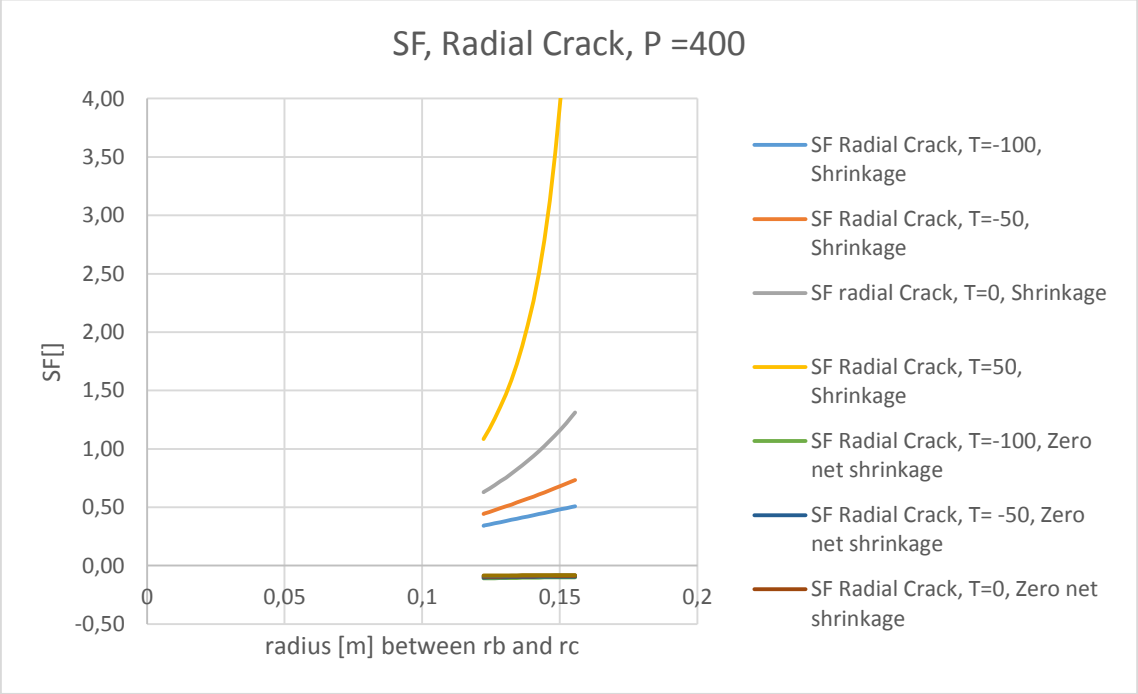

SF for debonding considering different temperatures, with constant pressure

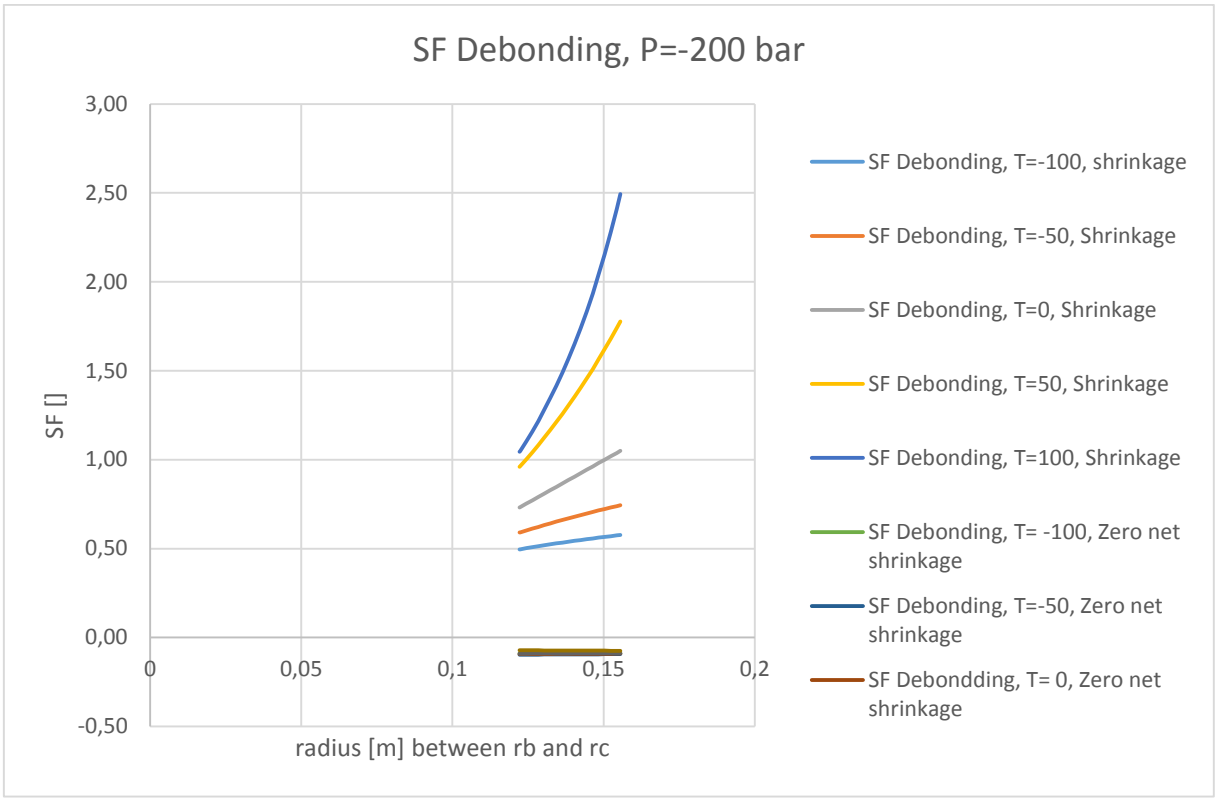

SF for shear failureconsidering different temperatures, with constant pressure

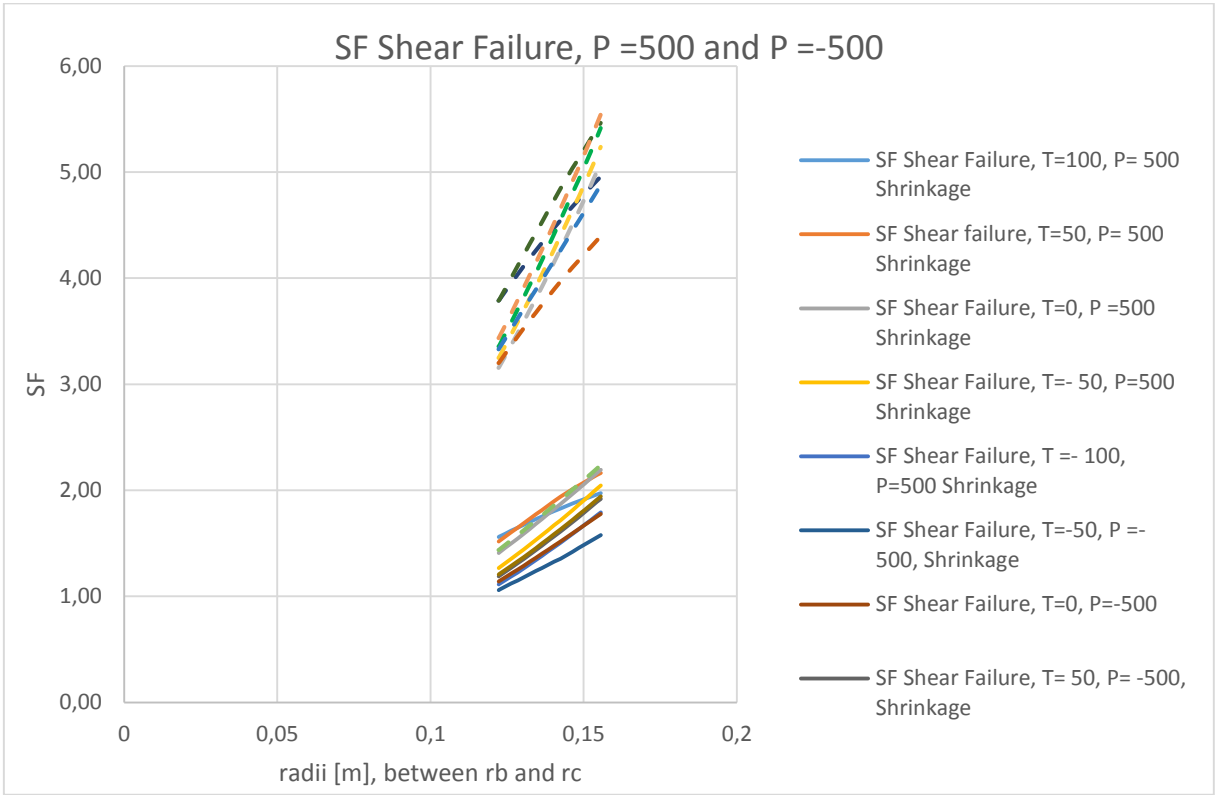

Cement Thickness

Debonding

At rb

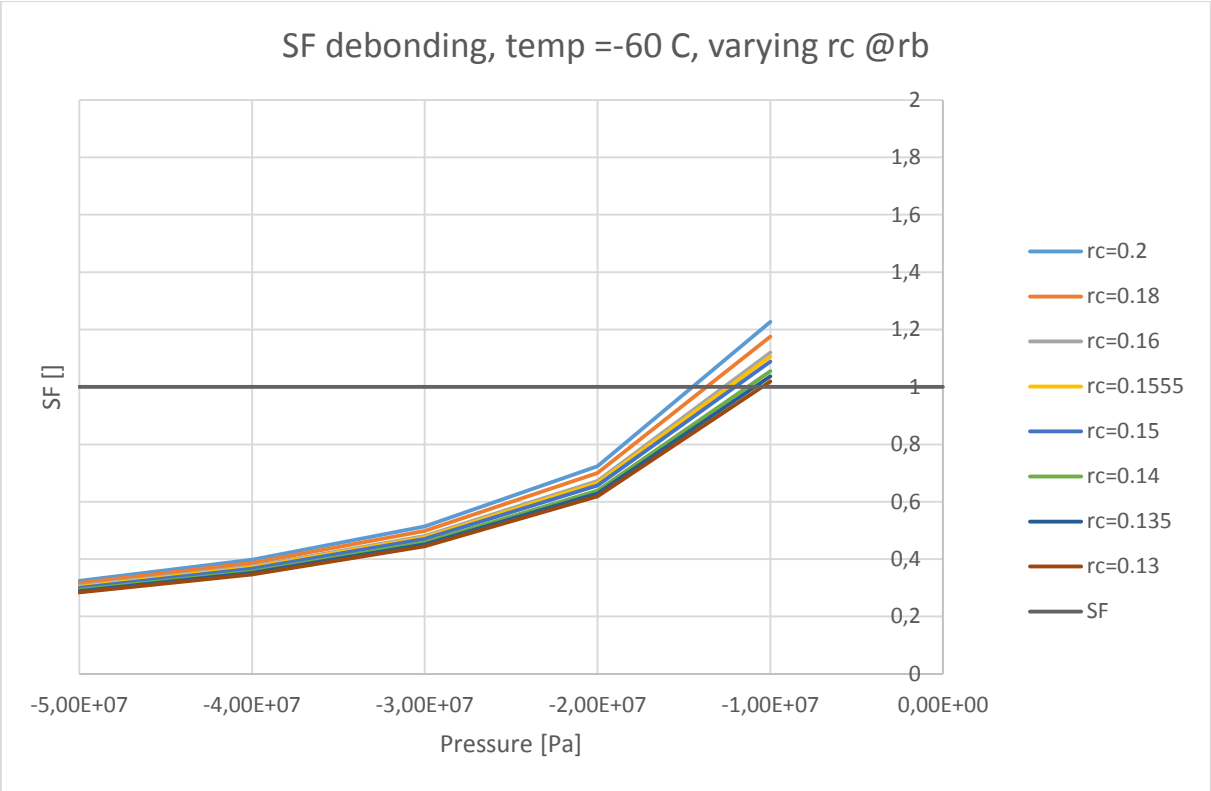

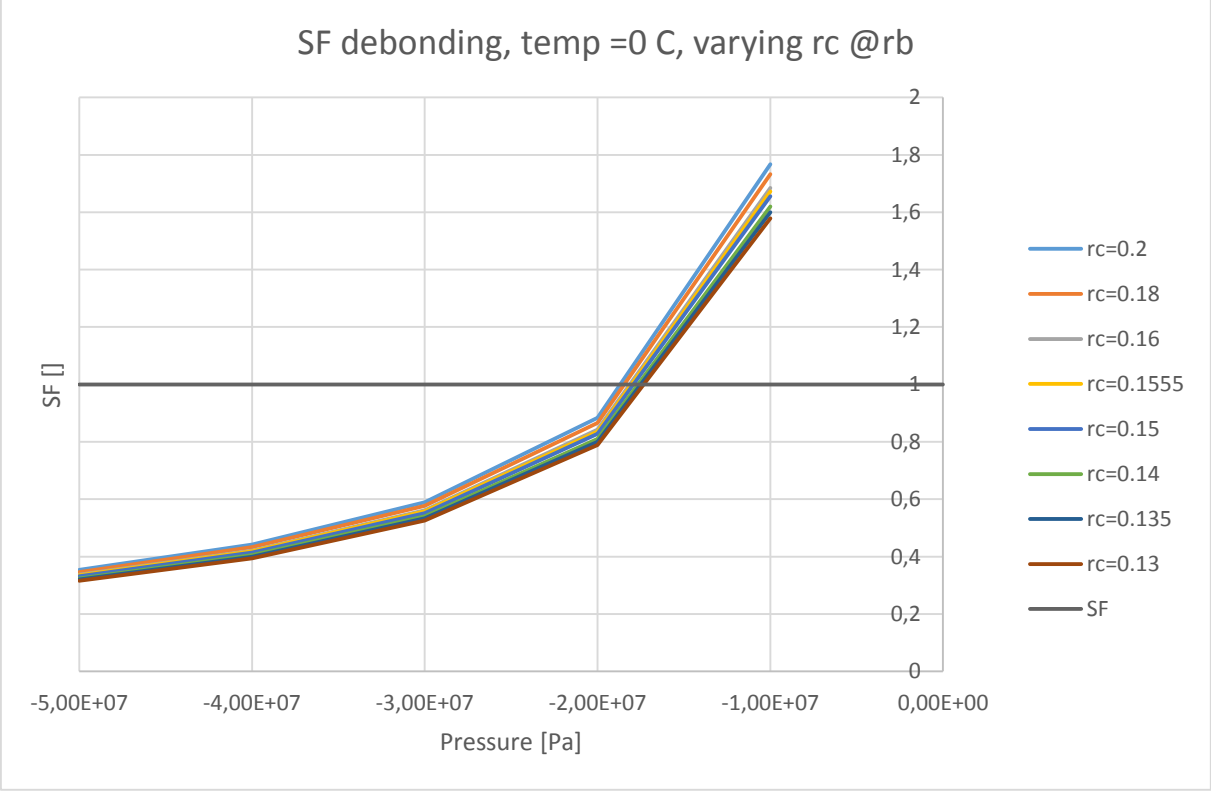

At r_c

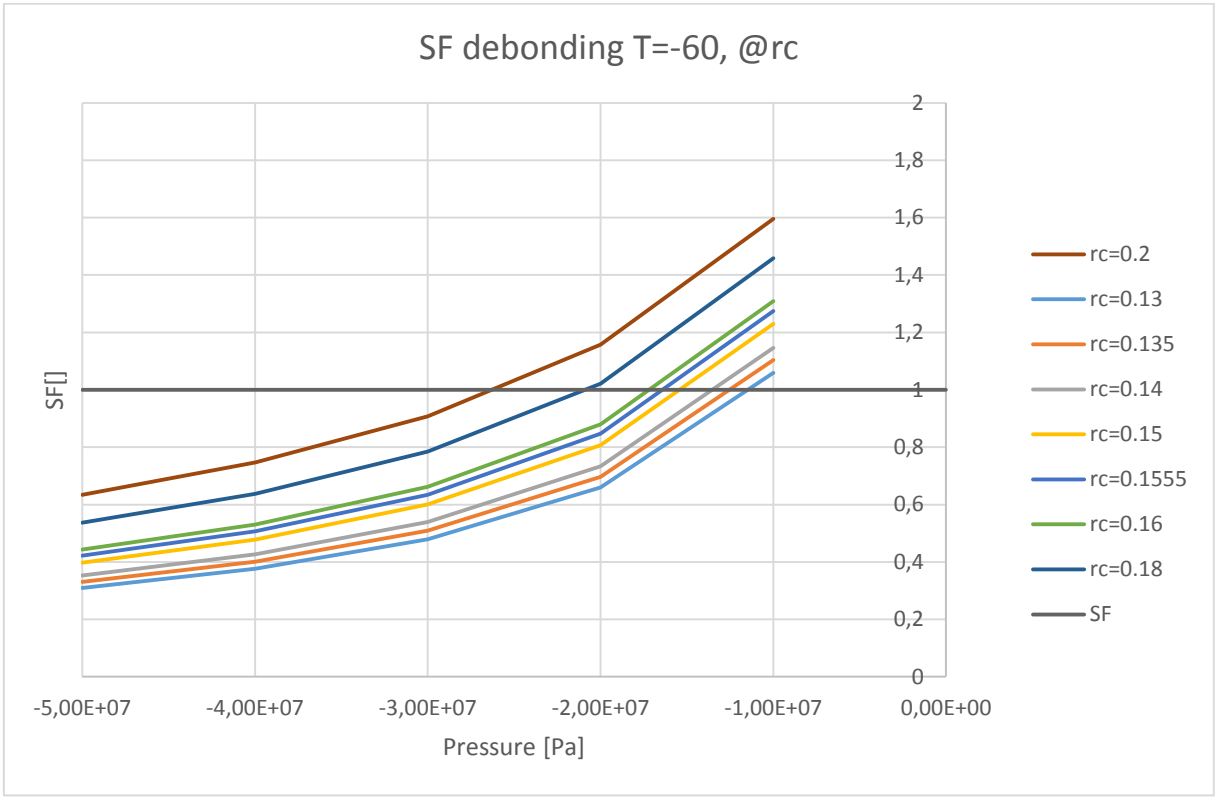
SF debonding T=-60, @rc
SF[]
2
1,8
1,6
1,4
1,2
1
0,8
0,6
0,4
0,2
0
-5,00E+07
-4,00E+07
-3,00E+07
-2,00E+07
-1,00E+07
0,00E+00
Pressure [Pa]
rc=0.2
rc=0.13
rc=0.135
rc=0.14
rc=0.15
rc=0.1555
rc=0.16
rc=0.18
SF

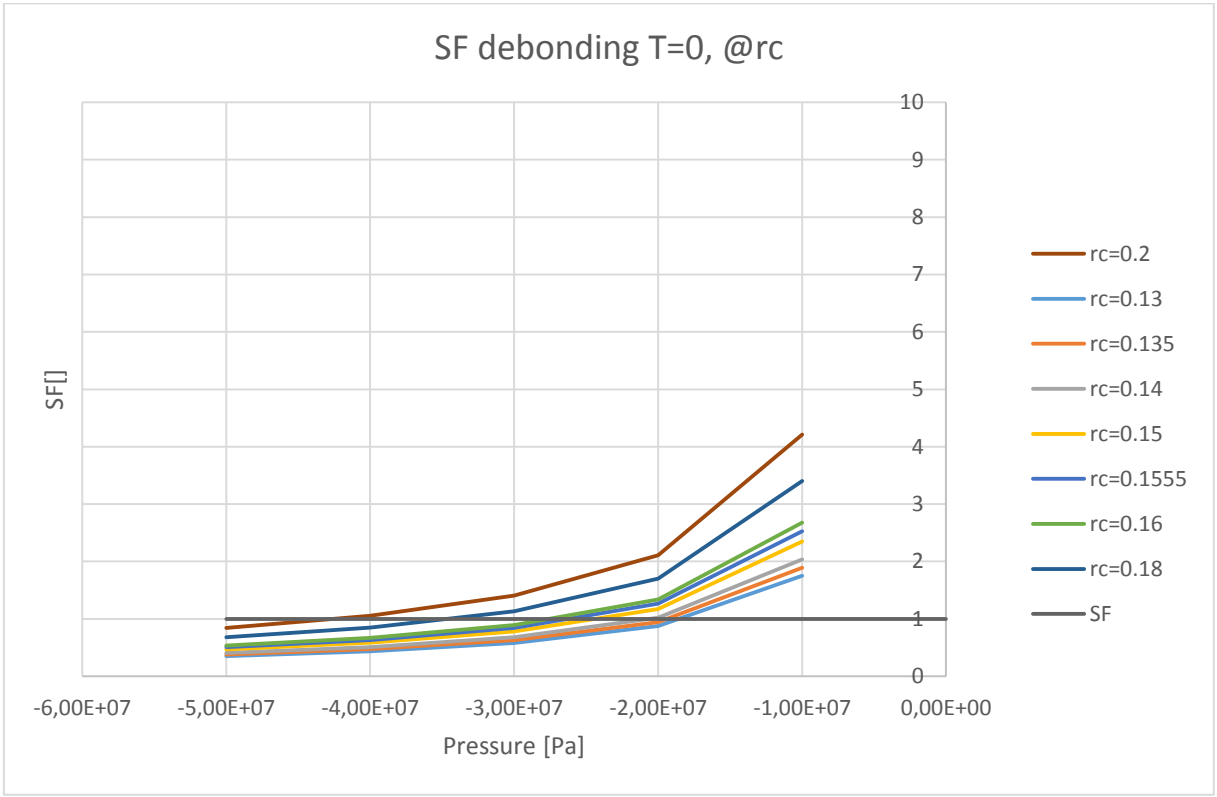
SF debonding T=0, @rc
SF[]
10
9
8
7
6
5
4
3
2
1
0
-6,00E+07
-5,00E+07
-4,00E+07
-3,00E+07
-2,00E+07
-1,00E+07
0,00E+00
Pressure [Pa]
rc=0.2
rc=0.13
rc=0.135
rc=0.14
rc=0.15
rc=0.1555
rc=0.16
rc=0.18
SF

Radial crack

At rb

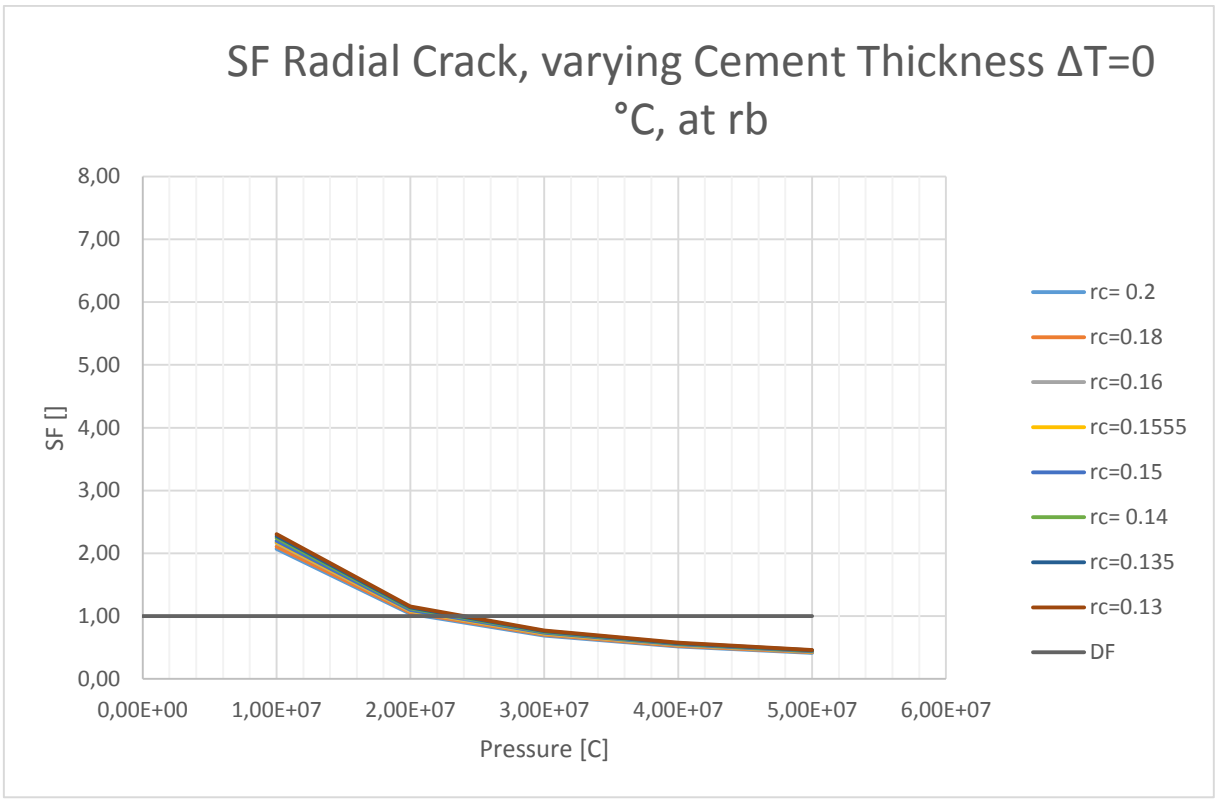

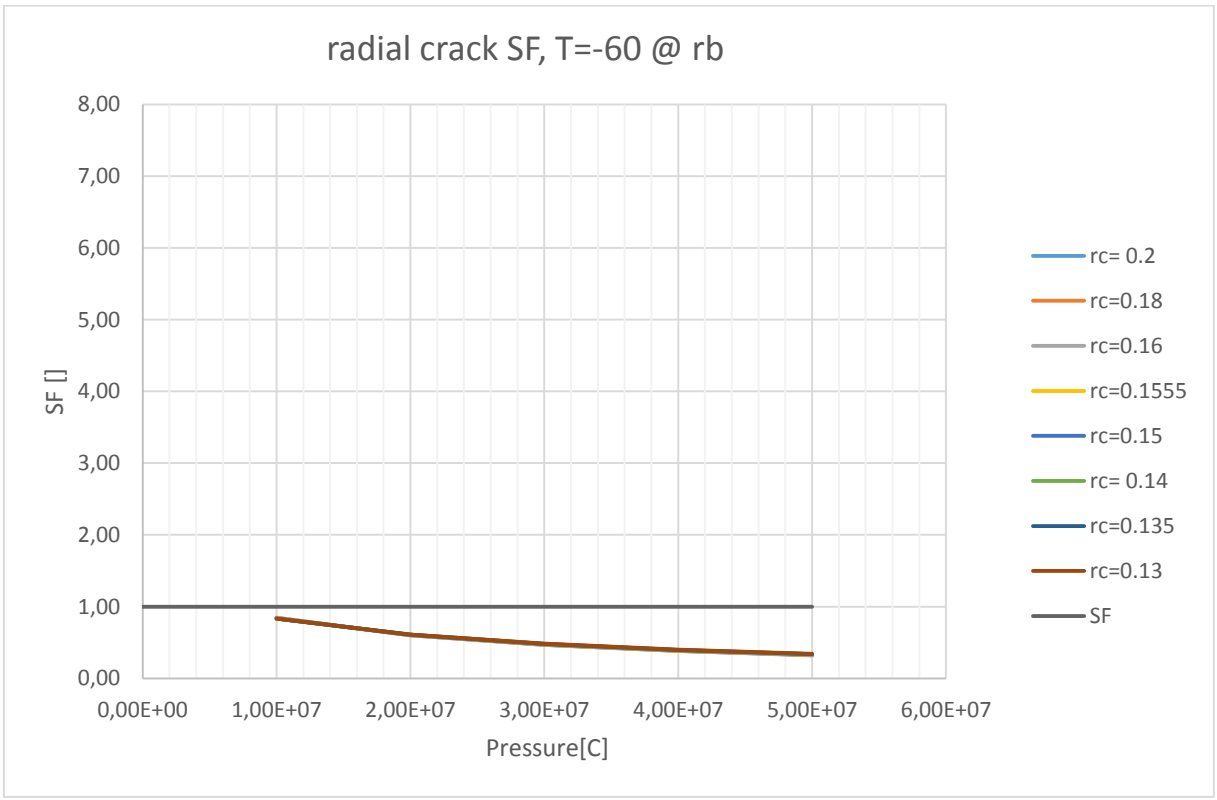

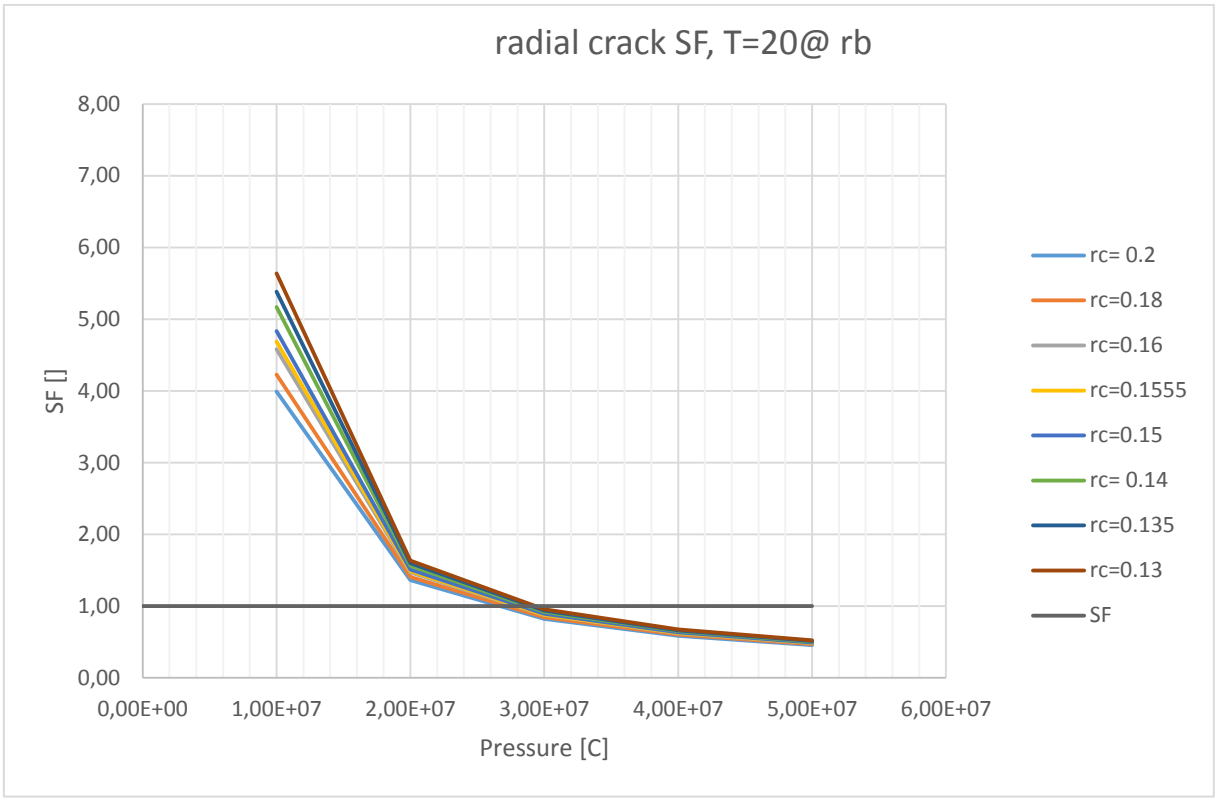
radial crack SF, T=20@ rb
8,00
7,00
6,00
5,00
4,00
3,00
2,00
1,00
0,00
SF []
0,00E+00
1,00E+07
2,00E+07
3,00E+07
4,00E+07
5,00E+07
6,00E+07
Pressure [C]
rc= 0.2
rc=0.18
rc=0.16
rc=0.1555
rc=0.15
rc= 0.14
rc=0.135
rc=0.13
SF

At r_c

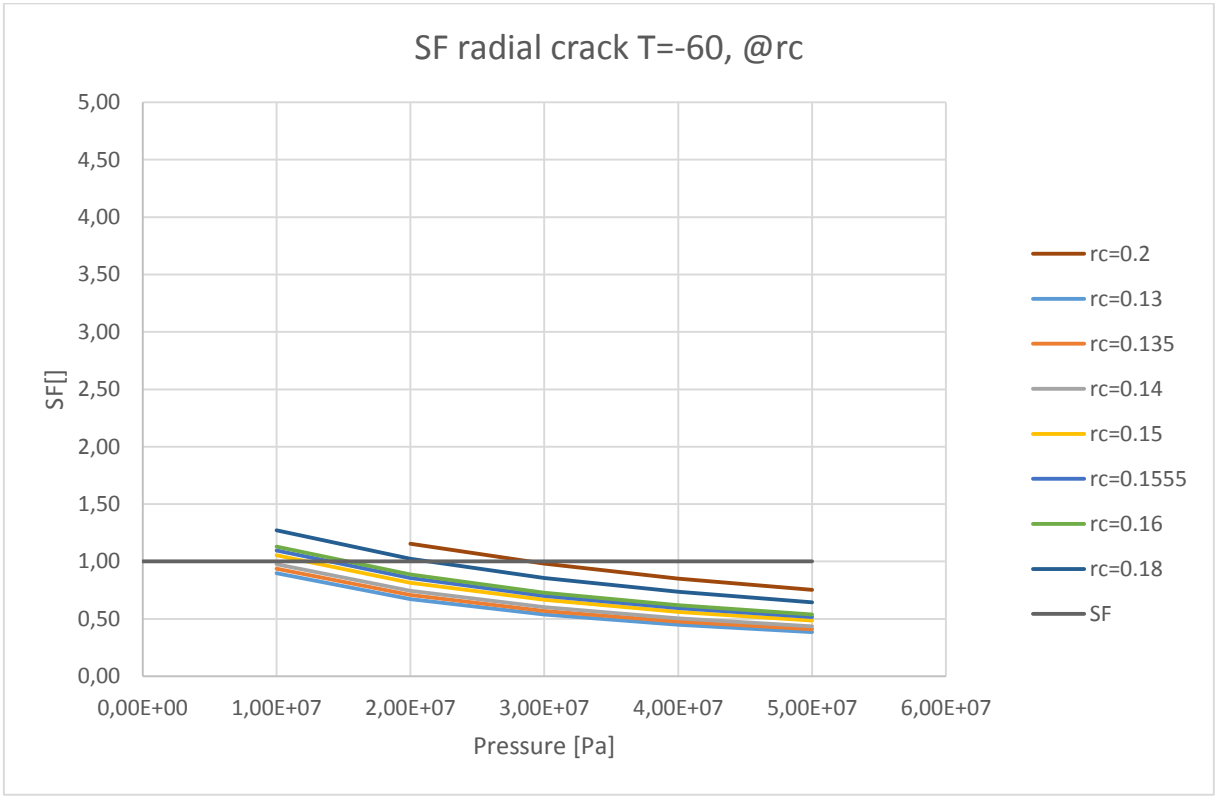
SF radial crack T=-60, @rc
5,00
4,50
4,00
3,50
3,00
2,50
2,00
1,50
1,00
0,50
0,00
SF[]
0,00E+00
1,00E+07
2,00E+07
3,00E+07
4,00E+07
5,00E+07
6,00E+07
Pressure [Pa]
rc=0.2
rc=0.13
rc=0.135
rc=0.14
rc=0.15
rc=0.1555
rc=0.16
rc=0.18
SF

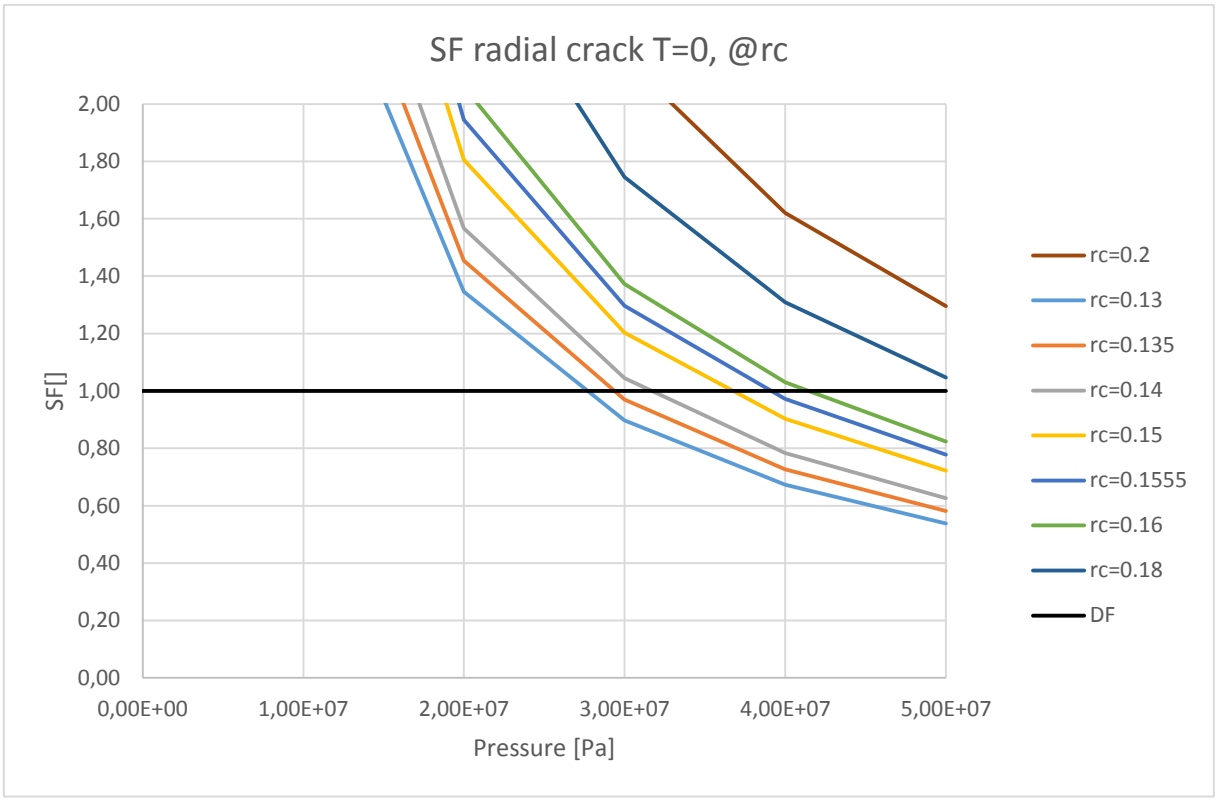
SF radial crack T=0, @rc
2,00
1,80
1,60
1,40
1,20
1,00
0,80
0,60
0,40
0,20
0,00
SF[]
0,00E+00
1,00E+07
2,00E+07
3,00E+07
4,00E+07
5,00E+07
Pressure [Pa]
rc=0.2
rc=0.13
rc=0.135
rc=0.14
rc=0.15
rc=0.1555
rc=0.16
rc=0.18
DF

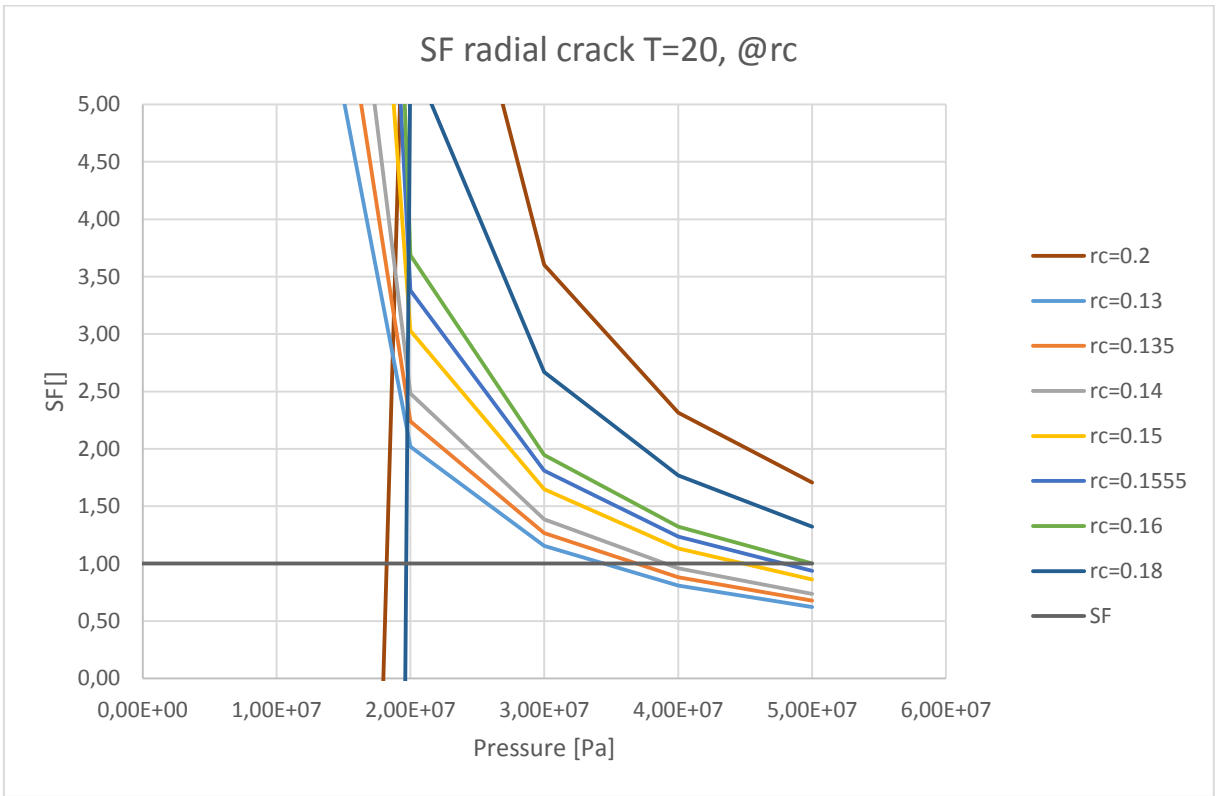
SF radial crack T=20, @rc
5,00
4,50
4,00
3,50
3,00
2,50
2,00
1,50
1,00
0,50
0,00
SF[]
0,00E+00
1,00E+07
2,00E+07
3,00E+07
4,00E+07
5,00E+07
6,00E+07
Pressure [Pa]
rc=0.2
rc=0.13
rc=0.135
rc=0.14
rc=0.15
rc=0.1555
rc=0.16
rc=0.18
SF

Shear

At rb

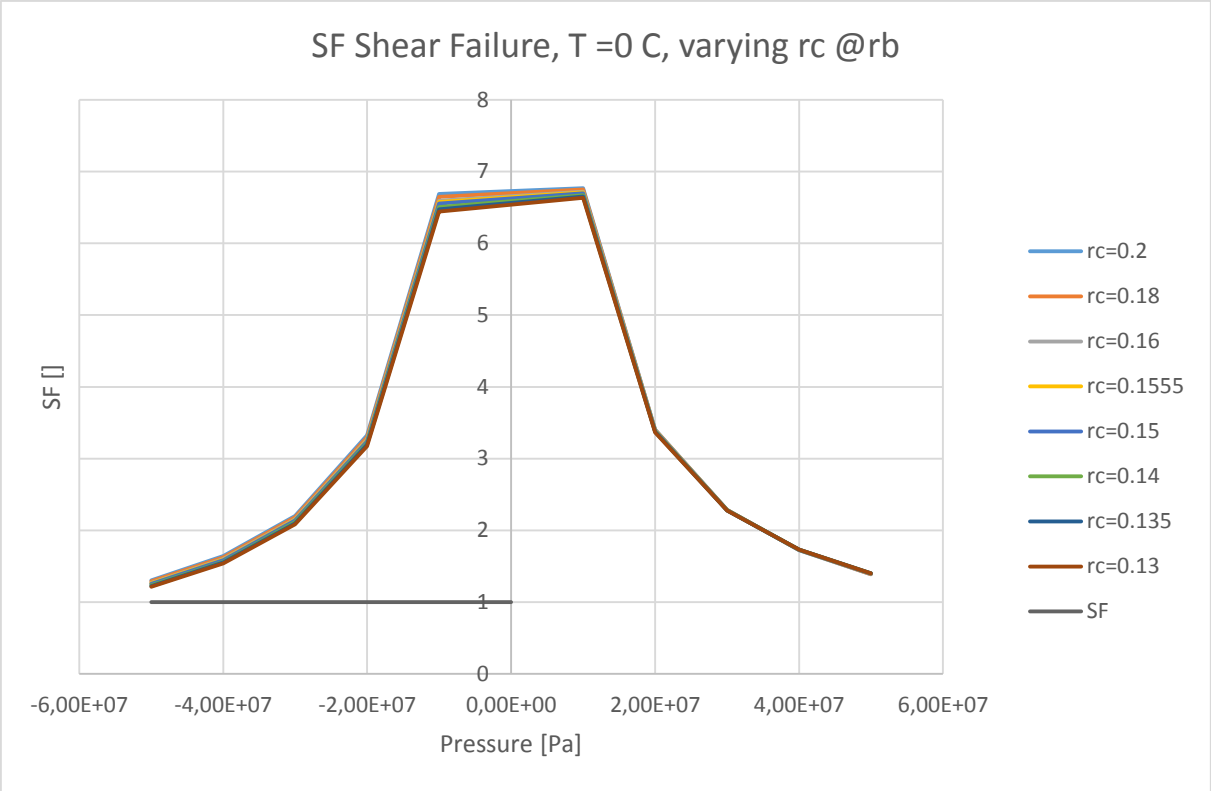
SF Shear Failure, T =0 C, varying rc @rb
SF []
Pressure [Pa]
-6,00E+07
-4,00E+07
-2,00E+07
0,00E+00
2,00E+07
4,00E+07
6,00E+07
0
1
2
3
4
5
6
7
8
rc=0.2
rc=0.18
rc=0.16
rc=0.1555
rc=0.15
rc=0.14
rc=0.135
rc=0.13
SF

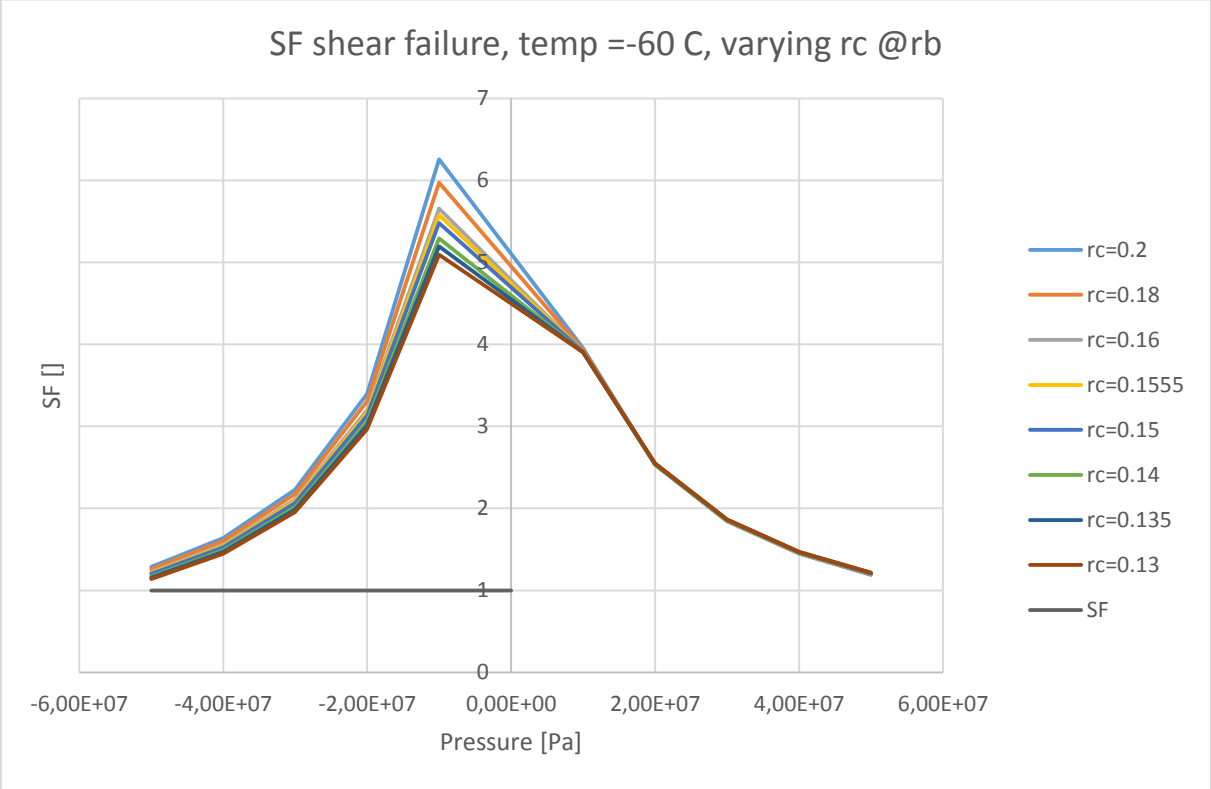
SF shear failure, temp =-60 C, varying rc @rb
SF []
Pressure [Pa]
-6,00E+07
-4,00E+07
-2,00E+07
0,00E+00
2,00E+07
4,00E+07
6,00E+07
0
1
2
3
4
5
6
7
rc=0.2
rc=0.18
rc=0.16
rc=0.1555
rc=0.15
rc=0.14
rc=0.135
rc=0.13
SF

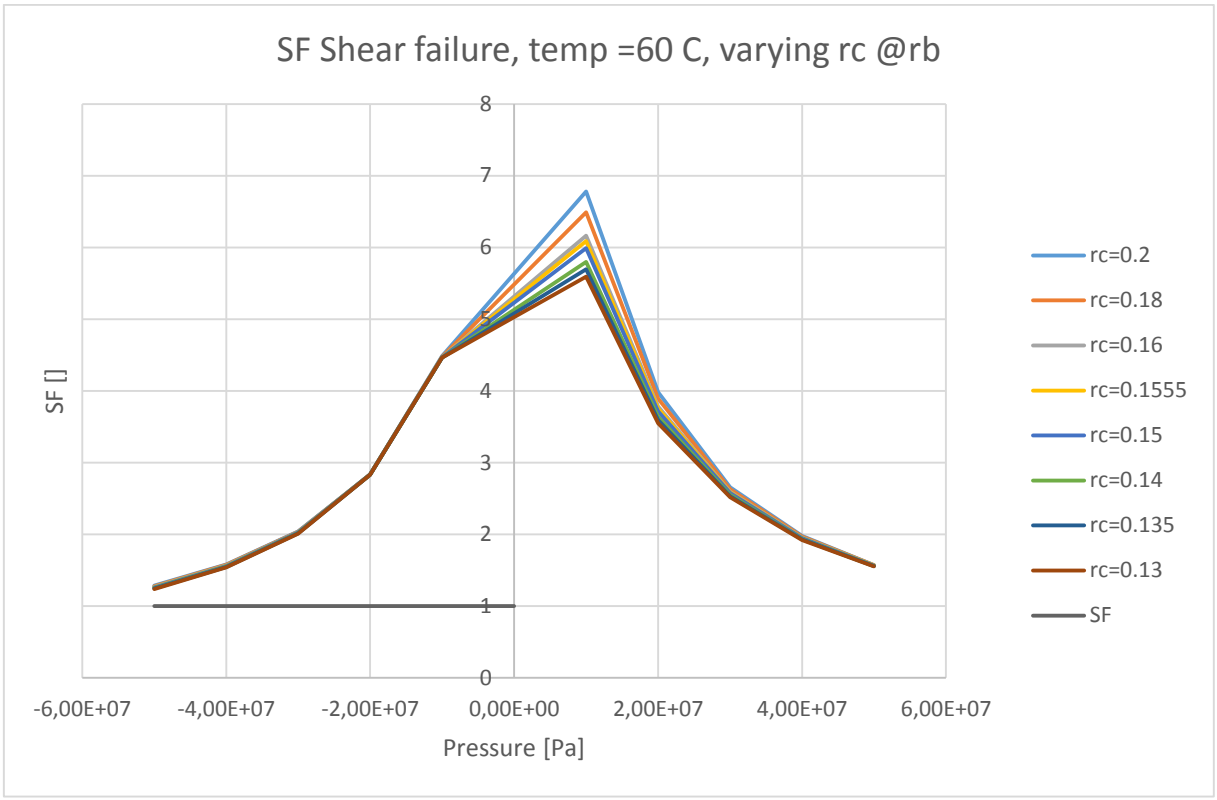
SF Shear failure, temp =60 C, varying rc @rb
SF []
Pressure [Pa]
-6,00E+07
-4,00E+07
-2,00E+07
0,00E+00
2,00E+07
4,00E+07
6,00E+07
0
1
2
3
4
5
6
7
8
rc=0.2
rc=0.18
rc=0.16
rc=0.1555
rc=0.15
rc=0.14
rc=0.135
rc=0.13
SF

At r_c

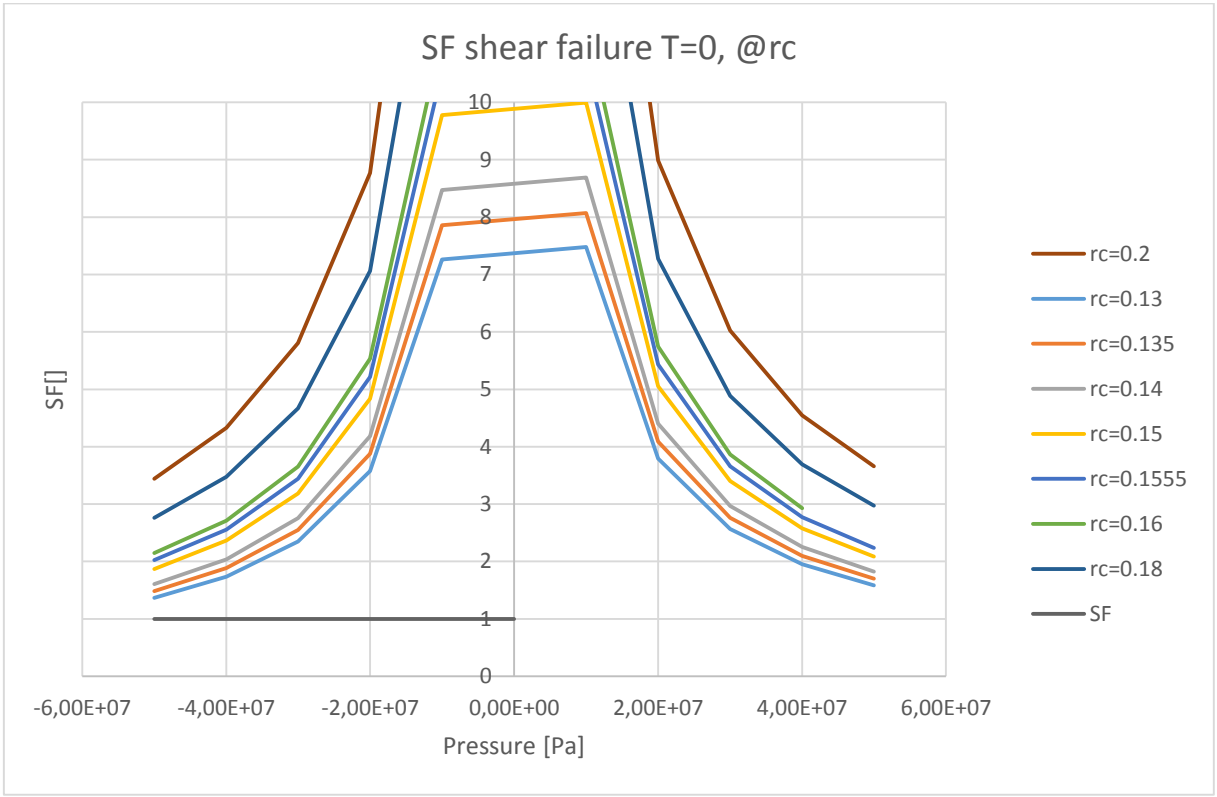
SF shear failure T=0, @rc
SF[]
Pressure [Pa]
-6,00E+07
-4,00E+07
-2,00E+07
0,00E+00
2,00E+07
4,00E+07
6,00E+07
0
1
2
3
4
5
6
7
8
9
10
rc=0.2
rc=0.13
rc=0.135
rc=0.14
rc=0.15
rc=0.1555
rc=0.16
rc=0.18
SF

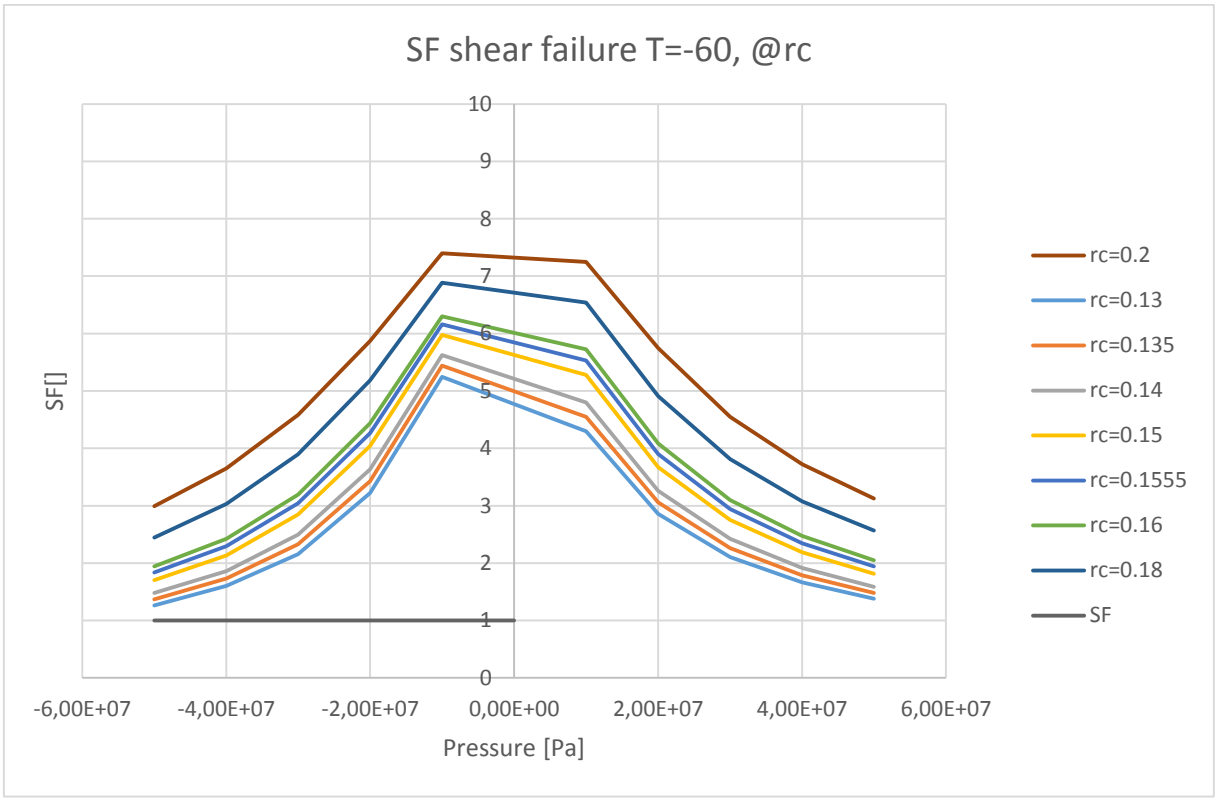
SF shear failure T=-60, @rc
SF[]
10
9
8
7
6
5
4
3
2
1
0
-6,00E+07
-4,00E+07
-2,00E+07
0,00E+00
2,00E+07
4,00E+07
6,00E+07
Pressure [Pa]
rc=0.2
rc=0.13
rc=0.135
rc=0.14
rc=0.15
rc=0.1555
rc=0.16
rc=0.18
SF

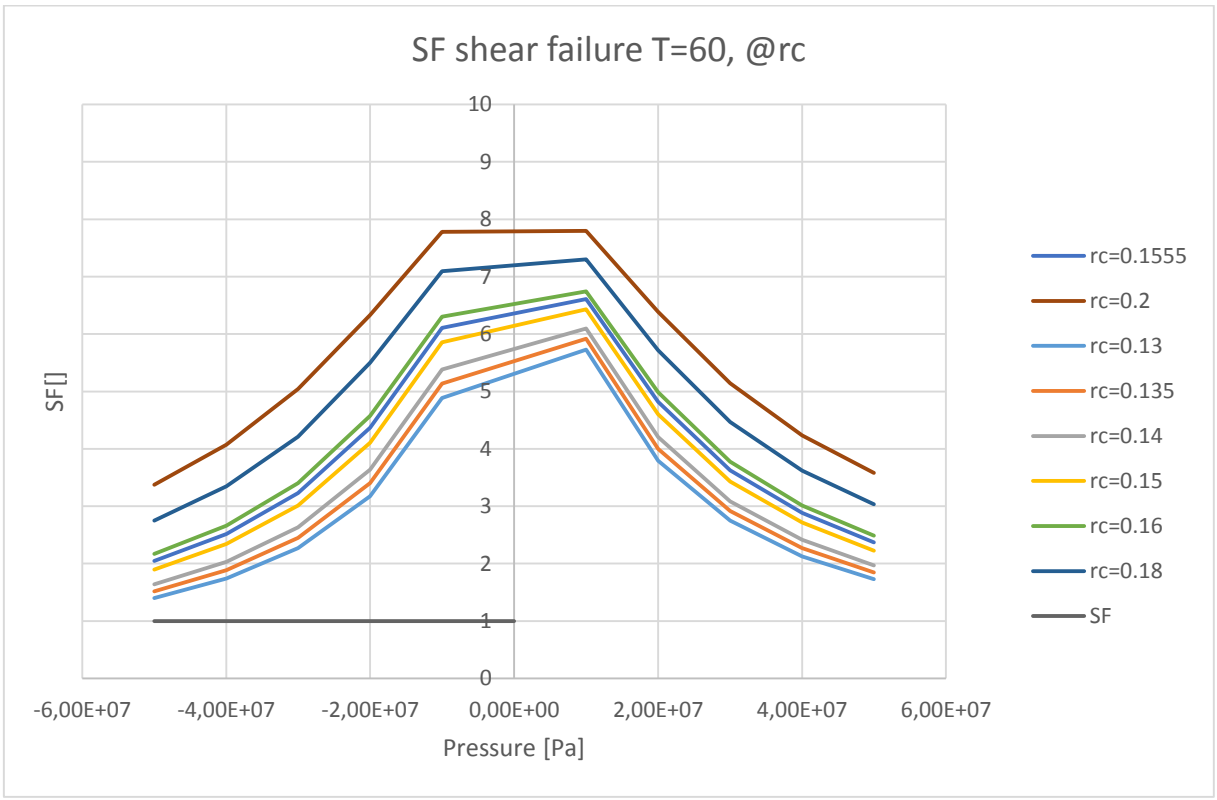
SF shear failure T=60, @rc
SF[]
10
9
8
7
6
5
4
3
2
1
0
-6,00E+07
-4,00E+07
-2,00E+07
0,00E+00
2,00E+07
4,00E+07
6,00E+07
Pressure [Pa]
rc=0.1555
rc=0.2
rc=0.13
rc=0.135
rc=0.14
rc=0.15
rc=0.16
rc=0.18
SF

I.1 Effect of Changing Rd on SFs for the Different Failure Modes

Radial Crack

At rb

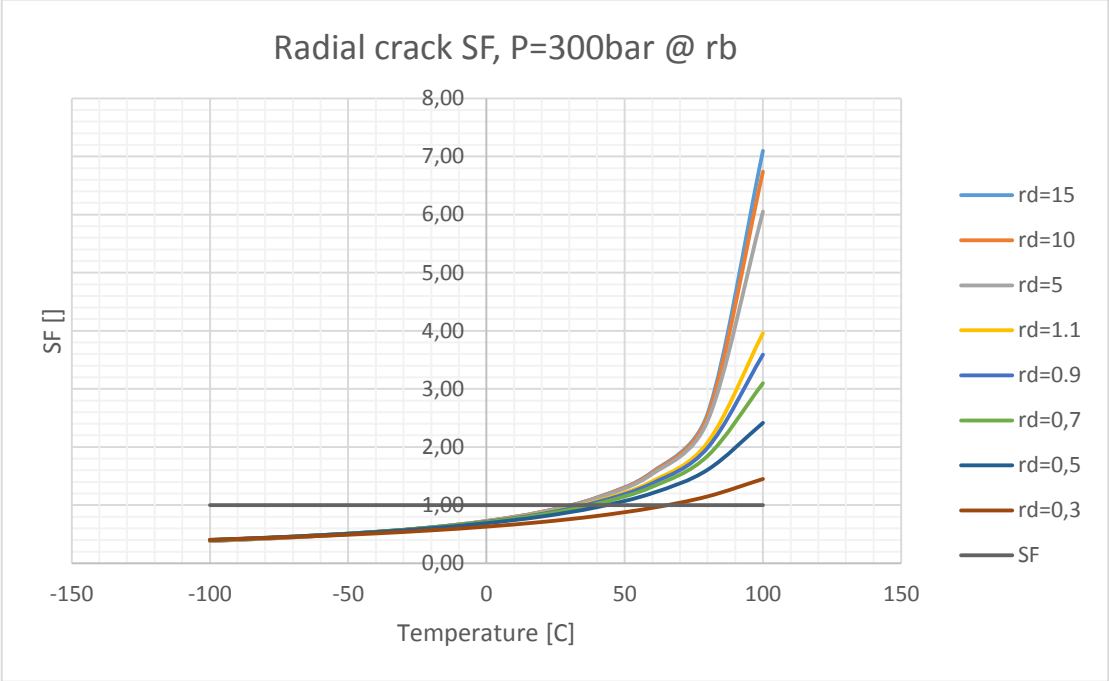

At r_c

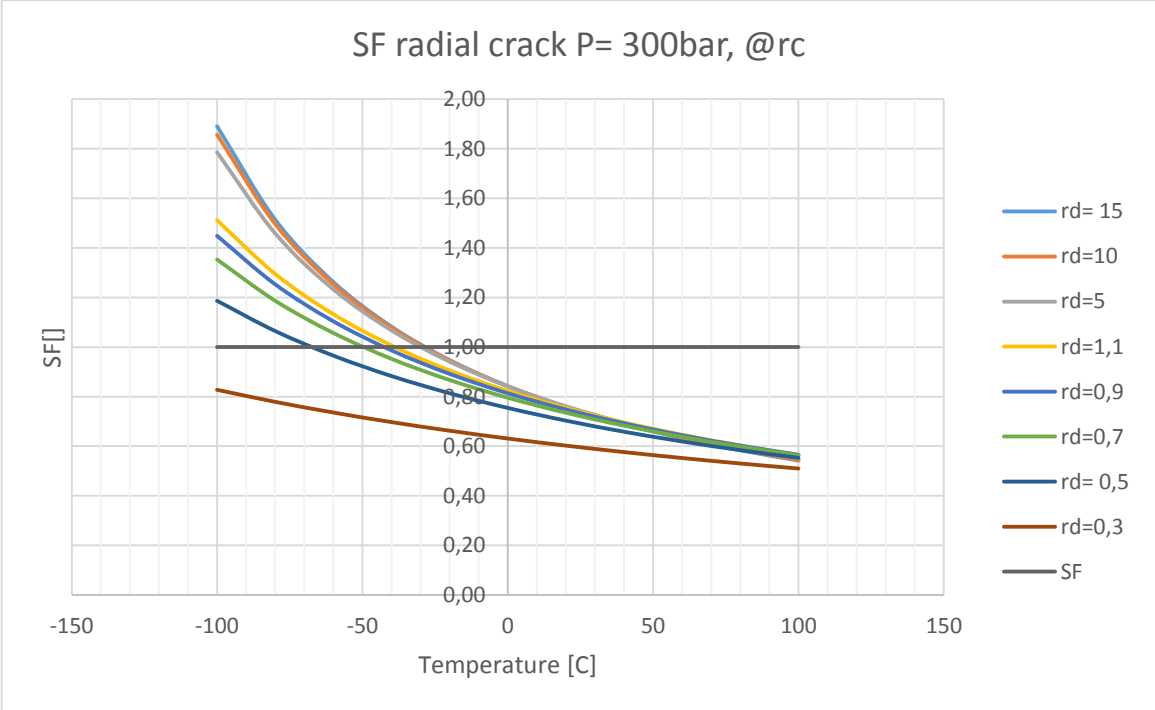

Debonding

At rb

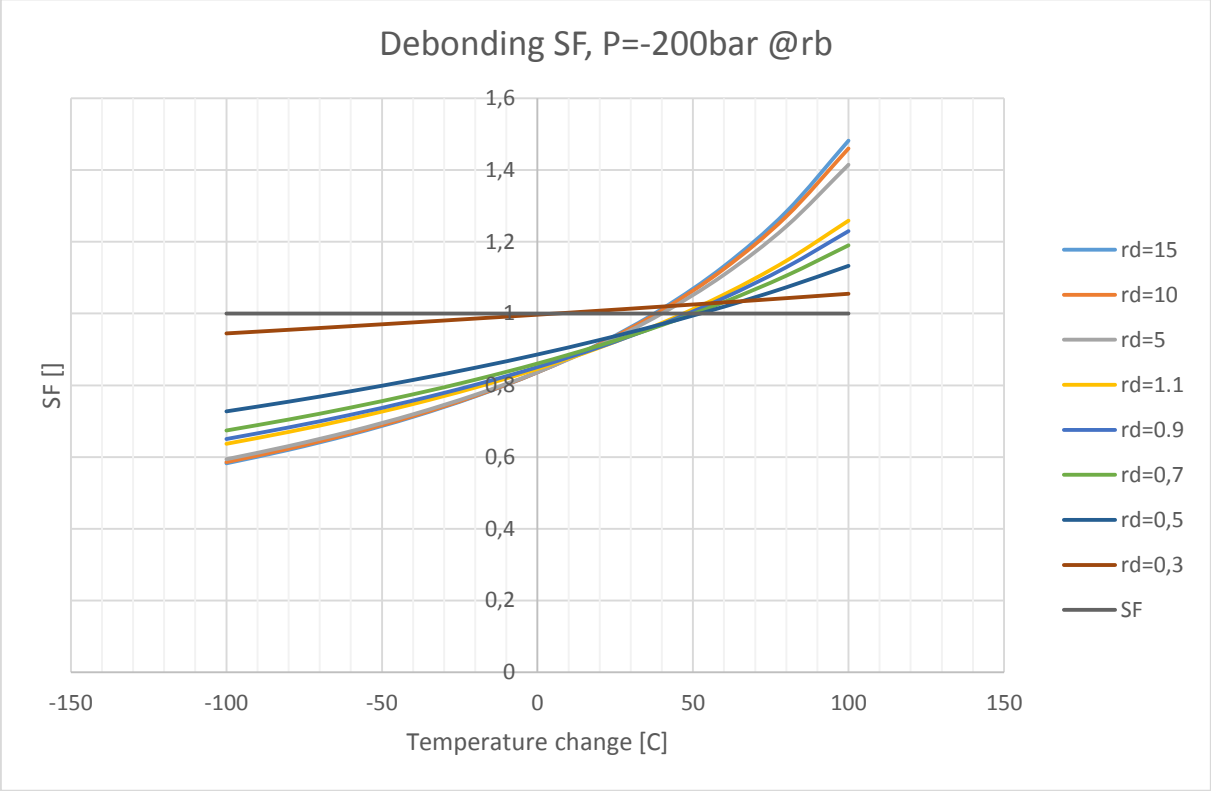

At r_c

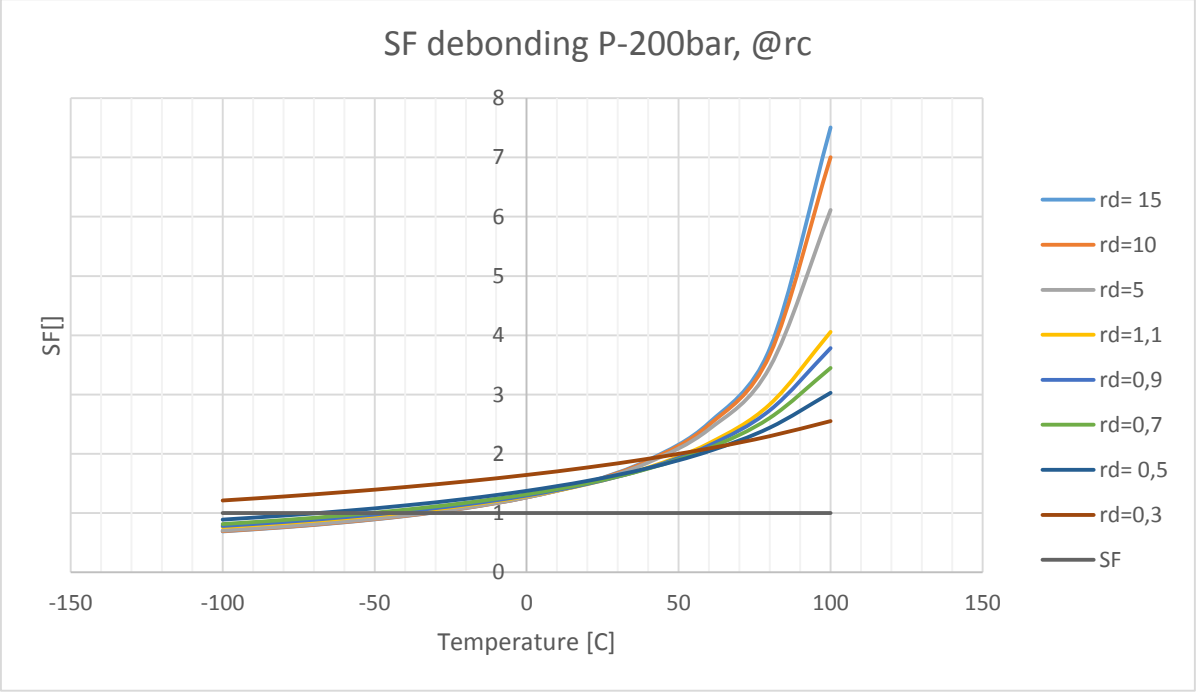

Shear Failure

At rb

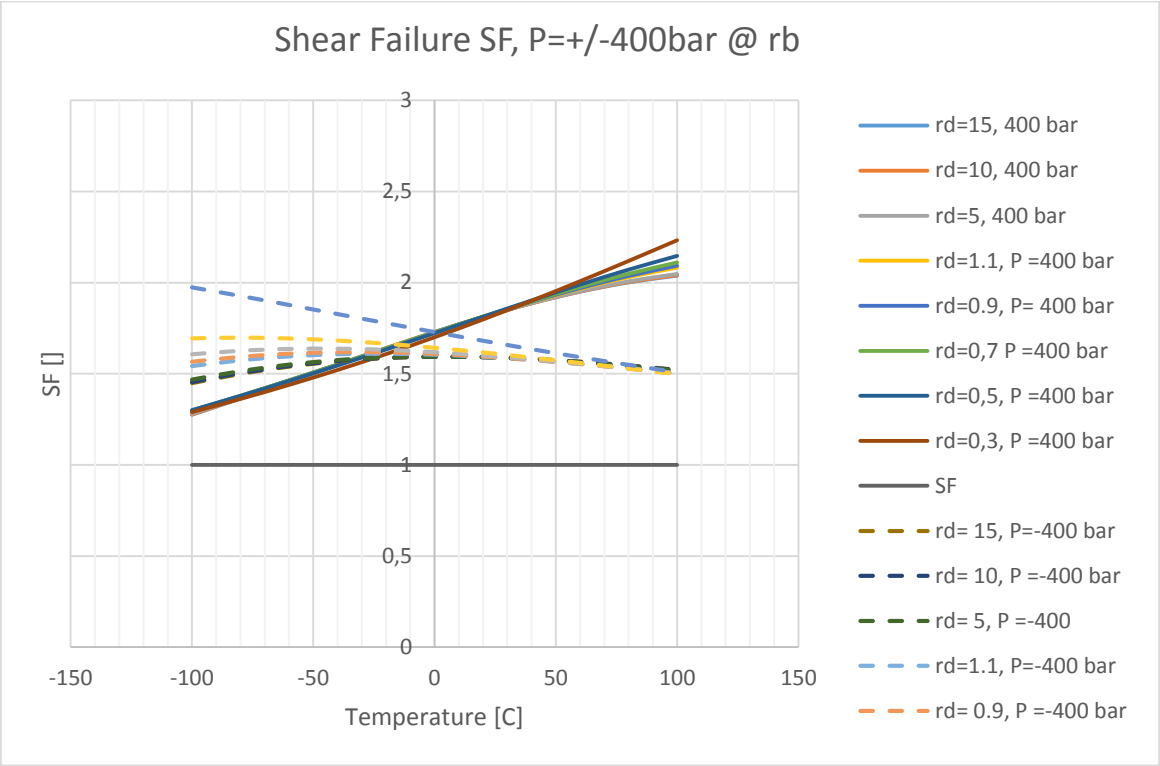

At rb

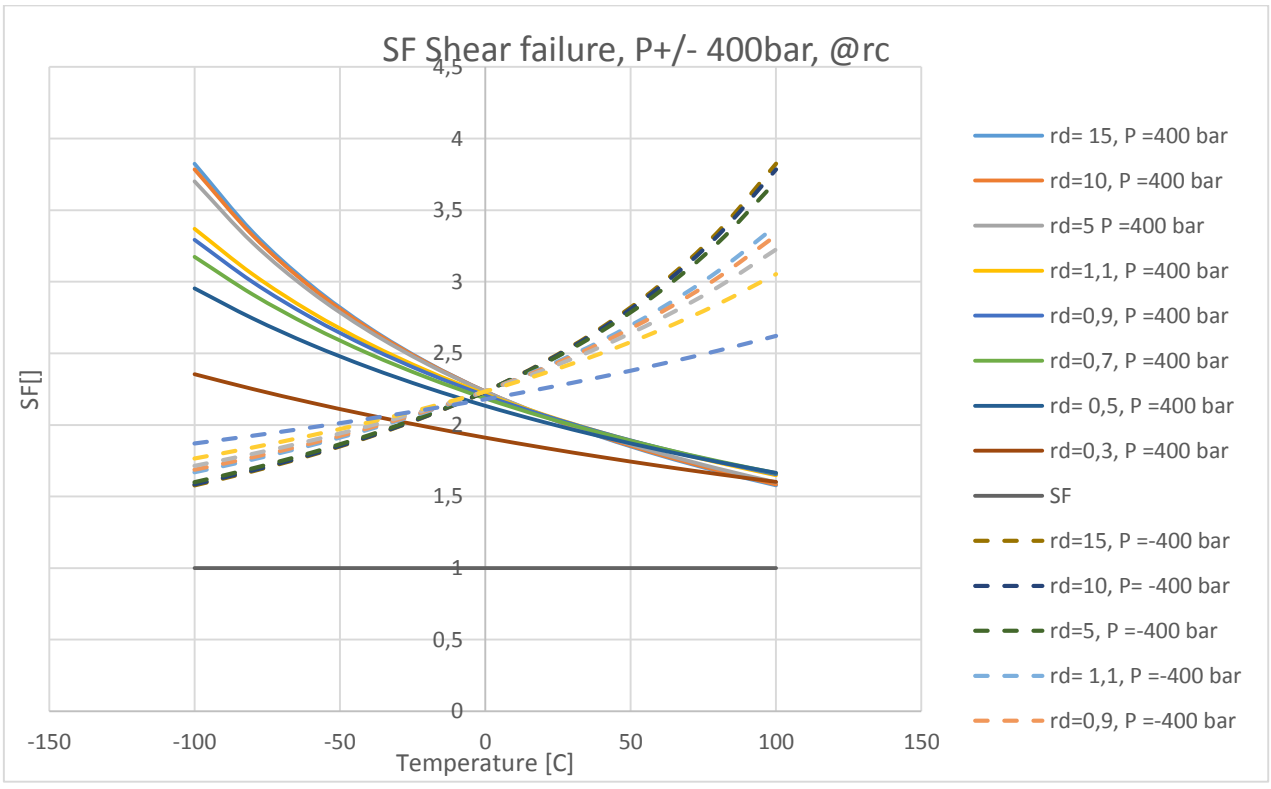

I.2 Change in External Pressure

Debonding

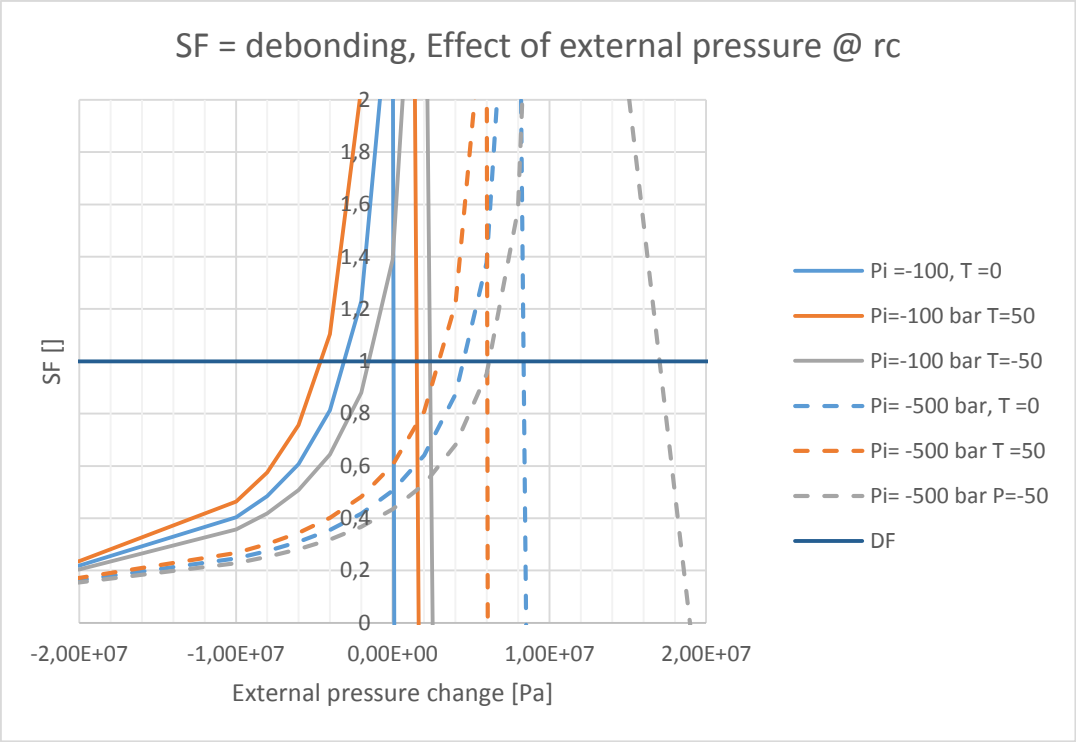

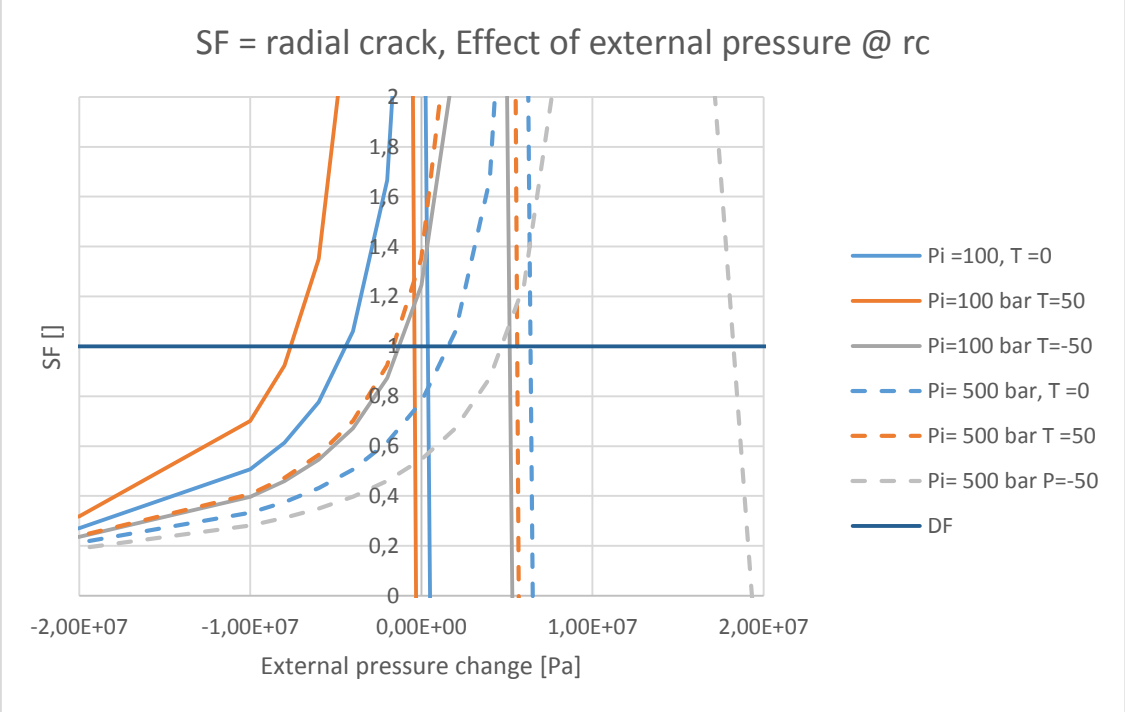

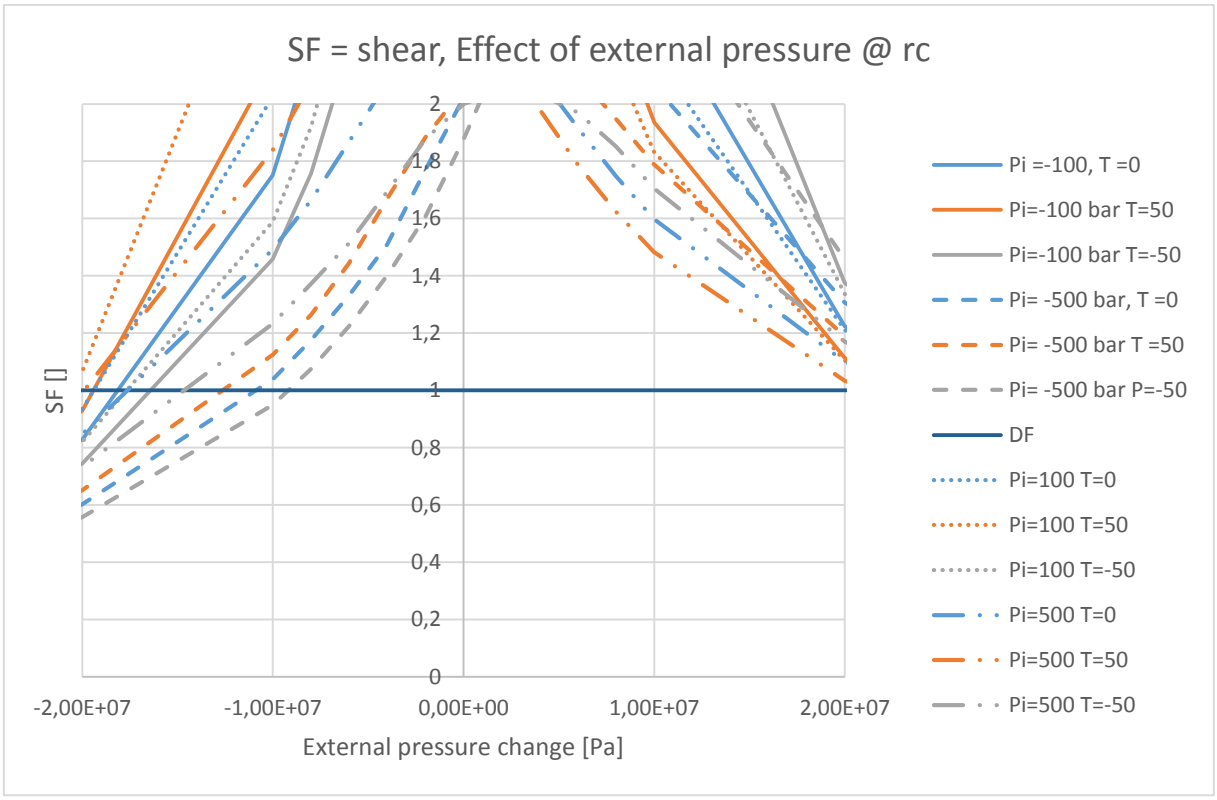
SF = shear, Effect of external pressure @ rc
SF []
2
1,8
1,6
1,4
1,2
1
0,8
0,6
0,4
0,2
0
-2,00E+07
-1,00E+07
0,00E+00
1,00E+07
2,00E+07
External pressure change [Pa]
Pi =-100, T =0
Pi=-100 bar T=50
Pi=-100 bar T=-50
Pi= -500 bar, T =0
Pi= -500 bar T =50
Pi= -500 bar P=-50
DF
Pi=100 T=0
Pi=100 T=50
Pi=100 T=-50
Pi=500 T=0
Pi=500 T=50
Pi=500 T=-50

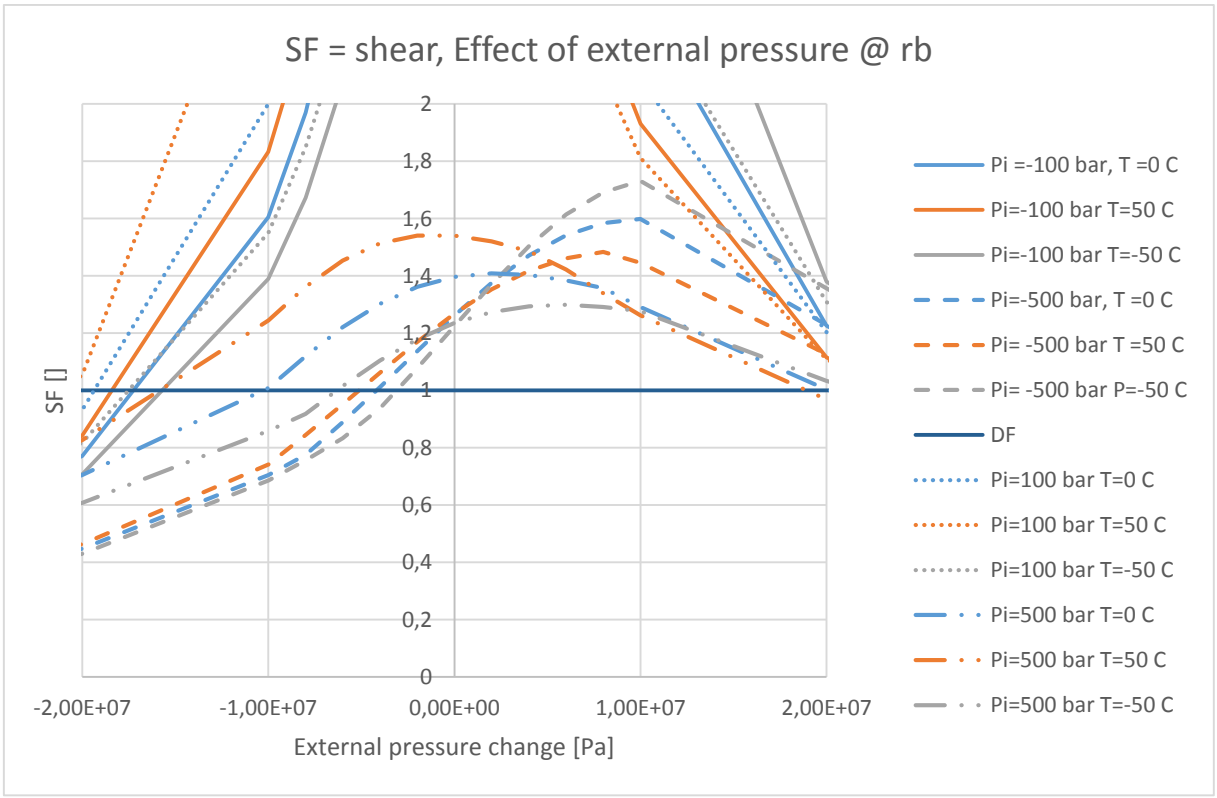
SF = shear, Effect of external pressure @ rb
SF []
2
1,8
1,6
1,4
1,2
1
0,8
0,6
0,4
0,2
0
-2,00E+07
-1,00E+07
0,00E+00
1,00E+07
2,00E+07
External pressure change [Pa]
Pi =-100 bar, T =0 C
Pi=-100 bar T=50 C
Pi=-100 bar T=-50 C
Pi=-500 bar, T =0 C
Pi= -500 bar T =50 C
Pi= -500 bar P=-50 C
DF
Pi=100 bar T=0 C
Pi=100 bar T=50 C
Pi=100 bar T=-50 C
Pi=500 bar T=0 C
Pi=500 bar T=50 C
Pi=500 bar T=-50 C